Photosensitizer, pH sensing and optical limiting properties of BODIPY dyes

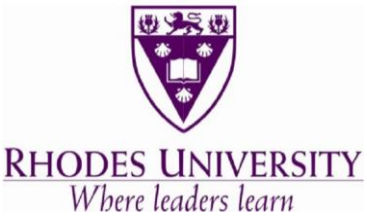

A thesis submitted in the fulfillment of the requirements for the degree of

Masters of Science

of

Rhodes University

by

Aviwe Khanya May

January 2018

Acknowledgements

I would like to thank my supervisor, Dr Mack, for the guidance and opportunities he provided for me during my MSc. I would also like to thank Prof Nyokong, my co-supervisor for the opportunities and support in all respects.

A special thanks also goes to Ms Gail Cobus for all the work she does, including the administrative work behind the scenes which has made my studies seamless and free of administrative clutter. I would also like to thank Dr Britton for the technical work and chemical order management for S22. On that note, great thanks also go to everyone in Laboratory S22: Thank you for the support, teaching me different techniques and approaches and above all, for making the lab nothing but fun.

I would also like to thank Professor Zhen Shen (Nanjing University, China) for hosting me during my exchange visit in 2016.

It would be a great injustice to not thank Dr Pitchou Ngoy for the support and guidance given. A very special thanks goes to him for his assistance with synthesis, and particularly that of the distyryl compounds studied herein. Thank you Dr Ngoy.

Above all, I would like to thank God almighty, my family and all my friends and acquaintances, without mentioning names. Thank you for your continuous support and for keeping the relationship alive even during the most challenging times of my studies.

Financial support from the National Research Foundation is acknowledged with a grateful heart.

Abstract

A series of BODIPY dyes have been successfully synthesised and structurally characterised to examine the effect of halogenation at the 2,6-positions and the introduction of styryl and vinylene groups at the 3,5-positions. The photophysical properties were studied, to assess the effect of the enhancement of the rate of intersystem crossing through halogenation on the fluorescence properties and the generation of reactive oxygen species. This is important in the assessment of the suitability of applying these molecules as photosensitizer dyes for photodynamic therapy and photodynamic antimicrobial chemotherapy. Upon bromination, the dyes showed moderately high singlet oxygen quantum yields. The inclusion of BODIPY dyes into cyclodextrins was explored since it makes them water soluble and hence suitable for biomedical applications, but no singlet oxygen was detected in aqueous media for the inclusion complexes.

In order to red-shift the main spectral band of the BODIPY dyes into the therapeutic window, styryl groups were introduced at the 3,5-positions via a modified Knoevenagel condensation reaction. Since the main spectral band lies well above 532 nm, the second harmonic of the Nd:YAG laser, there is relatively weak absorbance at this wavelength. The 3,5-distyryl and 3,5-divinylene BODIPY dyes were assessed for their potential utility for application in nonlinear optics (NLO), and they demonstrated typical nonlinear absorption behaviour characterised by reverse saturable absorption (RSA) in z-scan measurements. Furthermore, the dyes possess excellent optical limiting parameters, such as their third-order suspectibility and hyperpolarizability values, in a wide range of solvents. One dye containing dimethylamino moieties on styryl groups attached at the 3,5-positions was

assessed for potential application as an on/off fluorescence sensor. The dye proved to be successful, since intramolecular charge transfer in the S_1 state was eliminated in the presence of acid and this results in a fluorescence “turn on” effect. This process was found to be reversible with the addition of a base.

Table of Contents

List of Symbols

A	Absorbance
Å	Angstrom
β	Nonlinear absorption coefficient
ε	Molar extinction coefficient
γ	Second-order hyperpolarizability
I_{lim}	Optical limiting threshold
$Im[\chi^{(3)}]$	Third-order nonlinear susceptibility
λ	Wavelength
η	Refractive index
$^1O_2$	Singlet oxygen
Φ_Δ	Singlet oxygen quantum yield
Φ_F	Fluorescence quantum yield
S_n	n^{th} electronic excited state
S_0	Singlet ground state
S_1	First singlet excited state
S_2	Second excited state
T_1	First triplet excited state
τ_F	Fluorescence lifetime
t	Time

List of Abbreviations

Abs	Absorption
ADMA	Anthracene-9,10-bis-methylmalonate
BODIPY	4,4'-difluoro-4-bora-3a,4a-diaza-*s*-indacene
CD	Circular dichroism
CDx	Cyclodextrin
CGTase	Cyclodextrin glucanotransferase
CT	Charge transfer
DCM	Dichloromethane
DDQ	2,3-Dichloro-5,6-dicyano-1,4-benzoquinone
DMSO	Dimethyl sulfoxide
DPBF	1,3-Diphenylisobenzofuran
Em	Emission
EPR	Enhanced permeability and retention
ESA	Excited state absorption
Exc	Excitation
FRET	Förster resonance energy transfer
FT-IR	Fourier-transform infrared spectroscopy
HOMO	Highest occupied molecular orbital
ICT	Intramolecular charge transfer
ISC	Intersystem-crossing
LUMO	Lowest unoccupied molecular orbital
MALDI-TOF	Matrix-assisted laser desorption/ionisation-time of flight

MS	Mass spectrometry
NBS	*N*-bromosuccinimide
Nd:YAG	Neodymium-doped yttrium aluminium garnet
NLA	Nonlinear absorption
NLO	Nonlinear optics
NLS	Nonlinear light scattering
NMR	Nuclear magnetic resonance spectroscopy
NR	Nonlinear refraction
OL	Optical limiter/limiting
PACT	Photodynamic antimicrobial chemotherapy
PET	Photo-induced electron transfer
PS	Photosensitizer
PDT	Photodynamic therapy
ROS	Reactive oxygen species
RSA	Reverse saturable absorption
RT	Room temperature
SEM	Scanning electron microscopy
TCSPC	Time-correlated single photon counting
TEA	Triethylamine
TFA	Trifluoroacetic acid
THF	Tetrahydrofuran
TLC	Thin layer chromatography
2PA	Two-photon absorption

UV-Vis	Ultraviolet-visible
XRD	X-ray powder diffraction

List of Schemes

List of Figures

List of Tables

Chapter 1:

Introduction

What BODIPY dyes are: discovery, structure and general properties

Boradiazaindacenes or boron-dipyrromethene (BODIPY) fluorescent dyes consist of two pyrrole units linked by an interpyrrolic methene bridge, a boron atom and the heteroatoms bonded to the boron atom (typically a BF_2 moiety).[1–4] These dyes are structural analogues of porphyrins, hence the 8-position is typically termed the *meso*-carbon (**Figure 1**).[5] The synthesis of these dyes was first described by Treibs and Kreuzer in 1968 after they were prepared when the acylation of 2,4-dimethylpyrrole with acetic anhydride and boron trifluoride as a Lewis acid catalyst resulted in the serendipitous formation of a highly fluorescent compound.[6,7]

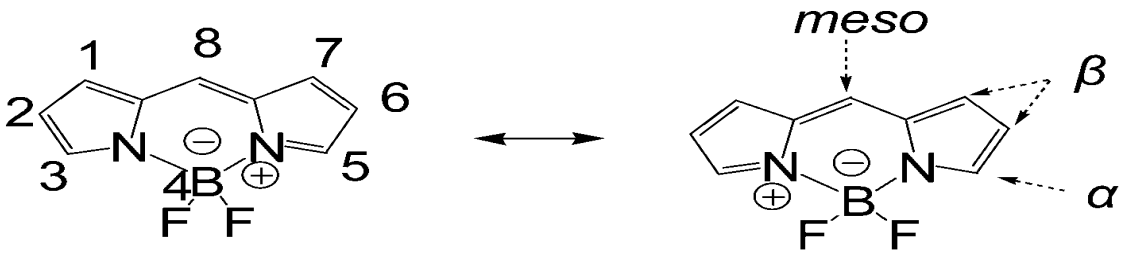

Figure 1. The numbering system of the BODIPY core. The 8-position is termed the *meso*-carbon following the naming system of porphyrins. Reprinted with permission from reference 3; Copyright Royal Society of Chemistry, 2014.

BODIPYs have been shown to have high fluorescence quantum yields (0.6–1.0), insensitivity to solvent polarity and pH changes, large extinction coefficients (60 000–80 000 $M^{-1}cm^{-1}$) and stability under common physiological conditions. These properties have led to research on a wide range of diverse applications.[8]

Synthetic routes towards the BODIPY core and possible structural modifications

Typically, the synthesis of the BODIPY core (**Figure 1**) is based on an acid-catalysed condensation reaction between a pyrrole unit and a highly electrophilic carbonyl compound such as an acid anhydride, acyl chloride or an aldehyde, forming an unstable dipyrromethane which is immediately oxidised with 2,3-dichloro-5,6-dicyano-1,4-benzoquinone (DDQ) or *p*-chloranil to form a dipyrromethene.[5] Finally, a boron atom is complexed by the dipyrromethene in the presence of a tertiary amine which provides basic conditions. To prevent polymerisation and porphyrin formation, the pyrrole used is typically substituted at the 3,5-positions adjacent to the nitrogen atom.[5] In this study, 2,4-dimethylpyrrole is used as a precursor to form a series of 1,3,5,7-tetramethylBODIPY dyes. The initial product formed through the condensation reaction with a carbonyl compound is normally referred to in the literature as a BODIPY core.

In addition to synthesising substituted BODIPYs using a starting pyrrole with the functional groups of interest, post-synthetic structural modifications are possible because the BODIPY core is highly robust. The stability of the BODIPY core and the various structural modifications which can also be performed allow for the enhancement of selected properties depending on the potential application of the dye being synthesised. Spectroscopic properties such as absorption, fluorescence (including the fluorescence quantum yields) can be altered by the substituents present on the core.[9,10] Various applications require different functional groups and properties, and these can also be introduced onto the starting pyrrole units, but the disadvantages of this approach are the long experimental times and low yields.[6]

Modifications to the structure can also be performed on the core subsequent to synthesis and purification. Among the various modifications, the following are possible:

a. Modifications at the *meso*-position: The *meso*-position, which usually contains an aryl group is the most used for the introduction of specific functional groups. This is mainly because when there are methyl groups at the 1,7-positions as is the case with all of the BODIPY dyes in this study, the *meso*-aryl group lies orthogonal to the BODIPY core and as such this modification usually does not give rise to changes in absorption and emission bands, i.e. the spectroscopic properties are not affected because there is typically minimal interaction between *meso*-aryl substituents and the BODIPY core.[3,9]

b. Electrophilic substitution: The 2- and 6-positions of the 1,3,5,7-tetramethylBODIPY core when they have no substituent attached, bear the least positive charge so they should be most susceptible to electrophilic attack (**Figure 2**).[9] This substitution does not result in any additional changes to the BODIPY structure, especially to the B-F bond.[5]

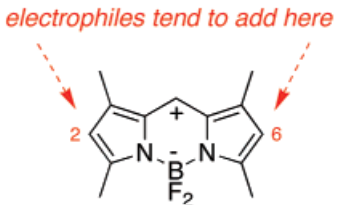

Figure 2. Possible positions for electrophilic attack. Reprinted with permission from reference 9; Copyright American Chemical Society, 2007.

c. Modification of methyl groups at the 3- and 5-positions: Methyl groups at the 3,5-positions can be modified, owing to their nucleophilic character, i.e. they can be deprotonated to give intermediates that readily add to electron-rich aromatic aldehydes, resulting in a styryl group.[11] Sometimes this modification method is used for

extending the degree of π-electron conjugation; an approach usually applied in the production of dyes that absorb and fluoresce at longer wavelengths; typically in the near-infrared region (NIR).[5] The most commonly used functional groups are phenyl, vinyl, or thiophene groups.[5,12]

d. Cross-coupling and functionalisation using palladium-catalysed coupling reactions: A halogen atom on the BODIPY core or on an aryl ring can be used in palladium-catalysed coupling reactions, such as the Heck, Sonogashira, Stille, or Suzuki reactions.[13] Similar to the electrophilic substitution reactions mentioned above, the B-F bonds remain intact.[5]

e. Nucleophilic substitution of leaving groups: Typically, substituents on the 3- and 5-positions come from substituted pyrroles which are used to synthesise the BODIPY of interest, but there has been a shift towards the use of good leaving groups such as chlorine atoms, i.e. leaving groups located on the 3- and/or 5-positions are nucleophilically substituted with functional groups like amines, alkoxides and thioalkoxides.[9,10] The substitution may be at either of the positions or at both to give monosubstituted or disubstituted products, respectively.[10]

f. Modifications at the boron centre: More recently, there has been a move to replace the fluorine atoms on the boron centre with various functional groups which are typically hard nucleophiles since this is a hard centre.[6,14]

Physicochemical properties

The numerous processes that a BODIPY dye can undergo upon interaction with electromagnetic radiation can be visualised using a Jablonski diagram (**Figure 3**).

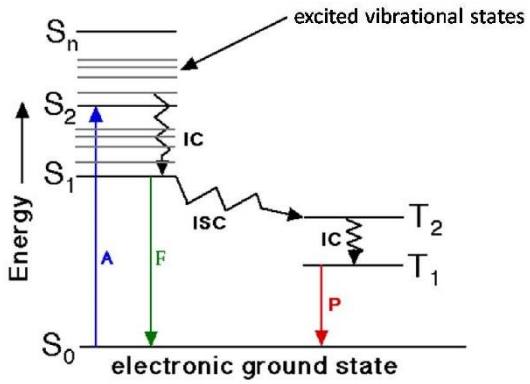

Figure 3. Jablonski diagram of possible electronic transitions. These include a transition from the ground state (S_0) to the second excited state (S_2), internal conversion (IC), fluorescence from the first excited state (S_1) to ground state (S_0), intersystem crossing (ISC) from the first excited state (S_1) to the first excited triplet state (T_1) and phosphorescence from the first excited triplet state (T_1) to ground state (S_0). Excitation can also access other n^{th} electronic states, exciting the molecule to higher S_n excited states.[15]

When a photon is absorbed, an electron is promoted to an S_n excited state, and it then relaxes to the lowest vibrational level of the S_1 state through internal conversion and eventually relaxes to the ground state by releasing a photon via fluorescence (**Figure 3**). Rapid internal conversion ensures that Kasha's rule is obeyed.[16,17] This rule states that the fluorescence (a photon emission process) usually only occurs from the lowest vibrational level of the S_1 state (lowest excited state). The presence of a heavy atom on the BODIPY enhances intersystem crossing to the T_1 state due to the heavy atom effect which promotes

spin-orbit coupling. A photon in the T_1 state can be emitted via phosphorescence (a lower energy process relative to fluorescence). Energy transfer from the T_1 state to ground state molecular dioxygen can occur, producing radicals and other reactive oxygen species, among which is singlet oxygen which is utilised in some applications of BODIPYs.[5,18–20]

Absorption spectra of BODIPY dyes

Unfunctionalised BODIPY dyes typically absorb in the 490–520 nm region and are usually resistant to changes in pH and solvent polarity because they are zwitterionic molecules.[21] Their absorption spectrum is dominated by a single absorption band that arises from the S_0 to S_1 transition, whereas a shoulder band appears around 475–485 nm due to a vibrational overtone. Typically, a weaker absorption band observed in the 300–400 nm region is associated with the S_0 to S_2 transition.[3]

Applications of BODIPY dyes

Although Treibs and Kreuzer noted in the late 1960s that these compounds have intense absorbance around 500 nm and are highly fluorescent, there was minimal research activity on them until relatively recently. Interest in their possible use in applications has increased enormously over the past three decades.[5,7,22] Common research areas include chemosensing, fluorescent labelling of biomolecules, lasers dyes, cellular imaging, photodynamic therapy (PDT), biolabels and light harvesting systems.[1,8,23–28] The applications of interest to this thesis are listed below.

1. Photodynamic therapy

Cancer is defined as a disease characterised by an uncontrolled growth and spread of body cells as a result of damages to genetic material, which in most instances is DNA.[29] This damage, in turn leads to tumours which may be treated by surgical removal, through chemical drugs or chemotherapy and/or the use of radiation if there are remaining cancer cells after surgery.[29] During chemotherapy, the drugs are distributed via the circulatory system and accumulate in body cells, especially abnormal cells, tumours and cancer cells.[29] Radiation therapy relies on high energy ionisation particles in the form of x-rays, gamma rays or electrons.[29] As successful as these treatments have been, they have their limitations and disadvantages. Some of the limits and trade-offs of these treatment techniques are:

- The failure of surgery to remove non-accessible tumours such as non-primary tumours and those located in vital or poorly accessible tissues.[29,30]
- Radiation damages healthy cells close to the cancer cells or in the path of the radiation beam.[29]
- The reproductive life of patients may be compromised as a result of chemotherapy and/or radiotherapy.[31]

The limits listed above are some of the reasons that have resulted in new therapeutic approaches and the development of those which exist but are under-researched or are not given priority. One of these is PDT, which is a cancer treatment technique which uses light, oxygen and a photosensitizer (PS) dye. During PDT treatment, the PS is administered onto the targeted tumour(s) which are then irradiated with light of appropriate wavelength, allowing the PS to generate reactive oxygen species (ROS) which kill cells via apoptosis or

necrosis.[32,33] This is because the PS selectively localises in tumours as a result of leaky tumour blood vessels due to neovascularization and the absence of lymphatic drainage, a phenomenon known as the enhanced permeability and retention (EPR) effect.[33] PDT destroys cancer cells either by inducing direct cytotoxic effects on the cells, damage to the tumour vasculature or by induction of a robust inflammatory reaction that can lead to the development of systemic immunity.[33] This depends on factors such as the type and dose of PS used, the time between PS administration and light exposure, total light dose, its fluence rate and tumour oxygen concentration.[33]

The main ROS of interest in PDT is singlet oxygen. PDT occurs in a two-step process, where the photosensitizer absorbs a photon of light in the ground state which promotes the PS to the short-lived excited singlet state. The singlet excited state may decay to the ground state via the emission of a photon, a process known as fluorescence.[34] Apart from fluorescence, the PS molecule can also undergo intersystem crossing from the excited singlet state to the more stable, long-lived triplet excited state.[34] In the triplet state, the PS can undergo radiationless decay to the ground state or transfer its energy to molecular oxygen (O_2), which has a triplet ground state. The transfer of energy to oxygen generates singlet oxygen which is toxic, through what is termed a type II process. In a type I process, the PS reacts directly with an organic molecule in a cellular environment, acquiring a hydrogen atom or an electron to form reactive species, such as a superoxide, hydrogen peroxide or hydroxyl radicals.[33] Some of the advantages of PDT over the traditional therapies mentioned above are:

- In 2011, of all the PSs that were clinically approved, none accumulates in cell nuclei, and as such, no DNA damage that could be carcinogenic occurs.[33]

- The adverse effects of chemotherapy and radiotherapy are absent.[33]
- PDT procedures can be performed in an outpatient or ambulatory setting, thereby making the treatment patient-friendly.[33]
- The success of PDT is recognised even by the United States of America's Food and Drug Administration (FDA) which approved it for neoplastic and non-malignant diseases even though it lacks popularity and remains clinically underutilised.[33]

Light Sources used in PDT

In PDT, blue light is not efficient because it fails to penetrate through tissue.[33] Red and infrared radiations are the most efficient since light of 600 to 1200 nanometers (nm) wavelength is known as the optical window of tissue. Light of the appropriate wavelength can be generated from lasers and incandescent light sources, with diode lasers more preferable when compared to pumped dye lasers as a result of their small size, cost-effectiveness and longer operational life.[33]

BODIPY dyes in PDT

Photosensitizers are typically defined as "organic delocalised aromatic molecules consisting of large conjugated systems of double bonds that may be considered as a central chromophore with auxiliary side chains attached (auxochromes) which are responsible for further electron delocalisation of the PS thus altering the absorption spectra of the PS".[35] This electron delocalisation gives PSs their deep colour. Furthermore, electron delocalisation causes the energy required to excite the electrons in the HOMO to the LUMO to be low

compared to less delocalised molecules, hence PS absorption bands are in the longer wavelength (red) spectral region and ideally are very intense.

The traditional PSs for the treatment of cancer are mostly based on the tetrapyrrole nucleus, with porphyrins at the forefront. Due to their unfavourable absorption spectrum in the 630 nm region, however, porphyrins were replaced with other tetrapyrroles such as chlorins, bacteriochlorins, and phthalocyanines due to their more intense absorption peaks at longer red wavelengths.[36] The versatility of the BODIPY core allows modifications that enable the dyes to: (i) undergo intersystem crossing to the triplet state, hence generating singlet oxygen, (ii) have their main spectral band shifted to longer wavelengths so as to absorb light in the NIR region and (iii) possess π-conjugated systems. This has opened avenues for research as potential PDT agents.[28]

The most important properties of a useful PS agent are:

- It should be a single pure compound to allow quality control analysis.[33]
- Its manufacturing costs must be low and it must be stable in storage.[33]
- It should have a high absorption peak between 600 and 800 nm since long-wavelength photons do not provide enough energy to excite oxygen to its singlet state and subsequently lead to the formation of sufficient ROS.[33,37]
- It should have no dark toxicity and relatively rapid clearance from normal tissues, thereby minimising phototoxic side effects.[33,38]

2. Achieving water solubility of BODIPY dyes

There are various methods which can be utilised to achieve water solubility in BODIPY dyes. Among these, the incorporation of suitable functional groups such as sulfonates and quaternised amines; but in this thesis, the focus will be on cyclodextrin (CD_x) inclusion to induce water solubility. Cyclodextrins are also known as cycloamyloses, cyclomaltoses or Schardinger dextrins and they are cyclic oligosaccharides with a diameter of 5–8 Å; they are made up of six (α-cyclodextrin), seven (β-cyclodextrin), eight (γ-cyclodextrin) or more glucopyranose units linked by α-(1,4) bonds.[39–45] The chair conformation of the glucopyranose units gives the cyclodextrins a truncated cone or torus shape.[42–44] α-, β and γ-Cyclodextrin are known as the first generation or parent cyclodextrins.[39–41] Cyclodextrins were first discovered in 1891 by A. Villiers, a French scientist as a result of isolating a bacterial digest from starch and the first isolate was labelled as a dextrin named cellulosine.[42,46] This was followed by Franz Schardinger's isolation of two crystalline compounds from a bacterial digest of potato starch which he named α-dextrin and β-dextrin, with the latter referred to as Villiers' cellulosine.[42,47] Schardinger was also able to isolate an organism, *Bacillus macerans*, capable of producing acetone and ethyl alcohol from sugar and starch-containing plant material, which also produced dextrins from starch.[40,48] The discovery of γ-cyclodextrin came at a later stage as a result of work by Freudenberg and Jacobi, in 1935.[49] Although only α-CDx, β-CDx and γ-CDx and some of their derivatives are available in the market as white crystalline powders, there were other cyclodextrins discovered, particularly those referred to as large ring cyclodextrins (LR-CDs).[41–43] Their production was later described to be as a result of an "intramolecular transglycosylation reaction from degradation of starch by cyclodextrin glucanotransferase (CGTase) enzyme".[48]

Ability to form complexes and description of process of complex formation

There is one particularly important feature which makes cyclodextrins interesting research compounds for drug-related research, and that is their ability to form inclusion complexes with several compounds irrespective of whether they are in the solid, liquid or gaseous phase.[44] For this reason, the pharmaceutical, food, biotechnological, environmental protection, bioconversion, chemical, textile and cosmetic industries apply cyclodextrins in many of their products.[41,47,50–61] From the X-ray structures which were first elucidated in 1942, the cyclodextrins' secondary hydroxyl groups are located on the wider edge of the ring, and the primary hydroxyl groups are on the other edge, whereas the apolar hydrogens and ether-like oxygens are on the inside.[42,44,47,55,62,63] Such an arrangement gives cyclodextrins a hydrophilic outer surface and a hydrophobic internal cavity, with the former affording them their water solubility.[40,63]

Because the polarity of the cyclodextrin cavity is similar to that of an aqueous ethanolic solution, a hydration shell develops when the cyclodextrin is dissolved in aqueous media.[42,47,64–67] When a guest is present, the hydrophobic cavity accommodates the hydrophobic guest molecules, thereby forming inclusion complexes and conferring a certain degree of solubility onto the guest molecule which would otherwise be insoluble in aqueous media.[40] In this way, each cyclodextrin molecule can accommodate one or two guest molecules, or inversely, portions of a guest molecule can be entrapped by one, two or three cyclodextrins.[40] The process of complex formation between cyclodextrin and a guest molecule is a dimensional fit between the host cavity and the guest, with the lipophilic cavity of each cyclodextrin molecule providing a microenvironment which can only accommodate appropriately sized guests.[44] During this process, there are no covalent bonds

broken or formed and instead what occurs is the release of enthalpy-rich water molecules from the cavity which are included in the cyclodextrin cavity and are present in this part of the molecule in crystal structures due to crystallisation of the cyclodextrins from aqueous media.[41] These are displaced as a result of the presence of more hydrophobic guest molecules. This is favoured because it reduces the cyclodextrin ring strain resulting in a more stable lower energy state due to the apolar-apolar association formed.[48,68]

Although cyclodextrins are popular for their water solubility, this is dependent on temperature, and this means that they are usually not highly soluble under all conceivable circumstances. An obvious example is β-CDx which is less soluble than both α-CDx and γ-CDx at low temperatures, with their respective aqueous solubilities improving at higher temperatures.[41] This temperature dependent solubility tends to be lost in inclusion complexes because if the guest is highly soluble in water, the solubility of the inclusion complex increases whereas the opposite is also true for poorly water-soluble guests.[41] To improve the solubility, inclusion capacity/hydrophobic cavity volume, stability and other relevant properties observed in natural cyclodextrins, chemically modified cyclodextrin derivatives are usually synthesised.[41,47,55,62,69,70] The low solubility of naturally occurring cyclodextrins is attributed to the relatively strong intramolecular hydrogen bonding in the crystal lattice and the most common modifications to increase solubility are aminations, esterifications or etherifications of primary and secondary hydroxyl groups of the cyclodextrins.[40,42]

Toxicological considerations

The application of cyclodextrins in the medical field has advanced to the point that there are multiple drug formulations on the market, based on both solid and solution-based

cyclodextrin complexes, wherein the cyclodextrins increase the aqueous solubility of poorly water-soluble drugs.[42,71–76] In addition to being carriers for poorly soluble drugs, cyclodextrins are also used to reduce side effects such as gastrointestinal and ocular irritation, unpleasant smells and tastes and unwanted interactions between drugs.[42,77,78] Because of their large molecular weights ranging from about 1000 to 2000 Da; hydrophilicity with a significant number of H-donors and acceptors means that they are not easily absorbed from the gastrointestinal tract in their intact form and the inability of human salivary and pancreatic amylases to hydrolyse α-CDx and β-CDx (unlike γ-CDx), they are highly suitable for the biological applications listed above.[42,79] To this end, multiple toxicity studies have been performed, and it has been demonstrated that orally administered cyclodextrins are practically non-toxic due to the lack of absorption from the gastrointestinal tract.[40,79] The cytotoxicity of each of the parent cyclodextrins is discussed below:

A. α-*Cyclodextrin*

α-Cyclodextrin is known to be relatively irritating both to the eyes and when administered intramuscularly. It also has the ability to bind with some lipids while possessing very low absorption after oral administration to rats (between 2 and 3%) with no metabolism in the upper intestinal tract, since it is only cleaved by intestinal flora in the caecum and colon.[40,42,80]

B. β-*Cyclodextrin*

β-Cyclodextrin is a common food additive and is less irritating than α-cyclodextrin. It binds cholesterol in very small amounts (1–2%) and is absorbed in the upper intestinal tract after oral administration albeit with no metabolism until the caecum and colon. This is the most

common cyclodextrin in pharmaceutical formulations in the form of topical, buccal and rectal drug formulations.[42,47,81] Application of high doses may be harmful and is not recommended and is also only non-toxic when given orally and not parenterally. [42,47,81]

C. γ-*Cyclodextrin*

Intramuscular administration does not result in significant irritation, but it is rapidly and completely degraded to glucose in the upper intestinal tract by intestinal enzymes. There is almost no absorption after oral administration (0.1%) and practically no metabolism, making it the least toxic of the three natural cyclodextrins although its complexes are typically aggregates with limited solubility in aqueous solutions.[40,82] The main reason for it to have the lowest toxicity is that its metabolism is similar to that of starch and it is excreted unchanged when administered intravenously.[83,84]

Preparation methods: complexation techniques, solution dynamics & temperature effects and complex drying and storage

When in solution, more cyclodextrin molecules are available for complexation compared to when in crystalline form which only provides the surface molecules of the cyclodextrin. Water is the most commonly used solvent particularly because it is easier for water molecules to be displaced by a hydrophobic guest relative to organic media, to yield solvent-free complexes.[40] An important factor worth monitoring is the amount of water used since the solubility of both cyclodextrin and water-soluble guests increases with a fraction of increased water; when the medium becomes too dilute this minimises contact between the guest molecule and the cyclodextrin.[40] Since not all guests are water-soluble, organic solvents are used to dissolve the guest but, as is the case with ethanol and diethyl ether, the solvent should not be complexed by the cyclodextrin and should be easily removed by

evaporation.[40] Also, although heating tends to increase the solubility of the cyclodextrin and in some instances that of the guest and this can enhance complex formation,[40] this can also destabilise the complex and result in its decomposition at 50–60 °C, although this is not the case for all, especially for strongly bound guests or the highly insoluble complexes.[40]

Co-precipitation

This method is the most widely used method in the laboratory, wherein the cyclodextrin is dissolved in water and the guest is added while stirring the cyclodextrin solution, typically with controlled heating, followed by cooling while stirring to form a precipitate.[40,41,85] For the least soluble of the parent cyclodextrins (β-cyclodextrin), the cyclodextrin solution is heated to at least 60 °C to dissolve the β-cyclodextrin before adding the guest.[52] The precipitate is usually collected by centrifugation or filtration and washed with a small amount of solvent such as water or other water-miscible solvents such as ethyl alcohol, methanol or acetone although this is not always safe since organic solvents may destabilise some complexes.[40,41] On scaling up, the disadvantage is the large volumes of water used which requires large tank capacities, longer heating times and higher heating energies.[40,86]

Slurry complexation and paste complexation

With slurry complexation, it is not necessary to dissolve the cyclodextrin completely. The complex forms in media made up mostly of solids (50–60%) and water, and then stirred at ambient temperatures. As the cyclodextrin complex saturates the liquid phase, the complex crystallises or precipitates out and the complex can be collected like with the co-precipitation method.[40,41] Unlike with co-precipitation however, the amount of water used is far less.[40] The difference with paste complexation is the small amount of water used to

form a paste which is then mixed with the cyclodextrin using a mortar and pestle or using a kneader at large scale.[40]

Damp mixing and heating

Minimal water is used and the guest and cyclodextrin are thoroughly mixed and placed in a sealed container follower by heating to about 100 °C and then the complex is removed and dried.[40]

Extrusion

Cyclodextrin, guest and water are added to an extruder and extruded to yield a complex which may dry as it cools or needs to be dried in an oven. The disadvantage of this method is the decomposition of heat-labile guest molecules.[40]

Dry mixing

Oily and liquid guests are added to the cyclodextrin and mixed over time, typically at ambient temperature. Although no water is used, caking on scale-up results in poor mixing thereby leading to incomplete complexation after long time periods.[40]

Drying typically occurs in an oven, fluid bed dryer or other types of dryers, with care to avoid destroying the complex.[40] Depending on the boiling temperature of the guest, lower temperatures may need to be used. Alternatively, complexes may be spray-dried or dried at low temperatures. During spray-drying, particles may become too large as a result of precipitation or the complex can be lost if the guest is volatile and heat labile.[40] At low temperatures, a desiccator or freeze dryer may be used.[40]

Aims and objectives of cyclodextrin use:

The basis of the use of the cyclodextrin compounds here is their water solubility and their history in the inclusion of organic compounds in their cavities to form inclusion complexes in aqueous solutions.[87] These inclusion complexes, particularly those with porphyrin derivatives have been shown to modify the photochemical and photophysical properties of the included compounds.[87–90] The photophysical properties of the BODIPY dyes to be used have been assessed in organic media and their ability to generate singlet oxygen molecules in this context clearly demonstrated, thereby making them potential photosensitizers for various singlet oxygen applications. Their inclusion in cyclodextrins here, therefore is an attempt to show that cyclodextrins can be used as carrier agents for the photosensitizers for delivery in applications, such as photodynamic antimicrobial chemotherapy (PACT), which may require the photosensitizer to be water soluble.

3. Nonlinear optics (NLO)

Nonlinear optics (NLO) focuses on the study of changes in the optical properties of materials upon interacting with incident light of different intensities. One aspect of NLO that has gained momentum over the past few decades is the development of optical limiter materials that are capable of significantly reducing light transmittance at high incident intensities while remaining transparent under ambient light conditions. This normally involves processes such as two-photon absorption (2PA) and excited state absorption (ESA). 2PA is a third-order nonlinear process of materials wherein a molecule simultaneously absorbs two photons, whereas ESA is the absorption of a photon from a lower excited state to a higher excited state (**Figure 4**).[91]

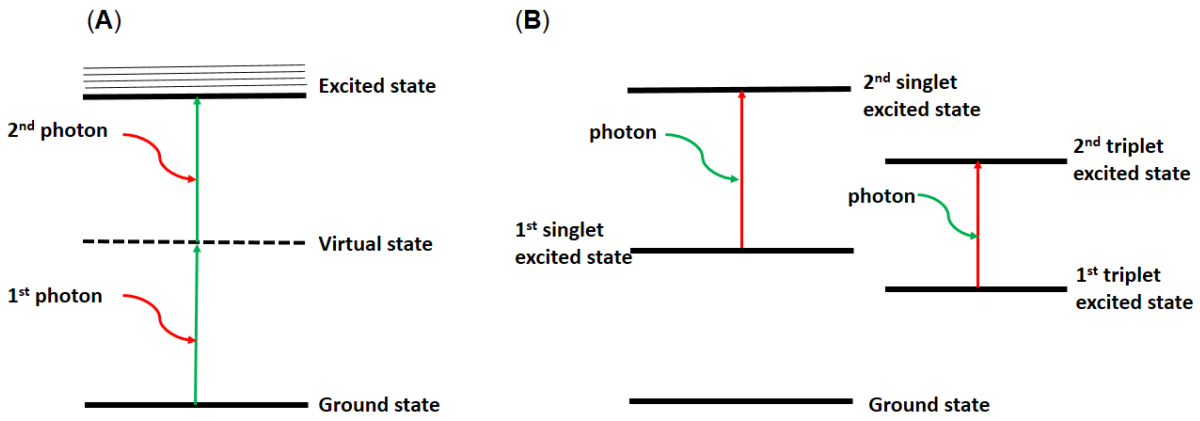

Figure 4. Jablonski diagrams showing two-photon absorption (A) and excited state absorption (B).

Optical limiting (OL) is characterised by a decrease of transmittance by a sample at high incident laser intensity. An ideal OL response shows constant transmittance of intensity or a decrease to a minimal value above a certain illumination intensity (**Figure 5A**), with a decrease of the initial linear transmittance above a threshold value (**Figure 5B**). This optical limiting process can occur via nonlinear absorption (NLA), nonlinear refraction (NR) or nonlinear light scattering (NLS) and the focus in this study is on NLA associated with molecular dyes. OL materials can be formed using organic dyes and other compounds that can be used to protect light-sensitive objects such as the human eye and optical sensors from intense incident laser beams.[92–94] The second harmonic of the Nd:YAG laser at 532 nm is particularly important in the context of OL applications and the continuous study of compounds for their potential use as OL materials at this wavelength is important because of, amongst other reasons, the ever-growing irresponsible use of laser pointers and the implications this has on aviation safety.[95,96] The organic compounds such as porphyrins and phthalocyanines that have been used as optical limiters typically have delocalised π-conjugation systems which possess high polarisabilities when interacting with intense laser

light.[97–100] BODIPYs have, however, seldom been studied for applications as OL materials. In order to study BODIPY dyes as OL materials at 532 nm, the optical properties of the dyes must be significantly modified to ensure their utility in this context, since this lies close to the main BODIPY spectral band. The structural versatility and stability of the highly robust BODIPY core and its facile structural modification for the enhancement of selected properties make it possible for these dyes to be studied as optical limiters. One of the most widely used methods to achieve a red-shift of the BODIPY main spectral band towards the NIR is to introduce styryl groups at the 3,5-positions.[5,11,12] Dyes modified in this fashion have an extended degree of π-conjugation and this results in a shift of the main absorption and fluorescence bands to longer wavelengths, hence achieving two necessary requirements for NLO studies at 532 nm: a π-conjugation system that results in high polarisability and a main absorption band that lies at a significantly longer wavelength than the second harmonic wavelength at 532 nm, typically with minimal absorbance at 532 nm.

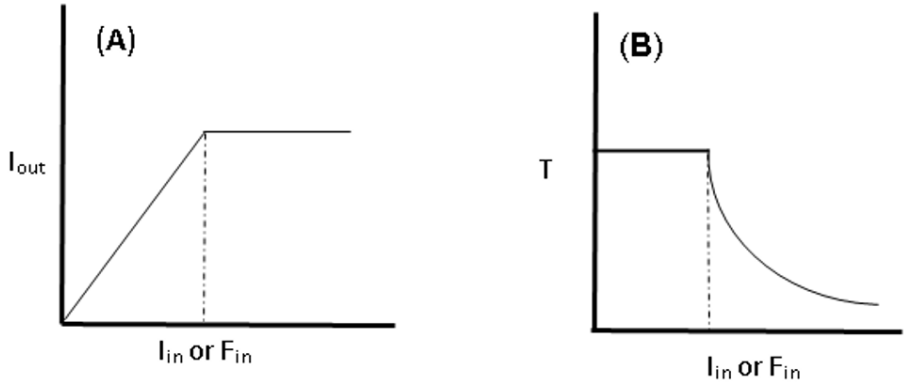

Figure 5. Ideal behaviour of an optical limiter. The limiting intensity is shown by the deviation of transmittance from linearity, as marked by a dashed line. A: Transmitted intensity, I_{out} vs. incident intensity I_{in}, B: transmittance, T vs. incident intensity, I_{in}. Reprinted with permission from reference 96; Copyright Royal Society of Chemistry, 1998.

NLA and NLR can be studied using the single-beam z-scan technique (**Figure 6A**) to determine optical limiting parameters.[93,101] During the scan, the sample is moved along the z-direction of a focussed Gaussian beam and an aperture can be optionally placed in front of D2.[102] When the aperture is absent, the total transmitted energy is detected, and this gives the results for nonlinear absorption alone.[102] When the aperture is present, the scan gives both nonlinear absorption and nonlinear refraction results. To derive the nonlinear refraction curve, the resultant z-scan curve obtained with an aperture is divided by the curve obtained in the absence of the aperture, hence eliminating nonlinear absorption. This curve, referred to as the divided z-scan curve, reveals the effect of nonlinear refraction alone.[102] In this study the focus is on the use of non-aggregated BODIPY molecular dyes for NLA, so only open aperture z-scan measurements are analysed to determine the most important NLO parameters that are related to OL.

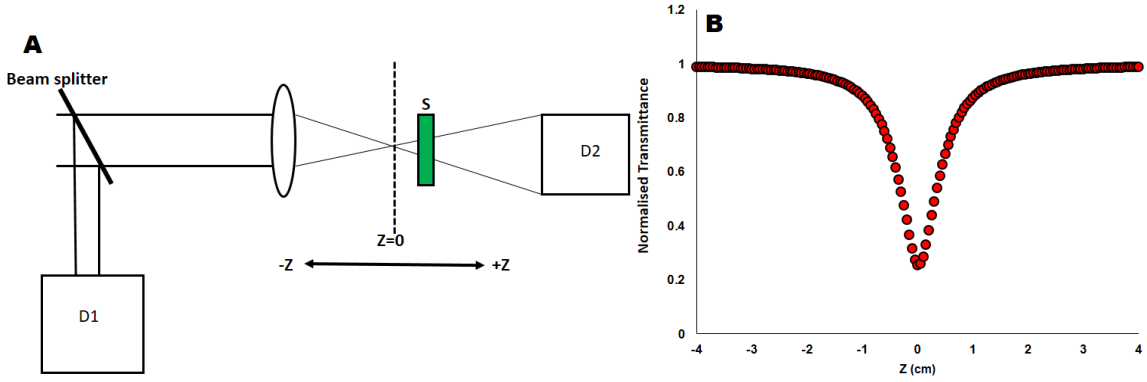

Figure 6. A: Open-aperture z-scan setup. The sample is moved along the z-direction of a focussed Gaussian beam. D1 and D2 are photodetectors, and S is the sample. B: Typical reverse saturable absorption response obtained from the z-scan setup.

Some optical limiters are known to strongly reduce the transmittance of light at high incident light intensities while remaining transparent at incident intensities, a phenomenon

known as reverse saturable absorption; this can be visualised by plotting the data obtained from the z-scan equipment (**Figure 6B**). The data is first analysed using the procedure described by Sheik-Bahae *et al.*, Equation (1):[103]

$$T(z) = \frac{1}{\sqrt{\pi} q_0(z)} \int_{-\infty}^{\infty} In\left[1 + q_0(z) e^{\tau^2}\right] d\tau \quad (1)$$

where $q_0(z)$ provides an indicator of the strength of the nonlinearity. For circular-shaped beams, the $q_0(z)$ value is provided by Equation (2):[104]

$$q_0(z) = \frac{2\beta_{eff} P_0 l_{eff}}{\pi \omega(z)^2} \quad (2)$$

where P_0 and l_{eff} are the peak power of the laser pulse and the effective pathlength, given by Equation (3):

$$l_{eff} = \frac{1 - e^{-\alpha l}}{\alpha} \quad (3)$$

where α and l are the linear absorption coefficient and the pathlength. The beam width as a function of sample position ω(z) in Equation (2) can be obtained from Equation (4):

$$\omega(z) = \omega_0 \sqrt{1 + \left(\frac{z}{z_0}\right)^2} \quad (4)$$

where ω_0 is the beam waist at the focus (z = 0), which is the distance from the centre of the beam to a point where intensity decreases to $1/e^2$ of its on-axis value. z_0 and z are the Rayleigh length and the translation distance for the sample relative to the focus, respectively. The Rayleigh length is defined as $\pi\omega_0^2/\lambda$ with λ being the laser wavelength.

The β_{eff} value, the effective nonlinear absorption coefficient, can be extracted from the experimentally measured transmittance using Equations (1–4). In this study, a nanosecond pulsed laser is used, so it is not possible to measure the β value that arises solely from 2PA, since an RSA response can also be associated with ESA (**Figure 4**). Equation (1) is not well

suited to fit directly to the data, however, so a numerical version of this formula (Equation (5)) is normally used to derive $q_0(z)$ from the normalised transmittance values obtained experimentally:

$$T(z) = 0.363e^{\left(\frac{-q_0(z)}{5.60}\right)} + 0.286e^{\left(\frac{-q_0(z)}{1.21}\right)} + 0.213e^{\left(\frac{-q_0(z)}{24.62}\right)} + 0.096e^{\left(\frac{-q_0(z)}{115.95}\right)} + 0.038e^{\left(\frac{-q_0(z)}{965.08}\right)} \quad (5)$$

On substituting Equation (4) into Equation (2), $q_0(z)$ can be defined by Equation (6):

$$q_0 = \frac{Q_0}{1 + \left(\frac{z}{z_0}\right)^2} \quad (6)$$

where Q_0 is given as:

$$Q_0 = \frac{2\beta P_0 l_{eff}}{\pi \omega_0^2} \quad (7)$$

A Gaussian-shaped curve with Q_0 as the maximum value at z = 0 can be obtained from Equation (7). The full width at half minimum and peak values derived from the plot provide values for z_0 and Q_0, respectively. Equation (8) is used to obtain the value of β_{eff}, and this provides an important parameter for assessing the suitability of materials for OL applications:

$$\beta = \frac{\lambda Z_0 Q_0}{2 P_0 l_{eff}} \quad (8)$$

The imaginary third-order susceptibility ($Im[\chi^{(3)}]$) is a measure of the speed of the response by an optical limiter to the perturbation induced by the incident laser pulse. The imaginary third-order susceptibility is directly proportional to the two-photon absorption coefficient, β_{eff} and can be calculated using Equation (9):

$$Im[\chi^{(3)}] = \frac{\eta^2 \varepsilon_0 C \lambda \beta_{eff}}{2\pi} \quad (9)$$

where η is the refractive index of the solvent, c is the speed of light, ε_0 is the permittivity of free space, and λ is the wavelength of the laser.

The second-order hyperpolarizability (γ) measures the interaction of the incident photon with the permanent dipole moments of the molecule. This parameter describes NLA per mole of the compound and can be determined using Equation (10):

$$\gamma = \frac{I_m[\chi^{(3)}]}{f^4 C_{mol} N_A} \quad (10)$$

where C_{mol} is the molar concentration of the active species, f is the Lorentz local field enhancement factor defined as $f = (\eta^2 + 2)/3$ (where η is the refractive index of the sample), and N_A is the Avogadro constant.

From the standpoint of optical limiting applications, the $Im[\chi^{(3)}]$ value has an optimal range of 10^{-9} to 10^{-15} whereas that of γ is 10^{-29} to 10^{-34}.[104]

The threshold limit intensity (I_{lim}), is defined as the input fluence at which the nonlinear transmittance is reduced to 50% of the linear transmittance value. The International Commission on Non-Ionizing Radiation Protection has published a guideline for exposure limits to a variety of lasers.[105] Equation (11) can be used to determine what the use of 10 ns laser pulses at 532 nm results in as an exposure limit:

$$\text{Exposure Limit} = 2.7 C_A t^{0.75}\ \text{J.cm}^{-2} \quad (11)$$

where C_A is a correction factor (= 1 for 400–700 nm), and t is the exposure time. This equation provides a limit of 0.95 $J.cm^{-2}$ for a 0.25 s exposure time corresponding to the normal blink reflex for the human eye.[106]

In this work, the suitability of a series of structurally diverse BODIPY dyes for optical limiting is assessed in a variety of organic solvents. These BODIPY dyes are structurally diverse in that some contain heavy atoms in the form of bromine whereas others contain electron

withdrawing and electron donating groups separated by a π-conjugation system. For heavy atom containing BODIPYs, an enhanced optical limiting response is expected as has been previously observed with phthalocyanines,[107–109] as a result of intersystem crossing to the triplet state, which in turn, typically results in ESA in this triplet manifold. An enhanced optical limiting response is also expected for the dyes containing electron withdrawing and electron donating groups separated by a π-system as this creates a dipole moment due to their asymmetrical nature.[110] These donor (D)–π–acceptor (A) or D–π–A systems, typically termed as push-pull systems, have been studied to better understand their nonlinear optical behaviour and are known to possess large second-order nonlinearities.[110,111] In the dyes being studied here, the respective functional groups, as will be discussed in Chapter 4, will act as electron donors and as electron acceptors while the BODIPY core electronic system will provide the polarisable electrons, and it is therefore expected that when these polarisable electrons interact with an oscillating electric field of light they will selectively shift from the donor to the acceptor, thereby creating a single charge transfer direction.[110,111] This is what drives the large second-order optical nonlinearities observed in asymmetric molecules.[111]

4. *Sensing*

One other widely studied application of BODIPY dyes is their use in sensing, as chemical sensors. During the sensing process, the chemical sensor which is composed of a receptor and a transducer provides analytical information about a species present in a chemical system.[112,113] The receptor binds with the analyte of interest whereas the transducer reports the binding process which may be a chemical or biological process, in the form of a recognisable and detectable signal.[112–115]

The focus here is on chemosensors which are made up of a molecule or molecules of abiotic origin and are able to detect varying substrates.[112] Using synthetic chemistry, organic molecules, inorganic metal complexes, macrocycles, polymers and nanomaterials, sensitive and selective sensors have been previously developed to detect not only biologically important materials but other substrates of environmental and medicinal importance, irrespective of size and charge. Examples of these include various heavy metals and explosives.[112,116–119] Heavy metals such as copper and mercury which are prevalent in the environment need to be constantly monitored. Copper, for example, should be maintained within the correct levels within the human body because it is linked to neurodegenerative disorders such as Alzheimer's disease while copper deficiency leads to anaemia and leukopenia.[112,120–123] Explosive devices and their potential link to terrorist organisations and rogue states raise the need for devices which can detect these explosives, and a lot of research has been carried out in this regard.[112,124,125]

The substrate-receptor binding process is typically detected as either an optical or electrochemical signal.[112,126] The optical approach includes changes in the electronic absorption spectrum of the probe or a change in the fluorescence properties of the probe. These colourimetric and fluorometric changes can be visualised and studied using UV-visible absorption and fluorescence spectroscopies, respectively.[126] The electrochemical signals are a result of changes in current or redox potential and voltammetry is the most common technique used to follow the electrochemical changes which occur as a result of the presence of an analyte.[112,126] The fluorometric approach has become the most favourable as a result of advantages such as high sensitivity and specificity, minimal cell disruption in biological applications and easily monitored turn-off/turn-on fluorescence switching, and

these have created avenues for applications in various research fields including, but not limited to biochemistry, biology and in medicinal and drug-related research and applications.[112,114,127,128] During these fluorescence sensing studies, the chemosensor can be modified structurally or otherwise to enhance either the selectivity of the receptor for the analyte of interest or the sensitivity and output of the transducer.[112]

BODIPY dye based chemosensors have been previously reported and studied in colourimetric and fluorometric applications.[129–133] These BODIPY based sensors, particularly the fluorometric ones are typically based on far-red and NIR absorbing dyes.[114] The main sensing mechanisms in these dyes are photo-induced electron transfer (PET), intramolecular charge transfer (ICT), and Förster resonance energy transfer (FRET) or a combination of these and there are two general designs for a fluorescence sensor, namely the fluorophore-spacer-receptor system and intrinsic fluorescent probes.[112,114,127] In the intrinsic fluorescent probes the receptor is part of the π-electron system of the fluorophore whereas, in the fluorophore-spacer-receptor system, the π-electron systems of the fluorophore and the receptor are electronically disconnected by a spacer, typically an aliphatic group.[114,127] The fluorophore-spacer-receptor system is the basis for PET, wherein the binding of an analyte to the sensor modifies either the fluorescence intensity or fluorescence wavelength.[114,127,134] The PET-based fluorescence probes do not show significant spectral shifts upon analyte binding. Instead, their fluorescence is either enhanced or quenched and as such are more often referred to as “off-on” and “on-off” fluorescent sensors, whereas ICT based probes possess changes in fluorescence wavelength.[114,134] During the PET process, the fluorophore may be the electron donor or acceptor and the process may either be reductive or oxidative depending on the relationship between the molecular orbitals of the fluorophore and

receptor. In reductive PET the highest occupied molecular orbital (HOMO) of the fluorophore is lower than the HOMO of the receptor and as such the fluorophore accepts electron(s) from the receptor.[114] In contrast, in oxidative PET the lowest unoccupied molecular orbital (LUMO) of the fluorophore lies higher than the LUMO of the receptor and the fluorophore is the electron donor.[114] During the ICT process, fluorescence changes result from electronic interactions between electron donating and electron accepting groups. During this process, charge transfer or electron density redistribution from the electron donating group to the electron accepting group creates a dipole moment within the molecule and this dipole moment is disturbed by analyte binding which may either enhance or reduce it, thereby altering the fluorescence properties.[112] What happens to the fluorescence spectrum depends on whether the dipole is enhanced or reduced, i.e. an enhanced dipole results in an increase in molar absorptivity and red-shifted absorbance and fluorescence.[112] FRET, on the other hand, is as a result of an interaction between two fluorophores that are joined in the same molecule. These act as a donor and acceptor, with an energy donor emitting at shorter wavelengths and the acceptor emitting at a longer wavelength.[114] The energy transfer process is non-radiative and is facilitated by a spectral overlap between the emission spectrum of the donor and the absorption spectrum of the acceptor.[114]

Given BODIPY dyes have been studied for their potential as molecules which can be used in the design of fluorescent probes, some of the dyes synthesised in this work will also be tested to this effect. BODIPY dyes have been extensively studied based on their potential in sensing pH changes, cations and anions, metal ions, enzymes and reactive oxygen species.[114,131,133,135] With this proliferation of potential applications, pH-sensitive fluorescent

probes have also been on the spotlight especially since pH is an indicator in many cellular events, e.g. abnormal cell growth, inflammation and cancer are all characterised by pH values lower than those of normal cells.[136] These BODIPY based pH probes are mostly based on PET and ICT, and they typically contain the dimethylaminophenyl group which has the potential to act as a receptor.[137] Under normal circumstances, dyes with this functional group have their fluorescence quenched in polar solvents due to the charge transfer process, but upon protonation, the fluorescence process is activated due to the inhibition of the process.[112,132,133,135,137]

Aims

The aim of this work is to synthesise a series of structurally modified BODIPY dyes that will, among other properties exhibit the following characteristics: i. pH-sensitivity, ii. ability to absorb in the NIR region, and iii. possess enhanced photophysical properties. The aims can thus be summarised as:

1. Synthesis and photophysical study of a series of heavy atom containing BODIPY dyes.
2. Study the pH-sensitivity of the dyes containing $N(CH_3)_2$ groups both at the *meso*-position and on the styryl groups of the extended π-system.
3. Study the nonlinear optical behaviour of certain distyryl-BODIPY dyes in organic media.
4. Study BODIPY dye-cyclodextrin inclusion complexes in aqueous solution using UV-visible absorption and circular dichroism spectroscopies; and in solid state using x-ray diffraction spectroscopy, infrared spectroscopy and scanning electron microscopy.

5. Perform molecular modelling of the BODIPY dyes synthesised to identify structure-property relationships.

The results for one of the dyes studied for nonlinear optical limiting have already been published:

- May, A. K.; Stone, J.; Ngoy, B. P.; Mack, J.; Nyokong, T.; Kimura, M.; Kobayashi, N., accepted for publication in the *Journal of Porphyrins and Phthalocyanines* in **2018** [doi: 10.1142/S1088424617500869]

Chapter 2:

Experimental

2.1. Materials

All reagents were used without further purification unless otherwise stated. Trifluoroacetic acid (TFA), 2,4-dimethylpyrrole, 3-ethyl-2,4-dimethylpyrrole, tetrachloro-1,4-benzoquinone (*p*-chloranil), 4-bromobenzaldehyde, 4-dimethylamino benzaldehyde, 4-nitrobenzaldehyde, methyl 4-formylbenzoate, Rhodamine-6-G, 1,3-diphenylisobenzofuran (DBPF), boron trifluoride diethyl etherate ($BF_3{\cdot}Et_2O$), *N*-bromosuccinimide (NBS), sodium sulphate, triethylamine (TEA), anthracene-9,10-bis-methylmalonatepiperidine (ADMA) and glacial acetic acid were purchased from Sigma Aldrich. Rose Bengal was purchased from Fluka. Silica gel 60 for flash column chromatography was purchased from Merck. The cyclodextrins were purchased from Tokyo Chemical Industry Co., Ltd. All solvents were dried using molecular sieves before use.

2.2. Instrumentation

- Ultraviolet-visible (UV–vis) absorption spectra were measured at room temperature on a Shimadzu UV-2550 spectrophotometer. A 1 cm path length quartz cuvette was used.
- Proton nuclear magnetic resonance (^{1}H-NMR) spectra were recorded at room temperature in acetone-d_6, chloroform-d_3, tetrahydrofuran-d_8 (THF-d_8), N,N-Dimethylformamide-d_7 (DMF-d_7) or dimethylsulfoxide-d_6 (DMSO-d_6) on Bruker AMX 600 and 300 instruments operating at 600 and 300 MHz, respectively.
- Fluorescence emission and excitation spectra were obtained using a Varian Cary Eclipse spectrofluorimeter.
- Mass spectra (MS) data were collected on a Bruker AutoFLEX III Smart-beam matrix-assisted laser desorption/ionisation-time of flight (MALDI-TOF) mass spectrometer using

an α-cyano-4-hydroxycinnamic acid matrix and positive mode of operation for BODIPYs **2**–**10.**

- Fourier-transform infrared spectra (FT-IR) were recorded on a Perkin Elmer Spectrum 100 FT-IR spectrometer.

- Fluorescence lifetimes were measured using a time-correlated single photon counting (TCSPC) setup (FluoTime 200, Picoquant GmbH). For the brominated BODIPY cores, an LDH-P-C-485 laser head driven by PDL 800-B single channel driver and a 10 MHz repetition rate was used. For the di-styryl BODIPYs, an LDH-P-670 laser head with a 20 MHz repetition rate was used. Fluorescence was detected under the magic angle with a Peltier cooled photomultiplier tube (PMT) (PMA-C 192-N M, Picoquant GmbH) and integrated electronics (PicoHarp 300E, Picoquant GmbH). A monochromator with a spectral width of about 4 nm was used to select the required emission wavelength band. The response function of the system, which was measured with a scattering Ludox solution (DuPont), had a full width at half maximum (FWHM) of about 300 ps. All fluorescence decay curves were measured at the emission peak maxima. The decay curves were analysed with the FluoFit program (Picoquant GmbH).

- The irradiations for most of the singlet oxygen experiments were conducted using an Ekspla NT342B-20-AW – Nd:YAG laser (max output – 1J, pulse duration 3–6 ns) with parametric generation (max output – 50 mJ, pulse duration 3–5 ns, wavelength 400–2400 nm).

- All z-scan experiments were performed using a frequency doubled Nd:YAG laser (Quanta-Ray, 1.5 J/10 ns FWHM pulse duration) as the excitation source. The laser was

operated in a near Gaussian transverse mode at 532 nm (second harmonic), with a pulse repetition rate of 10 Hz and energy range of 0.1–0.1 mJ, limited by the energy detectors (Coherent J5-09). The low repetition rate of the laser prevents cumulative thermal nonlinearities. The beam was spatially filtered to remove the higher order modes and tightly focused with a 15 cm focal length lens.

- Circular dichroism (CD) spectra were recorded on a Jasco J-720 spectrodichrometer in water at room temperature. All samples were prepared from aqueous stock solutions. The following conditions were used: bandwidth, 1.0 nm; slit width, 1.0 nm; auto, sensitivity, 10 mdeg; time constant, 1.0 s; step resolution, 0.2 nm; scan speed, 20 $nm.min^{-1}$; number of scans, 4.

- The irradiations for the cyclodextrin inclusion complex singlet oxygen measurements were carried out using a Thorlabs mounted M530L3 LED as the light source for 530 nm light. The LED was mounted into the housing for a Modulight medical laser system that was equipped with a sample holder with a spot diameter of 5.5 cm. The LED provided an irradiance of 350 $mW.cm^{-2}$ with spectral readings taken at various time intervals to monitor progress.

- Imaging of the BODIPY dyes, cyclodextrins and their inclusion complexes were captured using a TESCAN Vega TS 5136LM scanning electron microscopy (SEM) (Jeol Quanta 200 F FE-SEM) at an accelerating voltage of 20 kV. Before SEM analysis, non-conductive samples were coated with gold using a sputter coater (Balzers Union SKD 030).

- X-ray powder diffraction (XRD) patterns were recorded on a Bruker D8, Discover instrument equipped with a proportional counter, using Cu-Kα radiation (λ = 1.5405 Å,

nickel filter). Data were collected in the range from 2θ = 10 to 100°, scanning at 1° min^{-1} with a filter time-constant of 2.5 s per step and a slit width of 6.0 mm. Samples were placed on a zero background silicon wafer. The X-ray diffraction data were treated using the freely-available EVA (evaluation curve fitting) software.[138] Baseline correction was performed on each diffraction pattern by subtracting a spline fitted to the curved background.

- The Gaussian 09 software package running on an Intel/Linux cluster was used to perform all calculations.[139] Geometry optimisations were carried out at the B3LYP level of theory with 6-31G(d)basis sets. TD-DFT calculations employed the CAM-B3LYP level of theory with 6-31G(d) basis sets. Avogadro, an advanced molecule editor and visualiser was used for all visualisations of molecular orbitals.[140]

2.3. Photophysical Properties of BODIPY dyes

A. Fluorescence properties of BODIPY dyes

BODIPY dye fluorescence properties have been extensively researched and applied in different fields.[5] Typically, the fluorescence spectra of BODIPYs are mirror images of the S_0 to S_1 absorption band since fluorescence only occurs from the lowest vibrational level of the S_1 to the S_0, following Kasha's rule.[17] The narrow emission bands of BODIPY cores lie in the 500–550 nm region unless they are red-shifted after structural modification.[5] The Stokes shift, which is the wavelength difference between the band maxima of the absorbed and emitted light for the S_0 to S_1 transition is typically small (approximately 10 nm) because the S_0 and S_1 states have similar geometries.[17]

The fluorescence quantum yield (ϕ_F) which is the number of photons emitted relative to the photons absorbed can be very high for some BODIPYs.[17,141] Similar to the fluorescence emission spectra, the fluorescence quantum yield is also independent of the excitation wavelength because there is rapid deactivation from the populated excited state (S_n) to the fluorescent lowest excited state.[17,141] To determine the quantum yield, the intensity of the BODIPY dye is compared with that of a standard.[142] In this work, the quantum yield is determined using Equation (12):

$$\Phi_F = \Phi_{F(Std)} \frac{F.A_{Std}.n^2}{F_{Std}.A.n_{Std}^2} \quad (12)$$

where F and F_{Std} are the areas under the fluorescence curves for the sample and standard respectively. A and A_{Std} are the absorbance values of the sample and standard at the excitation wavelength, while η and η_{std} are the respective refractive indices of the solvents in which the sample and standard were dissolved. Rhodamine 6G and zinc Pc (ZnPc) can be used as standards for the determination of fluorescence quantum yields in ethanol and DMSO, respectively, with ϕ_F = 0.95 and 0.20.[143,144]

The other important fluorescence property is the fluorescence lifetime (τ_F).[21,137,145,146] This is a measure of the average amount of time an electron in the S_1 state spends in this state before returning to the ground state via radiative emission of a photon. TCSPC is one technique which can be used to determine τ_F.[146] Here, a decay curve is plotted and then deconvoluted to give the fluorescence lifetime.

B. Singlet oxygen quantum yield of BODIPY dyes

There are two methods that can be used to quantify the generation of singlet oxygen by a photosensitizer dye, namely the physical/luminescence method and a comparative chemical method. In this work, the comparative method was used. This method uses a singlet oxygen quencher such as 1,3-diphenylisobenzofuran (DPBF) which reacts with the produced singlet oxygen. Monitoring is done using UV-visible absorption spectroscopy because a decrease in the intensity of the main absorption peak of the quencher is expected. Equation (13), shown below, is used for calculating singlet oxygen quantum yields (Φ_Δ).[147,148]

$$\Phi_\Delta = \Phi_\Delta^{std} \cdot \frac{R^{sample} \cdot I^{std}}{R^{std} \cdot I^{sample}} \quad (13)$$

where (Φ_Δ^{std}) is the singlet oxygen quantum yield for the standard (Rose Bengal, Φ_Δ^{std} = 0.76 in DMSO).[149] R^{sample} and R^{std} are the DPBF photobleaching rates in the presence of the sample under investigation and the standard, respectively. I^{sample} and I^{std} are the rates of light absorption by the sample and the standard, respectively.

2.4. Synthesis

A series of BODIPY dyes were synthesised, as described below.

BODIPY cores (Scheme 1)

2,4-Dimethylpyrrole (2.0 mole eq) and the corresponding benzaldehyde (1.0 mole eq) were dissolved in dry dichloromethane (DCM) (50 ml) under argon. TFA (2–3 drops) was added, and the reaction mixture was stirred at room temperature. When the aldehyde was consumed (monitored by TLC), a solution of *p*-chloranil (1.2 mole eq) in dry DCM (10 ml) was added at 0 °C. The solution was allowed to warm up to room temperature while stirring for 30 min under argon. A deep purple colour was observed and TLC confirmed the

synthesis of the dipyrromethene. TEA (7 mole eq) and $BF_3{\cdot}Et_2O$ (11 mole eq) were added dropwise at 0 °C, and the mixture was left to stir at room temperature for 12 h. The mixture was then filtered and washed with water (100 ml), dried over anhydrous sodium sulphate and the residue purified by flash column chromatography eluting with ethyl acetate:petroleum ether (1:4).

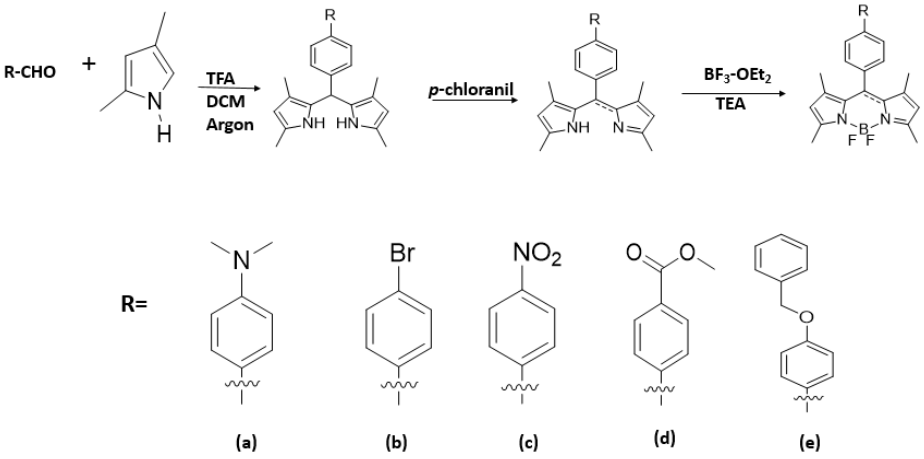

Scheme 1. Synthesis of BODIPYs **1(a–e)**.

BODIPY **1a**, **4,4'-difluoro-8-(4-dimethylaminophenyl)-1,3,5,7-tetramethyl-4-bora-3a,4a-diaza-*s*-indacene**, was obtained in 11% yield (0.27 g); FT-IR (cm^{-1}): 2918 (C-H stretch), 2848 (C-H stretch), 2773 (C-H stretch), 1499, 1357 (C-N stretch), 1185, 1055 (C-N stretch), 968 (=C-H bend), 468 (C-H); ^{1}H NMR (300 MHz, DMSO-d_6) δ 7.11–7.08 (d, J = 8.9 Hz, 2H), 6.86–6.83 (d, J = 8.8 Hz, 2H), 6.15 (s, 2H), 2.97 (s, 6H), 2.43 (s, 6H), 1.45 (s, 6H) ppm.

BODIPY **1b**, **4,4'-difluoro-8-(4-bromophenyl)-1,3,5,7-tetramethyl-4-bora-3a,4a-diaza-*s*-indacene**, was obtained in 16% yield (0.35 g); FT-IR (cm^{-1}): 2920 (C-H stretch), 2859 (C-H stretch), 1502, 1404 (C-N stretch), 1191, 1040 (C-N stretch), 970 (=C-H bend), 470 (C-H); ^{1}H NMR (300 MHz, DMSO-d_6) δ 7.78–7.76 (d, J = 8.3 Hz, 2H), 7.38–7.35 (d, J = 8.3 Hz, 2H), 6.20 (s, 2H), 2.44 (s, 6H), 1.37 (s, 6H) ppm.

BODIPY **1c**, **4,4'-difluoro-8-(4-nitrophenyl)-1,3,5,7-tetramethyl-4-bora-3a,4a-diaza-*s*-indacene**, was obtained in 25.8% yield (0.63 g); FT-IR (cm^{-1}): 2953 (C-H stretch), 2914(C-H stretch), 1712 (C=O), 1410 (C-N stretch), 1188, (C-N stretch), 1277, 1062 (C-O), 964 (=C-H bend), 465 (C-H); ^{1}H NMR (300 MHz, DMSO-d_6) δ 8.41–8.38 (d, J = 8.8 Hz, 2H), 7.77–7.74 (d, J = 8.8 Hz, 2H), 6.22 (s, 2H), 2.46 (s, 6H), 1.34 (s, 6H) ppm.

BODIPY **1d**, **4,4'-difluoro-8-(4-carbomethoxyphenyl)-1,3,5,7-tetramethyl-4-bora-3a,4a-diaza-*s*-indacene**, was obtained in 39% yield (0.9 g); FT-IR (cm^{-1}): 2953 (C-H stretch), 2914 (C-H stretch), 1712 (C=O), 1277, 1062 (C-O), 1459, 1410 (C-N stretch), 1188, 1062 (C-N stretch), 1277, 1062 (C-O), 965 (=C-H bend), 465 (C-H); ^{1}H NMR (300 MHz, DMSO-d_6) δ 8.14–8.11 (d, J = 8.4 Hz, 2H), 7.58–7.55 (d, J = 8.4 Hz, 2H), 6.20 (s, 2H), 3.90 (s, 3H), 2.45 (s, 6H), 1.32 (s, 6H) ppm.

BODIPY **1e**, **4,4'-difluoro-8-(4-benzyloxyphenyl)-1,3,5,7-tetramethyl-4-bora-3a,4a-diaza-*s*-indacene**, was obtained in 35% yield; FT-IR (cm^{-1}): 2918 (C-H stretch), 2854 (C-H stretch), 1455, 1408 (C-N stretch), 1188, 1070 (C-N stretch), 1102 (C-O-C), 969 (=C-H bend), 468 (C-H); ^{1}H NMR (600 MHz, $CDCl_3$) δ 7.48 (d, J = 7.3 Hz, 2H), 7.43 (t, J = 7.4 Hz, 2H), 7.38 (t, J = 7.3 Hz, 1H), 7.20–7.19 (d, J = 8.6 Hz, 2H), 7.12–7.10 (d, J = 8.6 Hz, 2H), 6.00 (s, 2H), 5.14 (s, 2H), 2.14 (s, 6H), 1.45 (s, 6H) ppm.

Brominated BODIPYs (Scheme 2)

BODIPYs **1a**, **b**, **c**, **d** and **e** (1 mole eq.) and NBS (3 mole eq.) were dissolved in DCM (20 mL). The mixture was left to stir under Ar/N_2 at room temperature; the reaction was followed by thin layer chromatography to completion. The product was washed with water and the organic phase dried over sodium sulphate. Finally, purification was achieved via flash column chromatography with ethyl acetate:petroleum ether (1:4) as the eluent.

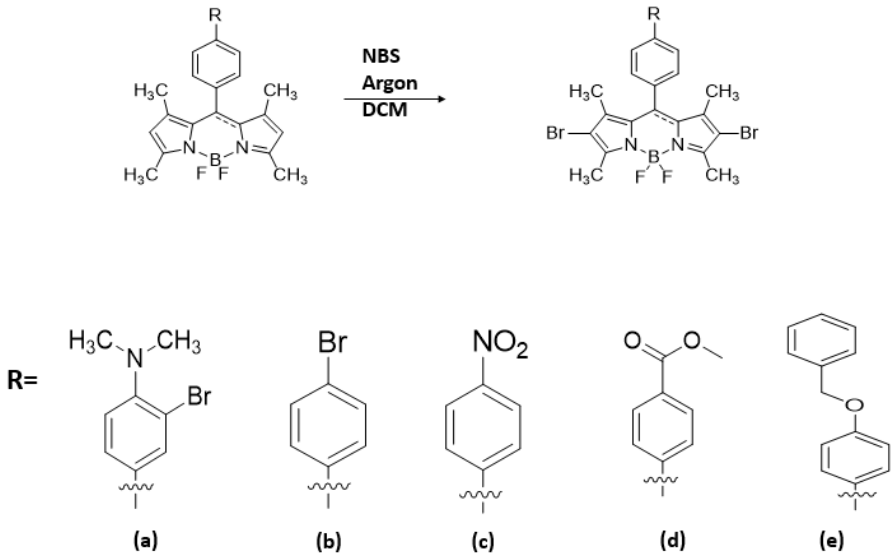

Scheme 2. Bromination of BODIPYs **1(a–d)** to form **2(a–d)**.

BODIPY **2a**, **4,4'-difluoro-8-(3-bromo-4-dimethylaminophenyl)-1,3,5,7-tetramethyl-2,6-dibromo-4-bora-3a,4a-diaza-*s*-indacene**, was obtained in 72% yield (0.82 g); FT-IR (cm^{-1}): 2919 (C-H stretch), 2854 (C-H stretch), 2781 (C-H stretch), 1535, 1308 (C-N stretch), 1170, 1088 (C-N stretch), 990 (=C-H bend), 522 (C-Br stretch); ^{1}H NMR (300 MHz, acetone-d_6) δ 7.69 (s, 1H), 7.40–7.39 (d, J = 1.1 Hz, 2H), 2.89 (s, 6H), 2.56 (s, 6H), 1.50 (s, 6H) ppm. MALDI-TOF Anal. calc. m/z 603.93; Found: $[M + 1H]^+$ 605.9.

BODIPY **2b**, **4,4'-difluoro-8-(4-bromophenyl)-1,3,5,7-tetramethyl-2,6-dibromo-4-bora-3a,4a-diaza-*s*-indacene** was obtained in 92% yield (0.18 g); FT-IR (cm^{-1}): 2917 (C-H stretch), 2856 (C-H stretch), 1458, 1394 (C-N stretch), 1174, 1086 (C-N stretch), 994 (=C-H bend), 523 (C-Br stretch); ^{1}H NMR (300 MHz, DMSO-d_6) δ 7.82–7.80 (d, J = 8.5 Hz, 2H), 7.44–7.41 (d, J = 8.5 Hz, 2H), 2.52 (s, 6H), 1.37 (s, 6H) ppm. MALDI-TOF Anal. calc. m/z 560.86; Found: $[M + 1H]^+$ 562.63.

BODIPY **2c**, **4,4'-difluoro-8-(4-nitrophenyl)-1,3,5,7-tetramethyl-2,6-dibromo-4-bora-3a,4a-diaza-*s*-indacene**, was obtained in 86.6% yield (0.68 g); FT-IR (cm^{-1}): 2921 (C-H stretch), 2850 (C-H stretch), 1526 (N=0), 1456, 1410 (C-N stretch), 1184, (C-N stretch), 997 (=C-H bend), 531 (C-Br stretch); ^{1}H NMR (600 MHz, $CDCl_3$) δ 8.57–8.56 (d, J = 8.7 Hz, 2H), 7.68–7.66 (d, J = 8.7 Hz, 2H), 2.76 (s, 6H), 1.50 (s, 6H) ppm. MALDI-TOF Anal. calc. m/z 526.97; Found: [M] 526.2.

BODIPY **2d**, **4,4'-difluoro-8-(4-carbomethoxyphenyl)-1,3,5,7-tetramethyl-2,6-dibromo-4-bora-3a,4a-diaza-*s*-indacene**, was obtained in 92% yield (0.18 g); FT-IR (cm^{-1}): 2995 (C-H stretch), 2951 (C-H stretch), 1724 (C=O), 1268, 1091 (C-O), 1458, 1399 (C-N stretch), 1188, 1091 (C-N stretch), 1268, 1091 (C-O), 998 (=C-H bend), 532 (C-Br stretch); ^{1}H NMR (300 MHz, DMSO-d_6) δ 8.16–8.14 (d, J = 8.5 Hz, 2H), 7.64–7.61 (d, J = 8.5 Hz, 2H), 3.91 (s, 3H), 2.52 (s, 6H), 1.31 (s, 6H) ppm. MALDI-TOF Anal. calc. m/z 539.99; Found: $[M + H]^+$ 541.271.

BODIPY **2e**, **4,4'-difluoro-8-(4-benzyloxyphenyl)-1,3,5,7-tetramethyl-2,6-dibromo-4-bora-3a,4a-diaza-*s*-indacene**, was obtained in 30% yield; FT-IR (cm^{-1}): 2918 (C-H stretch), 2856 (C-H stretch), 1457, 1395 (C-N stretch), 1085 (C-N stretch), 1178 (C-O-C), 866 (=C-H bend), 527 (C-Br); ^{1}H NMR (600 MHz, $CDCl_3$) δ 7.48 (d, J = 7.3 Hz, 2H), 7.43–7.42 (t, J = 7.4 Hz, 2H), 7.4–7.37 (m, 2H), 7.16–7.11 (dd, J = 20,8.6 Hz, 3H), 5.17 (s, 2H), 2.61 (s, 6H), 1.43 (s, 6H) ppm. MALDI-TOF Anal. calc. m/z 588.09; Found: [M] 588.29.

BODIPY 3: 4,4'-Difluoro-8-(4-carbomethoxyphenyl)-1,5,7-trimethyl-2,6-dibromo-3-mono-styryl-(4-dimethylamino)-4-bora-3a,4a-diaza-*s*-indacene (Scheme 3)

BODIPY **2d** (1 mole eq.), 4-dimethyl amino benzaldehyde (1.4 mole eq.) and glacial acetic acid (0.4 mL) were dissolved in dry benzene (20 mL) under Ar with stirring. Piperidine (0.4 mL) was added slowly and the solution was heated to reflux for 48 h under Ar. A Dean-Stark trap was deployed for the azeotropic removal of water formed during the condensation reaction. The reaction was quenched with water and the organic phase was dried over sodium sulphate. Separation was by flash column chromatography with ethyl acetate:petroleum ether (1:4). BODIPY **3** was obtained in 16.1% yield (0.02 g); FT-IR (cm^{-1}): 2852 (C-H stretch), 1715 (C=O), 1291 (C-O), 1434, 1351 (C-N stretch), 1064 (C-N stretch), 1163, 1106 (C-O), 937 (=C-H bend), 516 (C-Br stretch); ^{1}H NMR (600 MHz, $CDCl_3$) δ 8.19–8.14 (dd, J = 18.0, 12.3 Hz, 4H), 7.55–7.50 (dd, J = 18.5, 12.6 Hz, 4H), 7.39–7.37 (d, J = 8.2 Hz, 2H), 3.97 (s, 3H), 3.04 (s, 6H), 2.62 (s, 3H), 1.36 (s, 3H), 1.32 (s, 3H) ppm. MALDI-TOF Anal. calc. m/z 671.18; Found: $[M + 2H]^+$ 673.96.

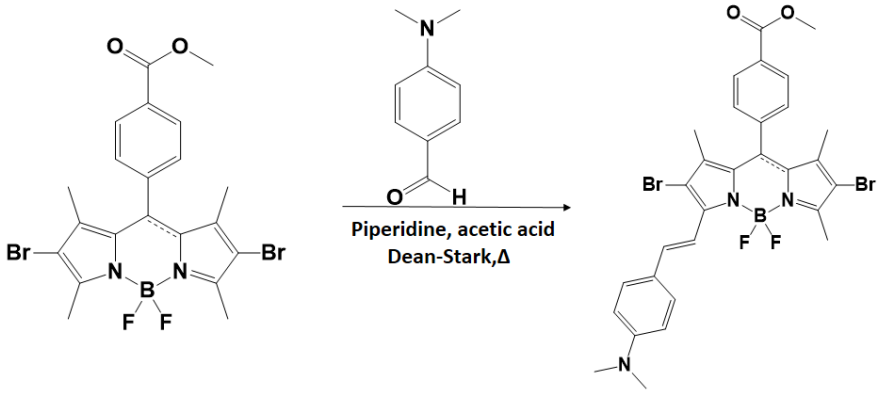

Scheme 3. Synthesis of BODIPY **3**.

BODIPY 4: 4,4'-Difluoro-8-(4-dimehtylamino)-1,7-dimethyl-2,6-dibromo-3,5-di-styryl-(4-benzo-15-crown-5)-4-bora-3a, 4a-diaza-*s*-indacene (Scheme 4)

The BODIPY dye was previously synthesised and characterised by another MSc student at Rhodes University.[150] For this thesis, the nonlinear optical studies of the di-styryl crown ether dye were the main focus and limited structural and photophysical characterisation was also performed to supplement the data already recorded.[150] ^{1}H NMR (600 MHz, THF-d_8) δ 8.13–8.10 (d, J = 16.6 Hz, 2H), 7.66–7.63 (d, J = 15.6 Hz, 3H), 7.32–7.31 (d, J = 11.7 Hz, 3H), 7.22–7.20 (d, J = 9.9 Hz, 4H), 6.97–6.95 (d, J = 8.0 Hz, 2H), 4.19–4.13 (d, J = 33.5 Hz, 8H), 3.88–3.85 (d, J = 20.6 Hz, 8H), 3.69 (s, 16H), 2.89 (s, 6H), 1.55 (s, 6H) ppm; MALDI-TOF Anal. calc. m/z 1082.6; Found: $[M + H]^+$ 1083.4.

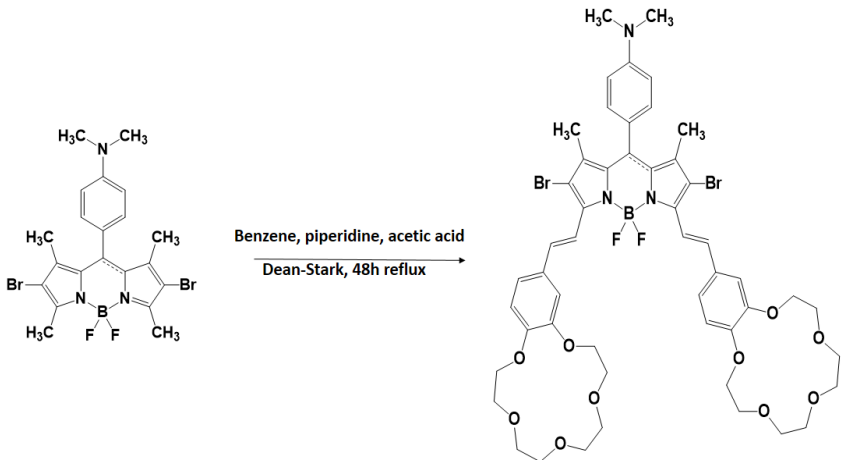

Scheme 4. Synthesis of the di-styryl crown ether BODIPY dye (BODIPY **4**).

BODIPY 5: 4,4'-Difluoro-8-(4-benzyloxyphenyl)-1,7-dimethyl-3,5-di-styryl-(4-benzyloxyphenyl)-4-bora-3a,4a-diaza-*s*-indacene (Scheme 5)

4,4'-Difluoro-8-(4-benzyloxyphenyl)-1,3,5,7-tetramethyl-4-bora-3a,4a-diaza-*s*-indacene (1 mole eq.), 4-benzyloxy benzaldehyde (1.4 mole eq.) and glacial acetic acid (0.4 mL) were dissolved in dry benzene (20 mL) under Ar with stirring. Piperidine (0.4 mL) was added

slowly and the solution was heated to reflux for 48 h under Ar. A Dean-Stark trap was deployed for the azeotropic removal of water formed during the condensation reaction. The reaction was quenched with water and the organic phase was dried over sodium sulphate. Separation was by flash column chromatography with ethyl acetate:petroleum ether (1:4). BODIPY **5** was obtained in 32% yield; FT-IR (cm^{-1}): 2926 (C-H stretch), 2856 (C-H stretch), 1501, 1438 (C-N stretch), 1103 (C-N stretch), 1166 (C-O-C), 876 (=C-H bend), 453 (C-H); ^{1}H NMR (600 MHz, $CDCl_3$) δ 7.60 (s, 4H), 7.47 (d, J = 8.2 Hz, 5H), 7.42 (s, 12H), 7.22–7.20 (d, J = 15.3 Hz, 3H), 7.11 (s, 2H), 7.02 (s, 3H), 6.92 (s, 2H), 6.62 (s, 2H), 5.13 (s, 4H), 5.03 (s, 2H), 1.59 (s, 6H) ppm. MALDI-TOF Anal. calc. m/z 818.35; Found: [M] 818.93.

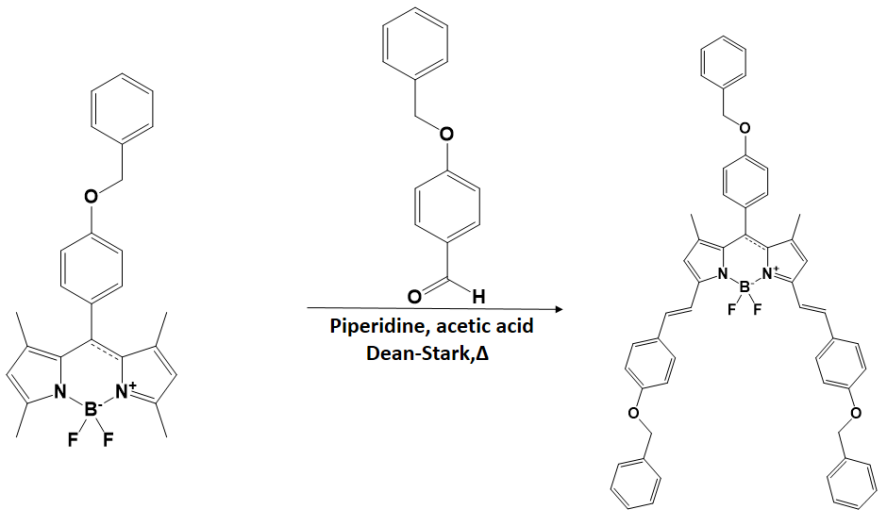

Scheme 5. Synthesis of BODIPY **5**.

BODIPY 6: 4,4'-Difluoro-8-(4-benzyloxyphenyl)-1,7-dimethyl-2,6-dibromo-3-di-styryl-(4-benzyloxyphenyl)-4-bora-3a,4a-diaza-*s*-indacene (Scheme 6)

BODIPY **2e** (1 mole eq.), 4-benzyloxy benzaldehyde (1.4 mole eq.) and glacial acetic acid (0.4 mL) were dissolved in dry benzene (20 mL) under Ar with stirring. Piperidine (0.4 mL) was added slowly and the solution was heated to reflux for 48 h under Ar. A Dean-Stark trap

was deployed for the azeotropic removal of water formed during the condensation reaction. The reaction was quenched with water and the organic phase was dried over sodium sulphate. Separation was by flash column chromatography with ethyl acetate:petroleum ether (1:4). BODIPY **6** was obtained in 20% yield; FT-IR (cm^{-1}): 2923 (C-H stretch), 2852 (C-H stretch), 1507, 1441 (C-N stretch), 1110 (C-N stretch), 1161 (C-O-C), 912 (=C-H bend), 522 (C-Br stretch) ^1H NMR (600 MHz, $CDCl_3$) δ 8.14–8.11 (d, J = 16.6 Hz, 2H), 7.65–7.62 (d, J = 15.4 Hz, 6H), 7.48 (s, 6H), 7.42 (s, 6H), 7.37 (s, 3H), 7.20 (s, 2H), 7.15 (s, 2H), 7.05 (s, 4H), 5.17 (d, J = 13.2 Hz, 6H), 1.49 (s, 6H) ppm. MALDI-TOF Anal. calc. m/z 976.17; Found: [M] 976.71.

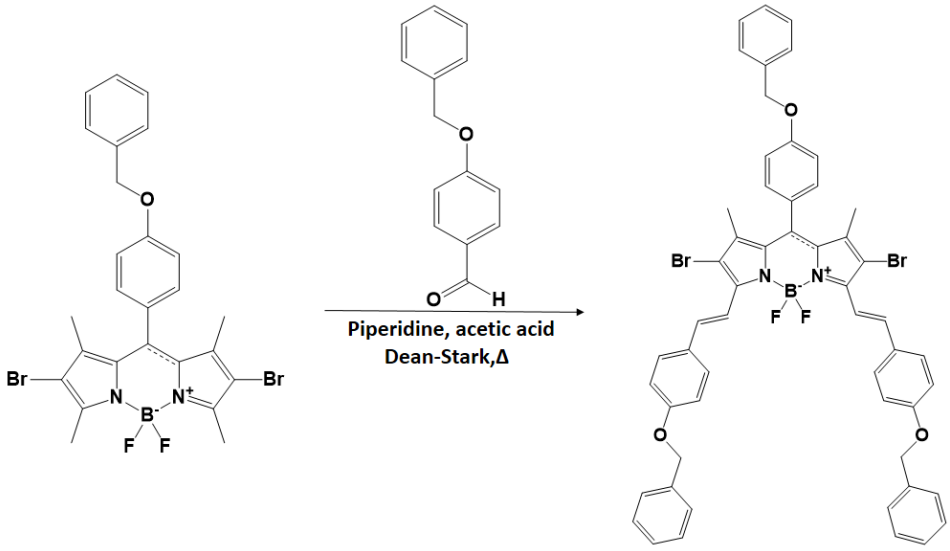

Scheme 6. Synthesis of BODIPY **6**.

BODIPY 7: 4,4'-Difluoro-8-(4-carbomethoxyphenyl)-1,7-dimethyl-3,5-di(thiophen-2-yl)vinyl-4-bora-3a,4a-diaza-*s*-indacene (Figure 7)

BODIPY **7** was previously synthesised and fully characterised by another MSc student at Rhodes Univerity;[95,151] the photophysical and optical limiting properties were revisited here.

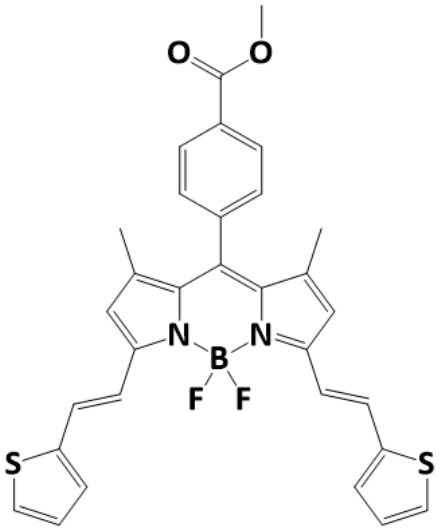

Figure 7. Structure of BODIPY **7**.

BODIPY 8: 4,4'-Difluoro-8-(4-carbomethoxyphenyl)-2,6-diethyl-1,7-dimethyl-3,5-di-styryl-(4-dimethylaminophenyl)-4-bora-3a,4a-diaza-*s*-indacene (Scheme 7)

3-Ethyl-2,4-dimethylpyrrole (2.0 mole eq) and methyl 4-formylbenzoate (1.0 mole eq) were dissolved in dry DCM (50 ml) under argon. TFA (2–3 drops) was added and the reaction mixture was stirred at room temperature. When the aldehyde was consumed (monitored by TLC), a solution of *p*-chloranil (1.2 mole eq) in dry DCM (10 ml) was added at 0 °C. The solution was allowed to warm up to room temperature while stirring for 30 min under argon. A deep purple colour was observed and TLC confirmed the synthesis of the dipyrromethene. TEA (7 mole eq) and $BF_3{\cdot}Et_2O$ (11 mole eq) were added dropwise at 0 °C and the mixture was left to stir at room temperature for 12 h. The mixture was then filtered and washed with water (100 ml), dried over anhydrous sodium sulphate and the residue purified by flash column chromatography eluting with ethyl acetate:petroleum ether (1:4). The product, 4,4'-difluoro-8-(4-carbomethoxyphenyl)-2,6-diethyl-1,3,5,7-tetramethyl-4-bora-3a,4a-diaza-*s*-indacene was obtained in powder form subsequent to drying.

4,4'-Difluoro-8-(4-carbomethoxyphenyl)-2,6-diethyl-1,3,5,7-tetramethyl-4-bora-3a,4a-diaza-*s*-indacene (1 mole eq.) was then mixed with 4-dimethyl amino benzaldehyde (1.4 mole eq.) and glacial acetic acid (0.4 mL) in dry benzene (20 mL) under Ar with stirring. Piperidine (0.4 mL) was added slowly and the solution was heated to reflux for 48 h under Ar. A Dean-Stark trap was deployed for the azeotropic removal of water formed during the condensation reaction. The reaction was quenched with water and the organic phase was dried over sodium sulphate. Separation was by flash column chromatography with ethyl acetate:petroleum ether (1:4). BODIPY **8** was obtained in 25–30% yield; FT-IR (cm^{-1}): 2916, 2853 (C-H stretch), 1712 (C=O), 1436, 1353 (C-N stretch), 1044 (C-N stretch), 1162, 1101 (C-O), 953 (=C-H bend); ^{1}H NMR (600 MHz, DMF-d_7) δ 8.40 (s, 2H), 8.26 (s, 3H), 7.71 (d, J = 40.1 Hz, 3H), 7.58 (s, 3H), 7.38 (s, 2H), 6.86 (s, 3H), 4.08 (s, 3H), 3.07 (s, 12H), 1.98 (s, 4H), 1.38 (s, 6H), 1.29 (s, 6H) ppm. MALDI-TOF Anal. calc. m/z 700.38; Found: [M] 700.94.

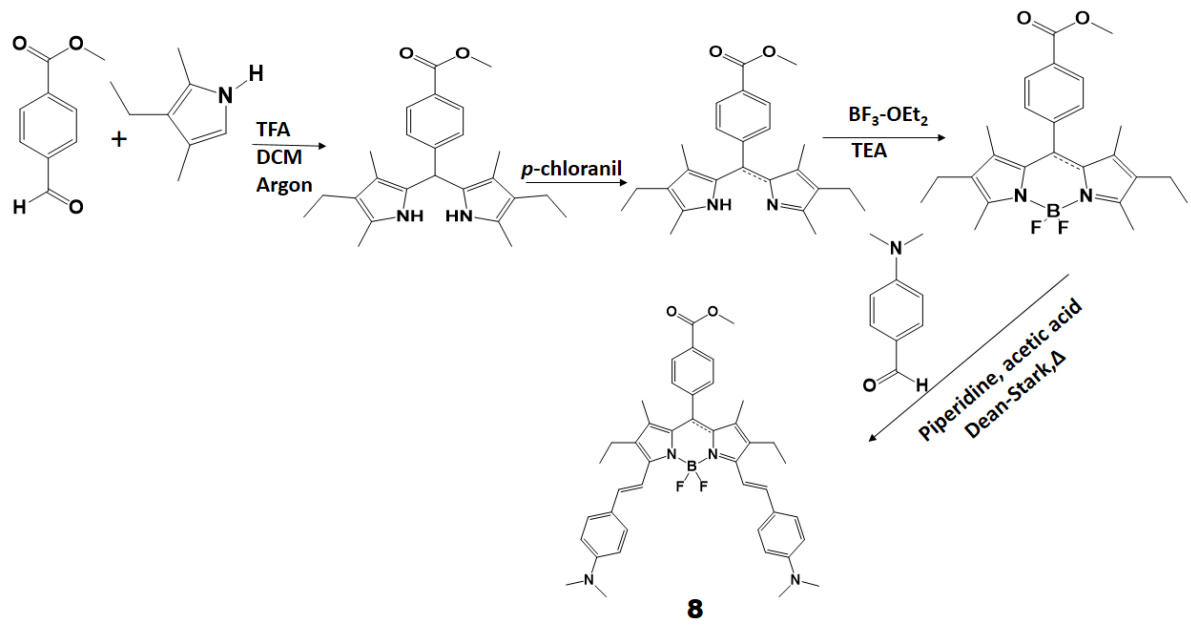

Scheme 7. Synthesis of BODIPY **8**.

BODIPY 9: 4,4'-Difluoro-8-(4-carbomethoxyphenyl)-2,6-diethyl-1,7-dimethyl-3,5-di-styryl-(4-hydroxyphenyl)-4-bora-3a,4a-diaza-*s*-indacene (Scheme 8)

3-Ethyl-2,4-dimethylpyrrole (2.0 mole eq) and methyl 4-formylbenzoate (1.0 mole eq) were dissolved in dry DCM (50 ml) under argon. TFA (2–3 drops) was added and the reaction mixture was stirred at room temperature. When the aldehyde was consumed (monitored by TLC), a solution of *p*-chloranil (1.2 mole eq) in dry DCM (10 ml) was added at 0 °C. The solution was allowed to warm up to room temperature while stirring for 30 min under argon. A deep purple colour was observed and TLC confirmed the synthesis of the dipyrromethene. TEA (7 mole eq) and $BF_3{\cdot}Et_2O$ (11 mole eq) were added dropwise at 0 °C and the mixture was left to stir at room temperature for 12 h. The mixture was then filtered and washed with water (100 ml), dried over anhydrous sodium sulphate and the residue purified by flash column chromatography eluting with ethyl acetate:petroleum ether (1:4). The product, 4,4'-difluoro-8-(4-carbomethoxyphenyl)-2,6-diethyl-1,3,5,7-tetramethyl-4-bora-3a,4a-diaza-*s*-indacene was obtained in powder form subsequent to drying.

4,4'-Difluoro-8-(4-carbomethoxyphenyl)-2,6-diethyl-1,3,5,7-tetramethyl-4-bora-3a,4a-diaza-*s*-indacene (1 mole eq.) was then mixed with 4-hydroxybenzaldehyde (1.4 mole eq.) and glacial acetic acid (0.4 mL) in dry benzene (20 mL) under Ar with stirring. Piperidine (0.4 mL) was added slowly and the solution was heated to reflux for 48 h under Ar. A Dean-Stark trap was deployed for the azeotropic removal of water formed during the condensation reaction. The reaction was quenched with water and the organic phase was dried over sodium sulphate. Separation was by flash column chromatography with ethyl acetate:petroleum ether (1:4). BODIPY **9** was obtained in 25–30% yield; FT-IR (cm^{-1}): 3250 (O-H stretch), 2923, 2858 (C-H stretch), 1718 (C=O), 1437, 1373 (C-N stretch), 1048 (C-N stretch), 1169, 1107 (C-

O), 966 (=C-H bend); ^{1}H NMR (600 MHz, acetone-d_6) δ 8.79 (s, 2H), 8.26 (d, J = 8.2 Hz, 2H), 7.67 (dd, J = 20.2, 12.5 Hz, 4H), 7.56 (d, J = 8.5 Hz, 4H), 7.36 (d, J = 16.8 Hz, 2H), 6.95 (d, J = 8.5 Hz, 4H), 3.98(s, 3H), 2.68 (m, 4H), 1.39 (s, 6H), 1.17 (t, J = 7.5 Hz, 6H) ppm. MALDI-TOF Anal. calc. m/z 646.28; Found: [M] 646.83.

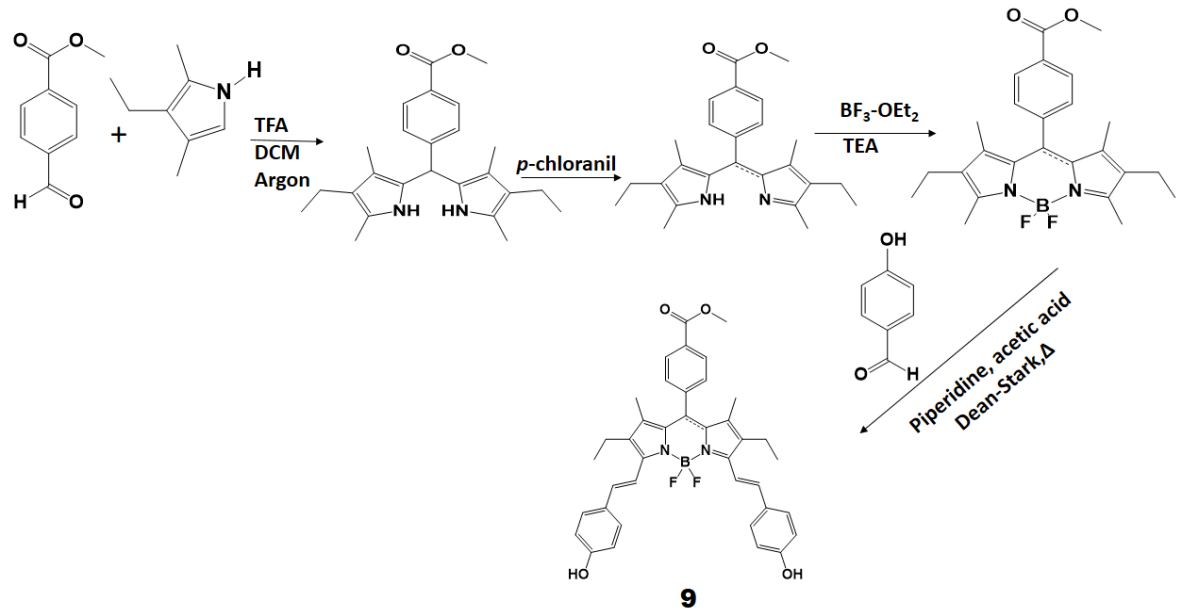

Scheme 8. Synthesis of BODIPY **9**.

BODIPY 10: 4,4'-Difluoro-8-(4-carbomethoxyphenyl)-2,6-diethyl-1,7-dimethyl-3,5-di-styryl-(4-methoxyphenyl)-4-bora-3a,4a-diaza-*s*-indacene (Scheme 9)

3-Ethyl-2,4-dimethylpyrrole (2.0 mole eq) and methyl 4-formylbenzoate (1.0 mole eq) were dissolved in dry DCM (50 ml) under argon. TFA (2–3 drops) was added and the reaction mixture was stirred at room temperature. When the aldehyde was consumed (monitored by TLC), a solution of *p*-chloranil (1.2 mole eq) in dry DCM (10 ml) was added at 0 °C. The solution was allowed to warm up to room temperature while stirring for 30 min under argon. A deep purple colour was observed and TLC confirmed the synthesis of the dipyrromethene. TEA (7 mole eq) and $BF_3{\cdot}Et_2O$ (11 mole eq) were added dropwise at 0 °C,

and the mixture was left to stir at room temperature for 12 h. The mixture was then filtered and washed with water (100 ml), dried over anhydrous sodium sulphate, and the residue purified by flash column chromatography eluting with ethyl acetate:petroleum ether (1:4). The product, 4,4'-difluoro-8-(4-carbomethoxyphenyl)-2,6-diethyl-1,3,5,7-tetramethyl-4-bora-3a,4a-diaza-*s*-indacene was obtained in powder form subsequent to drying.

4,4'-Difluoro-8-(4-carbomethoxyphenyl)-2,6-diethyl-1,3,5,7-tetramethyl-4-bora-3a,4a-diaza-*s*-indacene (1 mole eq.) was then mixed with 4-methoxybenzaldehyde (1.4 mole eq.) and glacial acetic acid (0.4 mL) in dry benzene (20 mL) under Ar with stirring. Piperidine (0.4 mL) was added slowly, and the solution was heated to reflux for 48 h under Ar. A Dean-Stark trap was deployed for the azeotropic removal of water formed during the condensation reaction. The reaction was quenched with water and the organic phase was dried over sodium sulphate. Separation was by flash column chromatography with ethyl acetate:petroleum ether (1:4). BODIPY **10** was obtained in 25–30% yield; FT-IR (cm^{-1}): 2920, 2855 (C-H stretch), 1722 (C=O), 1446, 1328 (C-N stretch), 1099 (C-N stretch), 1162 (C-O), 1027 (C-O-C stretch), 966 (=C-H bend) 529 (C-O-C bend); ^{1}H NMR (600 MHz, $CDCl_3$) δ 8.23 (d, J = 7.4 Hz, 2H), 7.71 (d, J = 16.8 Hz, 2H), 7.61 (d, J = 8.0 Hz, 4H), 7.50 (d, J = 7.5 Hz, 2H), 7.30 (s, 2H), 6.99 (d, J = 8.0 Hz, 4H), 4.03 (s, 3H), 3.90 (s, 6H), 2.65 (q, J = 7.1 Hz, 4H), 1.36 (s, 6H), 1.20 (t, J = 7.5 Hz, 6H) ppm. MALDI-TOF Anal. calc. m/z 674.31; Found: [M] 674.91.

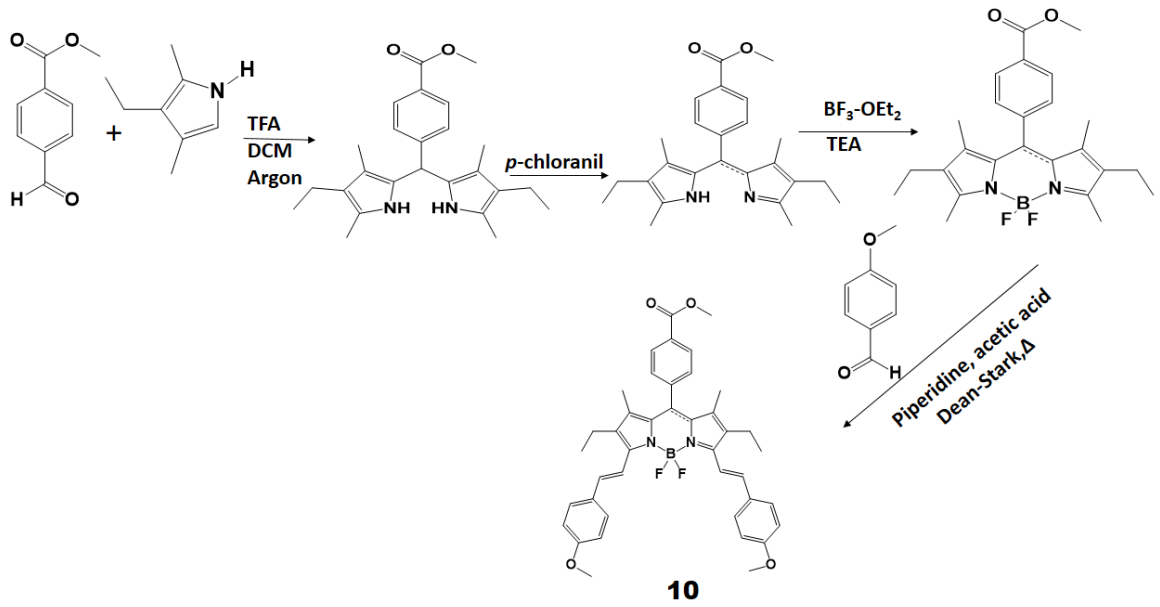

Scheme 9. Synthesis of BODIPY **10**.

Chapter 3:

Synthesis and spectroscopic characterisation of BODIPY Dyes

The focus of this chapter is on the synthesis of a series of BODIPY cores and their respective 2,6-dibrominated; and 3,5-substituted, red-shifted π-extended analogues. The BODIPY cores, **1a**–**e** (**Scheme 1**) were prepared for use in further reactions, to produce BODIPY dyes with more complex structures. Bromination of these BODIPYs at the 2,6-positions (and on one carbon of the *meso*-phenyl ring for BODIPY **1a**) yielded BODIPYs **2a**–**e** (**Scheme 2**). BODIPY **1e** was used as a starting reagent for BODIPY **5** (**Scheme 5**) and BODIPY **2e** as a starting reagent for BODIPY **6** (**Scheme 6**), both intended for use in optical limiting applications. BODIPYs **2a**–**c** were synthesised for application in the formation of cyclodextrin inclusion complexes, while BODIPY **2d** was used as a starting reagent for BODIPY **3**. Unlike the other dyes, BODIPYs **8**, **9** and **10** were synthesised from 3-ethyl-2,4-dimethylpyrrole and were intended for application in optical limiting studies and in addition, pH-sensing in the case of BODIPY **8**. Extending the π-conjugation of the BODIPY dyes results in significantly red-shifted main spectral bands; the photophysical properties of some of these dyes with an extended π-conjugation system were partially investigated to demonstrate singlet oxygen-generating capability, particularly for those derived from the 2,6-dibrominated dyes.[3] The singlet oxygen quantum yields of the brominated dyes before styryl extension were also investigated by using the comparative chemical method, with DPBF as a singlet oxygen quencher.[147–151]

3.1. 4,4'-Difluoro-8-(4-dimethylaminophenyl)-1,3,5,7-tetramethyl-4-bora-3a,4a-diaza-*s*-indacene (1a)

3.1.1. Synthesis of BODIPY **1a**

BODIPY **1a**, a previously reported dye was synthesised both as a precursor for a more complex BODIPY dye intended for use in optical limiting applications and for the formation of cyclodextrin inclusion complexes.[152] The synthesis route was the commonly-used "one-pot three-step" trifluoroacetic acid-catalysed condensation of 2,4-dimethylpyrrole and 4-dimethylaminobenzaldehyde using trifluoroacetic acid in DCM (**Scheme 10**). Unwanted polymerisation of the pyrrole unit is eliminated by the presence of the methyl groups on the pyrrole 2,4-positions.

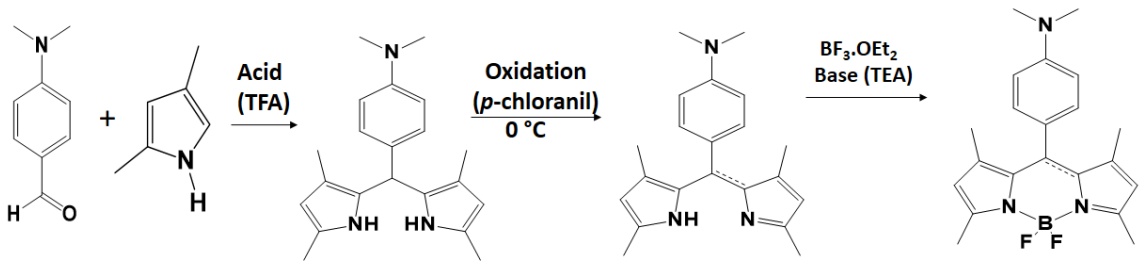

Scheme 10. Acid-catalysed one-pot synthesis of BODIPY **1a**.

3.1.2 Structural Analysis of BODIPY **1a**

The signals for all twenty-four protons can be identified in the ^{1}H NMR spectrum. The doublets at 7.11–7.08 and 6.86–6.83 ppm each integrate to two protons can be assigned to the four phenyl protons. The twelve proton signals that lie at 1.45 and 2.43 ppm can be attributed to the twelve methyl protons on the pyrrole core. The singlet signal at 2.97 ppm integrates as six protons and can be assigned to the six methyl protons on the dimethylamino group. The signal at 6.15 ppm is for the protons at the 2,6-positions of the

BODIPY core. The FT-IR spectra contained the peaks anticipated for the BODIPY core.[150,151,153] Between 2750 and 2950 cm^{-1} there are bands attributed to the C-H stretch of the terminal methyl groups, whereas the N-C stretch bands corresponding to the pyrrolic nitrogen atoms lie in the 1050–1360 cm^{-1} region. The C-H stretch for the bonds at the 2,6-positions are observed at 468 cm^{-1}

3.1.3 Spectroscopic properties of BODIPY **1a**

The electronic absorption spectrum for BODIPY **1a** is typical of that of a *meso*-substituted BODIPY, with no signs of aggregation and an absorbance maximum at 500 nm in DMSO. BODIPY **1a** is soluble in both ethanol and DMSO with only a slight blue-shift (ca. 2 nm) observed on increased solvent polarity from ethanol to DMSO. It has been suggested that this blue-shift arises from the polarisability of the solvent as a similar effect has been reported in cyanine-based dyes.[154] The absorption, excitation and emission band maxima values in the two solvents are summarised below (**Table 1**) in the absence and presence of TFA; the absorption (Abs), excitation (Exc) and emission (Em) spectra in DMSO in the presence of TFA are also provided (**Figure 8**). Additionally, the dye has an emission spectrum that is typical for a 1,3,5,7-tetramethyl BODIPY core. Upon protonation, both the absorption and emission spectra in DMSO exhibit a 4 nm red shift. As can be seen from the fluorescence quantum yield values (**Table 1**), BODIPY **1a** is highly fluorescent in the presence of TFA as intense fluorescence emission is only observed when the nitrogen lone pairs in the dimethylamino group are protonated. This is due to the elimination of intramolecular charge transfer from the nitrogen lone pairs into the BODIPY core. The dye has a negligible singlet oxygen quantum yield; this was studied using the comparative method and the dye

could not degrade DPBF, as is expected since there are no heavy atoms on the BODIPY core, and hence there is no intersystem crossing to the triplet state.

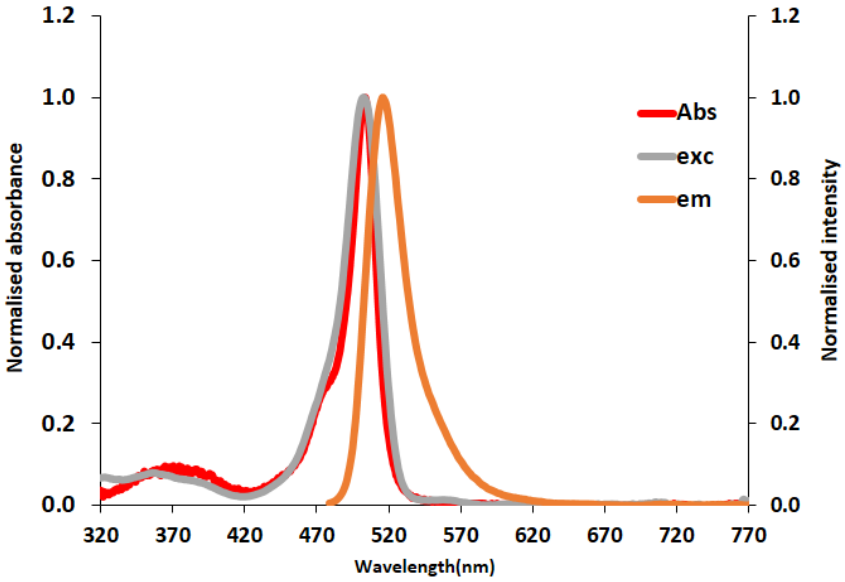

Figure 8. Normalised absorption (red), excitation (grey) and emission (orange) spectra of BODIPY **1a** in DMSO in the presence of TFA.

Table 1. Photophysical data for BODIPY **1a** in different organic solvents.

Solvent	λ_{Abs} (nm)	λ_{Exc} (nm)*	λ_{Em} (nm)	Stokes shift (cm^{-1})	Φ_F	log ε*
DMSO	500	n.d	512	469	0.022	5.30
Ethanol	498	505	511	511	0.02	NS
DMSO + TFA	504	503	516	461	0.35	4.84
Ethanol + TFA	502	501	515	503	0.29	NS

*NS = not studied; n.d = not detected

3.2. 4,4'-Difluoro-8-(4-bromophenyl)-1,3,5,7-tetramethyl-4-bora-3a,4a-diaza-*s*-indacene (1b)

3.2.1. Synthesis of BODIPY **1b**

BODIPY **1b**, a previously reported dye was synthesised for use in cyclodextrin inclusion complex formation.[155–160] The synthesis route was similar to that of BODIPY **1a** (**Scheme 11**).

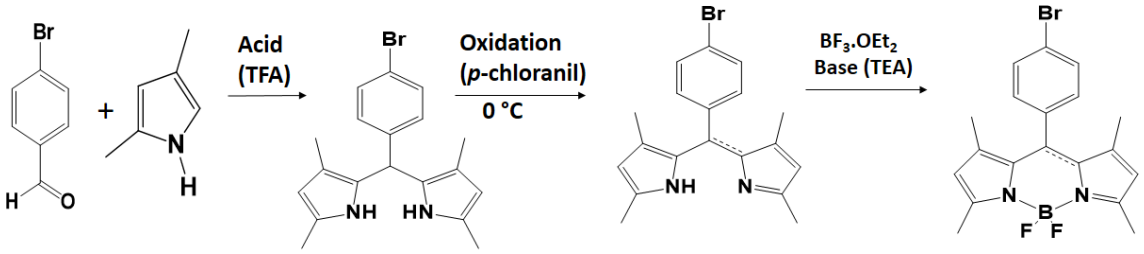

Scheme 11. Acid-catalysed one-pot synthesis of BODIPY **1b**.

3.2.2 Structural Analysis of BODIPY **1b**

The signals for all eighteen protons can be identified in the ^{1}H NMR spectrum. The doublets at 7.78–7.76 and 7.38–7.35 ppm each integrate to two protons can be assigned to the four phenyl protons. The twelve proton signals that lie at 1.37 and 2.44 ppm can be attributed to the twelve methyl protons on the pyrrole core. The signal at 6.20 ppm arises from the protons at the 2,6-positions of the BODIPY core. The FT-IR spectra contained the peaks anticipated for the BODIPY core.[150,151,153] Between 2850 and 2930 cm^{-1} there are bands attributed to the C-H stretch of the terminal methyl groups, whereas the N-C stretch bands corresponding to the pyrrolic nitrogen atoms lie in the 1040–1410 cm^{-1} region. The C-H stretch for the bonds at the 2,6-positions are observed at 470 cm^{-1}

3.2.3 Spectroscopic properties of BODIPY **1b**

The electronic absorption spectrum for BODIPY **1b** is typical of that of a *meso*-substituted BODIPY, with no signs of aggregation and with an absorbance maximum at 503 nm in DMSO, similar to a previously reported value.[151] The absorption, excitation and emission band maxima values in three different solvents are summarised below (**Table 2**) and the absorption, excitation and emission spectra in DMSO are also provided (**Figure 9**); the dye has an emission spectrum that is typical for a 1,3,5,7-tetramethyl BODIPY core. As can be seen from the fluorescence quantum yield values (**Table 2**), BODIPY **1b** is highly fluorescent as an intense fluorescence emission is observed. As with **1a,** the dye has a negligible singlet oxygen quantum yield, since there are no heavy atoms on the BODIPY core.

Table 2. Photophysical data for BODIPY **1b** in different organic solvents.

Solvent	**λ_{Abs} (nm)**	**λ_{Exc} (nm)**	**λ_{Em} (nm)**	**Stokes shift (cm^{-1})**	**Φ_F**	**log ε***
DMSO	503	503	516	501	0.83	4.52
Ethanol	501 (501[#]	503	513 (513)[#]	467	0.94	NS
Chloroform	504	504	516	461	0.83	NS

*NS = not studied

[#]Previously reported[157]

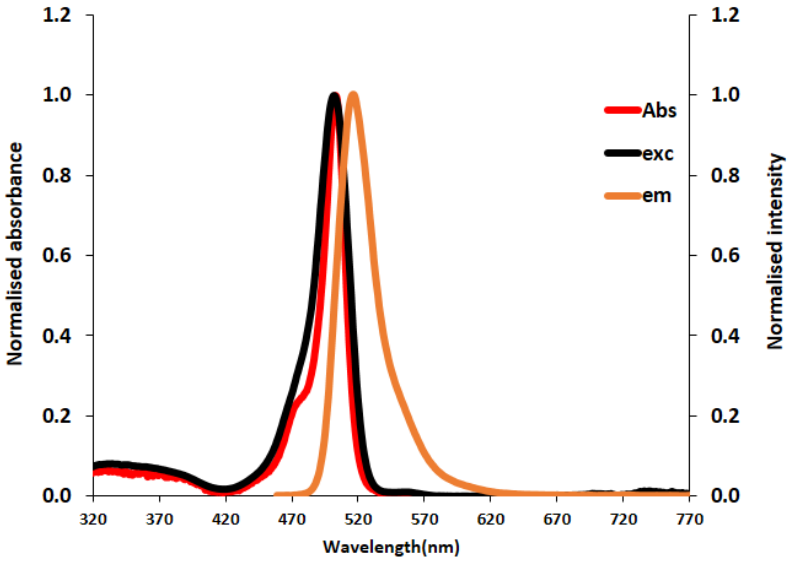

Figure 9. Normalised absorption (red), excitation (black) and emission (orange) spectra of BODIPY **1b** in DMSO.

3.3. **4,4'-Difluoro-8-(4-nitrophenyl)-1,3,5,7-tetramethyl-4-bora-3a,4a-diaza-*s*-indacene (1c)**

3.3.1. Synthesis of BODIPY **1c**

BODIPY **1c**, a previously reported dye was synthesised for use in cyclodextrin inclusion complex formation.[152,161] The synthesis route was similar to that of BODIPYs **1a** and **1b** (**Scheme 12**).

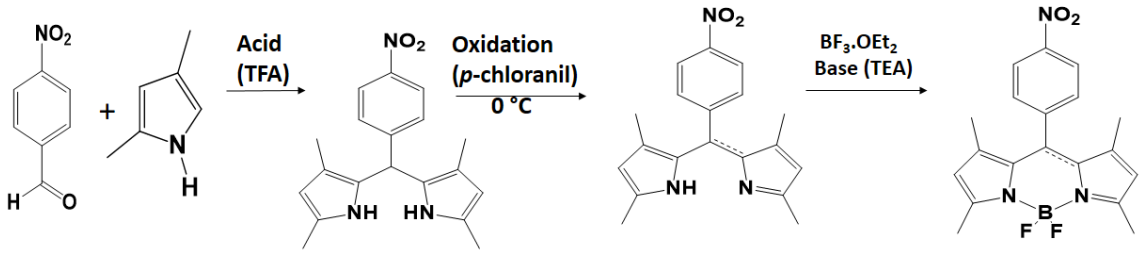

Scheme 12. Acid-catalysed one-pot synthesis of BODIPY **1c**.

3.3.2 Structural Analysis of BODIPY **1c**

The signals for all eighteen protons can be identified in the ^{1}H NMR spectrum. The doublets at 8.41–8.38 and 7.77–7.74 ppm each integrate to two protons can be assigned to the four phenyl protons. The twelve proton signals that lie at 1.34 and 2.46 ppm can be attributed to the twelve methyl protons on the pyrrole core. The signal at 6.22 ppm is for the protons at the 2,6-positions of the BODIPY core. The FT-IR spectra contained the peaks anticipated for the BODIPY core.[150,151,153] Between 2850 and 2920 cm^{-1} there are bands attributed to the C-H stretch of the terminal methyl groups, whereas the N-C stretch bands corresponding to the pyrrolic nitrogen atoms lie in the 1070–1410 cm^{-1} region. The C-H stretch for the bonds at the 2,6-positions are observed at 468 cm^{-1}.

3.3.3 Spectroscopic properties of BODIPY **1c**

The electronic absorption spectrum for BODIPY **1c** is typical of that of a *meso*-substituted BODIPY, with no signs of aggregation and with an absorbance maximum at 505 nm in DMSO. The absorption, excitation and emission band maxima values in DMSO are summarised below (**Table 3**) and the absorption, excitation and emission spectra are also provided (**Figure 10**); the dye has an emission spectrum that is typical for a 1,3,5,7-tetramethyl BODIPY core. As can be seen from the fluorescence quantum yield value (**Table 3**), BODIPY **1c** is not highly fluorescent and this can be attributed to the quenching effect of the nitro group which is known to strongly quench fluorescent dyes through what is suggested to be an electron-withdrawing effect.[161] As with **1a,** the dye has a negligible singlet oxygen quantum yield, since there are no heavy atoms on the BODIPY core.

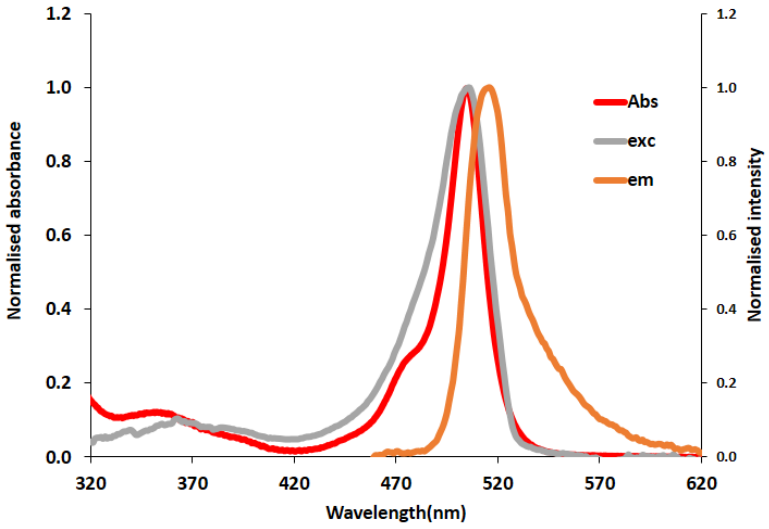

Figure 10. Normalised absorption (red), excitation (grey) and emission (orange) spectra of BODIPY **1c** in DMSO.

Table 3. Photophysical data for BODIPY **1c** in DMSO.

Solvent	λ_{Abs} (nm)	λ_{Exc} (nm)	λ_{Em} (nm)	Stokes shift (cm^{-1})	Φ_F	log ε
DMSO	505	506	514	347	0.05	4.77

3.4. 4,4'-Difluoro-8-(4-carbomethoxyphenyl)-1,3,5,7-tetramethyl-4-bora-3a,4a-diaza-*s*-indacene (1d)

3.4.1. Synthesis of BODIPY **1d**

BODIPY **1d**, a previously reported dye was synthesised as a precursor for a more complex BODIPY dye.[162–164] The synthesis route was similar to that of BODIPYs **1a**, **1b** and **1c** (**Scheme 13**).

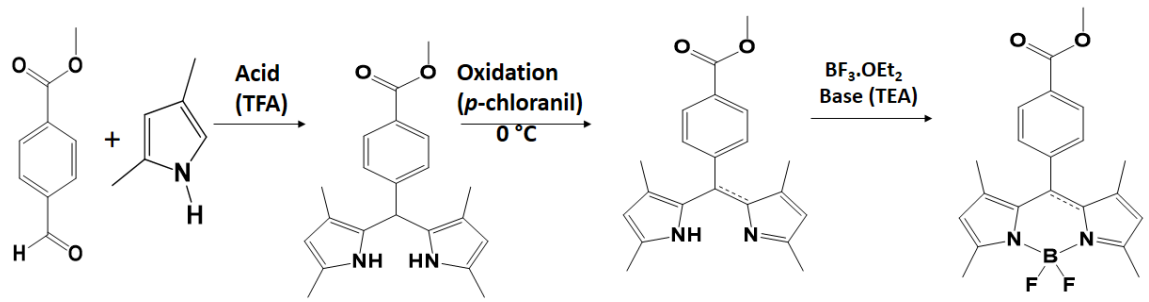

Scheme 13. Acid-catalysed one-pot synthesis of BODIPY **1d**.

3.4.2 Structural Analysis of BODIPY **1d**

The signals for all twenty-one protons can be identified in the ^{1}H NMR spectrum. The doublets at 8.14–8.11 and 7.58–7.55 ppm each integrate to two protons and can be assigned to the four phenyl protons. The twelve proton signals that lie at 1.32 and 2.45 ppm can be attributed to the twelve methyl protons on the pyrrole core. The signal at 6.20 ppm arises from the protons at the 2,6-positions of the BODIPY core. Finally, the signal at 3.90 ppm corresponds to the methyl protons of the ester group. The FT-IR spectra contained the peaks anticipated for the BODIPY core.[150,151,153] Between 2900 and 2960 cm^{-1} there are bands that can be attributed to the C-H stretch of the terminal methyl groups, whereas the N-C stretch bands corresponding to the pyrrolic nitrogen atoms lie in the 1180 cm^{-1} region. The C=O ester stretch is observed at 1712 cm^{-1}, whereas the C-O-C antisymmetric stretches lie at ca. 1277 and 1062 cm^{-1}. The C-H stretch for the bonds at the 2,6-positions is observed at 465 cm^{-1}.

3.4.3 Spectroscopic properties of BODIPY **1d**

The electronic absorption spectrum for BODIPY **1d** is typical of that of a *meso*-substituted BODIPY, with no signs of aggregation and with an absorbance maximum at 503 nm in DMSO. The absorption, excitation and emission band maxima values in three different

solvents are summarised below (**Table 4**) and the absorption, excitation and emission spectra in DMSO are also provided (**Figure 11**); the dye has an emission spectrum that is typical for a 1,3,5,7-tetramethyl BODIPY core. As can be seen from the fluorescence quantum yield values (**Table 4**), BODIPY **1d** is highly fluorescent as intense fluorescence emission is observed. As with **1a,** the dye has a negligible singlet oxygen quantum yield, since there are no heavy atoms on the BODIPY core.

Table 4. Photophysical data for BODIPY **1d** in DMSO and ethanol.

Solvent	**λ_{Abs} (nm)**	**λ_{Exc} (nm)**	**λ_{Em} (nm)**	**Stokes shift (cm^{-1})**	**Φ_F**	**log ε***
DMSO	503	503	518	576	0.59	4.42
Ethanol	501	500	514	505	0.39	NS

*NS = not studied

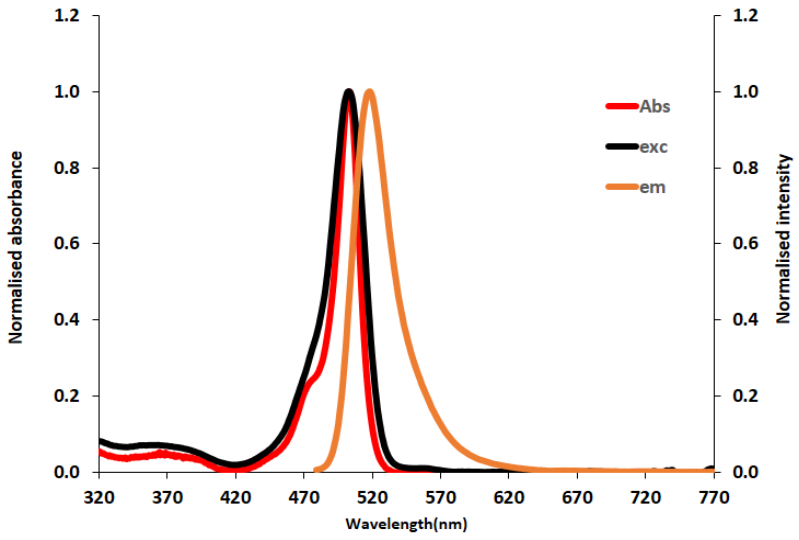

Figure 11. Normalised absorption (red), excitation (black) and emission (orange) spectra of BODIPY **1d** in DMSO.

3.5. 4,4'-Difluoro-8-(4-benzyloxyphenyl)-1,3,5,7-tetramethyl-4-bora-3a,4a-diaza-*s*-indacene (1e)

3.5.1. Synthesis of BODIPY **1e**

BODIPY **1e** was synthesised as a precursor for two more complex BODIPY dyes intended for use in optical limiting applications. The synthesis route was similar to that of BODIPYs **1a**, **1b**, **1c** and **1d** (**Scheme 14**)

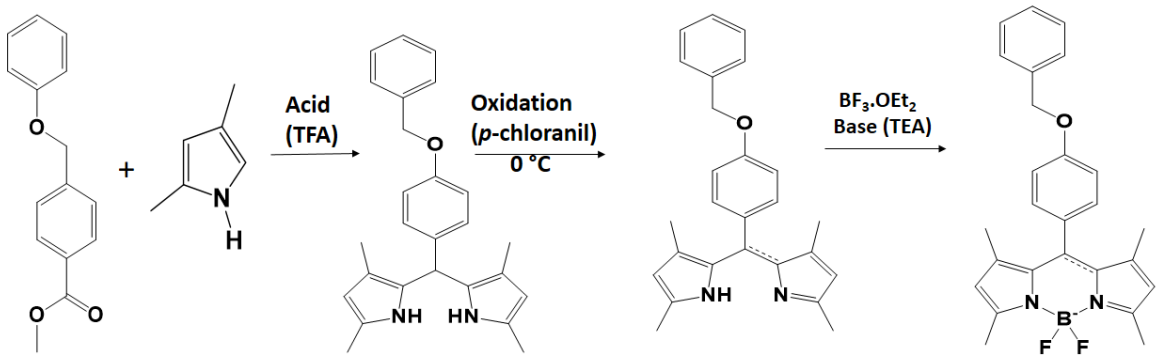

Scheme 14. Acid-catalysed one-pot synthesis of BODIPY **1e**.

3.5.2 Structural Analysis of BODIPY **1e**

All twenty-five protons can be identified in the ^{1}H NMR spectrum of BODIPY **1e**. The protons of the benzyloxy phenyl ring appear as a doublet at 7.49 ppm, a triplet at 7.38 ppm and another triplet at 7.43 ppm, integrating to two, one and two protons, respectively. The two CH_2 protons adjacent to the oxygen atom of the benzyloxy group appear at 5.14 ppm. The doublet signal at 7.20–7.19 ppm integrates to two protons and represents two of the *meso*-phenyl ring protons, with the remaining *meso*-phenyl ring protons appearing as a doublet integrating to two protons, at 7.12–7.10 ppm. The two protons at the 2,6-positions appear as a singlet at 6.0 ppm. The singlets at 2.14 and 1.45 ppm each integrate to six protons, representing the four methyl groups on the BODIPY core. The FT-IR spectrum of BODIPY **1e**

contained the peaks anticipated for the BODIPY core.[150,151,153] Between 2920 and 2850 cm^{-1} there are bands attributed to the C-H stretch of the terminal methyl groups, whereas the N-C stretch bands corresponding to the pyrrolic nitrogen atoms lie in the 1070–1460 cm^{-1} region. The C-O-C stretch for the benzyloxy ether group is observed at 1102 cm^{-1}. The C-H stretch for the bonds at the 2,6-positions lies at 468 cm^{-1}.

3.5.3 Spectroscopic properties of BODIPY **1e**

Spectroscopic characterisation of BODIPY **1e** was not carried out, as for the purposes of this thesis, there was no intended application for it but it was only used as a starting reagent in the syntheses of BODIPYs **2e** and **5**.

3.6. 4,4'-Difluoro-8-(3-bromo-4-dimethylaminophenyl)-1,3,5,7-tetramethyl-2,6-dibromo-4-bora-3a,4a-diaza-*s*-indacene (2a)

3.6.1. Synthesis of BODIPY **2a**

Halogenation has long been known to be employed in red-shifting the main spectral band of BODIPY dyes, with the 2,6-positions of the tetramethyl BODIPY core being the most vulnerable to electrophilic attack. BODIPY **2a**, a new BODIPY dye was synthesised from BODIPY **1a** using NBS (**Scheme 15**).

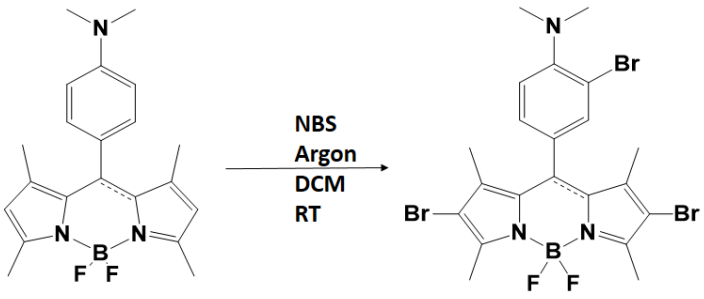

Scheme 15. Synthesis of the brominated BODIPY **2a**.

BODIPY **1a** and NBS were stirred together in DCM under argon and the reaction monitored by TLC. The duration of the reaction was very short due to the high reactivity of NBS. The aim was to brominate the 2,6-positions only but upon structural characterisation, an additional bromine was found to be present in the *meso*-phenyl ring.

3.6.2 Structural Analysis of BODIPY **2a**

All twenty-one protons can be identified in the ^{1}H NMR spectrum of BODIPY **2a** (**Figure 12**). The doublet at 7.40–7.39 ppm integrates as two protons and is attributed to two phenyl protons; whereas the singlet at 7.69 ppm is representative of the remaining phenyl proton. The singlet at 2.89 ppm is attributed to the six methyl group protons of the dimethylamino group. The singlets at 2.56 and 1.50 ppm each integrate to six protons, representing the four methyl groups on the BODIPY core. The absence of a singlet at 6.22 ppm confirms that the hydrogen atoms at the 2,6-positions of BODIPY **1a** have been replaced with bromine atoms. In the FT-IR spectrum of BODIPY **2a**, similar vibrations to that of BODIPY **1a** are observed. The appearance of a peak at 522 cm^{-1} confirms bromination, since the peak can be attributed to the C-Br stretch associated with bromination of the 2,6-positions of the BODIPY core. The predicted molecular mass of 603.93 amu for BODIPY **2a** was confirmed by MALDI-TOF mass spectrometry as the primary peak occurred at 605.9 amu (+ $1H^{+}$) (**Figure 13**).

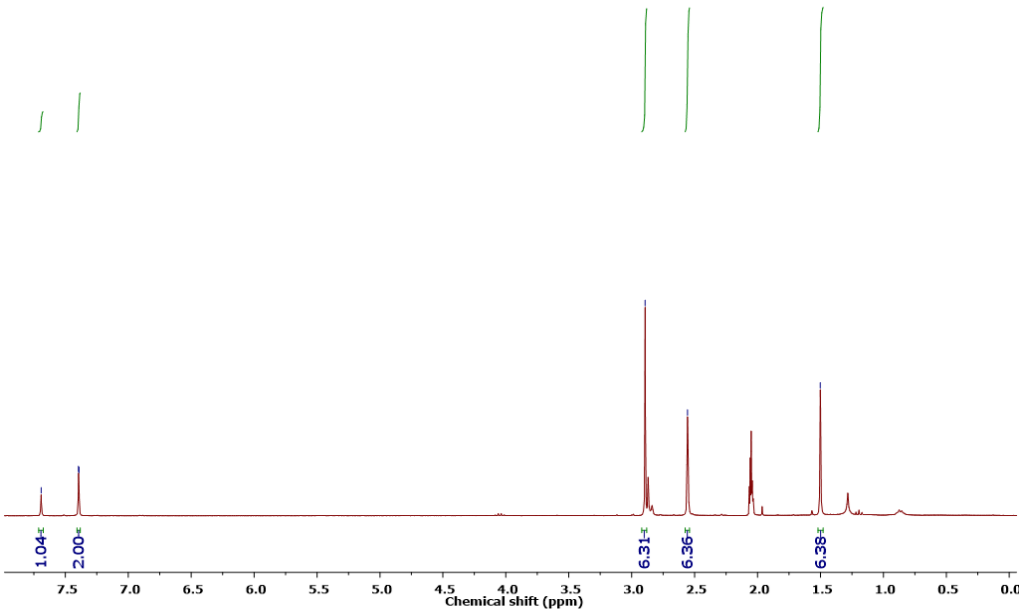

Figure 12. ^{1}H NMR spectrum of BODIPY **2a** in acetone-d_6.

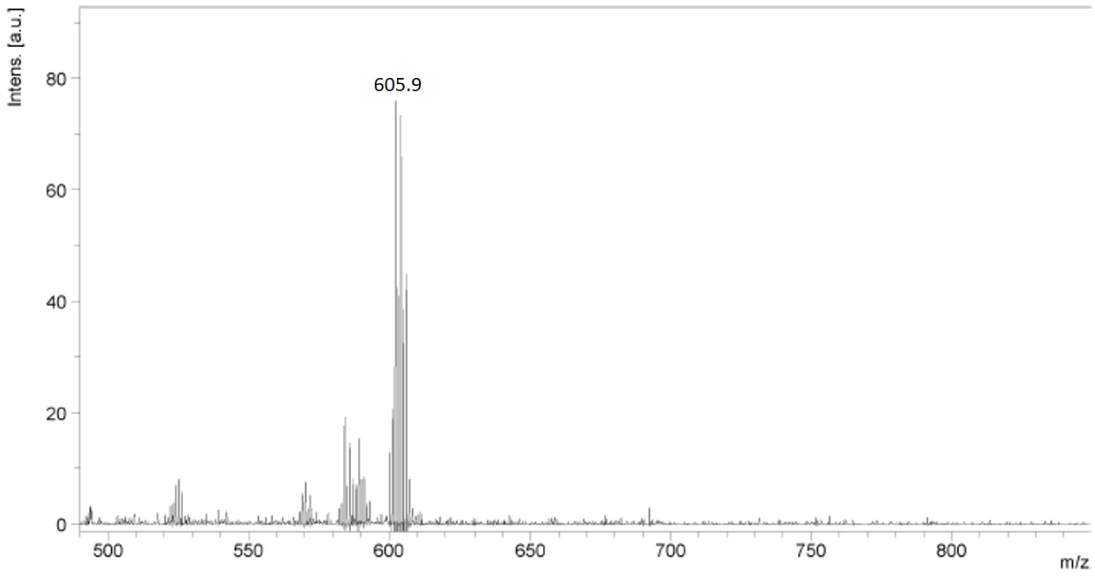

Figure 13. Mass spectrum of BODIPY **2a** with the primary peak at 605.9 (**2a** + 1H^{+}).

3.6.3 Spectroscopic properties of BODIPY **2a**

The electronic absorption spectrum for BODIPY **2a** is typical of that of a tetramethyl substituted BODIPY containing heavy atoms at the 2,6-positions, as can be seen in the absorbance maximum at 534 nm in DCM. The absorption, excitation and emission band

maxima values in different solvents are summarised below (**Table 5**) in the absence and presence of TFA; the absorption, excitation and emission spectra in DMSO in the presence of TFA are also provided and show no signs of aggregation (**Figure 14**). Upon protonation, the absorption and emission spectra in DCM exhibit 4 and 14 nm red shifts, respectively.

Table 5. Photophysical data for BODIPY **2a** in different organic solvents.

Solvent	λ_{Abs} (nm)	λ_{Exc} (nm)	λ_{Em} (nm)	Stokes shift (cm^{-1})	Φ_F	τ_F (ns)*	log ε*	Φ_Δ*
DCM	534	537	546	412	0.04	2.23	NS	NS
DCM + TFA	538	540	560	730	0.22	2.42	NS	NS
DMSO	529	532	552	788	0.19	1.98	5.30	NS
DMSO + TFA	528	532	552	824	0.19	1.37	5.34	0.81
Ethanol	527	531	549	760	0.29	NS	NS	NS
Ethanol + TFA	530	531	549	653	0.27	NS	NS	0.64

*NS = not studied

As can be seen from the fluorescence quantum yield values (**Table 5**), BODIPY **2a** only fluoresces in the presence of TFA in the less polar DCM but in the more polar ethanol and DMSO it is significantly fluorescent even when no TFA is added to eliminate intramolecular charge transfer from the nitrogen lone pairs into the BODIPY core (albeit possessing lower fluorescence than BODIPY **1a** due to the presence of bromines as heavy atoms). The dye has significant singlet oxygen quantum yield values; this was studied using the comparative

method and the dye degraded the singlet oxygen quencher DPBF, as is expected since there are heavy atoms on the BODIPY core, thereby increasing the rate of intersystem crossing to the triplet manifold.

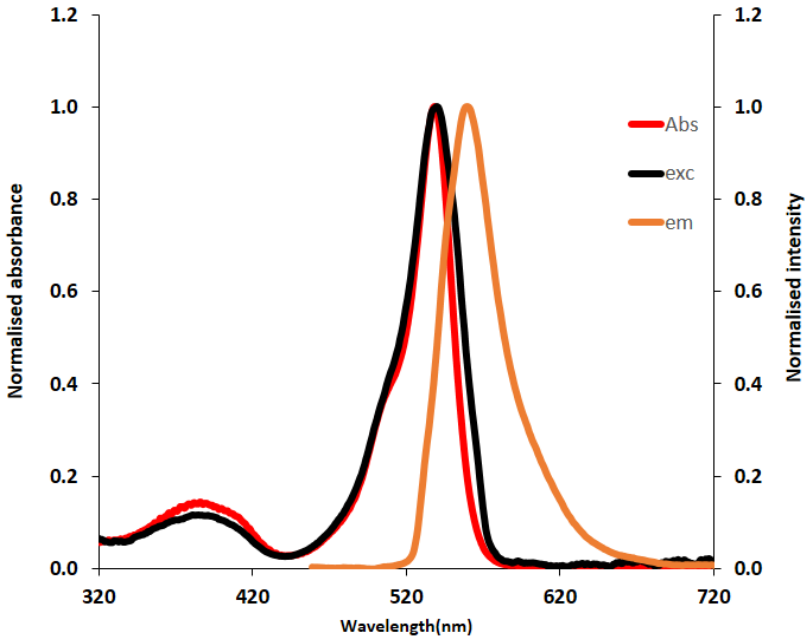

Figure 14. Normalised absorption (red), excitation (black) and emission (orange) spectra of BODIPY **2a** in DCM.

3.7. 4,4'-Difluoro-8-(4-bromophenyl)-1,3,5,7-tetramethyl-2,6-dibromo-4-bora-3a,4a-diaza-*s*-indacene (2b)

3.7.1. Synthesis of BODIPY **2b**

In a similar manner to BODIPY **2a**, BODIPY **2b**, a previously reported dye was synthesised from BODIPY **1b** (**Scheme 16**) by using NBS.[160,165]

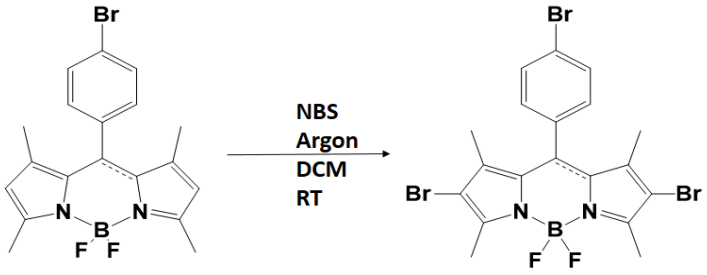

Scheme 16. Synthesis of the 2,6-dibrominated BODIPY **2b**.

3.7.2 Structural Analysis of BODIPY **2b**

All sixteen protons can be identified the ^{1}H NMR spectrum of BODIPY **2b**. The doublets at 7.82–7.80 and 7.44–7.41 ppm each integrate as two protons and can be attributed to the four phenyl protons. The singlets at 2.52 and 1.37 ppm each integrate to six protons, representing the four methyl groups on the BODIPY core. The absence of the singlet at 6.20 ppm confirms that the hydrogen atoms at the 2,6-positions of BODIPY **1b** have been replaced with bromine atoms. In the FT-IR spectrum of BODIPY **2b**, similar vibrations to that of BODIPY **1b** are observed. The appearance of a peak at 523 cm^{-1} confirms bromination, since this peak can be attributed to the C-Br stretch associated with bromination of the 2,6-positions of the BODIPY core. The predicted molecular mass of 560.86 amu for BODIPY **2b** was confirmed by MALDI-TOF mass spectrometry as the primary peak occurred at 562.63 amu (+ $1H^{+}$).

3.7.3 Spectroscopic properties of BODIPY **2b**

The electronic absorption spectrum for BODIPY **2b** is typical of that of a tetramethyl substituted BODIPY containing heavy atoms, as can be seen in the absorbance maximum at 529 nm in DMSO. The absorption, excitation and emission band maxima values in different

solvents are summarised below (**Table 6**) and the absorption, excitation and emission spectra in ethanol are also provided and show no signs of aggregation (**Figure 15**).

Table 6. Photophysical data for BODIPY **2b** in different organic solvents.

Solvent	λ_{Abs} (nm)	λ_{Exc} (nm)	λ_{Em} (nm)	Stokes shift (cm^{-1})	Φ_F	τ_F (ns)*	log ε*	Φ_Δ*
DCM	531 (528) #	530	547 (551) #	551	0.44 (0.08)#	1.48	NS	NS
DMSO	529	529	548	655	0.25	1.44	4.65	0.57
Ethanol	528	526	544	557	0.36	1.48	NS	NS

*NS = not studied

#Previously reported[165]

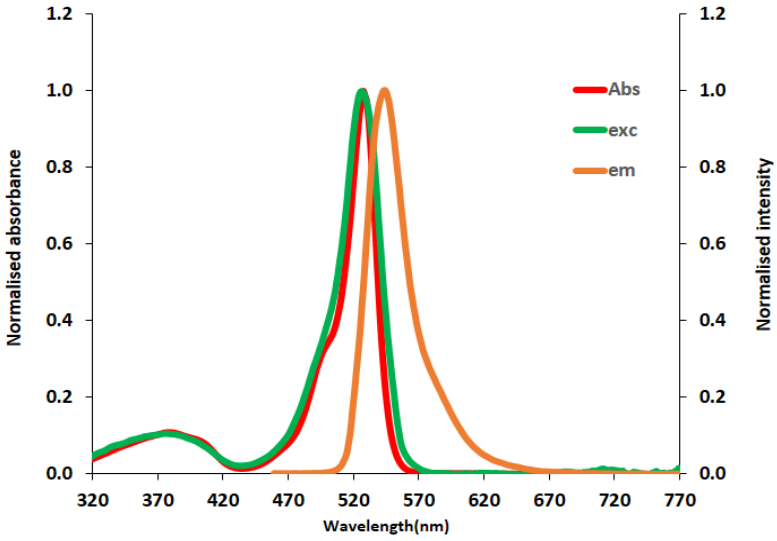

Figure 15. Normalised absorption (red), excitation (green) and emission (orange) spectra of BODIPY **2b** in ethanol.

BODIPY **2b** has moderately high fluorescence quantum yields albeit with a lower quantum yield than BODIPY **1b** due to the presence of the heavy atoms. As with **2a**, the dye has a significant singlet oxygen quantum yield value, since there are heavy atoms on the BODIPY core and this enhances the rate of intersystem crossing to the triplet manifold.

3.8. 4,4'-Difluoro-8-(4-nitrophenyl)-1,3,5,7-tetramethyl-2,6-dibromo-4-bora-3a,4a-diaza-*s*-indacene (2c)

3.8.1. Synthesis of BODIPY **2c**

In a similar manner to BODIPYs **2a** and **2b**, BODIPY **2c** was synthesised from BODIPY **1c** (**Scheme 17**) by using NBS.

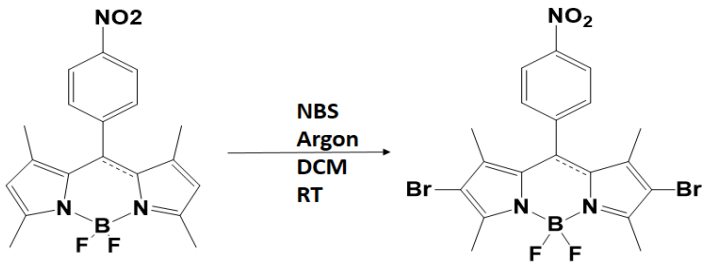

Scheme 17. Synthesis of the 2,6-dibrominated BODIPY **2c**.

3.8.2 Structural Analysis of BODIPY **2c**

All sixteen protons can be identified in the ^{1}H NMR spectrum of BODIPY **2c**. The doublets at 8.57–8.56 and 7.68–7.66 ppm each integrate as two protons and can be attributed to the four phenyl protons. The singlets at 2.76 and 1.50 ppm each integrate to six protons, representing the four methyl groups on the BODIPY core. The absence of the singlet at 6.22 ppm confirms that the hydrogen atoms present at the 2,6-positions of BODIPY **1c** have been replaced with bromine atoms. In the FT-IR spectrum of BODIPY **2c**, similar vibrations to that of BODIPY **1c** are also observed. The appearance of a peak at 531 cm^{-1} confirms

bromination; the peak can be attributed to the C-Br stretch associated with bromination of the 2,6-positions of the BODIPY core. The predicted molecular mass of 526.97 amu for BODIPY **2c** was confirmed by MALDI-TOF mass spectrometry as the primary peak occurred at 526.2 amu.

3.8.3 Spectroscopic properties of BODIPY **2c**

The electronic absorption spectrum for BODIPY **2c** is typical of that of a tetramethyl substituted BODIPY containing heavy atoms, as can be seen in the absorbance maximum at 532 nm in DMSO. The absorption, excitation and emission band maxima values in different solvents are summarised below (**Table 7**) and the absorption, excitation and emission spectra in DCM are also provided and show no signs of aggregation (**Figure 16**). BODIPY **2c** has moderately high fluorescence quantum yields in DCM and ethanol, while in the more polar DMSO the low fluorescence quantum yield value is not significantly different to that of BODIPY **1c**. As with **2a**, the dye has a significant singlet oxygen quantum yield value in DMSO, since there are heavy atoms on the BODIPY core.

Table 7. Photophysical data for BODIPY **2c** in different organic solvents.

Solvent	λ_{Abs} (nm)	λ_{Exc} (nm)	λ_{Em} (nm)	Stokes shift (cm^{-1})	Φ_F	τ_F (ns)*	log ε*	Φ_Δ*
DCM	535	534	555	674	0.33	1.3	NS	NS
DMSO	532	n.d	556	811	0.04	0.56	5.30	0.64
Ethanol	530	530	551	719	0.23	n.d	NS	NS

*NS = not studied; *n.d = not detected

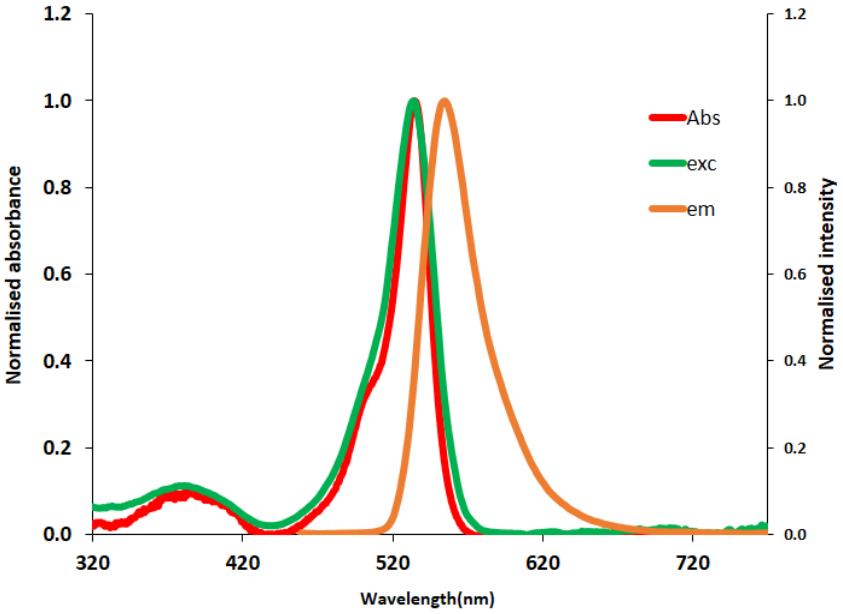

Figure 16. Normalised absorption (red), excitation (green) and emission (orange) spectra of BODIPY **2c** in DCM.

3.9. 4,4'-Difluoro-8-(4-carbomethoxyphenyl)-1,3,5,7-tetramethyl-2,6-dibromo-4-bora-3a,4a-diaza-*s*-indacene (2d)

3.9.1. Synthesis of BODIPY **2d**

In a similar manner to BODIPYs **2a**, **2b** and **2c**, BODIPY **2d** was synthesised from BODIPY **1d** (**Scheme 18**) by using NBS.

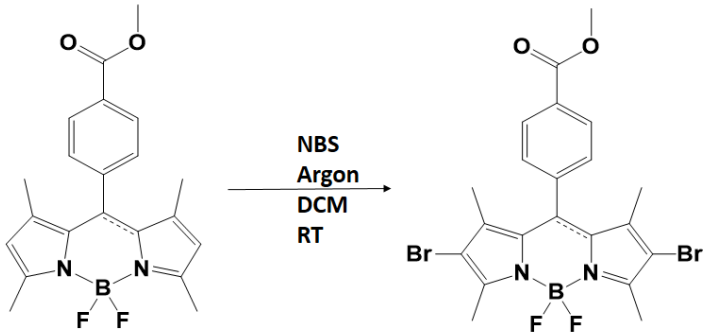

Scheme 18. Synthesis of the 2,6-dibrominated BODIPY **2d**.

3.9.2 Structural Analysis of BODIPY **2d**

All nineteen protons can be identified in the ^{1}H NMR spectrum of BODIPY **2d**. The doublets at 8.16–8.14 and 7.64–7.61 ppm each integrate as two protons and can be attributed to the four phenyl protons. The signal at 3.91 integrates to three protons, representing the three methyl group protons on the ester group. The singlets at 2.52 and 1.31 ppm each integrate to six protons, representing the four methyl groups on the BODIPY core. The absence of the singlet at 6.20 ppm confirms that the hydrogen atoms present at the 2,6-positions of BODIPY **1d** have been replaced with bromine atoms. In the FT-IR spectrum of BODIPY **2d**, similar vibrations to that of BODIPY **1d** are observed. The appearance of a peak at 532 cm^{-1} confirms bromination, since the peak can be attributed to the C-Br stretch associated with bromination of the 2,6-positions of the BODIPY core. The predicted molecular mass of 539.99 amu for BODIPY **2d** was confirmed by MALDI-TOF mass spectrometry as the primary peak occurred at 541.27 amu (+ $1H^{+}$).

3.9.3 Spectroscopic properties of BODIPY **2d**

The electronic absorption spectrum for BODIPY **2d** is typical of that of a tetramethyl substituted BODIPY containing heavy atoms, as can be seen in the absorbance maximum at 530 nm in DMSO. The absorption, excitation and emission band maxima values in different solvents are summarised below (**Table 8**) and the absorption, excitation and emission spectra in ethanol are also provided and show no signs of aggregation (**Figure 17**). BODIPY **2d** has moderately high fluorescence quantum yields. As with **2a**, the dye has a significant singlet oxygen quantum yield value, since there are heavy atoms on the BODIPY core.

Table 8. Photophysical data for BODIPY **2d** in different organic solvents.

Solvent	λ_{Abs} (nm)	λ_{Exc} (nm)	λ_{Em} (nm)	Stokes shift (cm^{-1})	Φ_F	τ_F (ns)*	log ε*	Φ_Δ*
DCM	531	530	548	584	0.36	1.78	NS	NS
DMSO	530	530	549	653	0.20	1.33	5.0	0.4
Ethanol	528	527	546	624	0.26	NS	NS	0.73

*NS = not studied

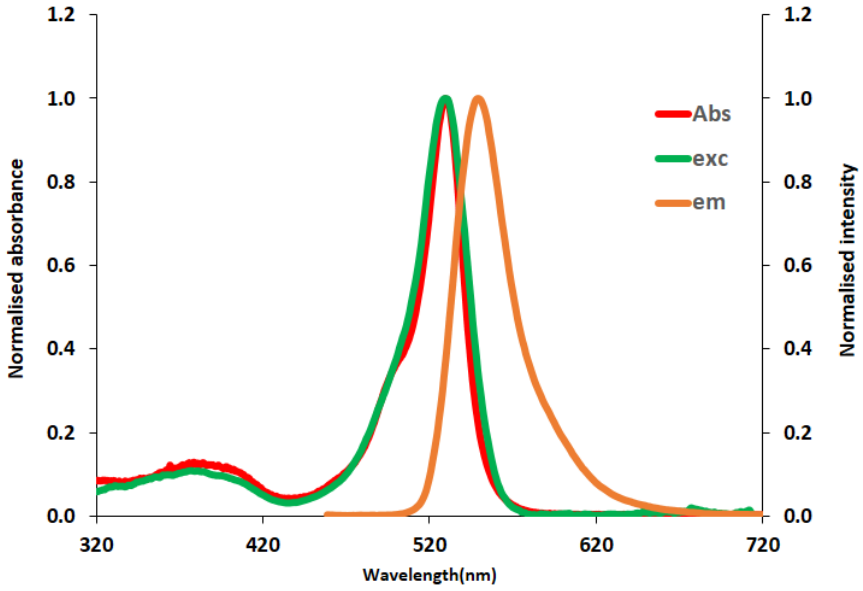

Figure 17. Normalised absorption (red), excitation (green) and emission (orange) spectra of BODIPY **2d** in ethanol.

3.10. 4,4'-Difluoro-8-(4-benzyloxyphenyl)-1,3,5,7-tetramethyl-2,6-dibromo-4-bora-3a,4a-diaza-*s*-indacene (2e)

3.10.1. Synthesis of BODIPY **2e**

In a similar manner to BODIPYs **2a**, **2b**, **2c** and **2d**, BODIPY **2e** was synthesised from BODIPY **1e** (**Scheme 19**) using NBS.

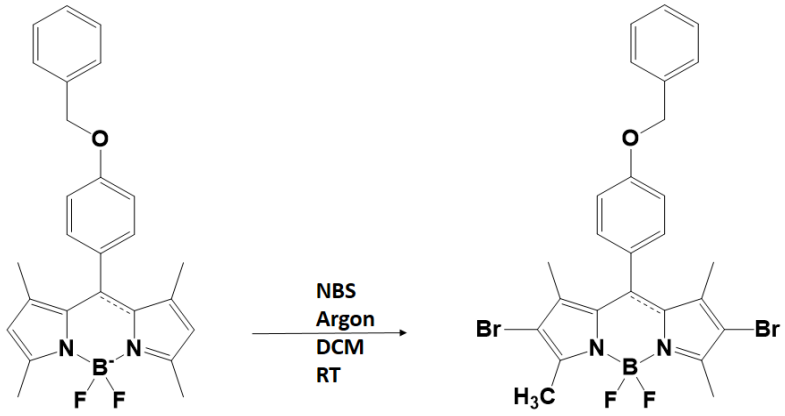

Scheme 19. Synthesis of the 2,6-dibrominated BODIPY **2e**.

3.10.2 Structural Analysis of BODIPY **2e**

All twenty-three protons can be identified in the ^{1}H NMR spectrum of BODIPY **2e**. The protons of the benzyloxy phenyl ring appear as a doublet of doublets at 7.16–7.11 ppm and a triplet at 7.43–7.42 ppm, integrating to three and two protons, respectively. The two CH_2 protons adjacent to the oxygen atom of the benzyloxy group lie at 5.17 ppm. The doublet signal at 7.48 ppm integrates to two protons and represents two of the *meso*-phenyl ring protons, with the remaining *meso*-phenyl ring protons appearing as a multiplet integrating to two protons, at 7.4–7.37 ppm. The singlets at 2.61 and 1.43 ppm each integrate to six protons, representing the four methyl groups on the BODIPY core. The predicted molecular mass of 588.09 amu for BODIPY **2e** was confirmed by MALDI-TOF mass spectrometry as the

primary peak occurred at 588.3 amu. In the FT-IR spectrum of BODIPY **2e**, similar vibrations to that of BODIPY **1e** are observed. The appearance of a peak at 527 cm^{-1} confirms bromination, since the peak can be attributed to the C-Br stretch associated with bromination of the 2,6-positions of the BODIPY core.

3.10.3 Spectroscopic properties of BODIPY **2e**

Spectroscopic characterisation of BODIPY **2e** was not carried out for the purposes of this thesis, since there was no intended applications for it but it was only used as a starting reagent in the synthesis of BODIPY **6**.

3.11. **4,4'-Difluoro-8-(4-carbomethoxyphenyl)-1,5,7-trimethyl-2,6-dibromo-3-mono-styryl-(4-dimethylamino)-4-bora-3a,4a-diaza-*s*-indacene (3)**

Substitution at any of the acidic methyl groups typically red-shifts the main absorption bands of the BODIPY dye due to delocalisation of the π-system. Additionally, the dimethylamino group used here was intended for use in pH sensing applications.

3.11.1. Synthesis of BODIPY **3** (**Scheme 20**)

BODIPY **3** was synthesised using a modified Knoevenagel condensation reaction. BODIPY **2d** and 4-dimethylaminobenzaldehyde were dissolved in dry benzene with piperidine added to initiate the condensation; the reaction was heated to reflux for 48 h and allowed to continue under argon with stirring, with constant monitoring using TLC. A Dean-Stark trap was used for the azeotropic removal of water formed as a by-product during the condensation reaction. The solution changed colour from orange-red to semi-dark green. A di-styryl-BODIBPY was expected to form but when left for longer, the product decomposed

into a dark brown mixture. BODIPY **3** was obtained by column chromatography by using ethyl acetate:petroleum ether (1:4) as the eluent.

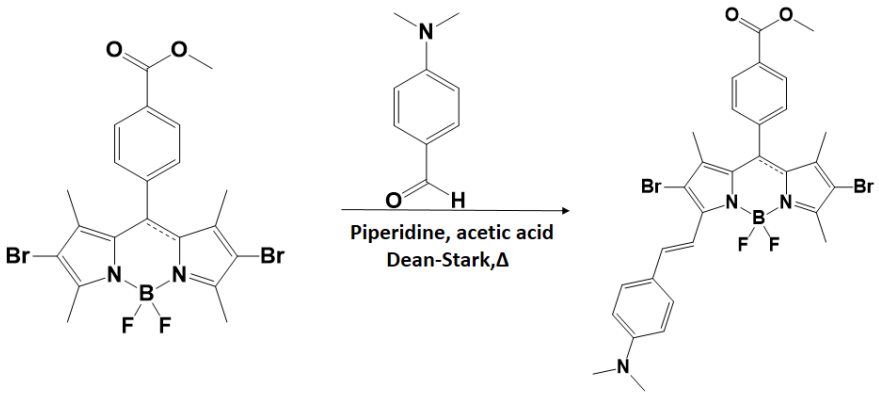

Scheme 20. Knoevenagel condensation to form BODIPY **3**.

3.11.2 Structural Analysis of BODIPY **3**

All twenty-eight protons can be identified in the ^{1}H NMR spectrum of BODIPY **2d** (**Figure 18**). The doublet of doublets at 8.19–8.14 ppm integrates as four protons and can be attributed to the four phenyl protons of the styryl group. The doublet of doublets at 7.55–7.50 ppm integrates as four protons and can be attributed to the four phenyl protons of *meso*-substituent. The signal at 7.39–7.37 is a doublet and integrates to the two protons of the bridging alkene between the styryl group and the core. The signal at 3.97 ppm integrates to three protons, representing the three methyl group protons on the ester group. The signal at 3.04 ppm integrates to six protons, representing the six dimethylamino group protons on the styryl ring. The singlets at 2.62, 1.36 and 1.32 ppm each integrate to three protons, representing the three methyl groups on the BODIPY core. The predicted molecular mass of 671.18 amu for BODIPY **3** was confirmed by MALDI-TOF mass spectrometry as the primary peak occurred at 673.96 amu (+ $2H^{+}$) (**Figure 19**). The FT-IR spectra were as expected for the BODIPY skeleton.[150,151,153] At ca. 2850 cm^{-1} there are bands attributed to the C-H stretch of

the terminal methyl groups attached to the BODIPY core, whereas the N-C stretch bands corresponding to both the pyrrolic nitrogen atoms and the styryl dimethylamino moiety lie in the 1060–1435 cm^{-1} region. The C=O ester stretch is observed at ca. 1715 cm^{-1}, whereas the C-O-C antisymmetric stretches are observed at 1163 and 1106 cm^{-1}. The C-Br stretch for the bonds at the 2,6-positions lie at 516 cm^{-1}.

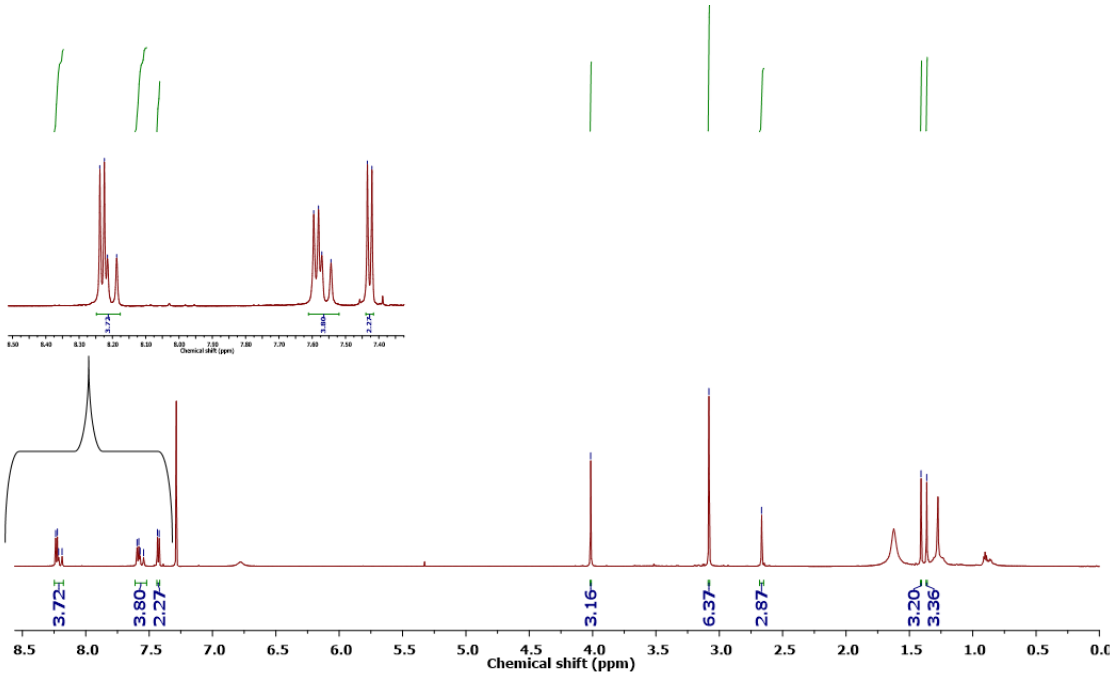

Figure 18. ^{1}H NMR spectrum of BODIPY **3** in $CDCl_3$.

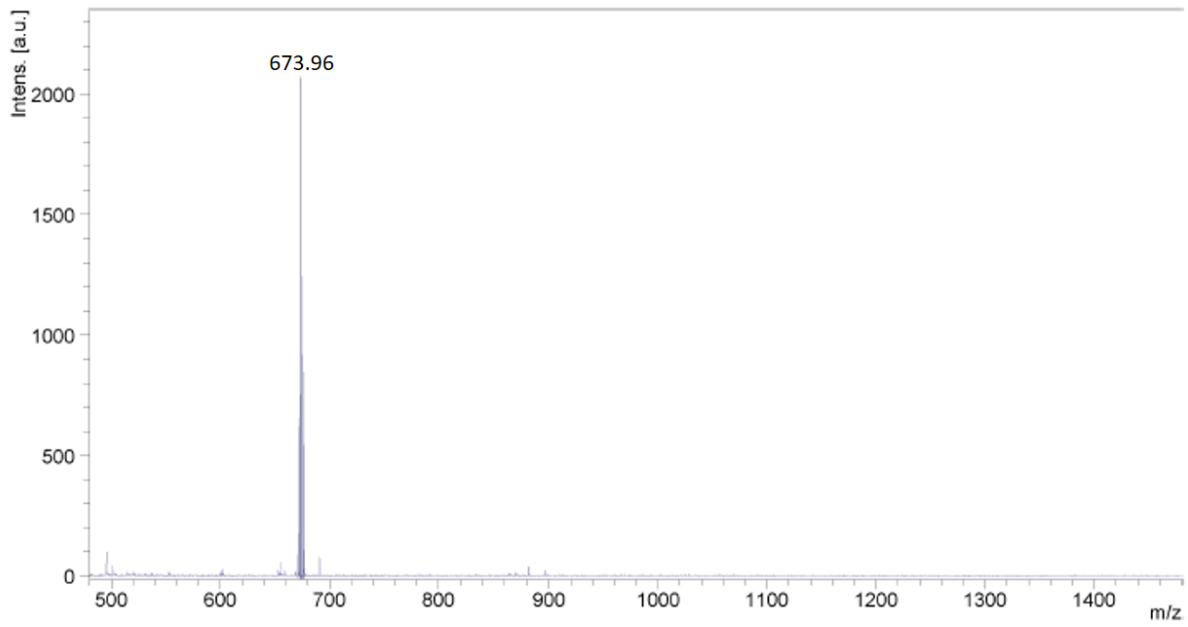

Figure 19. Mass spectrum of BODIPY **3** with the primary peak at 673.96 (**3** + $1H^+$).

3.12. **4,4'-Difluoro-8-(4-benzyloxyphenyl)-1,7-dimethyl-3-di-styryl-(4-benzyloxyphenyl)-4-bora-3a,4a-diaza-*s*-indacene (5)**

As previously mentioned, the substitution of any of the acidic methyl groups typically red-shifts the main absorption bands of the BODIPY dye due to delocalisation of the π-system and this is helpful in the intended application of BODIPY **5** which is optical limiting.

3.12.1. Synthesis of BODIPY **5** (**Scheme 21**)

BODIPY **5** was synthesised from BODIPY **1e** using a modified Knoevenagel condensation reaction. The solution changed colour from orange-red to deep ink-blue and when left for longer periods, the colour changes to green indicating the formation of a di-styryl-BODIPY from the blue mono-styryl. BODIPY **5** was obtained by column chromatography by using ethyl acetate:petroleum ether (1:4) as the eluent.

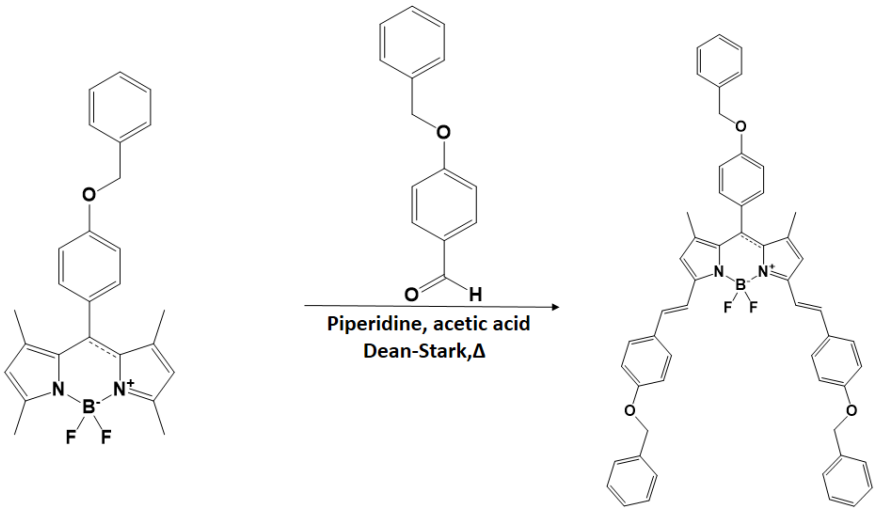

Scheme 21. Knoevenagel condensation to form BODIPY **5**.

3.12.2 Structural Analysis of BODIPY **5**

All forty-five protons can be identified in the ^{1}H NMR spectrum of BODIPY **5**. The singlet at 7.60 ppm integrates as four protons and can be attributed to four protons from the phenyl of the benzyloxy on the styryl group. The doublet at 7.47 ppm integrates as five protons and can be attributed to the five protons of the benzyloxy group. The singlet at 7.42 ppm integrates as twelve protons and can be attributed to the three phenyl rings of the benzyloxy group, each with four protons and close to the BODIPY core. The doublet at 7.22–7.20 ppm integrates as three protons and can be attributed to three protons on one of the phenyl rings of the benzyloxy group; these are the furthest protons from the BODIPY core. The singlet at 7.11 ppm integrates as two protons and can be attributed to one of the bridging alkenes between the styryl group and the core; with the second set integrating as two protons at 6.92 ppm. The singlet at 7.02 ppm integrates as three protons and can be attributed to the remaining three protons on one of the phenyl rings of the benzyloxy group. The protons at the 2,6-positions appear as a singlet which integrates to two protons, at 6.62 ppm. The singlet signal at 5.13 ppm integrates to four protons and is assigned to the

CH_2 protons adjacent to the oxygen atoms of the benzyloxy groups on the styryls; while the third CH_2 group which is of the benzyloxy group appears as a singlet integrating to two protons, at 5.03 ppm. The final signal at 1.59 ppm is a singlet which integrates to six protons, representing the two methyl groups on the BODIPY core. The predicted molecular mass of 818.35 amu for BODIPY **5** was confirmed by MALDI-TOF mass spectrometry as the primary peak occurred at 818.93 amu. In the FT-IR spectrum of BODIPY **5**, similar vibrations to that of BODIPY **1e** are also observed.

3.12.3 Spectroscopic properties of BODIPY **5**

The electronic absorption spectrum for BODIPY **5** is typical of that of a di-styryl substituted BODIPY, as can be seen in the absorbance maximum at 649 nm in DMSO. The absorption, excitation and emission band maxima values in different solvents are summarised below (**Table 9**) and the absorption, excitation and emission spectra in DMSO are also provided and show no signs of aggregation (**Figure 20**). The relatively intense absorption bands in the 300–400 nm region are believed to be associated with the benzyloxy substituents.

Table 9. Photophysical data for BODIPY **5** in DCM and DMSO.

Solvent	λ_{Abs} (nm)	λ_{Exc} (nm)	λ_{Em} (nm)	Stokes shift (cm^{-1})	Φ_F	τ_F (ns)	log ε
DCM	643	644	657	331	0.15	3.23	4.68
DMSO	649	649	665	371	0.13	3.74	5.23

BODIPY **5** has a relatively low but significant fluorescence quantum yield value. No singlet oxygen generation was observed when the comparative method was used with DPBF as the scavenger, due to the absence of heavy atoms to promote intersystem crossing.

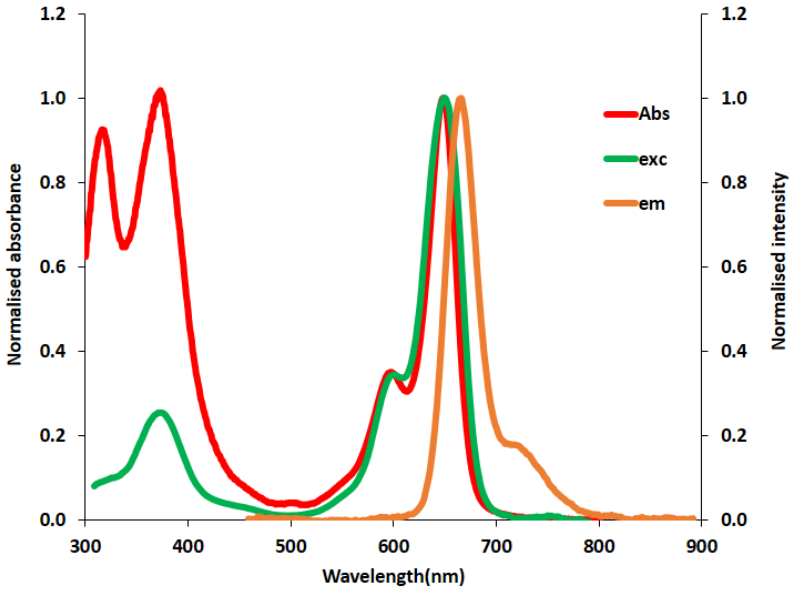

Figure 20. Normalised absorption (red), excitation (green) and emission (orange) spectra of BODIPY **5** in DMSO.

3.13. **4,4'-Difluoro-8-(4-benzyloxyphenyl)-1,7-dimethyl-2,6-dibromo-3-di-styryl-(4-benzyloxyphenyl)-4-bora-3a,4a-diaza-*s*-indacene (6)**

As previously mentioned, the substitution of any of the acidic methyl groups typically red-shifts the main absorption bands of the BODIPY dye due to delocalisation of the π-system and this is useful in the intended application of BODIPY **6** which is optical limiting. Also, it should be noted that the presence of the bromines as heavy atoms serves a function in studying the optical limiting applications (Chapter 4).

3.13.1. Synthesis of BODIPY **6** (**Scheme 22**)

BODIPY **6** was synthesised from BODIPY **2e** by using a modified Knoevenagel condensation reaction. The solution changed colour from orange-red to deep ink-blue and when left for longer periods, the colour changes to green indicating the formation of a di-styryl-BODIPY from the blue mono-styryl dye. BODIPY **6** was obtained by column chromatography by using ethyl acetate:petroleum ether (1:4) as the eluent.

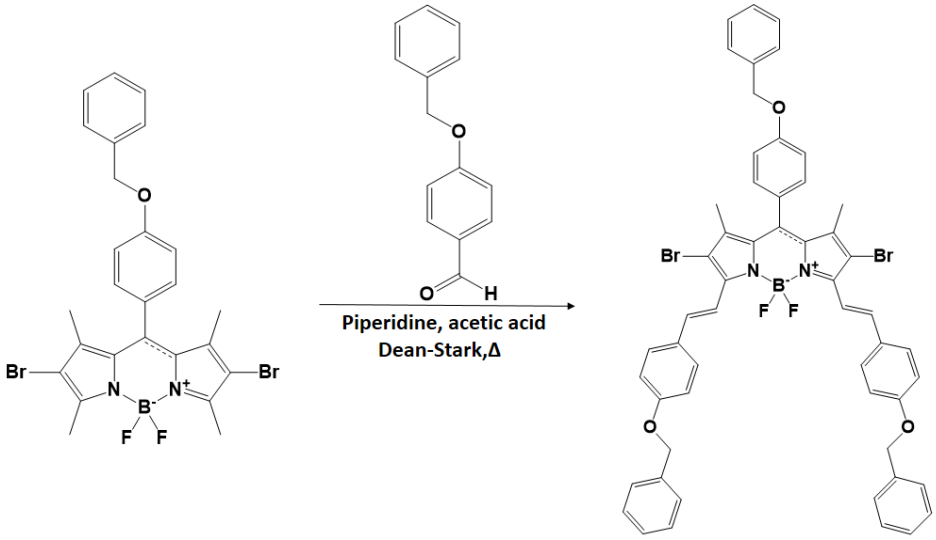

Scheme 22. Knoevenagel condensation to form BODIPY **6**.

3.13.2 Structural Analysis of BODIPY **6**

All forty-three protons can be identified in the ^{1}H NMR spectrum of BODIPY **6**. The three phenyl rings closest to the BODIPY core have their protons appearing as two sets, combined; at 7.65–7.62 ppm and 7.48 ppm there is a doublet and a singlet, respectively, each integrating to six protons and thereby totalling twelve protons with four on each ring. The doublet at 8.14–8.11 ppm integrates as two protons and can be attributed to the two protons of the benzyloxy group closest to the linking oxygen. The furthest protons from the BODIPY core for both styryl groups appear as a singlet integrating to six protons at 7.42

ppm, arising from three protons on each ring. The singlet at 7.37 ppm integrates as three protons and can be attributed to three protons on the phenyl rings of the benzyloxy group; these are the furthest protons from the BODIPY core for the *meso*-substituent. The singlet at 7.15 ppm integrates as two protons and can be attributed to one set of benzyloxy group phenyl protons furthest from the core; the second set is observed at 7.20 ppm. The singlet at 7.05 ppm integrates as four protons and can be attributed bridging alkenes between the styryl group and the core. The doublet signal at 5.17 ppm integrates to six protons and is assigned to the CH_2 protons adjacent to the oxygen atoms of the benzyloxy groups on both the styryls and the benzyloxy group. The final signal at 1.49 ppm is a singlet which integrates to six protons, representing the two methyl groups on the BODIPY core. The predicted molecular mass of 976.17 amu for BODIPY **6** was confirmed by MALDI-TOF mass spectrometry as the primary peak occurred at 976.71 amu. In the FT-IR spectrum of BODIPY **6**, similar vibrations to that of BODIPY **5** are also observed. The appearance of a peak at 522 cm^{-1} confirms bromination; the peak can be attributed to the C-Br stretch associated with bromination of the 2,6-positions of the BODIPY core.

3.13.3 Spectroscopic properties of BODIPY **6**

The electronic absorption spectrum for BODIPY **6** is typical of that of a di-styryl substituted BODIPY, as can be seen in the absorbance maximum at 667 nm in DMSO which is more red-shifted than BODIPY **5** due to the presence of heavy atoms at the 2,6-positions. The absorption, excitation and emission band maxima values in different solvents are summarised below (**Table 10**) and the absorption, excitation and emission spectra in DMSO are also provided and show no signs of aggregation (**Figure 21**). The absorption bands in the 300–400 nm region are associated with the benzyloxystyryl substituents. BODIPY **6** exhibits

moderate fluorescence. Due to the presence of heavy atoms, **6** has a significant singlet oxygen quantum yield value in DMSO.

Table 10. Photophysical data for BODIPY **6** in different organic solvents.

Solvent	λ_{Abs} (nm)	λ_{Exc} (nm)	λ_{Em} (nm)	Stokes shift (cm^{-1})	Φ_F	τ_F (ns)	log ε	Φ_Δ*
DCM	663	665	685	484	0.16	3.98	4.93	NS
DMSO	667	669	700	707	0.13	3.56	4.50	0.30

*NS = not studied

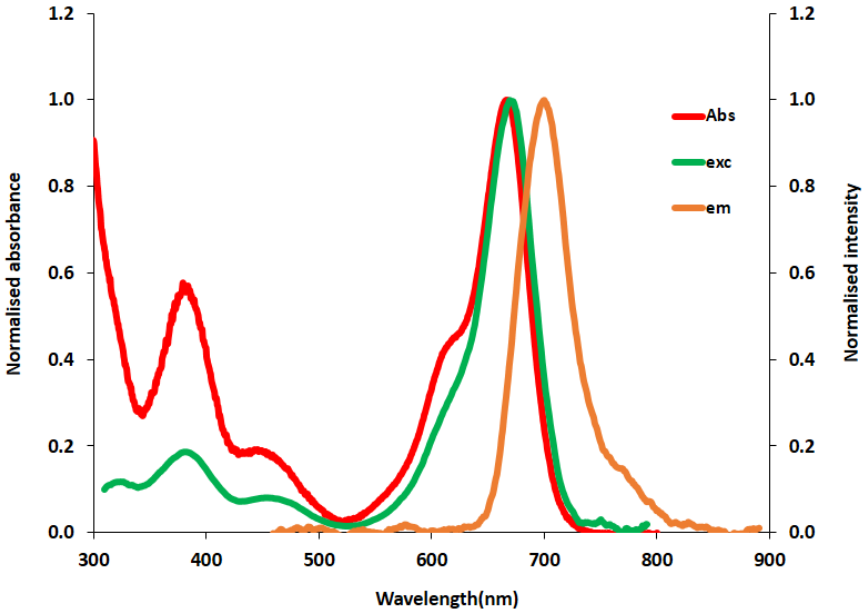

Figure 21. Normalised absorption (red), excitation (green) and emission (orange) spectra of BODIPY **6** in DMSO.

3.14. **4,4'-Difluoro-8-(4-carbomethoxyphenyl)-2,6-diethyl-1,7-dimethyl-3,5-di-styryl-(4-dimethylaminophenyl)-4-bora-3a,4a-diaza-*s*-indacene (8)**

The substitution of any of the acidic methyl groups on the BODIPY core typically red-shifts the main absorption bands of the BODIPY dye due to delocalisation of the π-system and this is helpful in optical limiting, one of the intended applications of BODIPY **8**.

3.14.1. Synthesis of BODIPY **8** (**Scheme 23**)

BODIPY **8** was synthesised from 4,4'-difluoro-8-(4-carbomethoxyphenyl)-2,6-diethyl-1,3,5,7-tetramethyl-4-bora-3a,4a-diaza-*s*-indacene by using a modified Knoevenagel condensation reaction. The solution changed colour from orange-red to light brown-red indicating the formation of a di-styryl-BODIPY. BODIPY **8** was obtained by column chromatography by using ethyl acetate:petroleum ether (1:4) as the eluent.

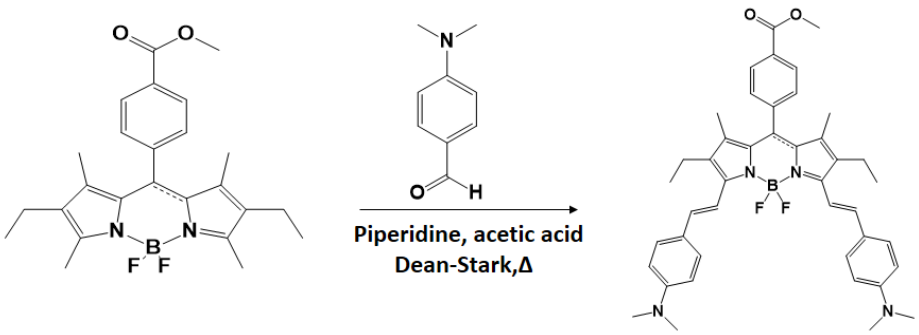

Scheme 23. Knoevenagel condensation to form BODIPY **8**.

3.14.2 Structural Analysis of BODIPY **8**

All forty-seven protons can be identified in the ^{1}H NMR spectrum of BODIPY **8**. The singlet at 8.40 ppm integrates as two protons and can be attributed to two protons from one of the phenyl rings on the styryls, while the singlet at 8.26 ppm integrates as three protons and can

be attributed to three protons from the other phenyl ring on the styryls. The rest of the styryl phenyl protons appear as a doublet which integrates as three protons, at 7.71 ppm. The singlet at 7.58 ppm integrates as three protons and can be attributed to three protons from the *meso*-phenyl ring, with the remaining proton found in the singlet at 7.38 ppm (notwithstanding the fact that the singlet integrates to two protons). The singlet at 6.86 ppm integrates as three protons and can be attributed to three protons from the bridging alkenes between the styryl group and the core, with the remaining proton of the bridging alkenes found at 7.38 ppm. The ester group protons appear as a singlet integrating to three protons, at 4.08 ppm. The dimethylamino protons from the styryls are found as a singlet integrating to twelve protons, at 3.07 ppm. At 1.98 ppm, a singlet integrating to four protons appears and it represents the two CH_2 groups of the ethyl groups at the 2,6-positions, with the CH_3 groups of the same group appearing as a singlet which integrates to six protons at 1.29 ppm. The final signal at 1.38 ppm is a singlet which integrates to six protons, representing the two methyl groups on the BODIPY core. The predicted molecular mass of 700.38 amu for BODIPY **8** was confirmed by MALDI-TOF mass spectrometry as the primary peak occurred at 700.94 amu. The FT-IR spectrum, with bands attributed to the C-H stretch of the terminal methyl groups attached to the BODIPY core found at 2916 and 2853 cm^{-1}. The C=O ester stretch is observed at 1712 cm^{-1}, whereas the C-O-C antisymmetric stretches are at 1162 and 1101 cm^{-1}. The N-C stretch bands corresponding to both the pyrrolic nitrogen atoms and the styryl dimethylamino moiety lie in the 1044–1436 cm^{-1} region.

3.14.3 Spectroscopic properties of BODIPY **8**

The electronic absorption spectrum for BODIPY **8** in the presence of an acid is typical of that of a di-styryl substituted BODIPY, as can be seen in the absorbance maximum at 730 nm in DMSO which is more red-shifted than all the other BODIPYs previously mentioned in this thesis. The absorption, excitation and emission band maxima values in different solvents are summarised below (**Table 11**) and the absorption, excitation and emission spectra in benzene with excess TFA are also provided and show no signs of aggregation (**Figure 22**). BODIPY **8** exhibits moderate fluorescence in the presence of acid due to the elimination of charge transfer.

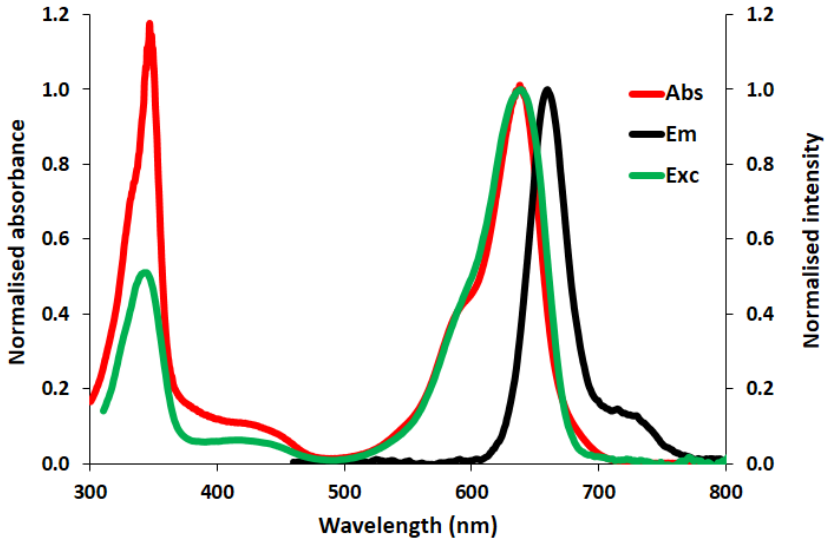

Figure 22. Normalised absorption (red), excitation (green) and emission (black) spectra of BODIPY **8** in benzene in the presence of TFA.

Table 11. Photophysical data for BODIPY **8** in different organic solvents in the presence and absence of TFA.

Solvent	λ_{Abs} (nm)	λ_{Exc} (nm)*	λ_{Em} (nm)*	Stokes shift (cm^{-1})	Φ_F	τ_F (ns)*	log ε*
Benzene	714	660	680; 754	743	0.09	2.63	5.07
Benzene + TFA	638	639	658	476	0.27	4.60	NS
DCM	715	657	673; 761	845	0.04	2.05	4.25
DCM + TFA	636	641	660	572	0.16	4.60	NS
Acetonitrile	711	717	794	1470	0.02	NS	4.60
Acetonitrile + TFA	622	633	655	810	0.02	NS	NS
DMSO	730	n.d	n.d	-	0.02	0.75 (97%) 3.301 (3.2%)	4.05

DMSO + TFA	633	633	662	692	0.03	0.26 (73%) 1.99 (27.1%)	NS

*NS = not studied; *n.d =not detected

3.15. 4,4'-Difluoro-8-(4-carbomethoxyphenyl)-2,6-diethyl-1,7-dimethyl-3,5-di-styryl-(4-hydroxyphenyl)-4-bora-3a,4a-diaza-*s*-indacene (9)

The substitution of any of the acidic methyl groups on the BODIPY core typically red-shifts the main absorption bands of the BODIPY dye due to delocalisation of the π-system and this is helpful in the intended application of BODIPY **9**, which is optical limiting.

3.15.1. Synthesis of BODIPY **9** (**Scheme 24**)

BODIPY **9** was synthesised from 4,4'-difluoro-8-(4-carbomethoxyphenyl)-2,6-diethyl-1,3,5,7-tetramethyl-4-bora-3a,4a-diaza-*s*-indacene using a modified Knoevenagel condensation reaction. The solution changed colour from orange-red to a deep green colour indicating the formation of a di-styryl-BODIPY. BODIPY **9** was obtained by column chromatography by using ethyl acetate:petroleum ether (1:4) as the eluent.

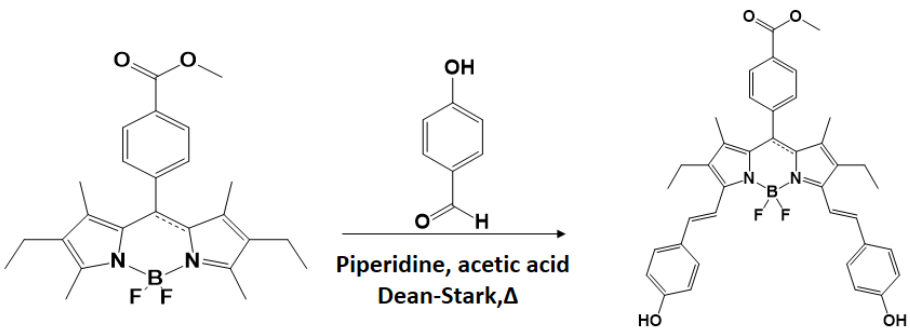

Scheme 24. Knoevenagel condensation to form BODIPY **9**.

3.15.2 Structural Analysis of BODIPY **9**

All thirty-seven protons can be identified in the ^{1}H NMR spectrum of BODIPY **9**. The singlet at 8.79 ppm integrates as two protons and can be attributed to two protons from the *meso*-phenyl ring, while the doublet at 8.26 ppm integrates as two protons and can be attributed to the two remaining protons of the *meso*-phenyl ring. The styryl phenyl protons appear as two doublets, each integrating as four protons, at 7.67 and 7.56 ppm. The doublet at 7.36 ppm integrates as two protons and can be attributed to the two protons from the hydroxyl groups on the styryls. At 6.95 ppm, the doublet integrates to four protons and can be attributed to the four protons of the bridging alkenes. The ester group protons appear as a singlet integrating to three protons, at 3.98 ppm. At 2.68 ppm, a multiplet integrating to four protons appears and it represents the two CH_2 groups of the ethyl groups at the 2,6-positions, with the CH_3 groups of the same ethyl groups appearing as a triplet which integrates to six protons at 1.17 ppm. The final signal at 1.39 ppm is a singlet which integrates to six protons, representing the two methyl groups on the BODIPY core. The predicted molecular mass of 646.28 amu for BODIPY **9** was confirmed by MALDI-TOF mass spectrometry as the primary peak occurred at 646.83 amu. The FT-IR spectrum contained the anticipated peaks, with bands attributed to the C-H stretch of the terminal methyl groups attached to the BODIPY core found at 2923 and 2858 cm^{-1}. The C=O ester stretch is observed at 1718 cm^{-1}, whereas the C-O-C antisymmetric stretches are at 1169 and 1107 cm^{-1}. The N-C stretch bands corresponding to the pyrrolic nitrogen atoms lie in the 1048–1437 cm^{-1} region. The O-H stretch from the styryls is found at ca. 3250 cm^{-1}.

3.15.3 Spectroscopic properties of BODIPY **9**

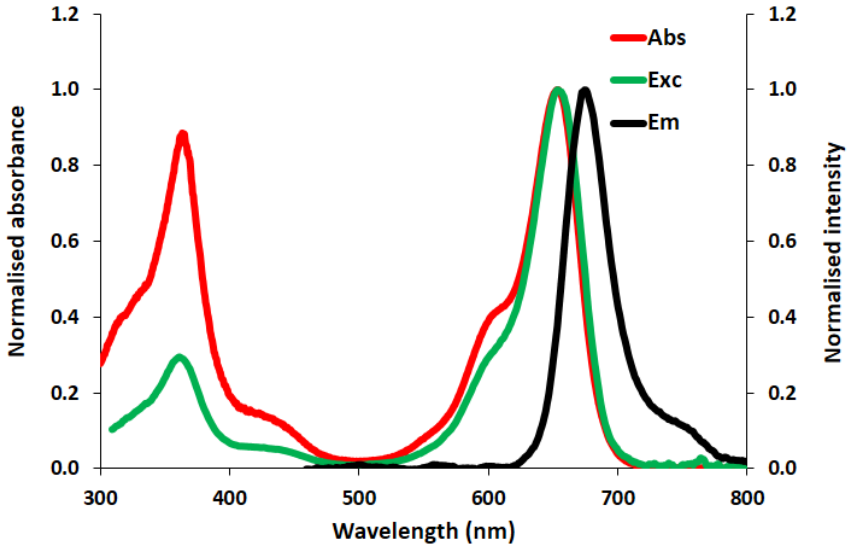

Figure 23. Normalised absorption (red), excitation (green) and emission (black) spectra of BODIPY **9** in DCM.

Table 12. Photophysical data for BODIPY **9** in different organic solvents.

Solvent	λ_{Abs} (nm)	λ_{Exc} (nm)	λ_{Em} (nm)	Stokes shift (cm^{-1})	Φ_F	τ_F (ns)	log ε
Benzene	658	659	676	405	0.18	3.49	4.50
DCM	653	653	674	477	0.19	3.73	4.56
Acetonitrile	651	657	680	655	0.14	3.66	5.40

The electronic absorption spectrum for BODIPY **9** is typical of that of a di-styryl substituted BODIPY, as can be seen in the absorbance maximum at 653 nm in DCM. The absorption, excitation and emission band maxima values in different solvents are summarised above

(**Table 12**) and the absorption, excitation and emission spectra in DCM are also provided and show no signs of aggregation (**Figure 23**). BODIPY **9** exhibits moderate fluorescence. The quantum yield and lifetime values are also recorded.

3.16. 4,4'-Difluoro-8-(4-carbomethoxyphenyl)-2,6-diethyl-1,7-dimethyl-3,5-di-styryl-(4-methoxyphenyl)-4-bora-3a,4a-diaza-*s*-indacene (10)

The substitution of any of the acidic methyl groups on the BODIPY core typically red-shifts the main absorption bands of the BODIPY dye due to delocalisation of the π-system and this is helpful in the intended application of BODIPY **10** which is optical limiting.

3.16.1. Synthesis of BODIPY **10** (**Scheme 25**)

BODIPY **10** was synthesised from 4,4'-difluoro-8-(4-carbomethoxyphenyl)-2,6-diethyl-1,3,5,7-tetramethyl-4-bora-3a,4a-diaza-*s*-indacene by using a modified Knoevenagel condensation reaction. The solution changed colour from orange-red to a deep green colour indicating the formation of a di-styryl-BODIPY. BODIPY **10** was obtained by column chromatography by using ethyl acetate:petroleum ether (1:4) as the eluent.

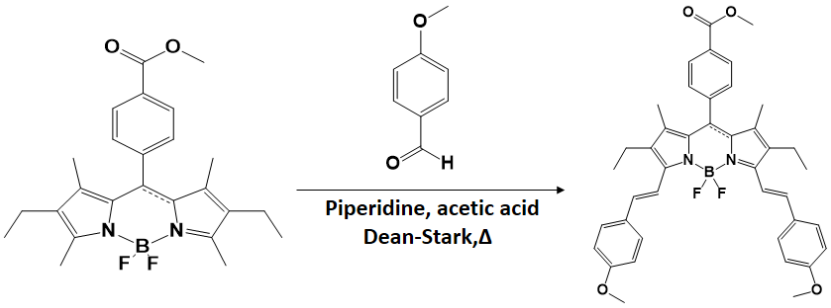

Scheme 25. Knoevenagel condensation to form BODIPY **10**.

3.16.2 Structural Analysis of BODIPY **10**

All forty-one protons can be identified in the ^{1}H NMR spectrum of BODIPY **10**. The doublet at 8.23 ppm integrates as two protons and can be attributed to two styryl phenyl protons, with the second set of two protons appearing as a doublet at 7.71 ppm. At 7.61 ppm, the doublet integrates as four protons and can be attributed to the four phenyl protons from the second styryl. The four *meso*-phenyl ring protons are represented by two different signals; a doublet at 7.50 ppm and a singlet at 7.30 ppm, each integrating to two protons. At 6.99 ppm, the doublet integrates to four protons and can be attributed to the four protons of the bridging alkenes. The ester group protons appear as a singlet integrating to three protons, at 4.03 ppm. The singlet at 3.90 ppm integrates as six protons and can be attributed to the six protons from the CH_3 groups of the methoxy groups on the styryls. At 2.65 ppm, a quartet integrating to four protons appears and it represents the two CH_2 groups of the ethyl groups at the 2,6-positions, with the CH_3 groups of the same ethyl groups appearing as a triplet which integrates to six protons at 1.20 ppm. The final signal at 1.36 ppm is a singlet which integrates to six protons, representing the two methyl groups on the BODIPY core. The predicted molecular mass of 674.31 amu for BODIPY **10** was confirmed by MALDI-TOF mass spectrometry as the primary peak occurred at 674.91 amu. The FT-IR spectrum contained the anticipated peaks, with bands attributed to the C-H stretch of both the terminal methyl groups attached to the BODIPY core and those of the methyl groups of the styryl methoxy moieties found at ca. 2920 and 2855 cm^{-1}. The C=O ester stretch is observed at 1722 cm^{-1}, whereas the C-O-C antisymmetric stretch of the ester group lies at 1162 cm^{-1}. The N-C stretch bands corresponding to the pyrrolic nitrogen atoms are observed in the 1099–1446 cm^{-1} region. The C-O-C stretch from the methyl groups of

the styryl methoxy moieties is found at 1027 cm^{-1}, whereas the corresponding C-O-C bend lies at 529 cm^{-1}.

3.16.3 Spectroscopic properties of BODIPY **10**

The electronic absorption spectrum for BODIPY **10** is typical of that of a di-styryl substituted BODIPY, as can be seen in the absorbance maximum at 654 nm in DCM. The absorption, excitation and emission band maxima values in benzene and DCM are summarised below (**Table 13**) and the absorption, excitation and emission spectra in benzene are also provided and show no signs of aggregation (**Figure 24**). BODIPY **10** exhibits moderate fluorescence. The quantum yield and lifetime values are also recorded.

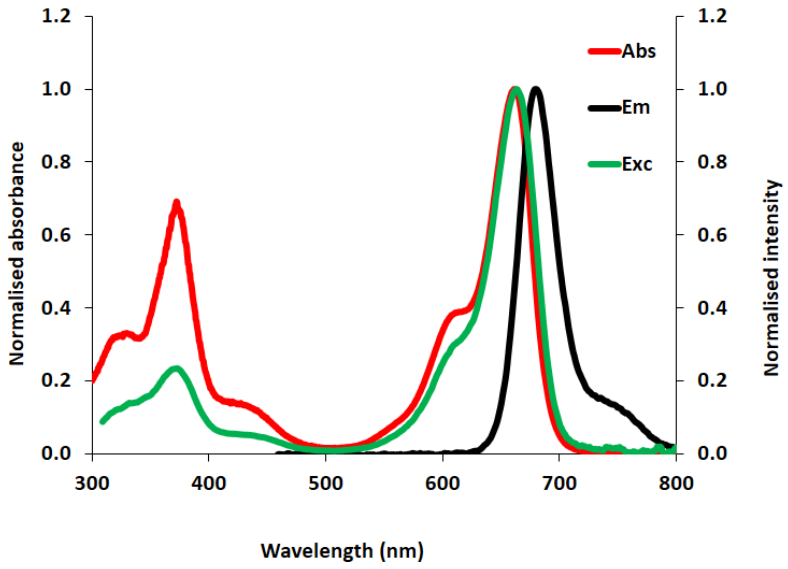

Figure 24. Normalised absorption (red), excitation (green) and emission (black) spectra of BODIPY **10** in benzene.

Table 13. Photophysical data for BODIPY **10** in benzene and DCM.

Solvent	λ_{Abs} (nm)	λ_{Exc} (nm)	λ_{Em} (nm)	Stokes shift (cm^{-1})	Φ_F	τ_F (ns)	log ε
Benzene	662	664	680	400	0.20	3.97	4.73
DCM	654	659	680	585	0.19	2.50 (46.2%) 4.89 (53.8%)	4.73

3.17. Spectroscopic characterisation of previously synthesised BODIPY Dyes

3.17.1 Spectroscopic properties of BODIPY **4**, 4,4'-difluoro-8-(4-dimethylamino)-1,7-dimethyl-2,6-dibromo-3,5-di-styryl-(4-benzo-15-crown-5)-4-bora-3a, 4a-diaza-*s*-indacene

The electronic absorption spectrum for BODIPY **4** is typical of that of a di-styryl substituted BODIPY, as can be seen in the absorbance maximum at 681 nm in DMSO which is highly red-shifted relative to BODIPY **1a** due to the presence of the bromines as heavy atoms at the 2,6-positions and the crown-ether-substituted styryl moieties at the 3,5-positions. The absorption, excitation and emission band maxima values in different solvents are summarised below (**Table 14**) and the absorption, excitation and emission spectra in DCM are also provided and show no signs of aggregation (**Figure 25**). The relatively intense absorption bands in the 300–400 nm region are believed to be associated with the crown ether substituents.

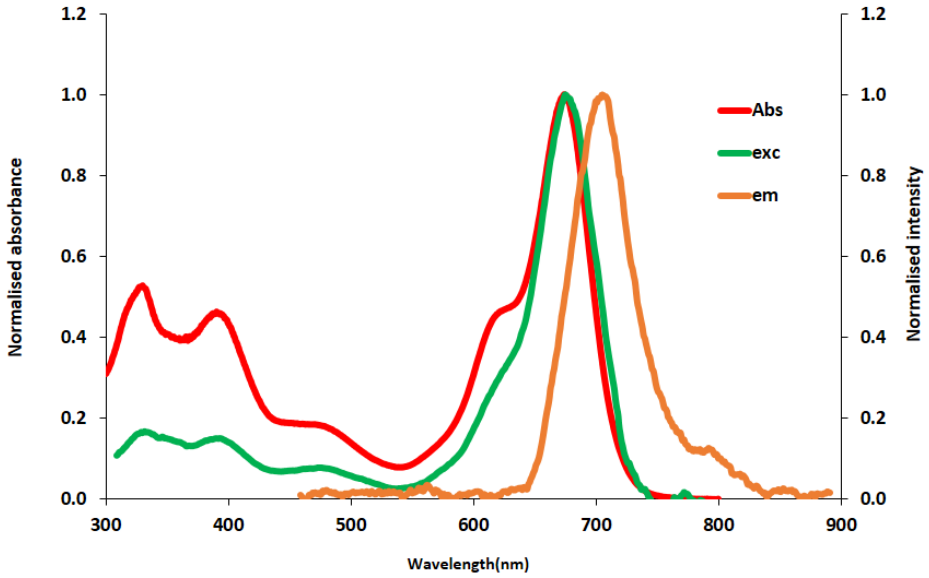

Figure 25. Normalised absorption (red), excitation (green) and emission (orange) spectra of BODIPY **4** in DCM.

Table 14. Photophysical data for BODIPY **4** in different organic solvents.

Solvent	λ_{Abs} (nm)	λ_{Exc} (nm)	λ_{Em} (nm)	Stokes shift (cm^{-1})	Φ_F	τ_F (ns)	log ε
Benzene	682	683	708	539	0.12	3.52	4.61
DCM	675	675	707	671	0.14	3.57	4.65
THF	676	678	709	689	0.11	3.41	4.80
Acetonitrile	676	676	707	649	0.05	2.02	4.97
DMSO	681	688	721	815	0.02	2.59	5.0

3.17.2 Spectroscopic properties of BODIPY **7**, 4,4'-difluoro-8-(4-carbomethoxyphenyl)-1,7-dimethyl-3,5-di(thiophen-2-yl)vinyl-4-bora-3a,4a-diaza-*s*-indacene

The electronic absorption spectrum for BODIPY **7** is typical of that of a di-styryl substituted BODIPY, as can be seen in the absorbance maximum at 660 nm in DMSO which is red-shifted due to the presence of the thienylvinylene substituents at the 3,5-positions. The absorption, excitation and emission band maxima values in different solvents are summarised below (**Table 15**) and the absorption, excitation and emission spectra in DMSO are also provided and show no signs of aggregation (**Figure 26**). The relatively intense absorption bands in the 300–400 nm region are believed to be associated with the thienylvinylene groups.

Table 15. Photophysical data for BODIPY **7** in different organic solvents.

Solvent	λ_{Abs} (nm)	λ_{Exc} (nm)	λ_{Em} (nm)	Stokes shift (cm^{-1})	Φ_F	τ_F (ns)	log ε
Benzene	659	659	672	294	0.56	2.99	4.13
DCM	654	656	667	298	0.50	2.95	4.89
THF	651	653	664	301	0.46	2.95	5.29
Acetonitrile	646	646	661	351	0.46	3.01	5.36
DMSO	660	661	677	381	0.13	2.80	5.44

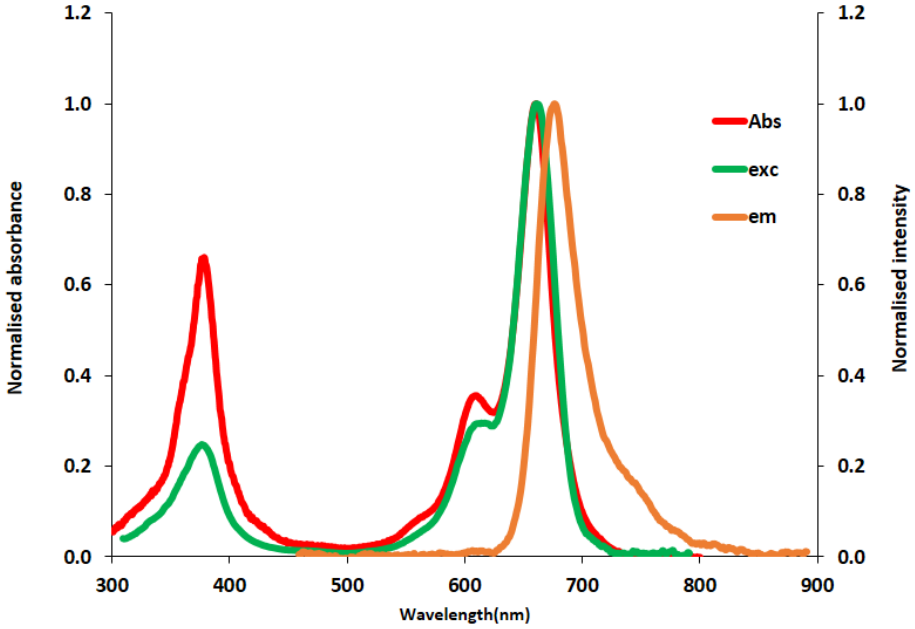

Figure 26. Normalised absorption (red), excitation (green) and emission (orange) spectra of BODIPY **7** in DMSO.

Concluding remarks

Five BODIPY cores, **1a**–**1e**, were synthesised using the classic "one-pot three-step" acid-catalysed condensation reaction and structurally characterised using various techniques. The only structural difference between these BODIPY dyes is the functional groups present on the *para*-position of the *meso*-phenyl ring. In addition to structural characterisation, photophysical characterisation were performed for **1a**–**1d**, which have broadly similar absorption properties as is typical from BODIPY dyes derived from 2,4-dimethylpyrrole, since the *meso*-aryl ring lies orthogonal to the BODIPY cores. The dyes do, however, differ significantly when it comes to fluorescence properties, although both the lifetimes and quantum yields lie in the range generally expected for BODIPY dyes.[5] BODIPY **1a** is only highly fluorescent in the presence of acid to eliminate charge transfer between the dimethylamino moiety and the BODIPY core, while BODIPY **1c** also possessed weak

fluorescence due to the quenching effect of the nitro group which is known to strongly quench fluorescent dyes through what is suggested to be an electron-withdrawing effect.[161] BODIPYs **1b** and **1d** are highly fluorescent in a manner that is independent of solvent polarity, since the absorption maximum was not significantly altered by changing the solvent. BODIPYs **1a**–**1e** were brominated at the 2,6-positions (and BODIPY **1a** on one of the carbons of the *meso*-phenyl ring), yielding BODIPYs **2a**–**2e** whose absorption spectra are red shifted by ca. 30 nm relative to their parent dyes (particularly BODIPYs **2a**–**2d** which were of spectroscopic interest here). BODIPYs **2a**–**2d** possessed significant singlet oxygen quantum yields. It is worth noting that BODIPYs **1a**–**1d** and **2b**–**2d** were not novel and have been previously reported in literature. To the best of our knowledge, the only novelty in this regard was the detailed photophysical characterisation undertaken herein.

BODIPY **2d** was used to synthesise BODIPY **3**, a new mono-styryl BODIPY dye whose structural characterisation was also successful. Five novel di-styryl BODIPYs, BODIPYs **5**, **6**, **8**, **9** and **10** were synthesised from BODIPYs **1e** and **2e** for BODIPYs **5** and **6**, respectively and from 4,4'-difluoro-8-(4-carbomethoxyphenyl)-2,6-diethyl-1,3,5,7-tetramethyl-4-bora-3a,4a-diaza-*s*-indacene which was synthesised using the classic "one-pot three-step" acid-catalysed condensation reaction, for BODIPYs **8**, **9** and **10** . BODIPYs **3**, **5**, **6**, **8**, **9** and **10** were synthesised using a modified version of the Knoevenagel condensation reaction from their respective starting BODIPYs. These dyes were characterised using ^{1}H-NMR, MALDI-TOF mass spectrometry and FT-IR. Their main absorption band maxima are significantly red-shifted far beyond 532 nm, the second harmonic of the Nd:YAG laser which is used to study the optical limiting properties of these dyes, as discussed in Chapter 4. BODIPY **6** was red-shifted into the therapeutic window, with absorption maxima at 663 in DCM and 667 nm in DMSO; this

red-shift coupled with the ability of the dye to generate singlet oxygen species (as is evident with the quantum yield of 0.3 in DMSO) makes the dye a potential photosensitizer for singlet oxygen applications such as PDT. In addition to studying the optical limiting properties of BODIPY **8**, this dye was also designed for study as a pH-sensitive fluorescent probe for potential biomedical applications, as discussed in Chapter 6.

Chapter 4:

Nonlinear optical (NLO) limiting properties of BODIPY dyes in solution

The goal of this chapter is to investigate the NLO properties of a series of 3,5-divinylene-substituted BODIPY dyes (**Figure 27**), some of which contain electron withdrawing and electron donating groups separated by a π-conjugation system to form D-π-A type systems. BODIPY **4** contains the electron donating dimethylaminophenyl group at the *meso*-position and crown ether moieties on the styryl rings and was studied in benzene, DCM, THF, acetonitrile and DMSO solutions to assess the effects of differences in solvent polarity. BODIPYs **5** and **6** were studied in DCM solutions and as is evident from their somewhat identical structures (**Figure 27**), the motivation for studying these compounds was to look at the effect of the presence of heavy atoms in the form of bromine. BODIPY **7** was studied in DCM, THF, acetonitrile and DMSO solutions to assess the effects of differences in solvent polarity with the added effect of the absence of heavy atoms to promote intersystem crossing which is known to enable ESA in the triplet manifold. BODIPYs **8**, **9** and **10** are 2,6-diethyl-substituted BODIPY dyes containing a moderately electron withdrawing ester group on the *meso*-phenyl ring and strongly electron donating groups at the 3,5-positions. This creates a strong permanent dipole moment in the ground state. All seven dyes possess an extended π-system and BODIPYs **4** and **6** contain bromine heavy atoms and as such an enhanced optical limiting response is expected since optical limiter materials with heavy atoms incorporated have previously shown to perform better in the context of phthalocyanines.[107–109] During the z-scan measurements on these compounds, there was a consistent effort to ensure that the dye being studied was not aggregated in solution by carefully checking the UV-visible absorption spectra before and after measurement, since aggregation could lead to significant NLS and as such interfere with the NLA results.

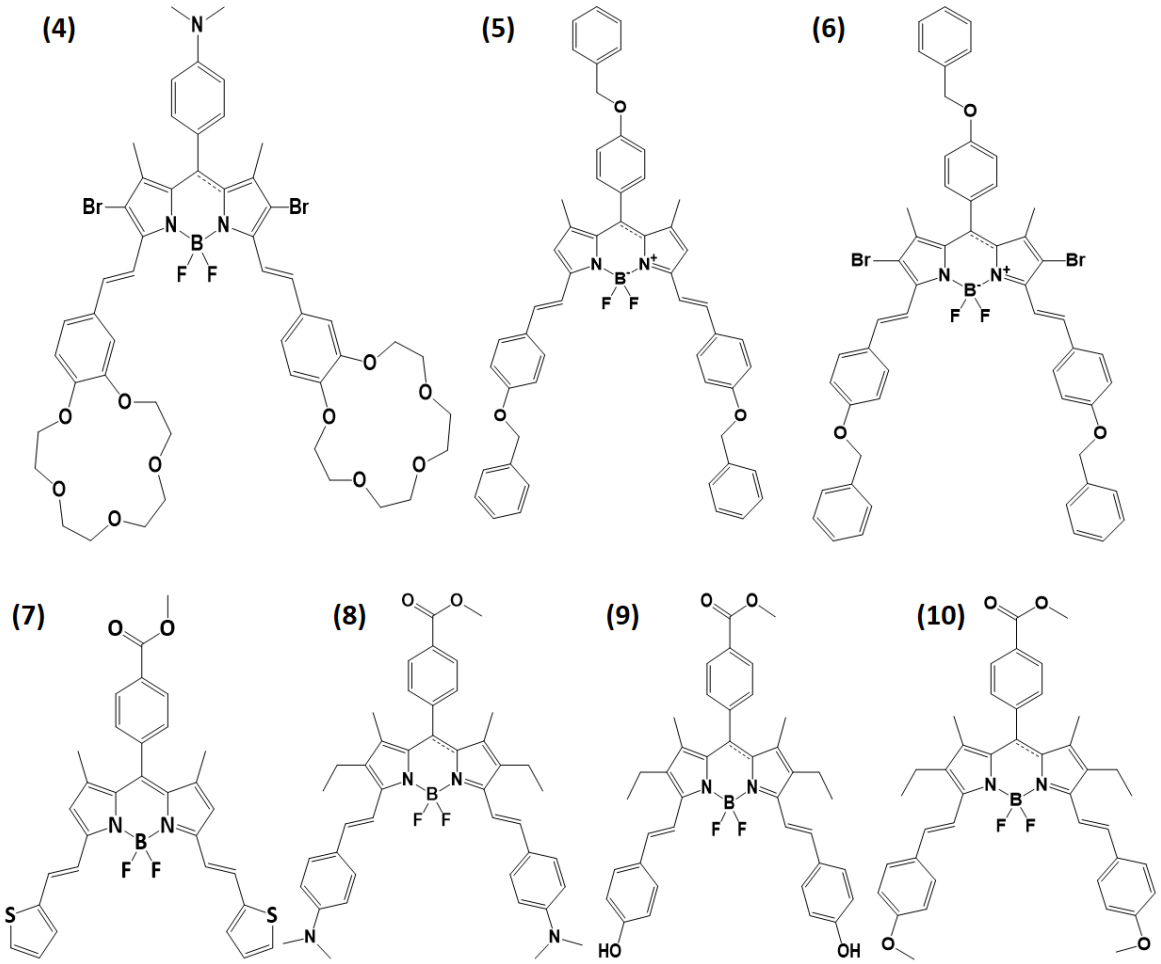

Figure 27. BODIPY dyes used for the NLO studies.

It is worth noting that the z-scan setup being used employs nanosecond and not femtosecond laser pulses, hence the RSA responses observed as the focal point is approached during the z-scan measurements are expected not to be strictly due to 2PA. This means that the 2PA intrinsic β value cannot be measured and instead, the effective nonlinear absorption coefficient (β_{eff}) is determined, since ESA that occurs on a nanosecond timescale can also result in an RSA response.[166,97] When ESA is more intense than ground state absorption, there is a positive nonlinear absorption coefficient and a decrease in

transmittance as the material approaches the zero position of the z-scan instrument at high-intensity incident light levels.[166]

I. Optical limiting properties of BODIPY **4**

The optical limiting ability of the di-styryl crown ether BODIPY was assessed in benzene, DCM, THF, acetonitrile and DMSO and in all solvents the main absorption band lies ca. 145 nm to the red of the Nd:YAG laser's second harmonic wavelength at 532 nm with minimal absorbance at this wavelength (**Figure 28**), and this provides the possibility of a good NLO response.

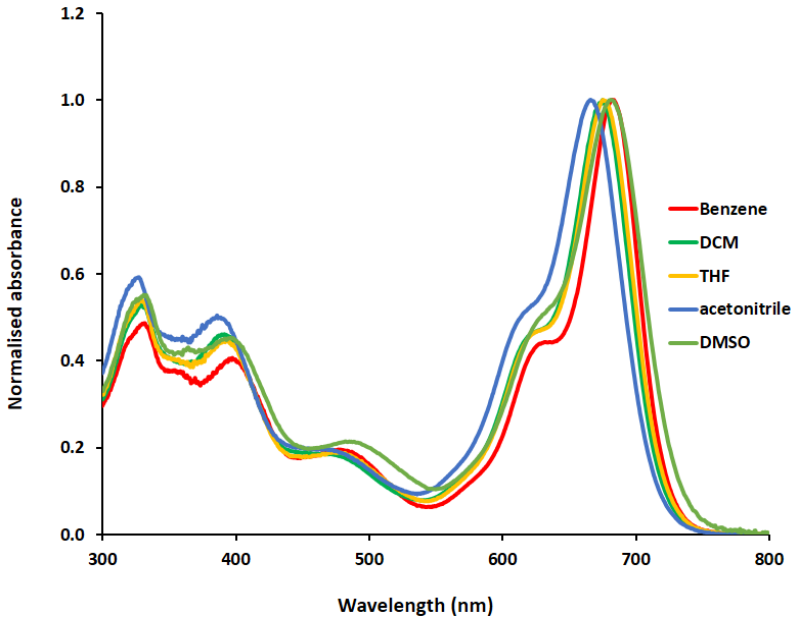

Figure 28. Normalised absorption spectra of the di-styryl crown ether BODIPY (**4**) in different organic solvents.

To study the effects of the amount of dye present, two different concentrations were studied for each solvent. NLO responses can be studied by following the reduction in transmittance along the z-axis, which shows a positive nonlinear absorption. The responses in this study were characteristic of RSA.[167–169] The studies were conducted at four energies

in terms of each incident laser pulse, in all solvents, but the z-scan plots (**Figure 29**–**Figure 33**) are limited only to two energies in terms of each incident laser pulse, i.e. a comparative study between a lower and a higher energy. The results for the other incident laser pulse intensities are included in the tables (**Table 16**–**Table 20**).

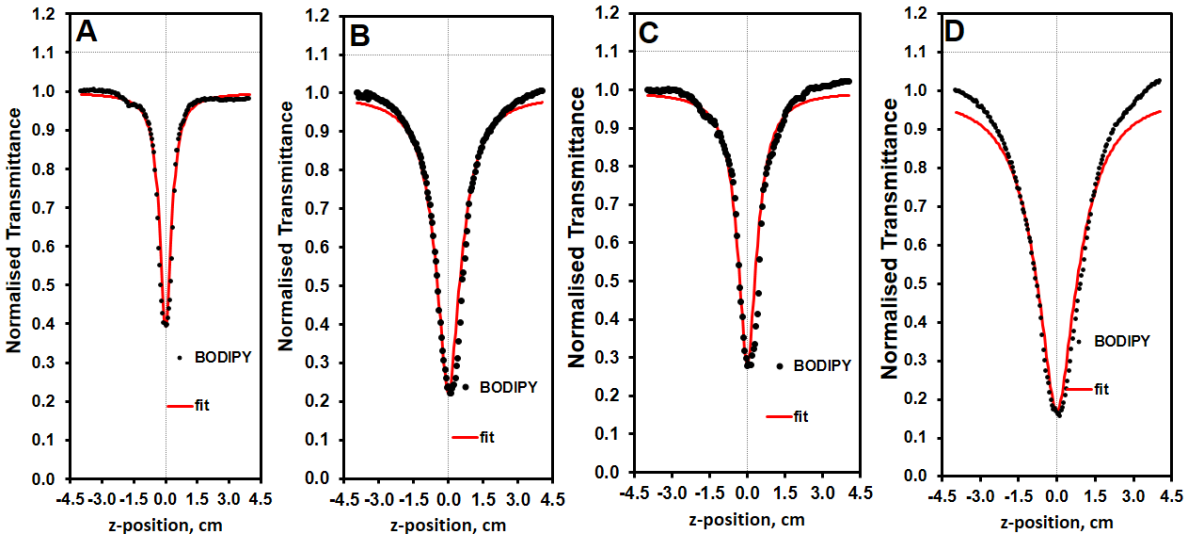

Figure 29. Characteristic open-aperture z-scans of the di-styryl crown ether BODIPY (**4**) in benzene at A: input intensity of 10 µJ for each laser pulse and a concentration of 3.35×10^{-6} M, B: input intensity of 40 µJ and a concentration of 3.35×10^{-6} M, C: input intensity of 10 µJ and a concentration of 6.85×10^{-6} M and D: input intensity of input intensity of 40 µJ and a concentration of 6.85×10^{-6} M.

The open-aperture z-scan plots obtained at both dye concentrations studied in benzene were able to reduce transmittance below 50% and an increase in dye concentration significantly reduces transmittance by the BODIPY solution (**Figure 29A** and **Figure 29C**). The transmittance is also reduced more when higher energy incident laser pulses are used at each concentration.

In order to study the efficiency of this dye as an OL material, the main OL parameters were studied. These parameters include the nonlinear absorption coefficient (β_{eff}), imaginary third-order susceptibility ($Im[\chi^{(3)}]$), second order hyperpolarizability (γ) and the limiting intensity (I_{lim}). The parameters that will be discussed here are limited only to those solutions which were able to reduce transmittance by at least 50%, since this is viewed as a prerequisite for a good optical limiter (**Table 16**). The β_{eff} value provides a measure of the effective degree of nonlinear absorptivity when measurements are made on a nanosecond timescale. A positive nonlinear absorption coefficient is an indication that the optical limiter being studied possesses reverse saturable absorption and as a result is characterised by a high transmittance at normal light intensities and a decrease in transmittance under high intensity.[93] The $Im[\chi^{(3)}]$ value is a measure of the rapidity of response by an optical limiter to the perturbation induced by incident laser pulses, whereas the γ value provides a measure of the interaction of the incident photon with the permanent dipole moments of the OL material. The I_{lim} value is defined as the threshold input energy or fluence at which a decrease to 50% transmittance is achieved.[93] The lower the optical limiting threshold, the better the optical limiting material. As described in Chapter 1, to avoid damage to the human eye, the limiting threshold should be 0.95 $J.cm^{-2}$ or lower for 10 ns laser pulses at 532 nm.[168,105,106]

For BODIPY **4**, the OL parameters are tabulated and are ordered according to increasing solvent polarity (**Table 16**–**Table 20**). In each case, the $Im[\chi^{(3)}]$ and γ values lie in the optimal range that has been reported for these parameters (see Chapter 1) and this clearly demonstrates that this dye is potentially useful as an optical limiting material and merits further study in this regard. This was not unexpected, since similar results were recently

obtained by Harris *et al.*[95] and Kubheka *et al.*[96] for BODIPY dyes and an aza-BODIPY dye, respectively.

In the optical limiting parameters for the benzene solutions (**Table 16**), a better optical limiting response is observed for the lower energy laser pulses, since the general trend is a decrease in β_{eff}, $Im[\chi^{(3)}]$ and γ values with an increase in pulse energy. Also, an increase in the concentration of the dye present in solution seems to give a significantly better optical limiting response, as seen with β_{eff} and $Im[\chi^{(3)}]$ values increasing with an increase in concentration. The γ values, however, follow an opposite trend with higher values observed for the lower concentration. The limiting intensity values were determined experimentally at 50% transmittance and a lower threshold response is obtained with an increase in concentration and a decrease in the laser pulse energy (**Table 16**).

Table 16. NLO parameters for the di-styryl crown ether BODIPY (**4**) in benzene.

Concentration (M)	**Energy (μJ)**	**α (cm^{-1})**	**β_{eff} ($cm.GW^{-1}$)**	**$Im[\chi^{(3)}]$ (esu)**	**γ (esu)**	**I_{lim} ($J.cm^{-2}$)**
3.35×10^{-6}	~10	1.26	343.1	8.29×10^{-10}	1.02×10^{-28}	0.46
	~20		277.7	6.71×10^{-10}	8.23×10^{-29}	0.56
	~30		249.3	6.03×10^{-10}	7.39×10^{-29}	0.87
	~40		209.6	5.07×10^{-10}	6.21×10^{-29}	1.02
6.85×10^{-6}	~10	2.41	563.7	1.36×10^{-9}	8.18×10^{-29}	0.40
	~20		440.9	1.07×10^{-9}	6.40×10^{-29}	0.47
	~30		369.0	8.92×10^{-10}	5.35×10^{-29}	0.57
	~40		270.5	6.54×10^{-10}	3.92×10^{-29}	0.78

The open-aperture z-scan plots obtained using DCM show that both concentrations studied were able to reduce transmittance far below 50%, demonstrating the ability of the dye to perform as an optical limiter. It was observed that an increase in concentration significantly reduces transmittance by the BODIPY solution (**Figure 30A** and **Figure 30C**). Additionally, the transmittance is reduced more for the higher energy at each concentration (**Figure 30C** and **Figure 30D**), as was the case in benzene solution.

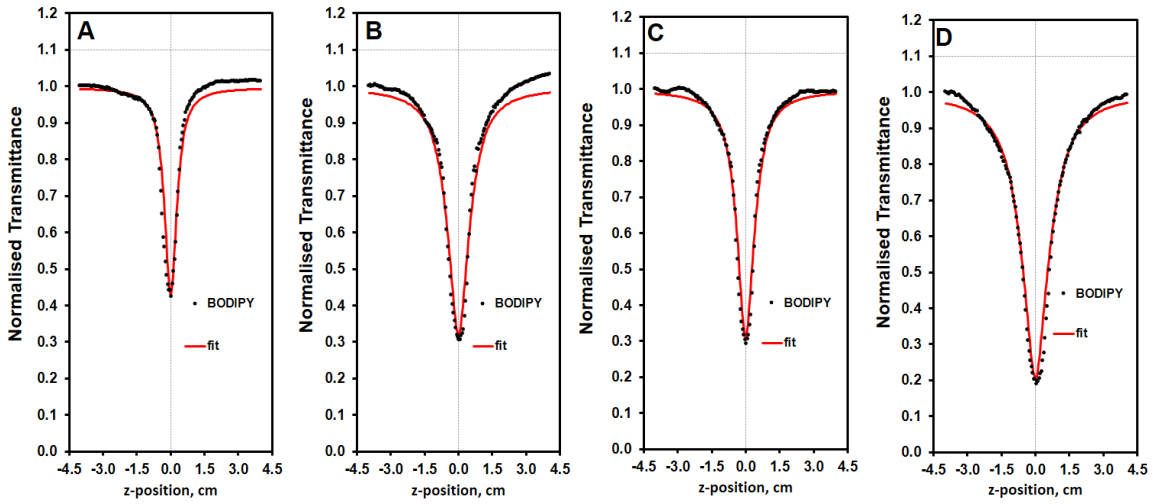

Figure 30. Characteristic open-aperture z-scans of the di-styryl crown ether BODIPY (**4**) in DCM at A: input intensity of 10 µJ for each laser pulse and a concentration of 2.22×10^{-5} M, B: input intensity of 40 µJ and a concentration of 2.22×10^{-5} M, C: input intensity of 10 µJ and a concentration of 5.54×10^{-5} M and D: input intensity of input intensity of 40 µJ and a concentration of 5.54×10^{-5} M.

In DCM, a better optical limiting response in terms of the β_{eff} and $Im[\chi^{(3)}]$ values is observed at higher concentrations and for the lower energy laser pulses in a similar manner to what was observed in benzene (**Table 17**). The γ values, however, did not follow any specific trend with somewhat similar values observed for both concentrations, but were generally

higher for the lower concentration. Lower I_{lim} values are obtained with an increase in concentration and a decrease in laser pulse energy (**Table 17**).

Table 17. NLO parameters for the di-styryl crown ether BODIPY (**4**) in DCM.

Concentration (M)	Energy (μJ)	α (cm^{-1})	β_{eff} ($cm.GW^{-1}$)	$Im[\chi^{(3)}]$ (esu)	γ (esu)	I_{lim} ($J.cm^{-2}$)
2.22×10^{-5}	~10	0.77	232.5	5.06×10^{-10}	1.17×10^{-29}	0.73
	~20		151.4	3.30×10^{-10}	7.60×10^{-30}	0.95
	~30		188.1	4.09×10^{-10}	9.44×10^{-30}	0.95
	~40		111.5	2.43×10^{-10}	5.59×10^{-30}	1.55
5.54×10^{-5}	~10	2.42	584.1	1.27×10^{-9}	1.17×10^{-29}	0.34
	~20		307.1	6.68×10^{-10}	6.16×10^{-30}	0.60
	~30		353.2	7.69×10^{-10}	7.09×10^{-30}	0.65
	~40		283.1	6.16×10^{-10}	5.68×10^{-30}	0.85

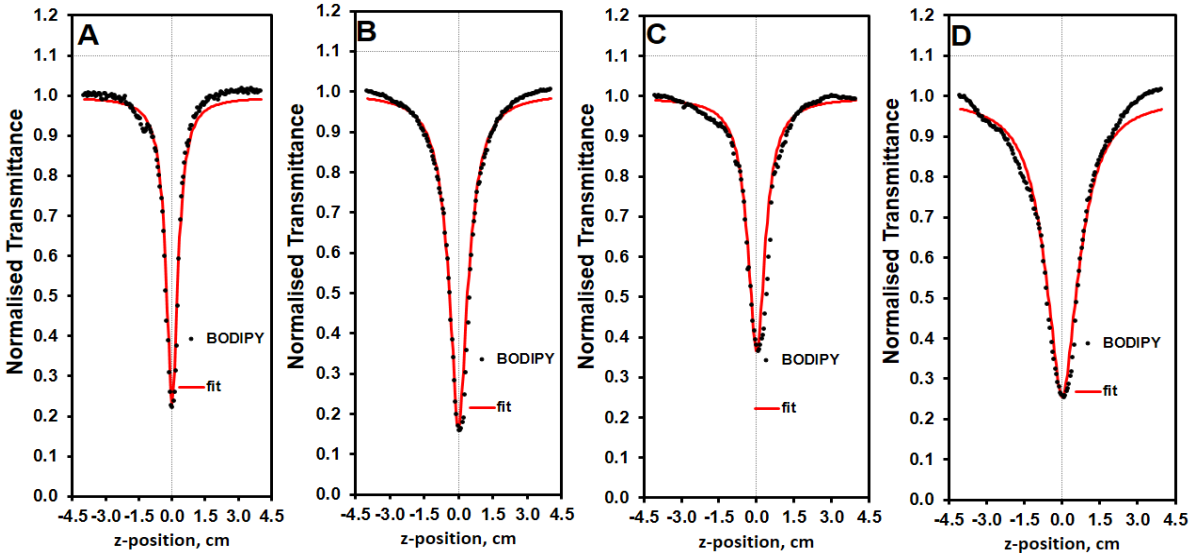

Figure 31. Characteristic open-aperture z-scans of the di-styryl crown ether BODIPY (**4**) in THF at A: input intensity of 10 μJ for each laser pulse and a concentration of 3.02×10^{-5} M, B: input intensity of 40 μJ and a concentration of 3.02×10^{-5} M, C: input intensity of 10 μJ and a concentration of 4.77×10^{-5} M and D: input intensity of input intensity of 40 μJ and a concentration of 4.77×10^{-5} M.

In THF solution, in contrast with the two previous solvents, an increase in concentration failed to significantly reduce transmittance by the BODIPY solution (**Figure 31A** and **Figure 31C**), but the anticipated trend of a decrease in transmittance with higher laser pulse energies was observed at each concentration. A better optical limiting response is again observed at lower laser pulse energies as is evident from the decrease in the β_{eff}, $Im[\chi^{(3)}]$ and γ values with increasing pulse energies (**Table 18**), and there is an increase in the values with an increase in dye concentration. Lower I_{lim} values were again obtained when there is an increase in the dye concentration and a decrease in laser pulse energy (**Table 18**).

Table 18. NLO parameters for the di-styryl crown ether BODIPY (**4**) in THF.

Concentration (M)	Energy (μJ)	α (cm^{-1})	β_{eff} ($cm.GW^{-1}$)	Im [$\chi^{(3)}$] (esu)	γ (esu)	I_{lim} ($J.cm^{-2}$)
3.02×10^{-5}	~10	2.02	274.6	5.81×10^{-10}	1.04×10^{-29}	0.73
	~20		240.2	5.08×10^{-10}	9.09×10^{-30}	0.90
	~30		209.3	4.43×10^{-10}	7.92×10^{-30}	1.05
	~40		193.7	4.10×10^{-10}	7.33×10^{-30}	1.42
4.77×10^{-5}	~10	2.95	581.2	1.23×10^{-9}	1.39×10^{-29}	0.40
	~20		537.9	1.14×10^{-9}	1.29×10^{-29}	0.42
	~30		405.0	8.57×10^{-10}	9.71×10^{-30}	0.55
	~40		466.1	9.86×10^{-10}	1.12×10^{-29}	0.57

In acetonitrile, both concentrations studied were able to reduce transmittance below 50% and an increase in laser pulse energy significantly reduces transmittance by the BODIPY solution (**Figure 32A** and **Figure 32C**). Unlike in the previous three solvents, however, there was significant trend observed related to an increase in dye concentration.

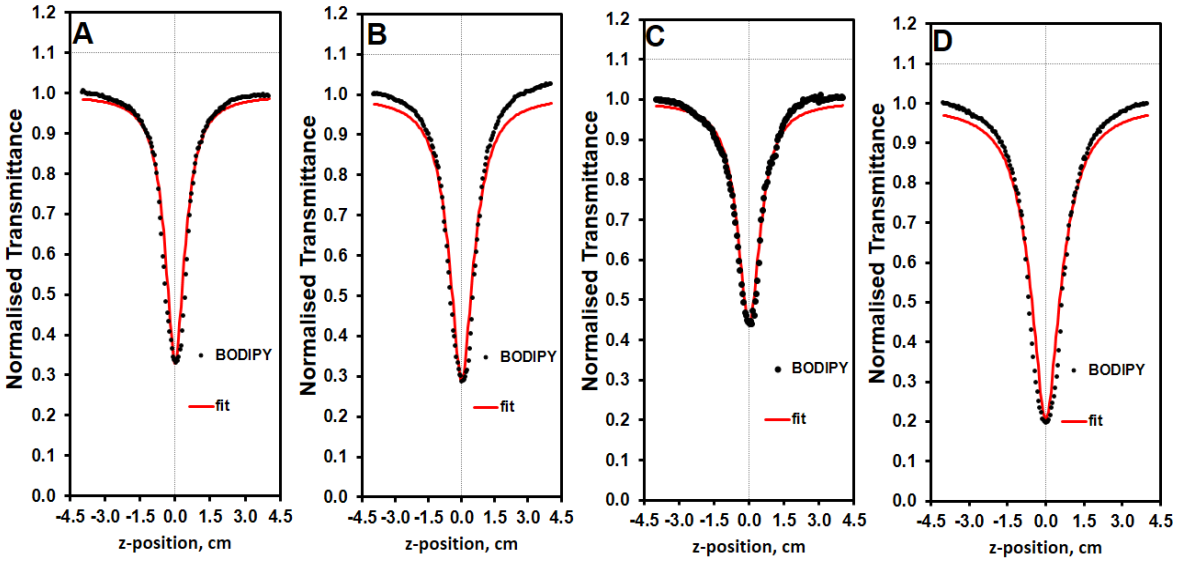

Figure 32. Characteristic open-aperture z-scans of the di-styryl crown ether BODIPY (**4**) in acetonitrile at A: input intensity of 10 µJ for each laser pulse and a concentration of 1.95 × 10^{-5} M, B: input intensity of 40 µJ and a concentration of 1.95 × 10^{-5} M, C: input intensity of 10 µJ and a concentration of 2.93 × 10^{-5} M and D: input intensity of input intensity of 40 µJ and a concentration of 2.93 × 10^{-5} M.

In acetonitrile solution, a better optical limiting response is observed at lower laser pulse energies since the general trend is a decrease in β_{eff}, Im[$\chi^{(3)}$] and γ values with an increase in energy (**Table 19**), and an increase in the dye concentration gives a significantly better optical limiting response as would normally be anticipated. The γ values follow the trend of having higher values at lower concentration as was observed in benzene and DCM. Lower I_{lim} values were again obtained at the higher concentration and at lower laser pulse energies (**Table 19**).

Table 19. NLO parameters for the di-styryl crown ether BODIPY (**4**) in acetonitrile.

Concentration (M)	Energy (μJ)	α (cm^{-1})	β_{eff} ($cm.GW^{-1}$)	$Im[\chi^{(3)}]$ (esu)	γ (esu)	I_{lim} ($J.cm^{-2}$)
1.95×10^{-5}	~10	1.48	365.0	7.07×10^{-10}	2.32×10^{-29}	0.45
	~20		229.3	4.44×10^{-10}	1.46×10^{-29}	0.93
	~30		193.8	3.76×10^{-10}	1.23×10^{-29}	0.95
	~40		173.1	3.35×10^{-10}	1.10×10^{-29}	1.06
2.93×10^{-5}	~10	1.95	422.5	8.19×10^{-10}	1.79×10^{-29}	0.41
	~20		293.1	5.68×10^{-10}	1.24×10^{-29}	0.47
	~30		249.0	4.83×10^{-10}	1.06×10^{-29}	0.82
	~40		238.9	4.63×10^{-10}	1.01×10^{-29}	0.85

In the DMSO solutions, only the higher concentration solution studied was able to reduce transmittance below 50% (**Figure 33B** and **Figure 33D**). Additionally, the transmittance is reduced more for the higher energy laser pulses at each concentration (**Figure 33C** and **Figure 33D**).

The results in **Table 20** are limited to the higher dye concentration of 2.50×10^{-5} M in DMSO, since only this concentration was able to reduce the transmittance by at least 50%. An increase in laser pulse energy seems to result in a poorer optical limiting response as can be seen in the decrease in β_{eff}, $Im[\chi^{(3)}]$ and γ values at higher laser pulse energies. A limiting threshold of below 0.95 $J.cm^{-2}$ was only obtained at the lowest laser pulse energy of 20 μJ.

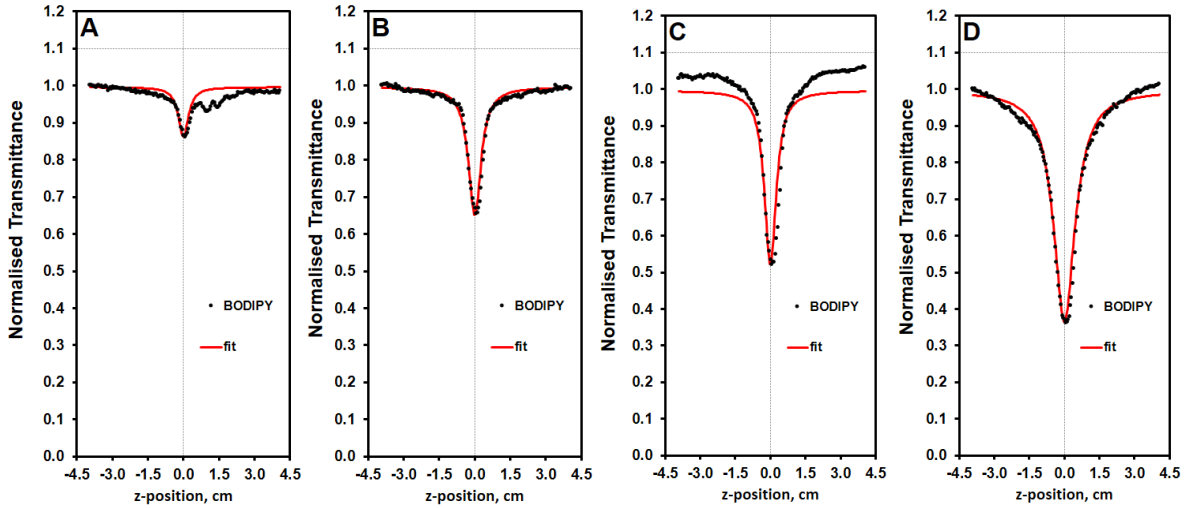

Figure 33. Characteristic open-aperture z-scans of the di-styryl crown ether BODIPY (**4**) in DMSO at A: input intensity of 10 µJ for each laser pulse and a concentration of 1.0×10^{-5} M, B: input intensity of 40 µJ and a concentration of 1.0×10^{-5} M, C: input intensity of 10 µJ and a concentration of 2.5×10^{-5} M and D: input intensity of input intensity of 40 µJ and a concentration of 2.5×10^{-5} M.

Table 20. NLO parameters for the di-styryl crown ether BODIPY (**4**) in DMSO.

Concentration (M)	α (cm^{-1})	Energy (µJ)	β_{eff} ($cm.GW^{-1}$)	$Im[\chi^{(3)}]$ (esu)	γ (esu)	I_{lim} ($J.cm^{-2}$)
2.50×10^{-5}	3.94	~20	250.0	5.87×10^{-10}	1.03×10^{-29}	0.93
		~30	218.1	5.12×10^{-10}	8.96×10^{-30}	1.23
		~40	181.4	4.26×10^{-10}	7.45×10^{-30}	1.42

A comparison for the response by the dye in each solvent was made by overlaying the z-scan responses at 20 µJ together with a plot of output fluence vs input fluence showing the extent of deviation from linear transmittance. Following the reduction in transmittance, benzene seems to perform best followed by DCM, THF and acetonitrile and then DMSO (**Figure 34**).

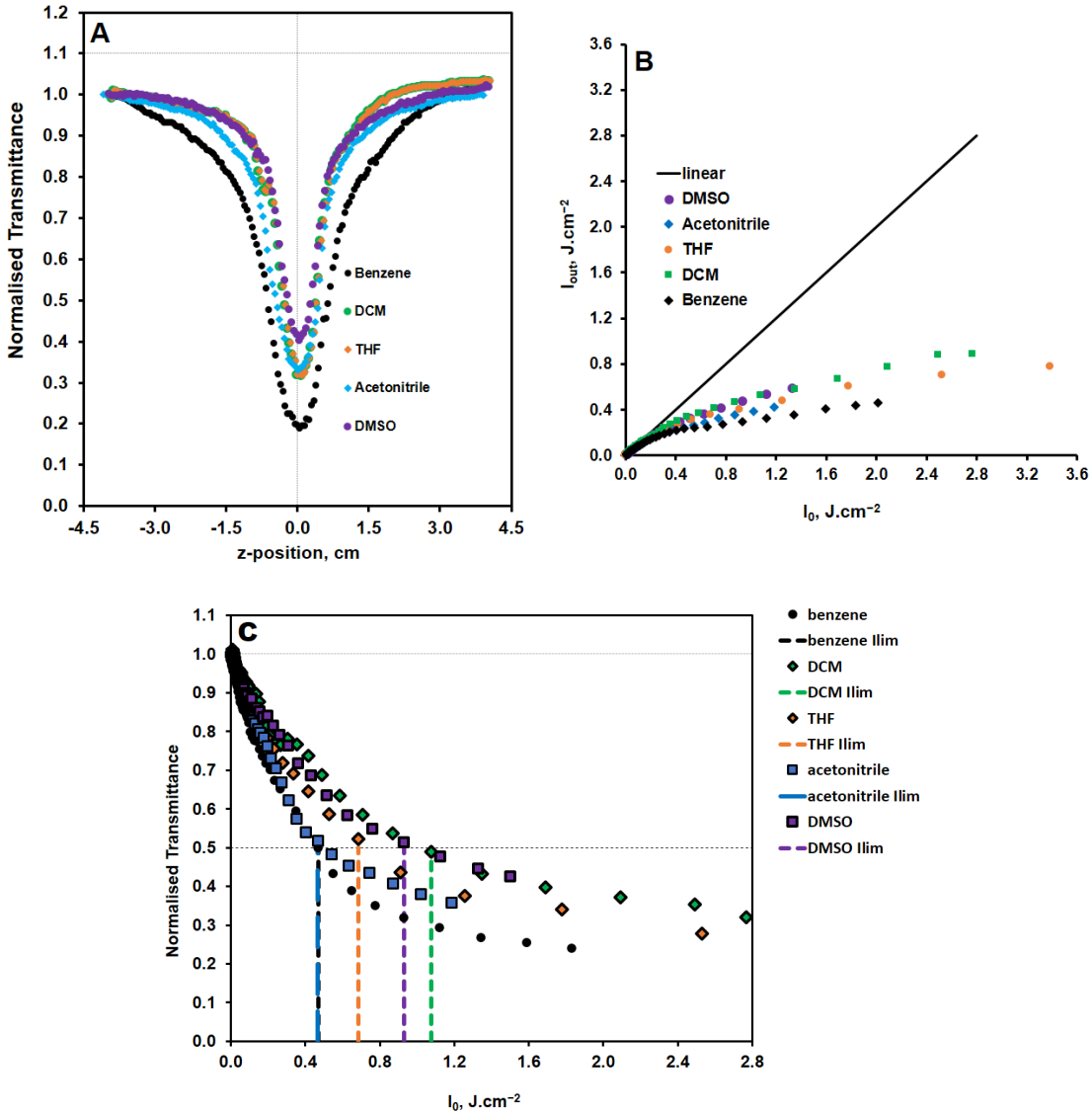

Figure 34. A: Characteristic open-aperture z-scans, B: plots of output fluence (I_{0Out}) vs input fluence (I_0) and C: normalised transmittance vs input fluence curves. Plots for the di-styryl crown ether BODIPY (**4**) were obtained at 20 µJ and the following concentrations: benzene-6.85 × 10^{-6} M, DCM-2.22 × 10^{-5} M, THF-3.02 × 10^{-5} M, acetonitrile-2.93 × 10^{-5} M and DMSO-2.5 × 10^{-5} M.

According to the parameters, the benzene solution, despite having the lowest concentration performs better than any other solvent followed by acetonitrile, THF, DMSO and then DCM as the poorest. There appears to be no clear relationship between the OL ability and both

the fluorescence quantum yield and lifetime for this dye, despite the fact that the lowest fluorescence lifetimes are obtained for the most polar solvents, acetonitrile and DMSO (**Table 14**). Kubheka *et al.*[96] have previously observed for the aza-BODIPY studied therein that the NLO responses obtained demonstrated strong solvent dependence and that this was consistent with differences in the fluorescence lifetimes and quantum yields. This mechanism was attributed to the absence of significant ground state absorbance and intersystem crossing, meaning that the 2PA-assisted ESA which causes an RSA response on the nanosecond timescale is dependent on the population of the S_1 state which is linked to both the fluorescence properties and solvent dependent population of this S_1 state.[96] For BODIPY **4**, this was not the case, however, and this is thought to be as a result of both the nonzero values for the linear absorption coefficient, α (**Table 16**–**Table 20**), and the presence of bromine heavy atoms to promote intersystem crossing which enables ESA in the triplet manifold.

II. Optical limiting properties of BODIPYs **5** and **6**

The NLO studies for BODIPYs **5** and **6** were performed in DCM, and as is typical for styryl-extended BODIPY dyes the main absorption band lies well to the red of the Nd:YAG laser's second harmonic wavelength at 532 nm with minimal absorbance at this wavelength (**Figure 35**). Five different concentrations were studied for each compound. Strong RSA responses were observed in the z-scan plots (**Figure 36** and **Figure 37**) and the NLO parameters (**Table 21** and **Table 22**) will be discussed in the context of two laser pulse energies.

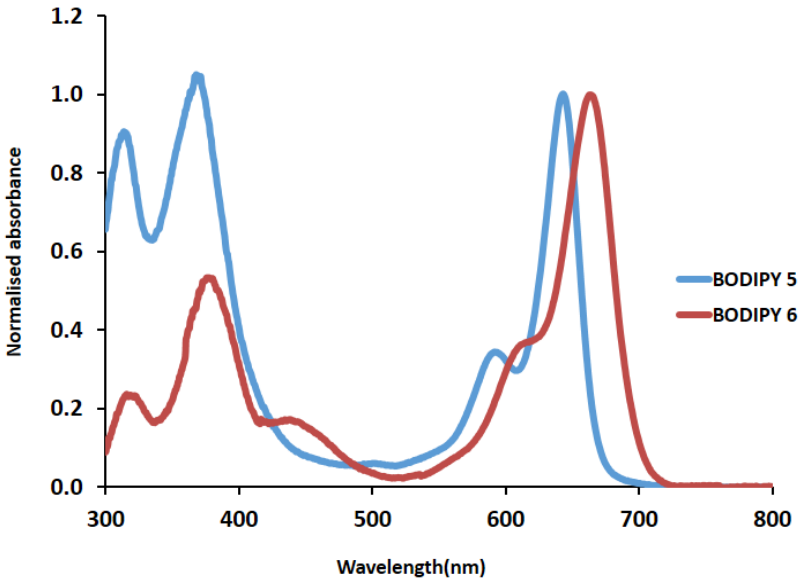

Figure 35. Normalised absorption spectra of BODIPYs **5** and **6** in DCM.

The open-aperture z-scan plots for BODIPY **5** show that all of the solution concentrations studied were able to reduce transmittance far below 50% and this provides a strong indication that the dye is able to perform highly favourably as an optical limiter (**Figure 36**). It was observed that an increase in concentration does not give any significant trend in relation to reduction in transmittance. The observations are generally similar for BODIPY **6** (**Figure 37**). As would normally be anticipated, the transmittance is reduced more for the higher energy laser pulse at each concentration for both compounds (**Figure 36** and **Figure 37**).

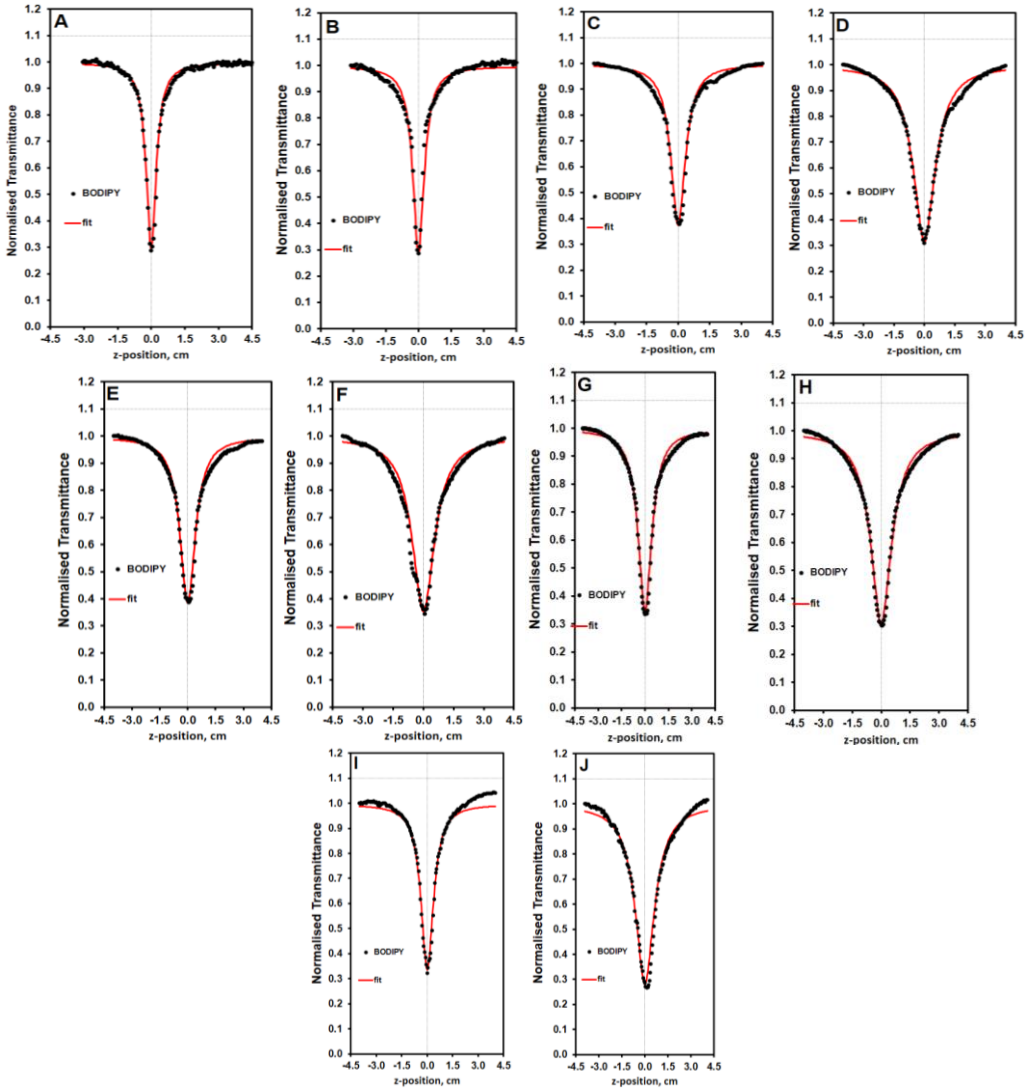

Figure 36. Characteristic open-aperture z-scans of BODIPY **5** in DCM at A: input intensity of 15 µJ for each laser pulse and a concentration of 2.31 × 10^{-5} M, B: input intensity of 35 µJ and a concentration of 2.31 × 10^{-5} M, C: input intensity of 15 µJ and a concentration of 3.35 × 10^{-5} M, D: input intensity of input intensity of 35 µJ and a concentration of 3.35 × 10^{-5} M, E: input intensity of 15 µJ and a concentration of 4.15 × 10^{-5} M, F: : input intensity of 35 µJ and a concentration of 4.15 × 10^{-5} M , G: input intensity of 15 µJ and a concentration of 5.24 × 10^{-5} M, H: input intensity of 35 µJ and a concentration of 5.24 × 10^{-5} M, I: input intensity of 15 µJ and a concentration of 6.91 × 10^{-5} M and J: input intensity of 35 µJ and a concentration of 6.91 × 10^{-5} M.

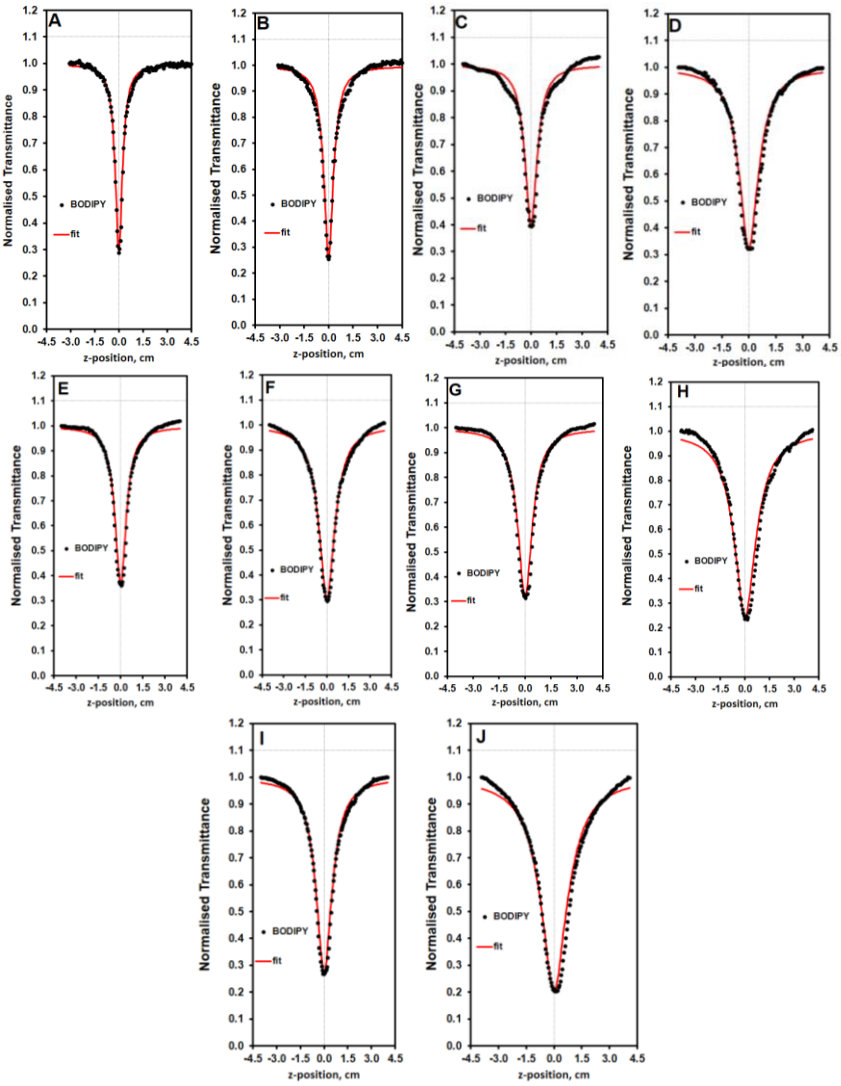

Figure 37. Characteristic open-aperture z-scans of BODIPY **6** in DCM at A: input intensity of 15 μJ for each laser pulse and a concentration of 1.19×10^{-5} M, B: input intensity of 35 μJ and a concentration of 1.19×10^{-5} M, C: input intensity of 15 μJ and a concentration of 1.9×10^{-5} M, D: input intensity of input intensity of 35 μJ and a concentration of 1.9×10^{-5} M, E: input intensity of 15 μJ and a concentration of 2.49×10^{-5} M, F: input intensity of 35 μJ and a concentration of 2.49×10^{-5} M, G: input intensity of 15 μJ and a concentration of 3.08×10^{-5} M, H: input intensity of 35 μJ and a concentration of 3.08×10^{-5} M, I: input intensity of 15 μJ and a concentration of 3.67×10^{-5} M and J: input intensity of 35 μJ and a concentration of 3.67×10^{-5} M.

The main OL parameters were studied and a better optical limiting response was observed for the lower energy laser pulses, since an increase in energy gives lower β_{eff}, $Im[\chi^{(3)}]$ and γ values (**Table 21** and **Table 22**). For both dyes, the $Im[\chi^{(3)}]$ and γ values lie in the optimal range that has been previously reported for these parameters and this clearly demonstrates that these dyes are potentially useful as optical limiting materials, warranting further study in this regard.

Table 21. NLO parameters for BODIPY **5** in DCM.

Concentration (M)	Energy (μJ)	α (cm^{-1})	β_{eff} ($cm.GW^{-1}$)	$Im[\chi^{(3)}]$ (esu)	γ (esu)	I_{lim} ($_{J.cm^{-2}}$)
2.31×10^{-5}	~15	0.71	173	3.77×10^{-10}	8.34×10^{-30}	1.74
	~35		135	2.94×10^{-10}	6.51×10^{-30}	1.35
3.35×10^{-5}	~15	1.27	219.5	4.78×10^{-10}	7.27×10^{-30}	0.74
	~35		191.4	4.17×10^{-10}	6.34×10^{-30}	0.90
4.19×10^{-5}	~15	1.62	294.8	6.42×10^{-10}	7.82×10^{-30}	0.67
	~35		214.5	4.67×10^{-10}	5.69×10^{-30}	0.66
5.24×10^{-5}	~15	1.59	305.1	6.64×10^{-10}	6.47×10^{-30}	0.59
	~35		216.8	4.72×10^{-10}	4.60×10^{-30}	0.95
6.91×10^{-5}	~15	0.98	385.8	8.40×10^{-10}	6.20×10^{-30}	0.44
	~35		249	5.42×10^{-10}	4.00×10^{-30}	0.92

For both dyes, an increase in dye concentration results in a significantly better OL response, as can be observed in the increase in the values of β_{eff} and $Im[\chi^{(3)}]$. The γ values, however, follow an opposite trend with significantly higher values observed at lower concentrations for both compounds. Differences in this regard are not unexpected, since γ is defined to factor in concentration, while the other parameters are not.[151] The I_{lim} values at the lowest

concentration were above 0.95 J.cm^{-2} for both BODIPYs, but lower values were observed with an increase in dye concentration and a decrease in the energy of the incident laser pulses.

Table 22. NLO parameters for BODIPY **6** in DCM.

Concentration (M)	Energy (μJ)	α (cm^{-1})	β_{eff} (cm.GW^{-1})	Im[$\chi^{(3)}$] (esu)	γ (esu)	I_{lim} (J.cm^{-2})
1.19 × 10^{-5}	~15	0.3	185.0	4.03 × 10^{-10}	1.7 × 10^{-29}	0.96
	~35		117.0	2.55 × 10^{-10}	1.1 × 10^{-29}	1.47
1.9 × 10^{-5}	~15	0.62	203.0	4.42 × 10^{-10}	1.2 × 10^{-29}	0.74
	~35		171.1	3.72 × 10^{-10}	1 × 10^{-29}	0.89
2.49 × 10^{-5}	~15	0.63	219.9	4.79 × 10^{-10}	9.8 × 10^{-30}	0.64
	~35		168.3	3.66 × 10^{-10}	7.5 × 10^{-30}	0.94
3.08 × 10^{-5}	~15	1.05	274.4	5.97 × 10^{-10}	9.9 × 10^{-30}	0.49
	~35		223.8	4.87 × 10^{-10}	8.1 × 10^{-30}	0.89
3.67 × 10^{-5}	~15	0.93	323.5	7.04 × 10^{-10}	9.8 × 10^{-30}	0.37
	~35		220.6	4.80 × 10^{-10}	6.7 × 10^{-30}	0.87

BODIPY **6** was found to perform somewhat better as an optical limiter than BODIPY **5** when studied in DCM. This is evident in both the increased reduction in transmittance at the focal point of the z-scan instrument and the enhanced NLO parameter values that were obtained at comparable concentrations (**Table 21** and **Table 22**). This is consistent with previous observations with phthalocyanines that optical limiters with heavy atoms have the ability to perform better as optical limiters,[107–109] and suggests that halogenation may be a useful strategy for enhancing the OL properties of BODIPY dyes.

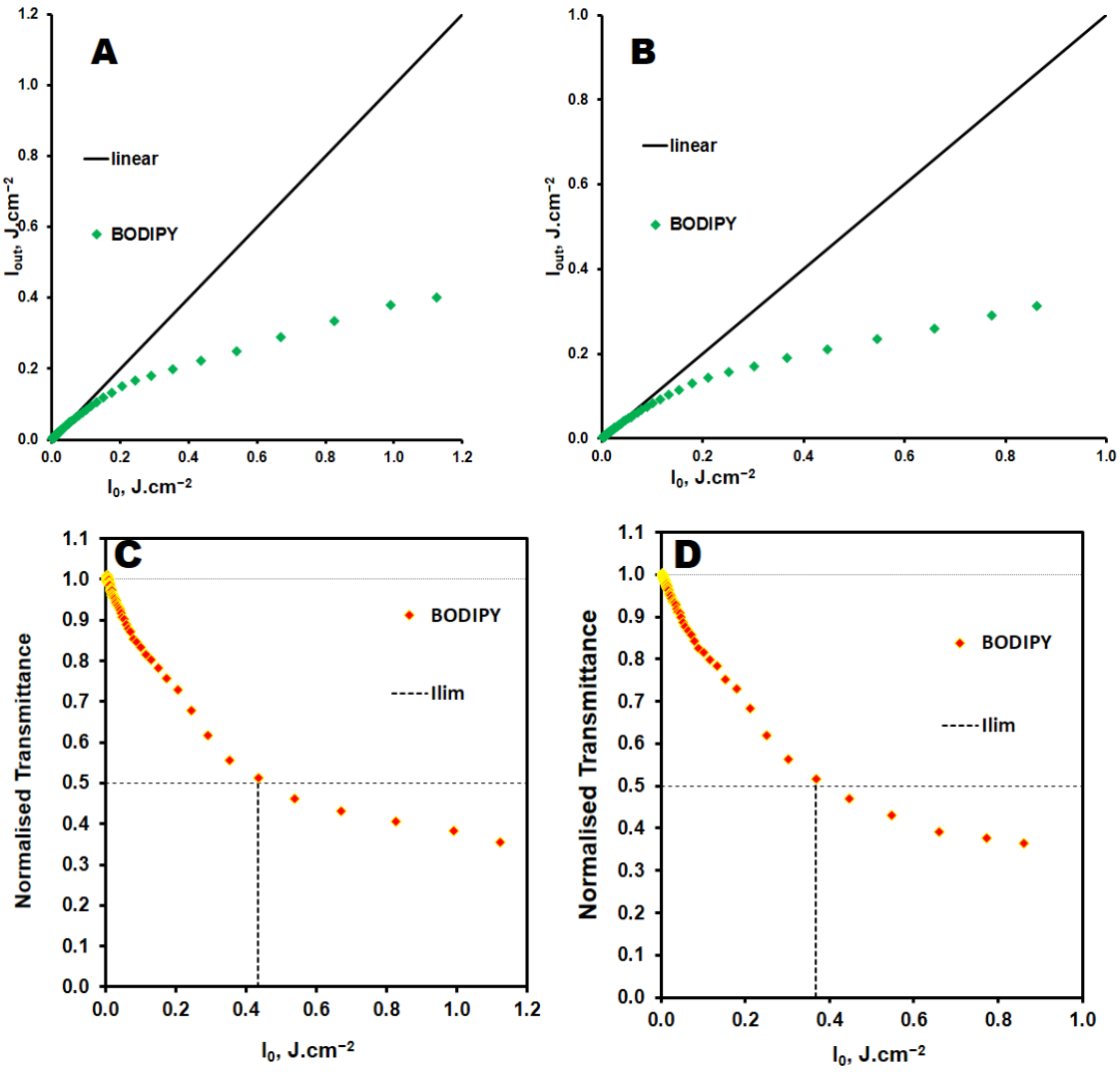

Figure 38. A: plots of output fluence (I_{0out}) vs input fluence (I_0) for BODIPY **5**, B: plots of output fluence (I_{0out}) vs input fluence (I_0) for BODIPY **6**, C: transmittance (T) vs input fluence curve for BODIPY **5** and D: transmittance (T) vs input fluence curve for BODIPY **6**. Data obtained at an input intensity of 15 µJ and concentrations of 6.91×10^{-5} M for BODIPY **5** and 3.67×10^{-5} M for BODIPY **6**.

III. Optical limiting properties of BODIPY **7**

The optical limiting ability of BODIPY **7** was assessed in DCM, THF, acetonitrile and DMSO and in all solvents the main absorption band lies well above the second harmonic wavelength at 532 nm and there is minimal absorbance at 532 nm and there is minimal absorbance at this wavelength (**Figure 39**).

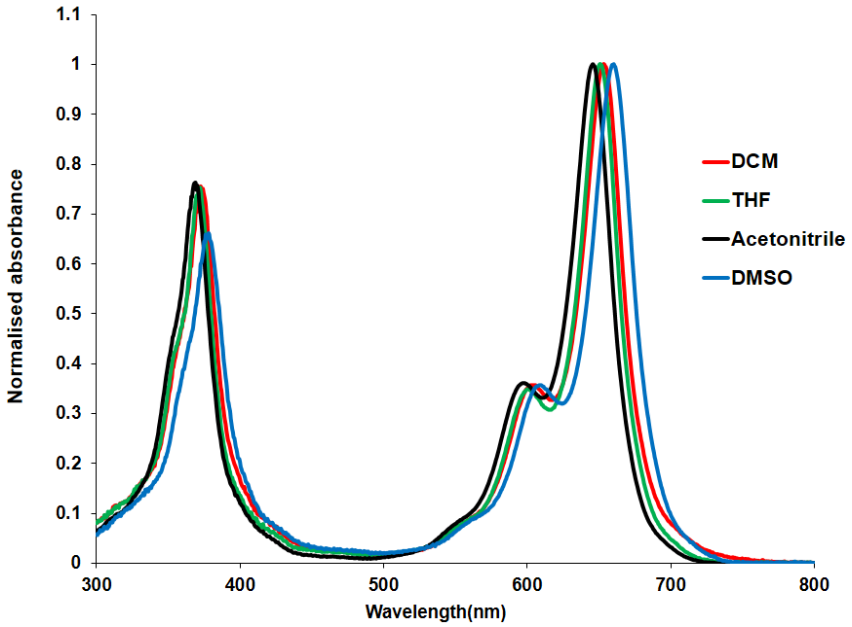

Figure 39. Normalised absorption spectra of BODIPY **7** in different organic solvents.

The optical limiting studies for BODIPY **7** were carried out using two different concentrations for each solvent and strong RSA responses[167–169] were observed in the z-scan plots in each solvent (**Figure 40**–**Figure 43**) at two different laser pulse energies.

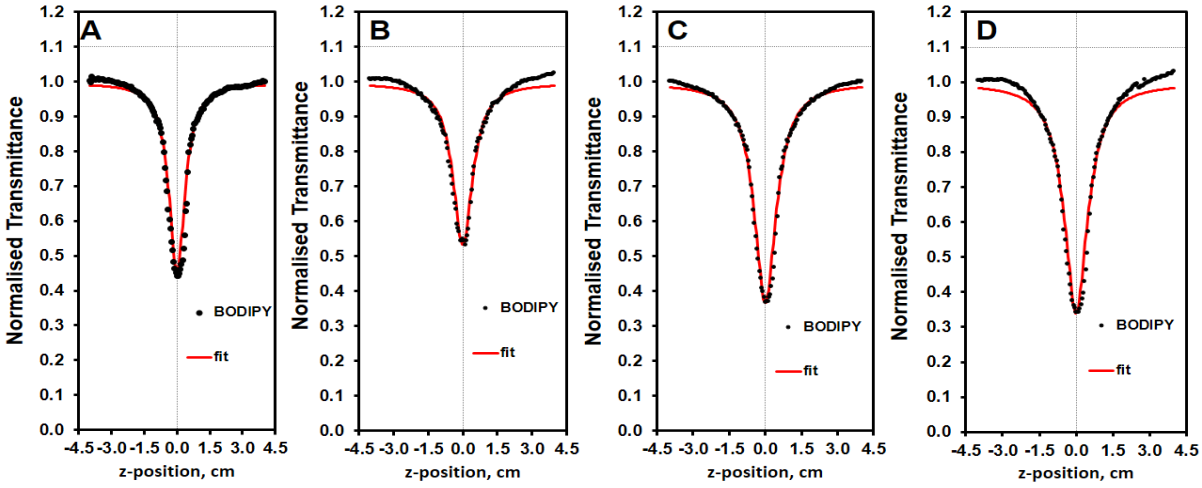

Figure 40. Characteristic open-aperture z-scans of BODIPY **7** in DCM at A: input intensity of 20 µJ for each laser pulse and a concentration of 2.0×10^{-5} M, B: input intensity of 40 µJ and a concentration of 2.0×10^{-5} M, C: input intensity of 20 µJ and a concentration of 3.12×10^{-5}M and D: input intensity of input intensity of 40 µJ and a concentration of 3.12×10^{-5}M.

Table 23. NLO parameters for BODIPY **7** in DCM.

Concentration (M)	Energy (µJ)	α (cm^{-1})	β_{eff} ($cm.GW^{-1}$)	$Im[\chi^{(3)}]$ (esu)	γ (esu)	I_{lim} ($J.cm^{-2}$)
2.00×10^{-5}	~20	0.86	141.2	3.07×10^{-10}	7.84×10^{-30}	1.20
	~30		136.9	2.98×10^{-10}	7.60×10^{-30}	1.25
3.12×10^{-5}	~10	1.19	290.8	6.33×10^{-10}	1.04×10^{-29}	0.65
	~20		223.4	4.86×10^{-10}	7.96×10^{-30}	0.87
	~30		186.4	4.06×10^{-10}	6.64×10^{-30}	1.40
	~40		125.8	2.74×10^{-10}	4.48×10^{-30}	1.34

In DCM, the β_{eff} and $Im[\chi^{(3)}]$ values increase with dye concentration. For both concentrations, an increase in incident laser pulse energy gives poorer/lower β_{eff}, $Im[\chi^{(3)}]$ and γ values (**Table 24**). The I_{lim} values appear to be lower at higher dye concentration as

would normally be anticipated and some of the values lie below the desired 0.95 J.cm^{-2} threshold for 10 ns laser pulses at 532 nm.

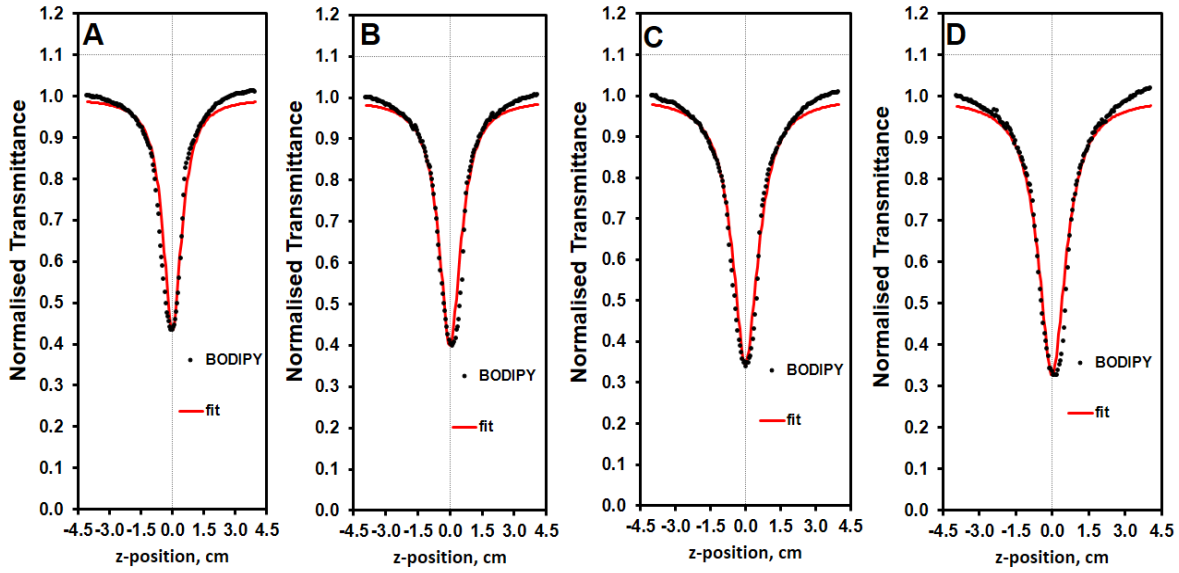

Figure 41. Characteristic open-aperture z-scans of BODIPY **7** in THF at A: input intensity of 20 µJ for each laser pulse and a concentration of 1.1 × 10^{-5} M, B: input intensity of 40 µJ and a concentration of 1.1 × 10^{-5} M, C: input intensity of 20 µJ and a concentration of 1.6 × 10^{-5} M and D: input intensity of input intensity of 40 µJ and a concentration of 1.6 × 10^{-5} M.

In THF, transmittance was consistently reduced below 50 % at the focal point of the z-scan instrument at all laser pulse energies studied except at 10 µJ for the low concentration of 1.32 × 10^{-4} M. An increase in both laser pulse energy and dye concentration reduces transmittance by the BODIPY solution, albeit only slightly with the pulse energy increases (**Figure 41C** and **Figure 41D**). The β_{eff} and Im[$\chi^{(3)}$] values increase with the dye concentration, whereas the γ value decreases. For both concentrations, an increase in incident laser pulse energy results in poorer/lower β_{eff}, Im[$\chi^{(3)}$] and γ values (**Table 24**). Lower I_{lim} values were

obtained at high concentration and low laser pulse energies. Some of the values lie above the desired value of 0.95 J.cm^{-2}.

Table 24. NLO parameters for BODIPY **7** in THF.

Concentration (M)	Energy (μJ)	α (cm^{-1})	β_{eff} ($cm.GW^{-1}$)	$Im[\chi^{(3)}]$ (esu)	γ (esu)	I_{lim} ($J.cm^{-2}$)
1.10×10^{-5}	~20	1.08	215.1	4.55×10^{-10}	2.23×10^{-29}	0.78
	~30		156.9	3.32×10^{-10}	1.63×10^{-29}	0.97
	~40		125.2	2.65×10^{-10}	1.30×10^{-29}	1.55
1.60×10^{-5}	~10	1.45	313.8	6.64×10^{-10}	2.24×10^{-29}	0.71
	~20		268.3	5.67×10^{-10}	1.92×10^{-29}	0.74
	~30		205.2	4.34×10^{-10}	1.47×10^{-29}	0.80
	~40		171.4	3.63×10^{-10}	1.22×10^{-29}	1.10

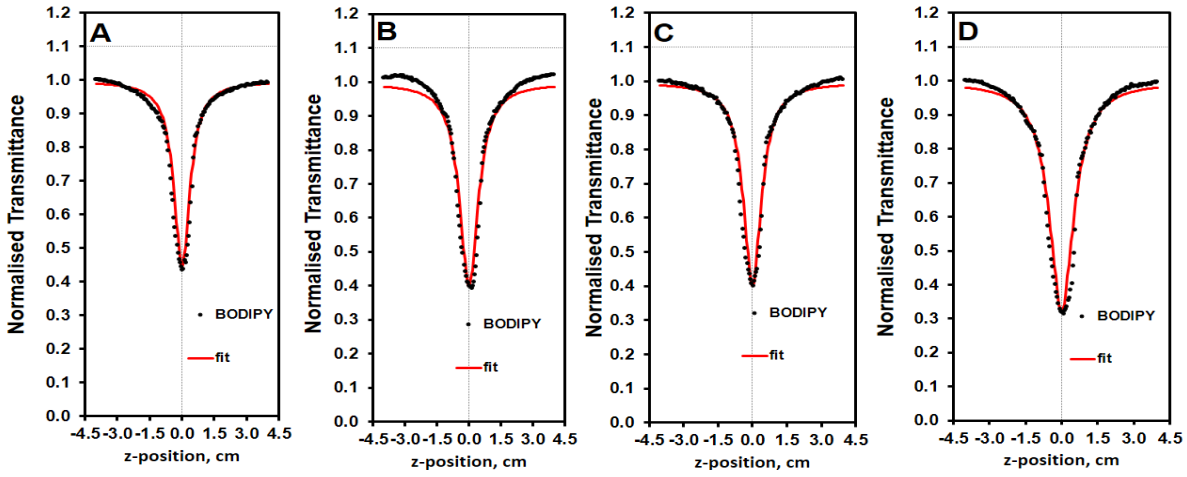

Figure 42. Characteristic open-aperture z-scans of BODIPY **7** in acetonitrile at A: input intensity of 20 μJ for each laser pulse and a concentration of 7.84×10^{-6} M, B: input intensity of 40 μJ and a concentration of 7.84×10^{-6} M, C: input intensity of 20 μJ and a concentration of 1.09×10^{-5} M and D: input intensity of input intensity of 40 μJ and a concentration of 1.09×10^{-5} M.

In acetonitrile, the transmittance was consistently reduced below 50% except for the studies at 10 μJ for both concentrations, and an increase in both laser pulse energy and dye concentration reduces transmittance by the BODIPY solution (**Figure 42**).

Table 25. NLO parameters for BODIPY **7** in acetonitrile.

Concentration (M)	Energy (μJ)	α (cm^{-1})	β_{eff} ($cm.GW^{-1}$)	$Im[\chi^{(3)}]$ (esu)	γ (esu)	I_{lim} ($J.cm^{-2}$)
7.84×10^{-6}	~20	1.16	173.9	3.37×10^{-10}	2.76×10^{-29}	1.08
	~30		118.5	2.30×10^{-10}	1.88×10^{-29}	1.75
	~40		108.5	2.10×10^{-10}	1.72×10^{-29}	1.70
1.09×10^{-5}	~20	1.46	194.3	3.77×10^{-10}	2.22×10^{-29}	0.80
	~30		214.6	4.16×10^{-10}	2.45×10^{-29}	0.70
	~40		185.9	3.60×10^{-10}	2.12×10^{-29}	0.83

The β_{eff} and $Im[\chi^{(3)}]$ values in acetonitrile increase with dye concentration (**Table 25**). An increase in incident laser pulse results in lower β_{eff}, $Im[\chi^{(3)}]$ and γ values observed with an increase in energy. The three parameters reach their highest values at 30 μJ for the higher concentration (**Table 25**). The I_{lim} values were lower at higher concentration and the values lie above 0.95 $J.cm^{-2}$ for the lower concentration solutions. The lowest I_{lim} value was obtained at 30 μJ, which appears to be the optimal energy for the OL response in this solvent.

The open-aperture z-scan plots of the DMSO solutions at a concentration of 6.46×10^{-6} M, at 10 and 20 μJ do not dip below 50% transmittance, in contrast with the other scans for this dye. As would normally be anticipated, an increase in both energy and concentration

significantly reduces transmittance by the BODIPY solution in this solvent (**Figure 43C** and **Figure 43D**).

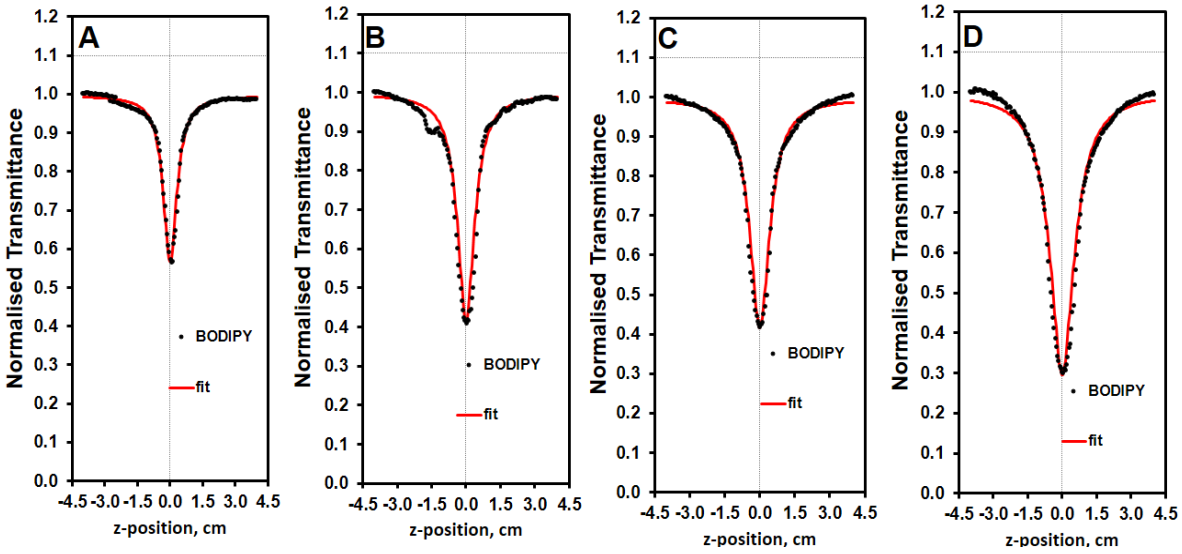

Figure 43. Characteristic open-aperture z-scans of BODIPY **7** in DMSO at A: input intensity of 20 µJ for each laser pulse and a concentration of 6.46 × 10^{-6} M, B: input intensity of 40 µJ and a concentration of 6.46 × 10^{-6} M, C: input intensity of 20 µJ and a concentration of 1.13 × 10^{-5} M and D: input intensity of input intensity of 40 µJ and a concentration of 1.13 × 10^{-5} M.

Table 26. NLO parameters for BODIPY **7** in DMSO.

Concentration (M)	Energy (µJ)	α (cm^{-1})	β_{eff} ($cm.GW^{-1}$)	$Im[\chi^{(3)}]$ (esu)	γ (esu)	I_{lim} ($J.cm^{-2}$)
6.46 × 10^{-6}	~30	0.85	114.2	2.68 × 10^{-10}	1.82 × 10^{-29}	1.52
	~40		102.6	2.41 × 10^{-10}	1.63 × 10^{-29}	1.74
1.13 × 10^{-5}	~10	1.28	291.2	6.83 × 10^{-10}	2.64 × 10^{-29}	0.87
	~20		213.7	5.02 × 10^{-10}	1.94 × 10^{-29}	0.79
	~30		191.6	4.50 × 10^{-10}	1.74 × 10^{-29}	0.87
	~40		192.4	4.52 × 10^{-10}	1.75 × 10^{-29}	0.82

In DMSO, as is the case with THF and acetonitrile, a better optical limiting response is observed for the lower laser pulse energy, since there is a decrease in the β_{eff}, $Im[\chi^{(3)}]$ and γ values (**Table 26**) with increasing laser pulse energy, and the OL response is enhanced by an increase in the dye concentration. The I_{lim} value in the higher concentration solutions lie below 0.95 $J.cm^{-2}$, while those of the low concentration solutions do not.

To make a comparison for the response by the dye in each solvent, an overlay of the z-scan responses at 30 µJ was made together with a plot of output fluence vs input fluence showing the extent of deviation from linear transmittance. Following the reduction in transmittance, DMSO seems to perform best followed by acetonitrile, and then DCM and THF (**Figure 44**). According to the parameters β_{eff}, $Im[\chi^{(3)}]$, γ and I_{lim}, acetonitrile and DMSO perform better followed by THF while DCM seems to possess the poorest optical limiting parameters. This is despite the acetonitrile solution having the lowest concentration.

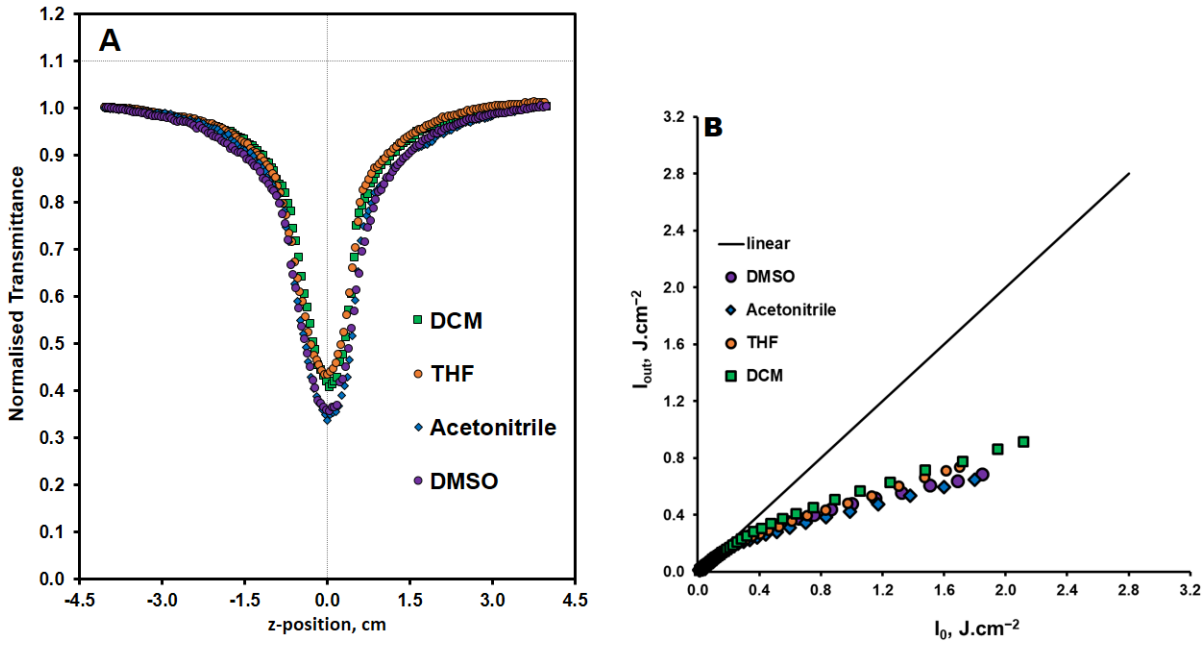

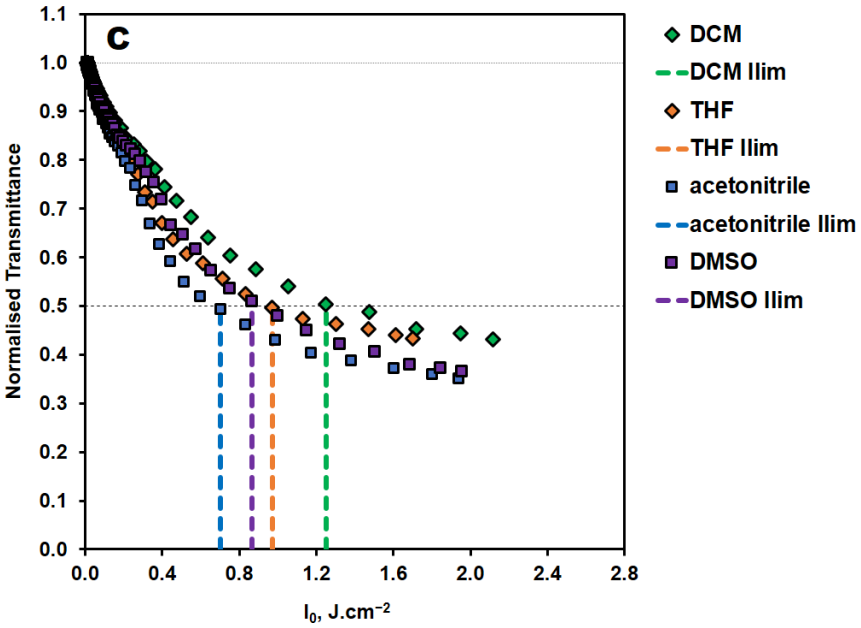

Figure 44. A: Characteristic open-aperture z-scans, B: plots of output fluence (I_{0out}) vs input fluence (I_0) and C: normalised transmittance vs input fluence curves. Plots for BODIPY **7** were obtained at 30 μJ and the following concentrations: DCM-2.0 × 10^{-5} M, THF-1.1 × 10^{-5} M, acetonitrile-1.09 × 10^{-5} M and DMSO-1.13 × 10^{-5} M.

For BODIPY **7**, the OL parameters Im[$\chi^{(3)}$] and γ values lie in the optimal range that has been reported for these parameters. This clearly demonstrates that this dye is potentially useful as an optical limiting material and merits further study in this regard. This was similar to results recently obtained by Harris *et al.*[95] and Kubheka *et al.*[96] for BODIPY dyes and an aza-BODIPY dye, respectively. As previously mentioned in the context of BODIPY **4**, Kubheka *et al.*[96] observed NLO responses with a strong solvent dependence for an aza-BODIPY dye, due to an 2PA-assisted ESA which causes an RSA response on the nanosecond timescale that is dependent on the population of the S_1 state which is linked to both the fluorescence properties and solvent dependent population of this S_1 state.[96] This was initially expected to also be the case for BODIPY **7** since the dye does not contain any heavy atoms to promote

intersystem crossing and ESA in the triplet manifold. The observations were not consistent with this, however, since there is no clear relationship between the OL responses, solvent polarity, and both the fluorescence quantum yields and lifetimes for this dye (**Table 15**). The difference in mechanism can be attributed to the nonzero values for the linear absorption coefficient, α (**Table 23**–**Table 26**). This suggests that the main mechanism for the RSA response of this dye results from an ESA mechanism which depends primarily on population of the S_1 state via linear absorption.

IV. Optical limiting properties of BODIPYs **8**, **9** and **10**.

This section focuses on the optical limiting ability of three 2,6-diethyl-substituted BODIPY dyes, **8**, **9** and **10**, which contain an electron withdrawing ester group on the *meso*-phenyl position and strongly electron donating styryl groups at the 3,5-positions to study the effect of the D-π-A type structure of these dyes on the OL properties. The main absorption band lies well above the Nd:YAG laser's second harmonic wavelength at 532 nm in benzene, DCM and acetonitrile and there is minimal absorbance at this wavelength (**Figure 45**) making the dye potentially suitable for use as an OL material.

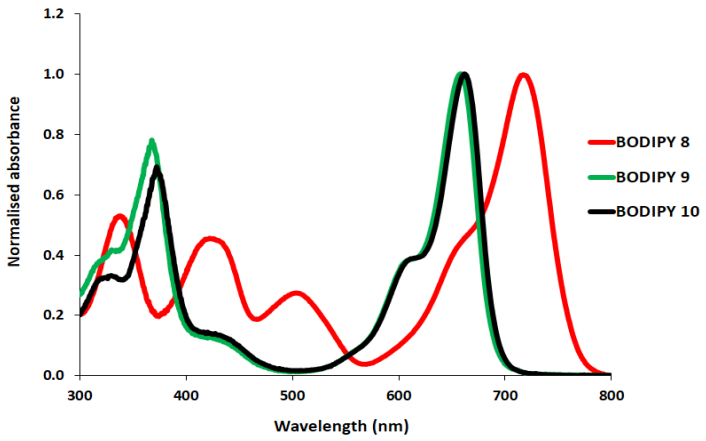

Figure 45. Normalised absorption spectra of BODIPYs **8**, **9** and **10** in benzene.

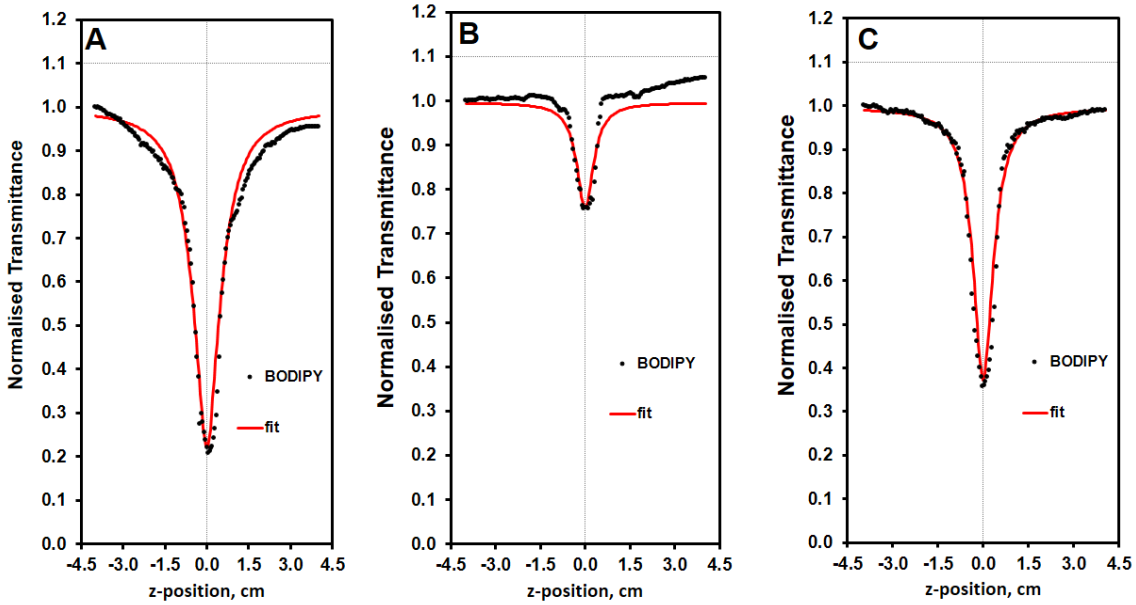

Figure 46. Characteristic open-aperture z-scans of BODIPY **8** in different organic solvents at an input intensity of 25 μJ for each laser pulse and a concentration of 3.0×10^{-5} M. A: benzene, B: DCM and C: acetonitrile.

BODIPY **8** was studied at a concentration of 3.0×10^{-5} M in all solvents. The benzene solution was able to reduce the transmittance by 79% at the focal point of the laser, followed by the acetonitrile solution with a 64% reduction and DCM with a 24% reduction (**Figure 46**). When the concentration was doubled in DCM, the OL response improved significantly and the transmittance was reduced by 79% (**Figure 47**). A comparison of the β_{eff}, $Im[\chi^{(3)}]$ and γ values shows that the best optical limiting response is observed for the benzene solution at a concentration of 3.0×10^{-5} M (**Table 27**). This is also evident in the plots showing the extent of deviation from linearity (**Figures 48A** and **49A**).

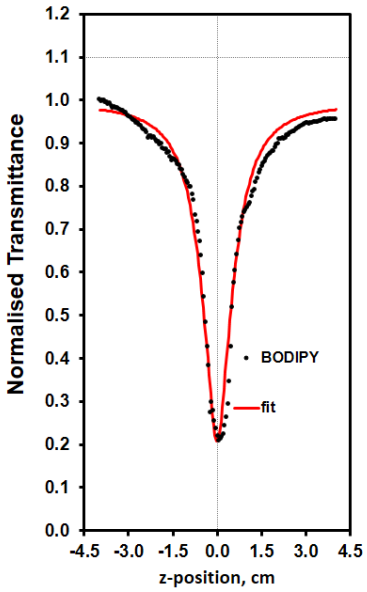

Figure 47. Open-aperture z-scan of BODIPY **8** in DCM at an input intensity of 25 µJ for each laser pulse and a concentration of 6.2×10^{-5} M.

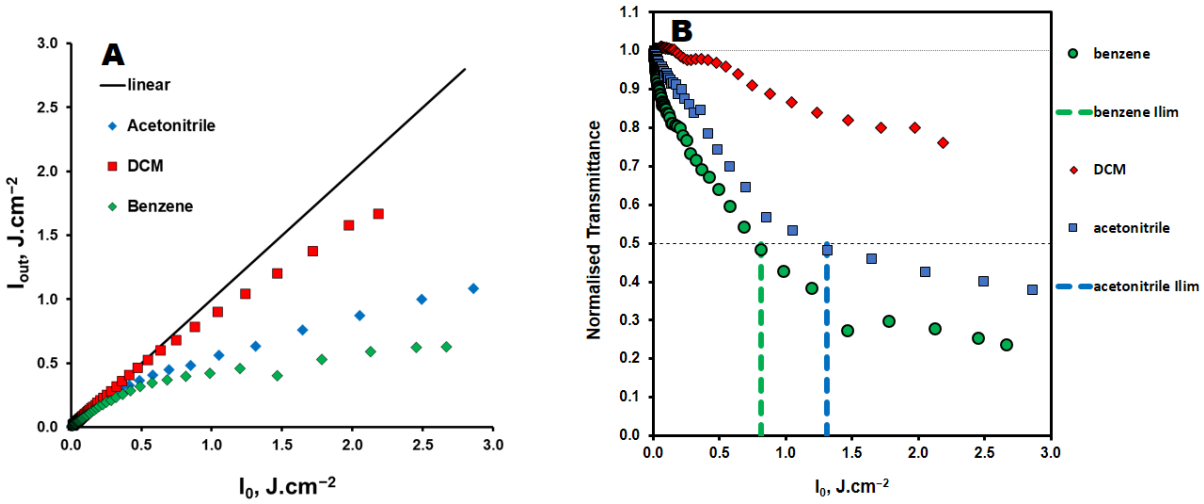

Figure 48. Overlayed data for BODIPY **8**. A: Plots of output fluence (I_{0out}) vs input fluence (I_0) and B: normalised transmittance vs input fluence curves. Data obtained at input intensity of 25 µJ for each laser pulse and a concentration of 3.0×10^{-5} M in all solvents.

Only the I_{lim} values in benzene at 3.0×10^{-5} M (**Figure 48B**) and in DCM at 6.2×10^{-5} M (**Figure 49B**) lie below 0.95 J.cm^{-2}. Overall, BODIPY **8** proved to be more effective as an optical limiter in the less polar benzene solvent, as is evident in both the z-scan plots

showing the extent of reduction in transmittance and in the OL parameters that were obtained (**Table 28**).

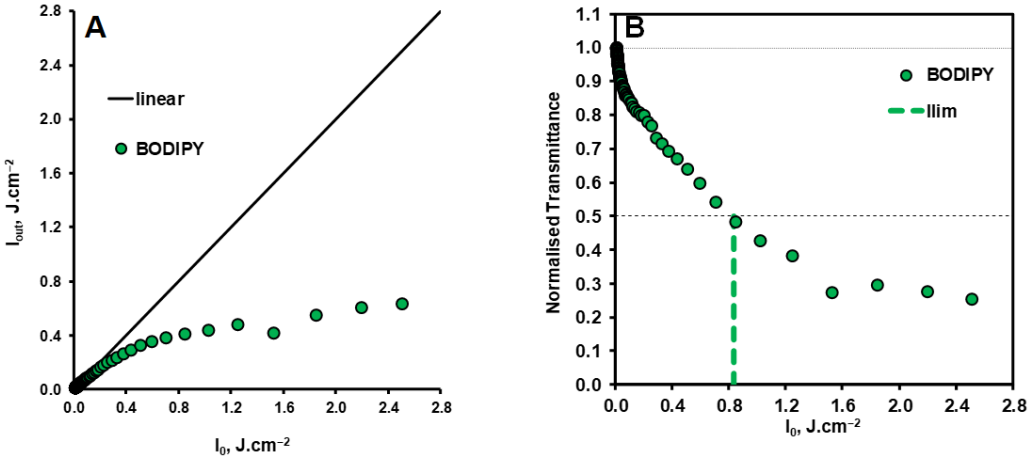

Figure 49. The optical limiting ability of BODIPY **8** at a higher concentration. A: Plot of output fluence (I_{0out}) vs input fluence (I_0) and B: normalised transmittance vs input fluence curve. Data obtained at input intensity of 25 µJ and a concentration of 6.2×10^{-5} M in DCM.

BODIPY **9** was studied at a concentration of 1.5×10^{-5} M in all solvents. Acetonitrile was able to reduce the transmittance by 80% at the focal point of the z-scan instrument, followed by DCM with a 74% reduction and benzene with a 59% reduction (**Figure 50**). When the concentration was increased to 8.0×10^{-5} M in benzene and DCM, the OL response improved significantly for benzene but not for DCM as the transmittance was reduced by 71% and 65%, respectively (**Figure 52**). The optical limiting parameters show that a better optical limiting response is observed for the acetonitrile solution at a concentration of 1.5×10^{-5} M, followed by DCM and then benzene (**Table 27**). The enhanced OL responses in acetonitrile and DCM are also evident in the plots showing the extent of deviation from linearity (**Figure 51A**).

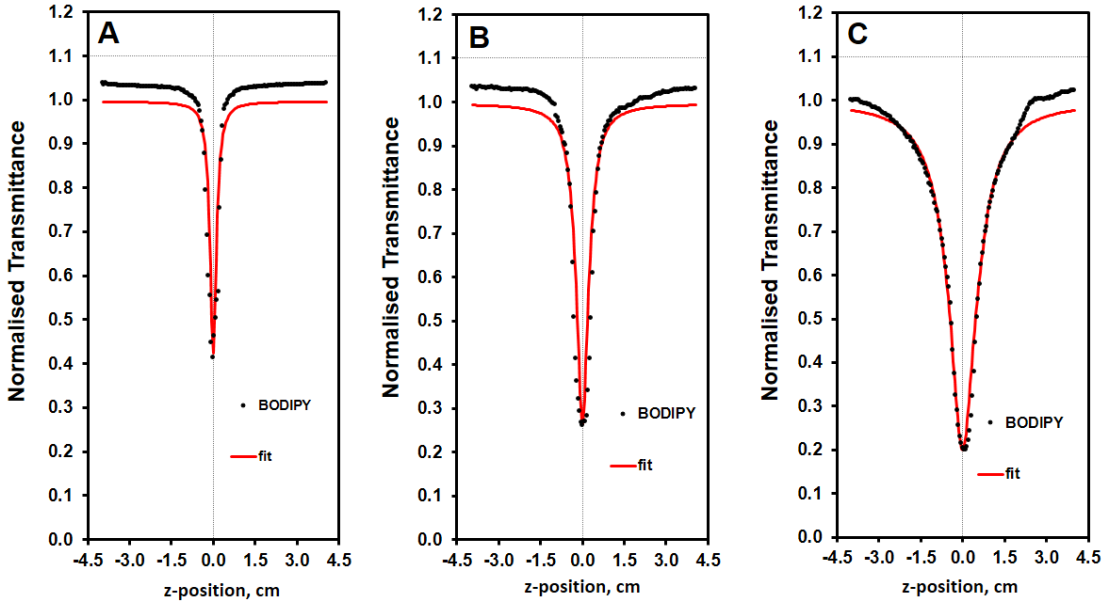

Figure 50. Characteristic open-aperture z-scans of BODIPY **9** in different organic solvents at an input intensity of 25 µJ for each laser pulse and a concentration of 1.5 × 10^{-5} M. A: benzene, B: DCM and C: acetonitrile.

The I_{lim} values were lowest in acetonitrile followed by the sample studied in DCM (**Figure 51B**), and the value obtained in benzene at higher concentration was also well below 0.95 J.cm^{-2} (**Figure 53B**). Overall, BODIPY **9** proved to be a more effective optical limiter in the more polar acetonitrile solvent followed by DCM as is evident in the OL parameters that were derived from the z-scan data (**Table 27**).

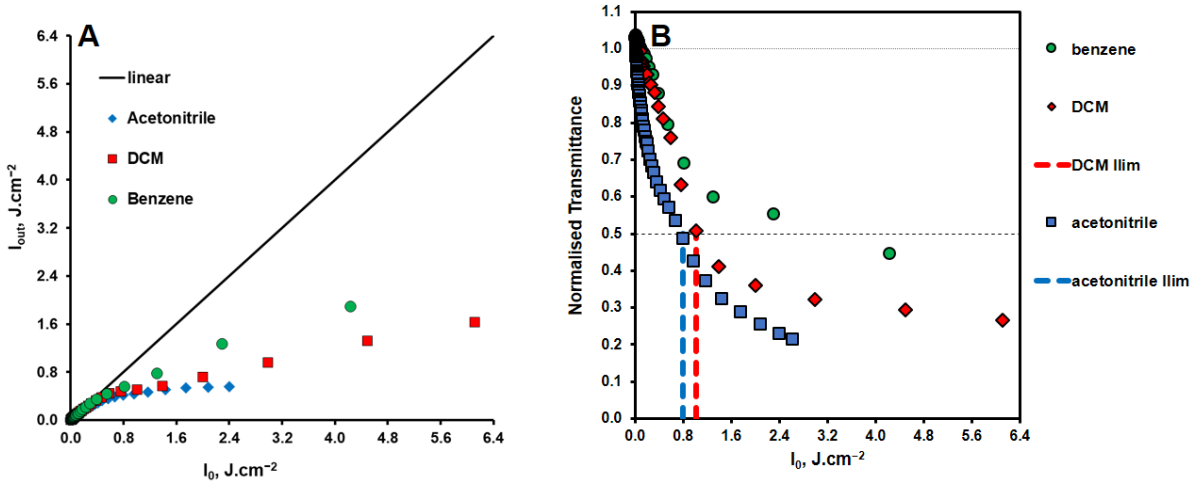

Figure 51. Overlayed data for BODIPY **9**. A: Plots of output fluence (I_{0out}) vs input fluence (I_0) and B: normalised transmittance vs input fluence curves. Data obtained at input intensity of 25 µJ for each laser pulse and a concentration of 1.5×10^{-5} M in all solvents.

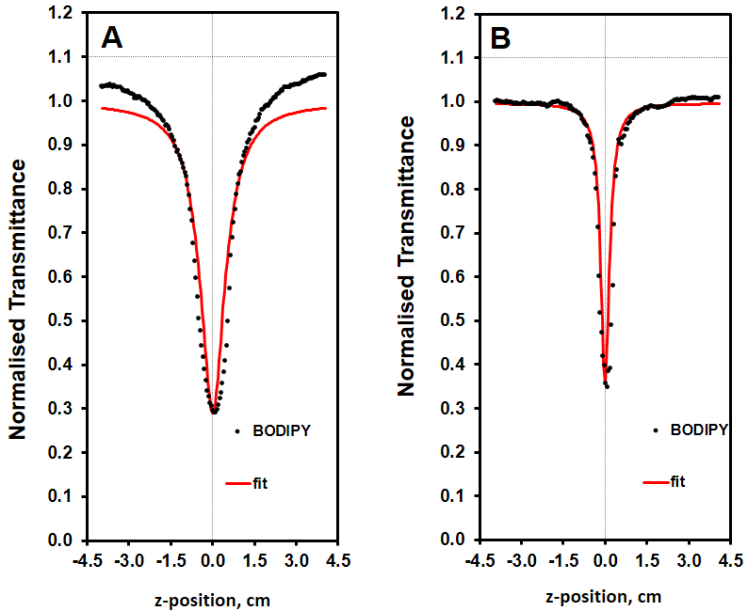

Figure 52. Characteristic open-aperture z-scans of BODIPY **9** at an input intensity of 25 µJ for each laser pulse and a concentration of 8.0×10^{-5} M. A: benzene and B: DCM.

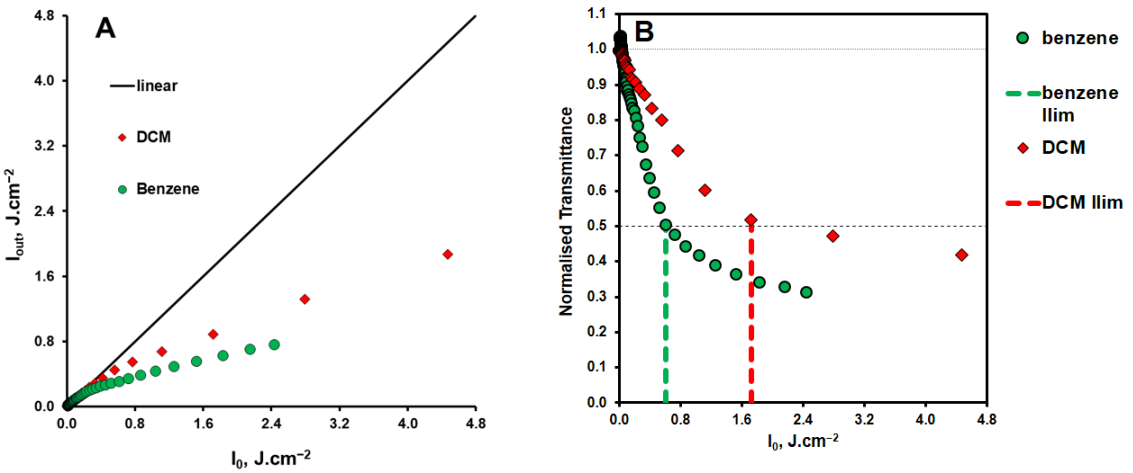

Figure 53. Overlayed data for BODIPY **9** at a higher concentration. A: Plots of output fluence (I_{0out}) vs input fluence (I_0) and B: normalised transmittance vs input fluence curves. Data obtained at input intensity of 25 µJ for each laser pulse and a concentration of 8.0×10^{-5} M in both solvents.

BODIPY **10** was studied at a concentration of 5.9×10^{-5} M in benzene and DCM, but not in acetonitrile due to poor solubility. The benzene solution was able to reduce the transmittance by 79% while DCM had an 83% reduction (**Figure 54**).

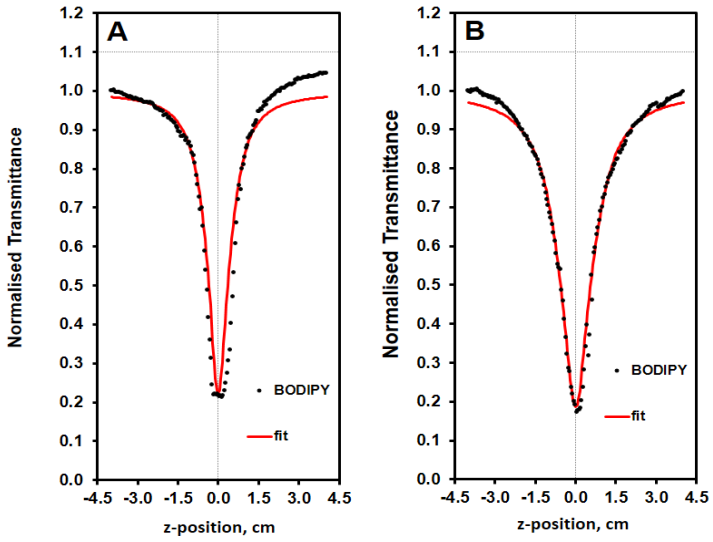

Figure 54. Characteristic open-aperture z-scans of BODIPY **10** at an input intensity of 25 µJ for each laser pulse and a concentration of 5.9×10^{-5} M. A: benzene and B: DCM.

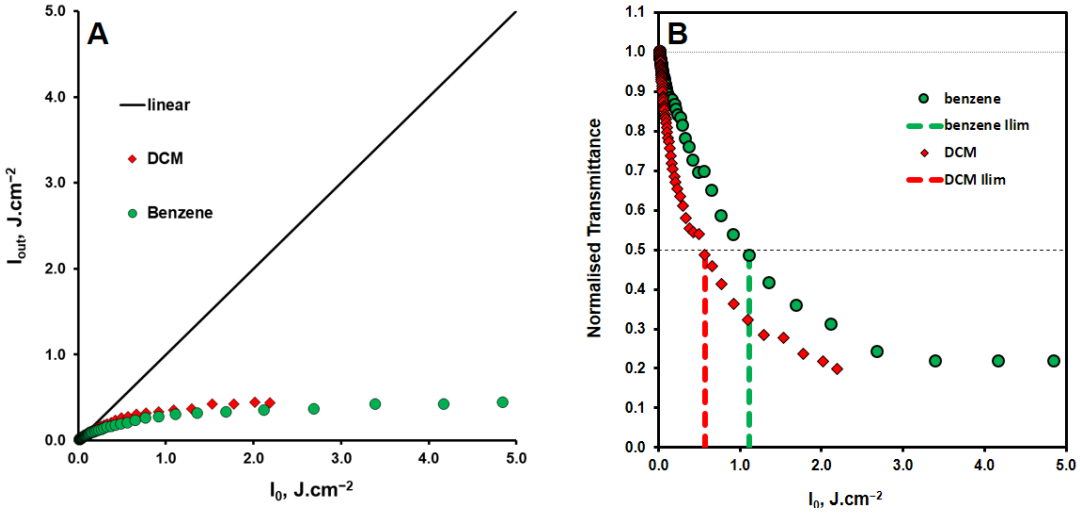

Figure 55. Overlayed data for BODIPY **10**. A: Plots of output fluence (I_{out}) vs input fluence (I_0) and B: normalised transmittance vs input fluence curves. Data obtained at input intensity of 25 µJ and a concentration of 5.9×10^{-5} M in both solvents

Table 27. NLO parameters for the 2,6-diethyl BODIPYs (**8**, **9** and **10**) in different organic solvents at an input energy of ~25 µJ.

BODIPY	Solvent	Conc. (M)	α (cm^{-1})	β_{eff} ($cm.GW^{-1}$)	Im [$\chi^{(3)}$] (esu)	γ (esu)	I_{lim} ($J.cm^{-2}$)
8	benzene	3.0×10^{-5}	6.98	471.9	1.14×10^{-9}	1.56×10^{-29}	0.82
	DCM		1.35	24.9	5.42×10^{-11}	9.30×10^{-31}	N/A
	acetonitrile		3.42	149.0	2.89×10^{-10}	6.19×10^{-30}	1.31
	DCM	6.2×10^{-5}	2.76	357.9	7.79×10^{-10}	6.44×10^{-30}	0.85
9	benzene	1.5×10^{-5}	0.16	43.9	1.06×10^{-10}	2.91×10^{-30}	N/A
	DCM		0.35	89.2	1.94×10^{-10}	6.61×10^{-30}	1.01
	acetonitrile		1.83	350.9	6.80×10^{-10}	2.90×10^{-29}	0.80
	benzene	8.0×10^{-5}	0.87	202.5	4.89×10^{-10}	2.52×10^{-30}	0.61
	DCM		1.33	71.9	1.57×10^{-10}	1.00×10^{-30}	1.72
10	benzene	5.9×10^{-5}	1.10	148.8	3.60×10^{-10}	2.51×10^{-30}	1.11
	DCM		1.38	426.8	9.29×10^{-10}	8.05×10^{-30}	0.57

The parameters β_{eff}, Im[$\chi^{(3)}$] and γ for BODIPY **10** show that there is a better optical limiting response for the DCM solution (**Table 27**). The I_{lim} values were also lower in DCM (**Figure 55B**).

For all three BODIPYs, **8**, **9** and **10**, the values for the OL parameters Im[$\chi^{(3)}$] and γ (**Table 27**) lie in the optimal range that has been previously reported for these parameters and this clearly demonstrates that these dyes are potentially useful as optical limiting materials and merit further study in this regard. There is no clear trend or relation between the fluorescence properties and the NLO responses for all the dyes (**Table 11**, **Table 12** and **Table 13**) and there was no significant solvent dependence of the NLO responses obtained. Also, the dyes did not contain heavy atoms to promote intersystem crossing which enables ESA in the triplet manifold, and it can therefore be concluded that an ESA mechanism which depends on population of the S_1 state via linear absorption is likely to be the main mechanism of interest, since each of the dyes possessed nonzero values for the linear absorption coefficient, α, in all solvents at 532 nm (**Table 27**).

Concluding remarks

The β_{eff}, Im[$\chi^{(3)}$], I_{lim} and γ values that were derived from the z-scan studies clearly demonstrate that BODIPYs **4**, **5**, **7**, **8**, **9** and **10** are potentially suitable for use in OL applications and merit further study in this regard, as was expected since the main spectral bands associated with the polarisable π-system lie beyond 600 nm with relatively weak absorbance at 532 nm, the second harmonic of Nd:YAG lasers that was used in these studies. The trends in the OL parameters are consistent with a positive nonlinear absorption

coefficient coupled with a decrease in transmittance as the material approaches the focal point of the z-scan instrument and high laser light intensity.[166]

BODIPY **4** was studied in five different solvents of differing polarity, while BODIPY **7** was studied in four solvents of differing polarity. For both dyes, there is no clear relationship between the OL ability and the fluorescence quantum yields and lifetime values. It was recently reported by Kubheka *et al*.[96] that there was significant solvent dependence in the NLO response for an aza-BODIPY dye containing no heavy atoms that was consistent with differences in the fluorescence lifetimes and quantum yields. In the absence of significant ground state absorbance and intersystem crossing to 2PA-assisted ESA which causes an RSA response on the nanosecond timescale, the mechanism was attributed to solvent dependent population of the S_1 state which is linked to the fluorescence properties.[96] These trends were initially expected to also be the observed for BODIPY **7** but the experimental data were not consistent with this. This can be attributed to the nonzero values for the linear absorption coefficient, α, which provides scope for significant ground-state absorption. In the context of BODIPY **4**, the presence of bromine heavy atoms to promote intersystem crossing which enables ESA from the triplet manifold is also likely to be a significant factor. Despite the absence of significant intersystem crossing, BODIPY **7** possesses favourable OL properties at 532 nm, providing further evidence that an ESA mechanism from the S_1 state can account for the OL properties of non-halogenated BODIPY dyes.[19,20,32,170-173]

BODIPYs **5** and **6** were studied in DCM at five different concentrations. BODIPY **6** contains bromine heavy atoms, hence for BODIPY **5** it is expected that the mechanism will involve ESA from the S_1 state due to the absence of intersystem crossing to the triplet state while

for BODIPY **6** the triplet manifold is likely to be involved. This sheds light on the relative efficiency of the OL mechanism for these BODIPY dyes, since dyes which undergo intersystem crossing are known to possess OL responses related to ESA from the T_1 state. Overall, BODIPY **6** performs better as an optical limiter when studied in DCM, thereby suggesting that optical limiters with heavy atoms can perform better as optical limiters due to ESA from the longer-lived T_1 state,[107–109] and that halogenation may prove to be a useful strategy for enhancing the OL properties of the BODIPY chromophore. BODIPYs **8**, **9** and **10** were also investigated in different solvents, with **8** and **9** studied in benzene, DCM and acetonitrile, while **10** was studied in benzene and DCM. For all three dyes, there is no significant trend between the OL responses observed and both solvent polarity and fluorescence lifetimes and quantum yields (**Table 11**, **Table 12** and **Table 13**). As with BODIPY **7**, this can again be attributed to the nonzero values for the linear absorption coefficient, α, since there are no heavy atoms, and an ESA mechanism which depends on the population of the S_1 state by linear absorption is the main mechanism.

In drawing all these conclusions, it is worth noting that BODIPY dyes have still not been extensively studied for their optical limiting ability at 532 nm. Within our research group, some articles have been published on the study of π-extended BODIPY dyes as nonlinear optical limiters.[95,96,171,174] Of all the studies undertaken both in this thesis and within the group, the optical limiting parameters $\mathrm{Im}[\chi^{(3)}]$ and γ lie within the ranges that are normally viewed as being suitable for optical limiting, as tabulated above for the studies conducted herein, and this demonstrates that further research in this area is merited. A final point worth noting is that the di-styryl crown-ether-substituted BODIPY (**4**) is predicted to have an unusually large permanent dipole moment introduced by the benzo-fused crown ether and

4-dimethylaminophenyl substituents and it has been experimentally demonstrated that the dye possesses good optical limiting properties at 532 nm, as is evident from the enhanced RSA profiles that are observed. The results for BODIPY **4** have been published,[174] and it is expected that highly favourable results for other D-π-A type BODIPY dyes studied in this thesis, such as BODIPYs **8**, **9** and **10**, will also be published soon. D-π-A type structures provide an obvious opportunity for further studies on the use of BODIPY dyes as optical limiters on the nanosecond timescale at 532 nm, and this approach could be extended in future to the other possible laser wavelengths of interest.

Chapter 5:

BODIPY-cyclodextrin inclusion complex formation and characterisation

As mentioned in Chapter 1, the main factors responsible for cyclodextrin inclusion complex formation are non-covalent forces such as Van der Waals and hydrophobic interactions which stabilise the complex.[41,44] Since the three parent cyclodextrins have a different number of glucopyranose units, they have different sizes and molecular dimensions and this enables them to include different guests. For example, α-cyclodextrin tends to complex low molecular weight molecules and compounds with aliphatic side chains while β-cyclodextrin complexes aromatic and heterocyclic compounds, while γ-cyclodextrin typically complexes larger molecules in the size range of macrocycles and steroids.[41,47] The inclusion complexes formed tend to be of a [guest]/[cyclodextrin] molar ratio of 1:1 but this is not always the case as higher or lower molar ratios are possible depending on how the guest and cyclodextrin relate when it comes to size and steric factors.[41,175] Another point worth noting is the fact that the inclusion of guest molecules in the cyclodextrin cavity is not fixed or permanent but is a dynamic equilibrium and the strength of the interaction depends on both the complementarity of how well the guest and cyclodextrin fit with each other and also the intermolecular interactions between surface atoms.[47] When included in the cyclodextrins, the physicochemical properties of the guest are usually modified or enhanced, depending on the conformation adopted by the guest within the cavity. This inclusion tends to protect the guest from specific properties which would otherwise render the guest incapable of performing its function. These include conferring solubility on insoluble guest molecules, protection and stabilisation of labile guests against the degradative effects of oxidation, visible or UV light and heat, and a decrease in and control of volatility and sublimation.[40]

The dyes used here contain various functional groups, particularly at the *meso*-position and it has been shown previously that cyclodextrins can encapsulate a wide range of functional groups and compounds within their cavity. These include but are not limited to straight or branched chain aliphatic compounds, aldehydes, ketones, alcohols, organic acids, fatty acids, aromatics, gases, and polar compounds such as halogens, oxyacids and amines.[40,176] These functional groups (present on the guest) serve two purposes; one is steric and the other one thermodynamic. Sterically, when the size of the guest molecule or its functional groups matches with the requirements of the cyclodextrin cavity, the guest is included in the cavity; and the same principle applies to the thermodynamic interactions between the different components of the system, i.e. guest-host interactions in a given solvent must pull the guest into the cyclodextrin cavity.[40] Energetically, there are four favourable interactions that promote the formation of the inclusion complex:[40]

- The displacement of polar water molecules from the apolar cyclodextrin cavity.
- The increased number of hydrogen bonds formed as the displaced water leaves the cavity.
- A reduction of the repulsive interactions between the hydrophobic guest and the aqueous environment as a result of inclusion into the hydrophobic cavity.
- An increase in the hydrophobic interactions as the guest inserts itself into the apolar cyclodextrin cavity.

For the studies in this thesis, conferring aqueous solubility on insoluble heavy atom containing BODIPY dyes is the main goal; the dyes are only soluble in organic media, and this is not suitable for most biological and green applications. The main aim, therefore, is to create suitable conditions for the BODIPY dyes to generate singlet oxygen in aqueous media.

5.1. Inclusion complex preparation

Following literature methods, the inclusion complexes of BODIPYs **2a**, **2b** and **2c** were studied.[41,177,178] This was carried out by following the co-precipitation method. Standard BODIPY-cyclodextrin solutions with total concentrations of 2.54×10^{-3} M, 2.38×10^{-3} M and 2.53×10^{-3} M for BODIPYs **2a**, **2b** and **2c**, respectively, were prepared as follows: the respective cyclodextrin, α or β, was dissolved in deionised water maintained at ca. 75 °C with stirring; the temperature was dropped to ca. 28 °C and the respective BODIPY dye, dissolved in ethanol, was added dropwise and after overnight with continuous stirring at room temperature, the precipitate was filtered and dried.

There are different techniques which can be used to study and characterise cyclodextrin complexes, both in solution and in the solid state.[41] Among these, the most referenced in literature are: phase solubility, high-performance liquid chromatography (HPLC), circular dichroism, NMR, (XRD), differential scanning calorimetry (DSC), thermogravimetric analysis (TGA), UV-visible absorption spectroscopy, FT-IR, and FT-Raman Spectroscopy.[45,52,179–184]

The following were employed in this study:

Fourier-transform infrared spectroscopy (FT-IR)

With FT-IR spectroscopy, when the guest is complexed with the cyclodextrin, there are shifts or changes in the spectrum relative to that of the uncomplexed guest, and there are typically interferences from the cyclodextrin.[52,183] These changes and shifts tend to be very small hence each spectrum needs to be carefully studied and analysed.[52] The typical method carefully following changes in the spectra is recording the spectrum of the guest alone, cyclodextrin alone, a physical mixture made by mixing the guest and cyclodextrin in the absence of a solvent and then finally that of the inclusion complex.[41,52,183]

Circular dichroism

Marconi and Mayer[45] have studied the conformational and circular dichroism responses of cyclodextrin inclusion complexes and were able to "elucidate different geometrical configurations and to gain insight into the relationship between structural and dynamic properties of the complexes".[41,45]

X-ray powder diffraction analysis (XRD)

XRD is a technique used to study the crystal arrangement and geometry of materials. Osadebe *et al*., [178] have used this technique to study the diffraction patterns of piroxicam and β-cyclodextrin inclusion complexes. A sample in powder or crystalline form is usually used and the absence or presence of peaks in the respective diffractograms of the guest, cyclodextrin, physical mixture or complex are carefully analysed. The diffractogram of the physical mixture is usually a superimposition of the patterns of the guest and host, while that of the inclusion complex does not correspond to those of both the guest and host.[184]

UV-visible absorption spectroscopy

UV-visible absorption spectroscopy is not only useful in studying changes in the guest spectra when complexed, but can also be used to determine complex stoichiometries.[41,42]

Scanning electron microscopy (SEM)

The SEM technique enables the visualization of surface morphological changes of the physical mixture and inclusion complex relative to those of the guest and cyclodextrin.[184–186] Similar to the superimposition usually observed in FT-IR and XRD analyses, the physical mixture tends to show a combined morphology of the guest and cyclodextrin, with the complex not showing the original morphologies and instead forming a new one.[184]

5.2. Results and discussion

5.2.1. UV-visible absorption studies

The UV-visible absorption spectra recorded in deionised water were observed to be more broadened for the inclusion complexes (**Figure 56** and **Figure 57**) relative to the sharp bands observed for the BODIPY dyes in organic media. Although this is thought to be the effect of aggregation of the inclusion complexes in water, it is not conclusive as the dyes were completely insoluble in water before complexation and as such no direct comparisons can be drawn between inclusion complex spectra in water and BODIPY dye spectra in water. As a result of this aggregation, fluorescence studies were not successful, which was expected because aggregates are known not to fluoresce.

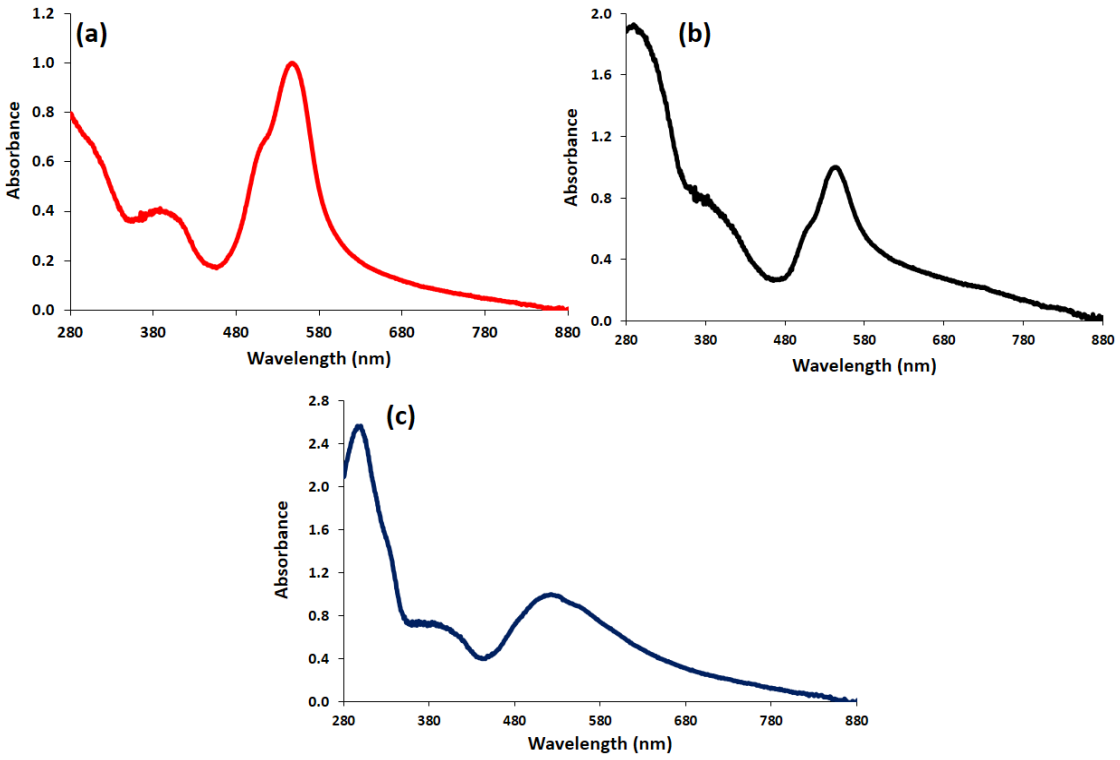

Figure 56. Normalised absorption spectra of BODIPY-(α-cyclodextrin) inclusion complexes in deionised water.(a) BODIPY **2a**-(α-cyclodextrin), (b) BODIPY **2b**-(α-cyclodextrin) and (c) BODIPY **2c**-(α-cyclodextrin).

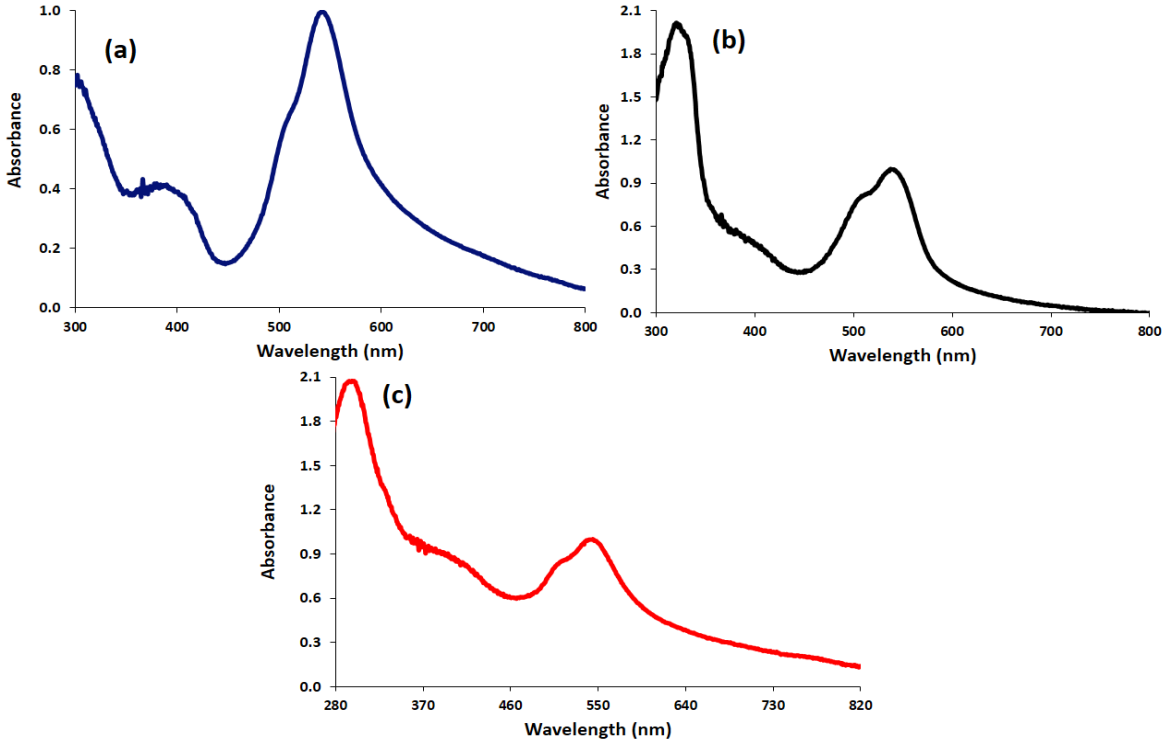

Figure 57. Normalised absorption spectra of BODIPY-(β-cyclodextrin) inclusion complexes in deionised water.(a) BODIPY **2a**-(β-cyclodextrin), (b) BODIPY **2b**-(β-cyclodextrin) and (c) BODIPY **2c**-(β-cyclodextrin).

Table 28. Differences in the spectra of BODIPY dyes in organic media and when included in α-cyclodextrin, in water.

Sample	Absorption maximum λ (Ethanol) (nm)	Absorption maximum λ (water) (nm)
BODIPY 2a	**531**	**N/A**
α + BODIPY 2a incl. comp	**N/A**	**547**
BODIPY 2b	**521**	**N/A**
α + BODIPY 2b incl. comp	**N/A**	**542**
BODIPY 2c	**531**	**N/A**
α + BODIPY 2c incl. comp	**N/A**	**522**

In addition to being broadened, the spectra show changes in the wavelength of the main transition bands of the respective BODIPY dyes and inclusion complexes (**Table 28** and **Table 29**). Red-shifts in the 11–20 nm range were observed, except when BODIPY **2c** was included in α-cyclodextrin, since this resulted in a 9 nm blue shift (**Table 28** and **Table 29**).

Table 29. Differences in the spectra of BODIPY dyes in organic media and when included in β-cyclodextrin, in water.

Sample	Absorption maximum λ (Ethanol) (nm)	Absorption maximum λ (water) (nm)
BODIPY 2a	**531**	**N/A**
α + BODIPY 2a incl. comp	**N/A**	**542**
BODIPY 2b	**521**	**N/A**
α + BODIPY 2b incl. comp	**N/A**	**538**
BODIPY 2c	**531**	**N/A**
α + BODIPY 2c incl. comp	**N/A**	**545**

The complex stoichiometries of inclusion complexes can also be determined. The most common method to determine these complex stoichiometries is the continuous variation/Job plot method using changes in a quantitative spectroscopic property such as absorbance.[187–189] To obtain the Job plots, absorbance is plotted against mole fraction, *r* (*r* = *m*/*m* + *n*), where *m* represents the proportion of BODIPY dye present in solution and *n* represents that of cyclodextrin; for the equimolar solutions with varying molar ratios i.e. ($BODIPY_m$:$CYCLODEXTRIN_n$). The plot is then used to infer the stoichiometric ratio at the maximum absorbance value; for example, if maximum absorbance occurs at *r* = 0.33, this

implies a ratio of 1BODIPY:2CYCLODEXTRINS (m = 1 and n = 2). In this study, a series of inclusion complex aqueous solutions with a fixed final concentration for each BODIPY dye inclusion complex (**2a**-2.54 × 10^{-3} M, **2b**-2.38 × 10^{-3} M and **2c**-2.53 × 10^{-3} M), were prepared by varying the molar ratios of $BODIPY_m$:$CYCLODEXTRIN_n$. The results indicated different mole ratios (**Table 30**) but a representative job plot is included (**Figure 58**); the other complexes were also studied following similar procedures.

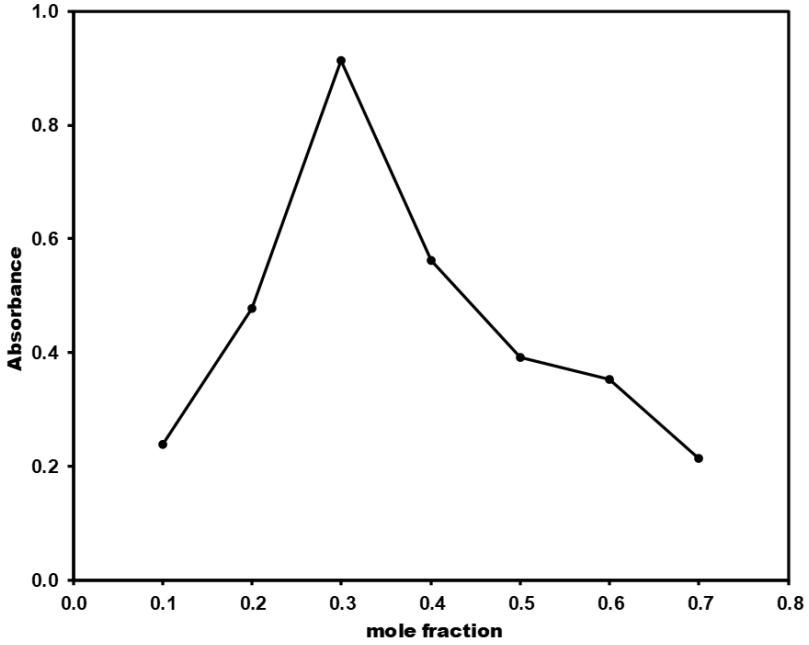

Figure 58. Continuous variation plot of the BODIPY **2b**-(β-cyclodextrin) inclusion complex.

Table 30. Inclusion complex stoichiometric ratios

Sample	Stoichiometric ratio (BODIPY:CYCLODEXTRIN)
BODIPY 2a α incl. comp	**1:1**
BODIPY 2b α incl. comp	**1:1**
BODIPY 2c α incl. comp	**1:1**
BODIPY 2a β incl. comp	**1:1**
BODIPY 2b β incl. comp	**1:2**
BODIPY 2c β incl. comp	**1:2**

5.2.2. Fourier-transform infrared spectroscopy (FT-IR)

The infrared spectra were recorded for the BODIPY dyes, cyclodextrins, physical mixtures and for the inclusion complexes. The IR plots are displayed (**Figure 59** and **Figure 60**) below and the characteristics of each spectrum discussed (**Table 31** and **Table 32**). The spectra provide the evidence for significant spectral differences that is required to infer inclusion of the BODIPY dyes into cyclodextrins; this is evident from the changes in the characteristic peaks which change subsequent to inclusion.

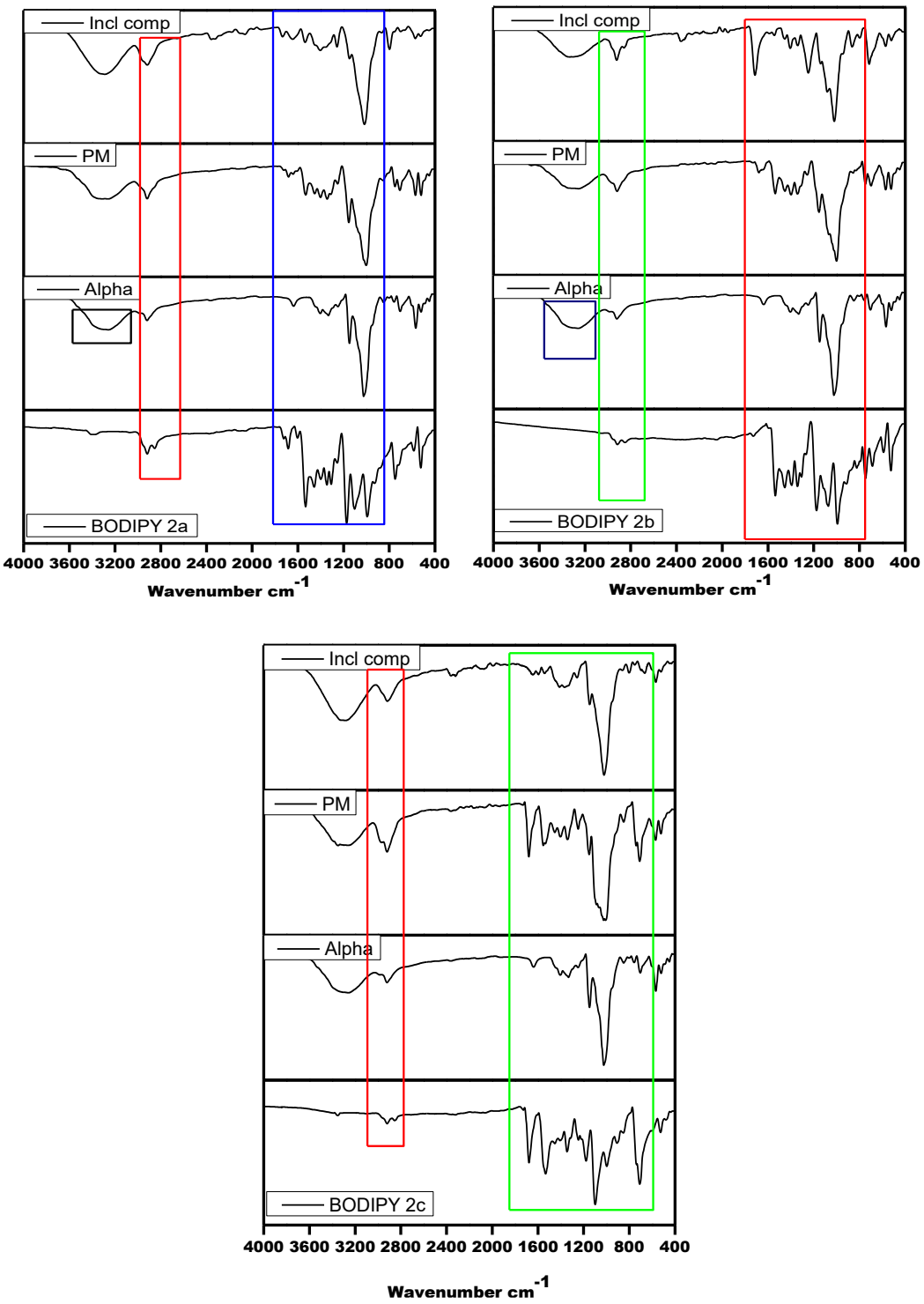

Figure 59. FT-IR spectra of BODIPY **2a**, BODIPY **2b** and BODIPY **2c** with α-cyclodextrin. Coloured boxes used to highlight changes in the respective characteristic peaks of the BODIPY and cyclodextrin upon formation of the inclusion complex.

Table 31. Discussion of FT-IR spectra of BODIPY dyes included in α-cyclodextrin.

Sample	Characteristics
α alone	500–1650 cm^{-1}: *cis* RCH=CHR, =CH and $=CH_2$ stretch, C-H bend, O-H, C-O, C-C-C bend, O-H bend, CH_2 deformation, O-C and C=O bands. At ca. 3300 cm^{-1}, there is an OH stretch.
BODIPY 2a alone	C-Br stretch at 522 cm^{-1}. 550–1600 cm^{-1}: multiple CH and CH_2 bands; C-N stretch. Ca. 2900 cm^{-1}: C-H stretches.
α + BODIPY 2a PM	500–1800 cm^{-1}: C-Br stretch, combined and superimposed BODIPY and CDx peaks, with broadening of the peak at ca. 1000 cm^{-1}. BODIPY C-H stretch at ca. 2918 cm^{-1} is maintained, but is less intense and characteristic shape lost. The O-H stretch of the CDx at 3261 cm^{-1} is maintained. Overall, the spectrum is a combination of CDx and BODIPY spectra.
α + BODIPY 2a incl. comp	500–600 cm^{-1}: All BODIPY stretches disappear, while those of the CDx are maintained. CDx O-H and C-O bands maintained at 1022 cm^{-1}. The C-C-C CDx bend at ca. 1150 cm^{-1} is drastically reduced in intensity but still maintained, whereas between 1150–1650 cm^{-1} the CDx and BODIPY spectra combine and peaks become less intense. At ca. 2921 cm^{-1}, the C-H stretch of the BODIPY is maintained, but loses the shape seen in the dye alone and is not significantly different to that of the physical mixture. Finally, the O-H stretch of the CDx at ca. 3289 cm^{-1} is maintained.
BODIPY 2b alone	C-Br stretch at 523 cm^{-1}. 550–1600 cm^{-1}: multiple CH and CH_2 stretches. Ca. 2900 cm^{-1}: C-H stretches.
α + BODIPY 2b PM	500–1600 cm^{-1}: BODIPY C-Br stretch maintained; CDx and BODIPY spectra maintained with some bands superimposed and most of the BODIPY peaks exhibiting decreased intensity. BODIPY C-H stretch at ca. 2918 cm^{-1} is maintained, but the characteristic shape is lost. The O-H stretch of the CDx at 3257 cm^{-1} is also maintained. Overall, the spectrum is a combination of CDx and BODIPY spectra.
α+ BODIPY 2b incl. comp	500–1600 cm^{-1}: Both BODIPY and CDx stretches are maintained. CDx O-H and C-O bands at 1022 cm^{-1} are combined and superimposed with the BODIPY spectrum,

	hence changing frequency to ca. 998 cm^{-1}. In the 2855–2925 cm^{-1} region, the C-H stretches of the BODIPY are maintained, but the characteristic shape is lost but not as drastically as in the physical mixture. Also, the O-H stretch of the CDx at ca. 3276 cm^{-1} is maintained.
BODIPY 2c alone	C-Br stretch at 531 cm^{-1}. 550–1700 cm^{-1}: multiple CH and CH_2 stretches; N=O band lies at 1526 cm^{-1}. Ca. 2850–2925 cm^{-1}: C-H stretches.
α+ BODIPY 2c PM	500–1800 cm^{-1}: C-Br stretch maintained; other BODIPY and CDx peaks are combined and superimposed, with significant broadening observed for the C=O/OH although it maintains the original frequency of 1026 cm^{-1}. N=O band is maintained at 1533 cm^{-1}. The BODIPY C-H stretch at 2919 cm^{-1} is maintained, but the characteristic shape is lost. The O-H stretch of the CDx at ca. 3300 cm^{-1} is fully maintained. Overall, the spectrum is a combination of the CDx and BODIPY spectra.
α+ BODIPY 2c incl. comp	500–1700 cm^{-1}: Most BODIPY stretches disappear, while those of the CDx are maintained. CDx O-H and C-O bands maintained and change frequency to 1023 cm^{-1} as a result of superimposition with BODIPY peaks. The C-C-C CDx bend at ca. 1150 cm^{-1} is fully maintained. The N=O band which was observed at ca. 1530 cm^{-1} in the BODIPY and physical mixture spectra is lost in that of the complex. This may indicate inclusion of the *meso*-phenyl ring which contains the nitro group inside the cyclodextrin cavity. At ca. 2900 cm^{-1}, the C-H stretches of the BODIPY are maintained and the characteristic shape is fully lost, more than in the physical mixture. Finally, the O-H stretch of the CDx at ca. 3260 cm^{-1} is maintained.

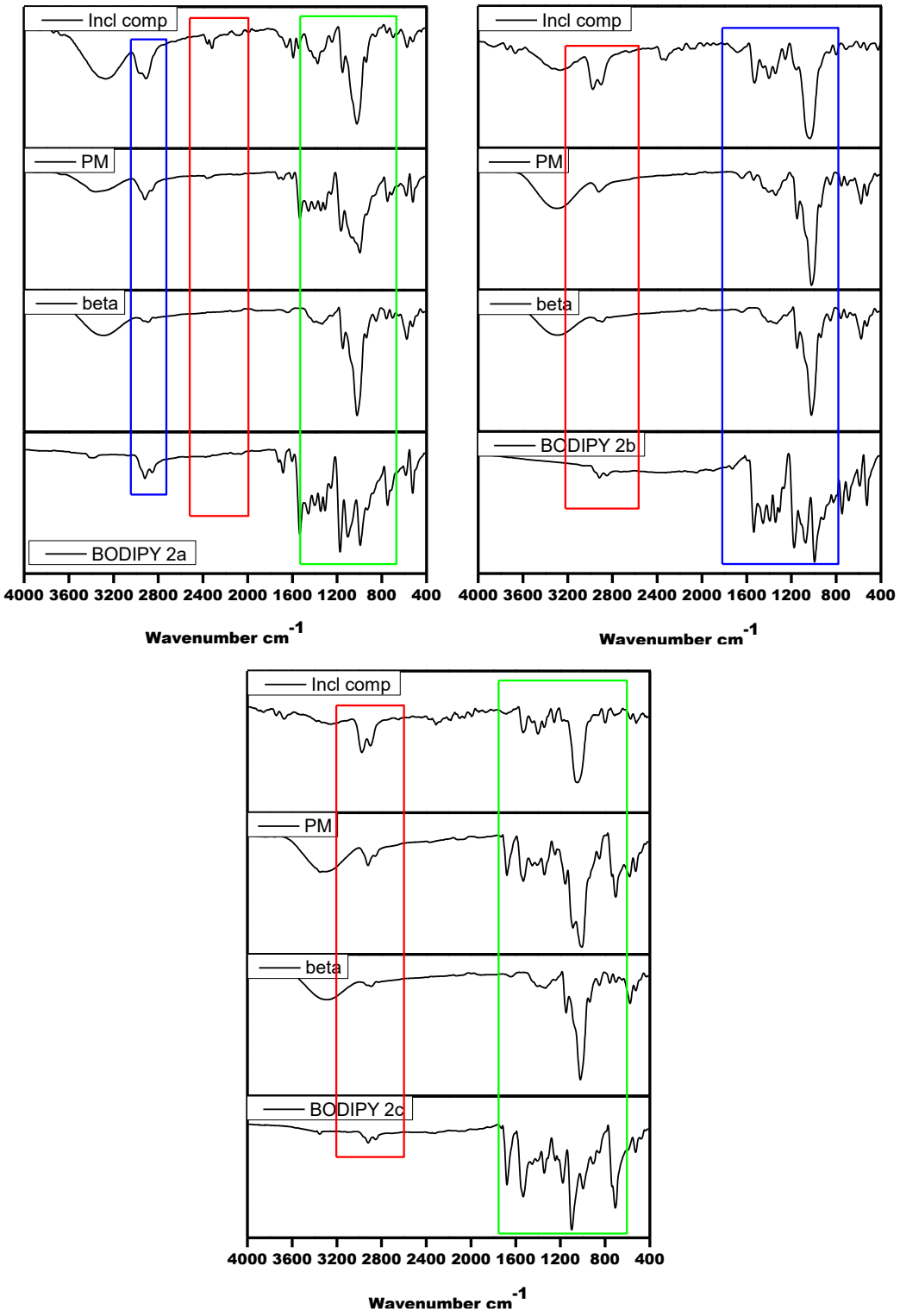

Figure 60. FT-IR spectra of BODIPY **2a**, BODIPY **2b** and BODIPY **2c** with β-cyclodextrin. Coloured boxes used to highlight changes in the respective characteristic peaks of the BODIPY and cyclodextrin upon formation of the inclusion complex.

Table 32. Discussion of FT-IR spectra of BODIPY dyes included in β-cyclodextrin.

Sample	Characteristics
β alone	500–1650 cm^{-1}: *cis* RCH=CHR, =CH and $=CH_2$ stretch, C-H bend, OH, C-O, C-C-C bend, O-H bend, CH_2 deformation, O-C and C=O. At ca. 3300 cm^{-1}, there is an O-H stretch.
BODIPY 2a alone	C-Br stretch at 522 cm^{-1}. 550–1600 cm^{-1}: multiple CH and CH_2; C-N stretch. Ca. 2900 cm^{-1}: C-H stretches.
β+ BODIPY 2a PM	The O-H stretch of the CDx at ca. 3350 cm^{-1} is maintained. 500–1800 cm^{-1}: C-Br stretch; combined and superimposed BODIPY and CDx peaks, with broadening of the peak at 996 cm^{-1}. BODIPY C-H stretch at 2918 cm^{-1} maintained, but characteristic shape lost. Overall, the spectrum is a combination of the CDx and BODIPY spectra.
β+ BODIPY 2a incl. comp	500–600 cm^{-1}: All BODIPY stretches disappear, with those of the CDx maintained, but are markedly less obvious, i.e. decreased intensity. CDx OH and C-O bands maintained, but shift from 1022 cm^{-1} in the CDx spectrum to 1031 cm^{-1} in that of the complex. The C-C-C CDx bend at ca. 1150 cm^{-1} is maintained, whereas around 1150–1650 cm^{-1}, the CDx spectrum combines with the less intense BODIPY peaks. At ca. 2900 cm^{-1}, the BODIPY C-H stretch is maintained, but it loses the shape seen in the dye alone. Finally, the O-H stretch of the CDx at 3290 cm^{-1} is maintained.
BODIPY 2b alone	C-Br stretch at 523 cm^{-1}. 550–1600 cm^{-1}: multiple C-H and CH_2 stretches. Ca. 2900 cm^{-1}: C-H stretches.
β+ BODIPY 2b PM	500–1100 cm^{-1}: BODIPY C-Br stretch maintained; other CDx and BODIPY bands superimposed with the CDx spectrum being more prominent. 1100–1600 cm^{-1}: the BODIPY spectrum is the only one maintained but with decreased intensity. BODIPY C-H stretch at 2919 cm^{-1} is maintained, but the characteristic shape is lost. The O-H stretch of the CDx at 3300 cm^{-1} is also maintained. Overall, the spectrum is a combination of CDx and BODIPY spectra.

β+ BODIPY 2b incl. comp	500–1600 cm^{-1}: BODIPY C-Br stretch disappears together with both the BODIPY and CDx stretches below 1000 cm^{-1}, while those around 1250–1600 cm^{-1} are maintained. CDx O-H and C-O bands are maintained and superimposed with those of BODIPY, and as such the peak shifts from 1022 to 1036 cm^{-1}. The C-C-C CDx bend at ca. 1160 cm^{-1} is drastically reduced in intensity but still maintained. In the 2905–2975 cm^{-1} region, the C-H stretch of the BODIPY is fully maintained. Finally, the O-H stretch of the CDx at ca. 3270 cm^{-1} is maintained.
BODIPY 2c alone	C-Br stretch at 531 cm^{-1}. 550–1700 cm^{-1}: multiple CH and CH_2 stretches; N=O band lies at 1526 cm^{-1}. 2850–2925 cm^{-1}: C-H stretches.
β+ BODIPY 2c PM	500–1800 cm^{-1}: C-Br stretch maintained, while other BODIPY and CDx peaks are combined and superimposed, with broadening of the C=O/OH band and change in frequency to ca. 1008 cm^{-1}. The N=O band is maintained at ca. 1530 cm^{-1}. The BODIPY C-H stretch at 2918 cm^{-1} is maintained, but the characteristic shape is lost. The O-H stretch of the CDx at ca. 3300 cm^{-1} is fully maintained. Overall, the spectrum is a combination of the CDx and BODIPY spectra.
β+ BODIPY 2c incl. comp	500–900 cm^{-1}: All BODIPY stretches disappear, while those of the CDx are maintained. CDx O-H and C-O bands maintained at 1023 cm^{-1}. The C-C-C CDx bend at ca. 1150 cm^{-1} is drastically reduced although still visible. Between 1150–1650 cm^{-1} the CDx and BODIPY spectra combine and peaks become the less intense. The N=O band at ca. 1530 cm^{-1} in the BODIPY and physical mixture spectra is lost in that of the complex. This may indicate inclusion of the *meso*-phenyl ring which contains the nitro group inside the cyclodextrin cavity. At ca. 2900 cm^{-1}, the C-H stretches of the BODIPY are maintained, and the characteristic shape becomes more pronounced than in the physical mixture. Finally, the O-H stretch of the CDx at ca. 3260 cm^{-1} is maintained but loses significant intensity.

5.2.3. Scanning electron microscopy (SEM)

The SEM images for the BODIPY dyes, cyclodextrins, physical mixtures and inclusion complexes were recorded (**Figure 61**–**Figure 66**) and they are discussed below (**Table 33** and **Table 34**).

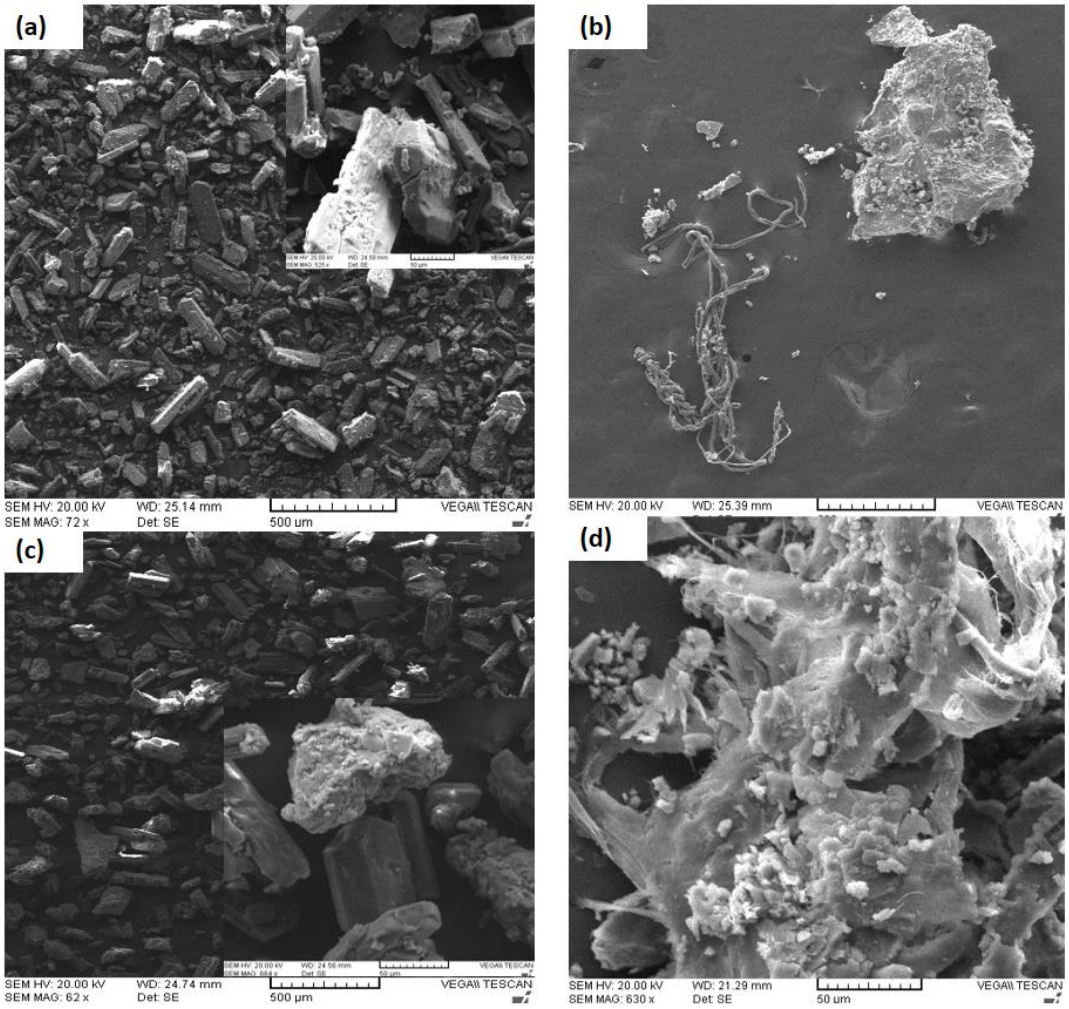

Figure 61. SEM micrographs of BODIPY **2a** with α-cyclodextrin: (a) α-cyclodextrin, (b) BODIPY **2a**, (c) BODIPY **2a**-(α-cyclodextrin physical mixture and (d) BODIPY **2a**-(α-cyclodextrin) inclusion complex.

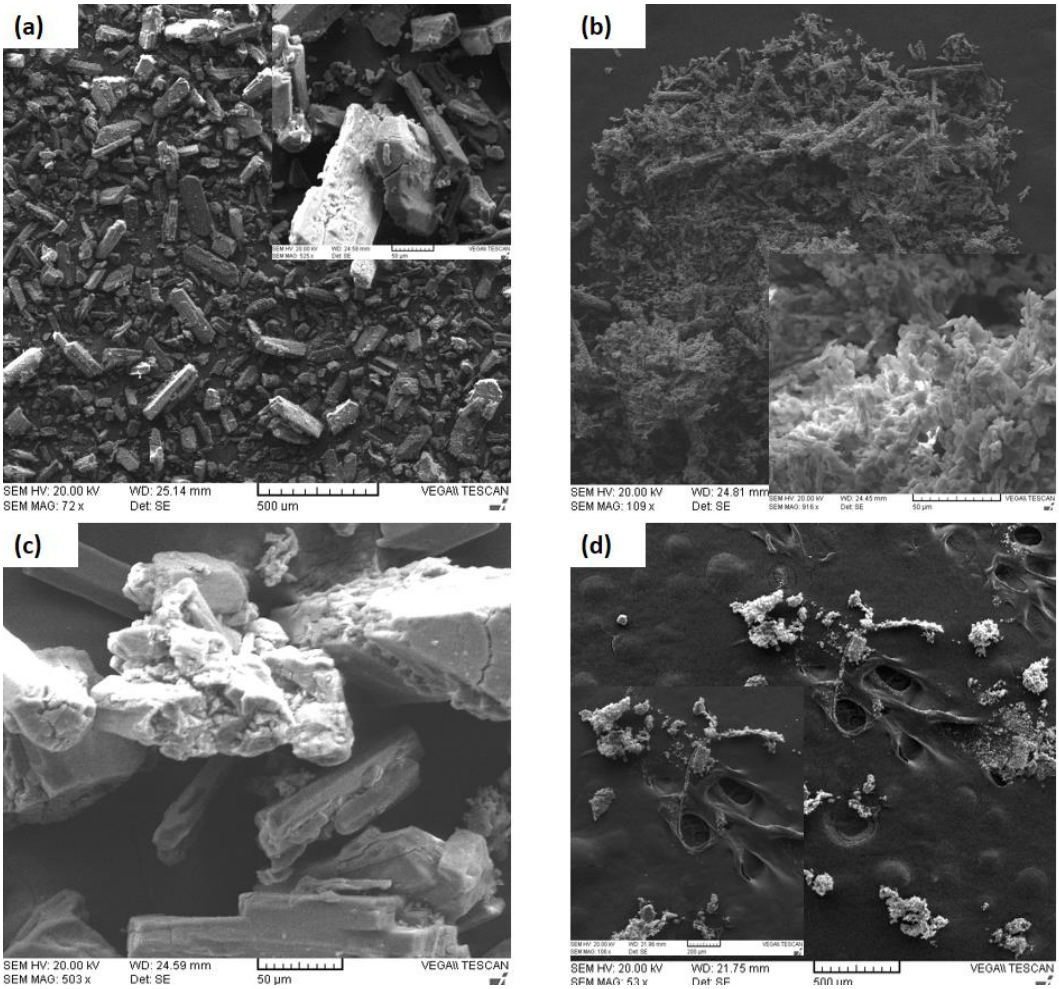

Figure 62. SEM micrographs of BODIPY **2b** with α-cyclodextrin: (a) α-cyclodextrin, (b) BODIPY **2b**, (c) BODIPY **2b**-(α-cyclodextrin physical mixture and (d) BODIPY **2b**-(α-cyclodextrin) inclusion complex.

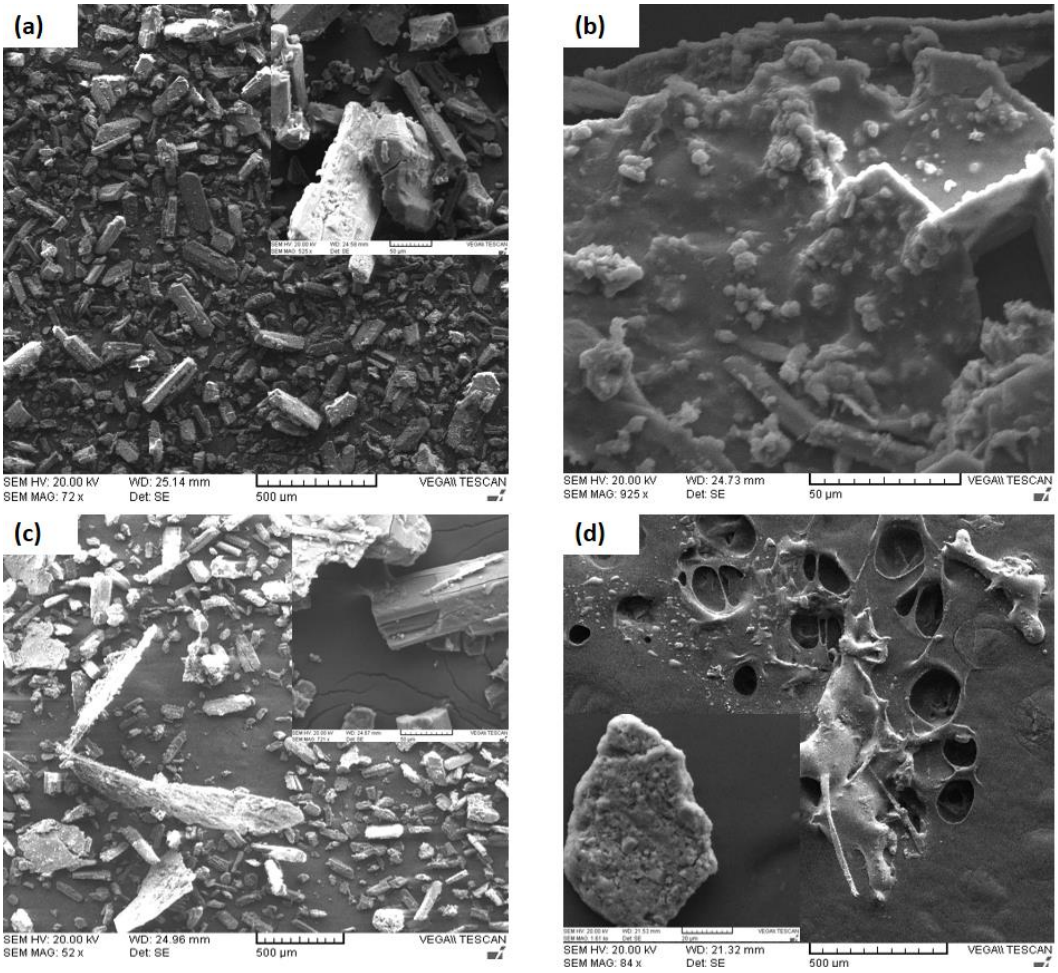

Figure 63. SEM micrographs of BODIPY **2c** with α-cyclodextrin: (a) α-cyclodextrin, (b) BODIPY **2c**, (c) BODIPY **2c**-(α-cyclodextrin physical mixture and (d) BODIPY **2c**-(α-cyclodextrin) inclusion complex.

Table 33. Discussion of SEM images of BODIPY dyes included in α-cyclodextrin.

Sample	Characteristics
α alone	Cubic, well-defined structures.
BODIPY 2a alone	Some fibrous structures, coupled with aggregated amorphous to cubic shape.
α+ BODIPY 2a PM	Mixed morphology.
α+BODIPY 2a incl. comp	Aggregated and amorphous. Different from both parent shapes.

BODIPY 2b alone	Aggregated/close-lying with a semi-cylindrical shape.
α+BODIPY 2b PM	Mixed morphology.
α+ BODIPY 2b incl. comp	New morphology. The dendrous and amorphous nature of the BODIPY is completely lost.
BODIPY 2c alone	Amorphous aggregates.
α+ BODIPY 2c PM	Mixed morphology, with CDx being more prominent.
α+ BODIPY 2c incl. comp	New morphology. Pore-like structures also present.

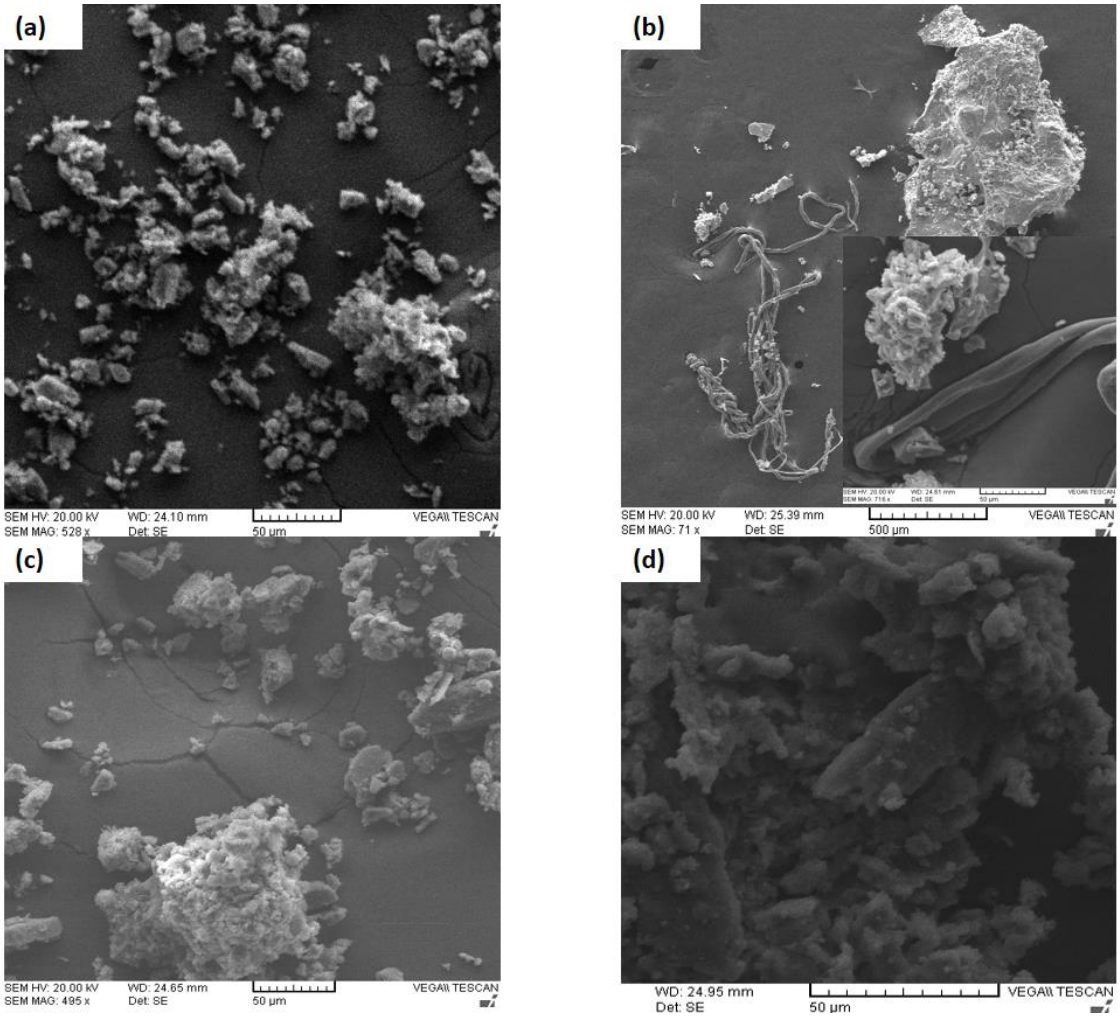

Figure 64. SEM micrographs of BODIPY **2a** with β-cyclodextrin: (a) β-cyclodextrin, (b) BODIPY **2a**, (c) BODIPY **2a**-(β-cyclodextrin physical mixture and (d) BODIPY **2a**-(β-cyclodextrin) inclusion complex.

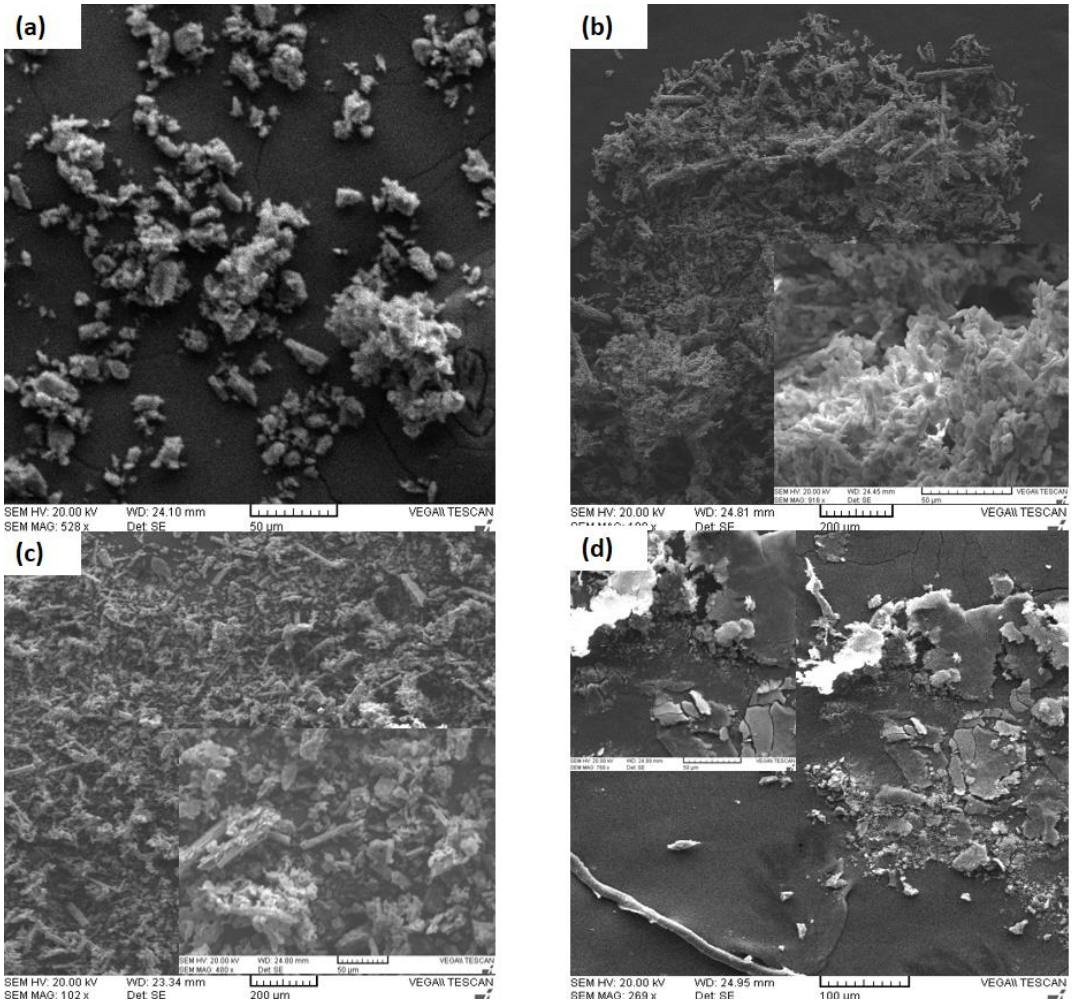

Figure 65. SEM micrographs of BODIPY **2b** with β-cyclodextrin: (a) β-cyclodextrin, (b) BODIPY **2b**, (c) BODIPY **2b**-(β-cyclodextrin physical mixture and (d) BODIPY **2b**-(β-cyclodextrin) inclusion complex.

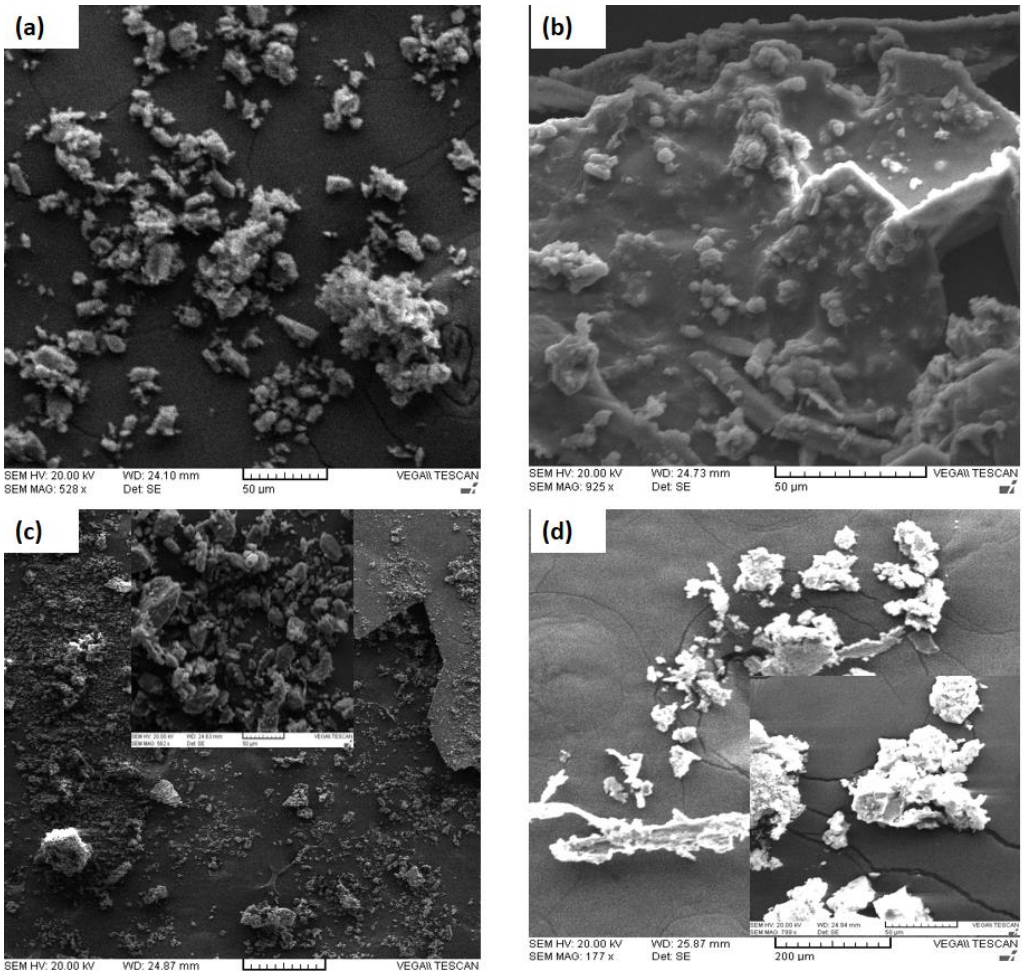

Figure 66. SEM micrographs of BODIPY **2c** with β-cyclodextrin: (a) β-cyclodextrin, (b) BODIPY **2c**, (c) BODIPY **2c**-(β-cyclodextrin physical mixture and (d) BODIPY **2c**-(β-cyclodextrin) inclusion complex.

Table 34. Discussion of SEM images of BODIPY dyes included in β-cyclodextrin.

Sample	Characteristics
β alone	Somewhat amorphous.
BODIPY 2b alone	Aggregated/close-lying with a semi-cylindrical shape.
β+ BODIPY 2b PM	Combined amorphous and semi-cylindrical.
β+ BODIPY 2b incl. comp	Both CDx alone and BODIPY alone shapes were lost. New flaky, amorphous morphologies observed, combined with some fibrous structures.

BODIPY 2a alone	Some fibrous structures, coupled with aggregated amorphous to cubic shape.
β+ BODIPY 2a PM	Both CDx amorphous and BODIPY cubic to amorphous morphologies maintained, with the BODIPY losing the aggregated nature and fibrous structures.
β+ BODIPY 2a incl. comp	New flaky structure observed. Increased aggregation, losing original shapes.
BODIPY 2c alone	Amorphous aggregates.
β+ BODIPY 2c PM	Both CDx and BODIPY morphologies maintained, with the CDx being more prominent.
β+ BODIPY 2c incl. comp	New morphologies: flaky and rod-like, coupled with aggregated amorphous ball-like structures.

5.2.4. X-ray powder diffraction analysis (XRD)

The X-ray diffraction patterns of the BODIPY dyes, cyclodextrins, physical mixtures and inclusion complexes have also been analysed (**Figure 67** and **Figure 68**). The α-cyclodextrin was crystalline (**Figure 67**) whereas the β-cyclodextrin was amorphous (**Figure 68**). The BODIPY dyes were all observed to be amorphous, with BODIPY **2a** exhibiting minimal crystallinity. The physical mixtures obtained with α-cyclodextrin were a superimposition of the diffraction patterns of the respective BODIPY dye and α-cyclodextrin, with the cyclodextrin being more prominent for BODIPYs **2a** and BODIPY **2b**, whereas for the BODIPY **2c**-(α-cyclodextrin) physical mixture the BODIPY pattern was more pronounced. Upon inclusion of the respective dyes into α-cyclodextrin, all diffraction patterns were mainly amorphous with a minor degree of crystallinity, albeit being different from the parent ones.

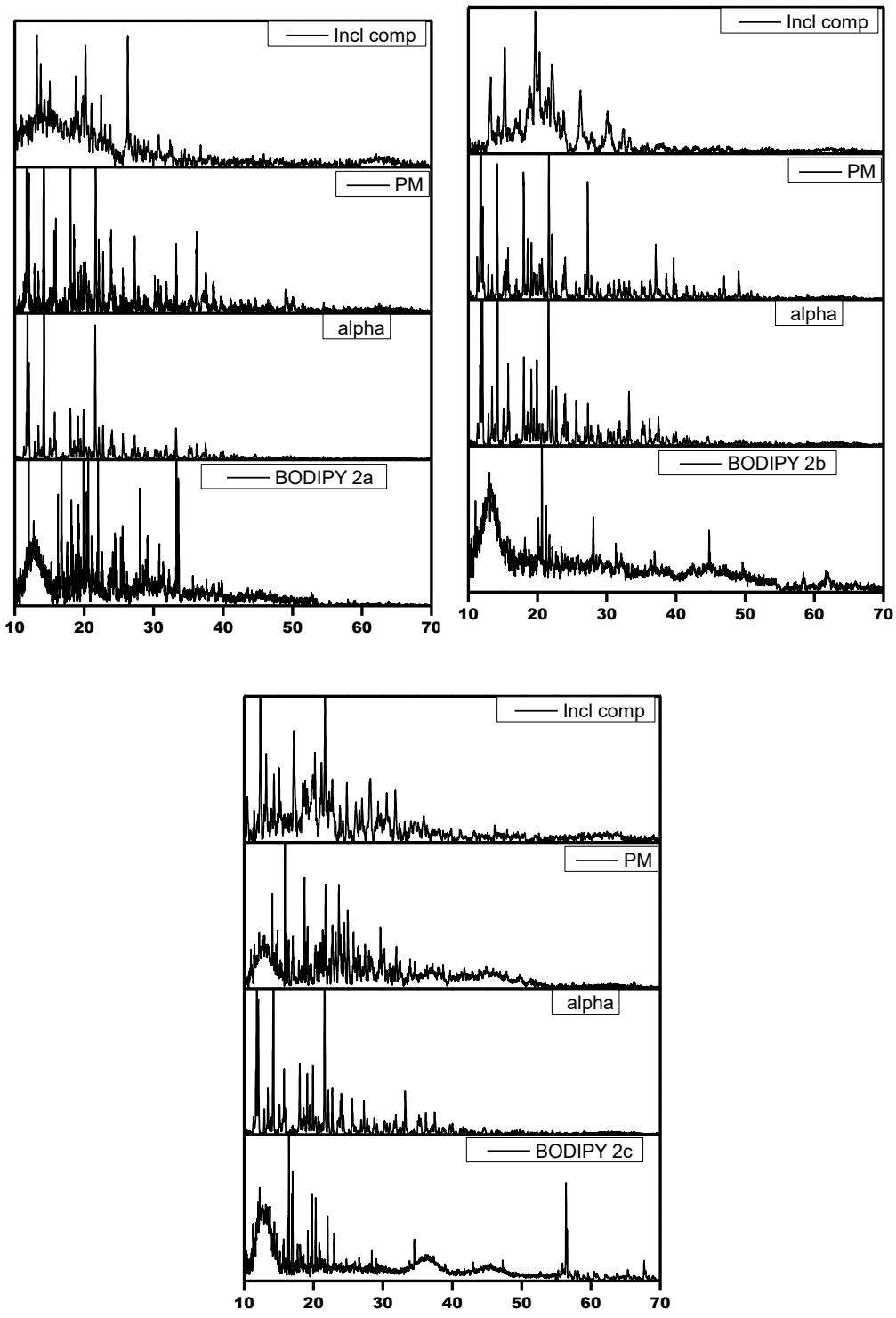

Figure 67. X-ray diffraction patterns of BODIPY **2a**, BODIPY **2b** and BODIPY **2c** with α-cyclodextrin.

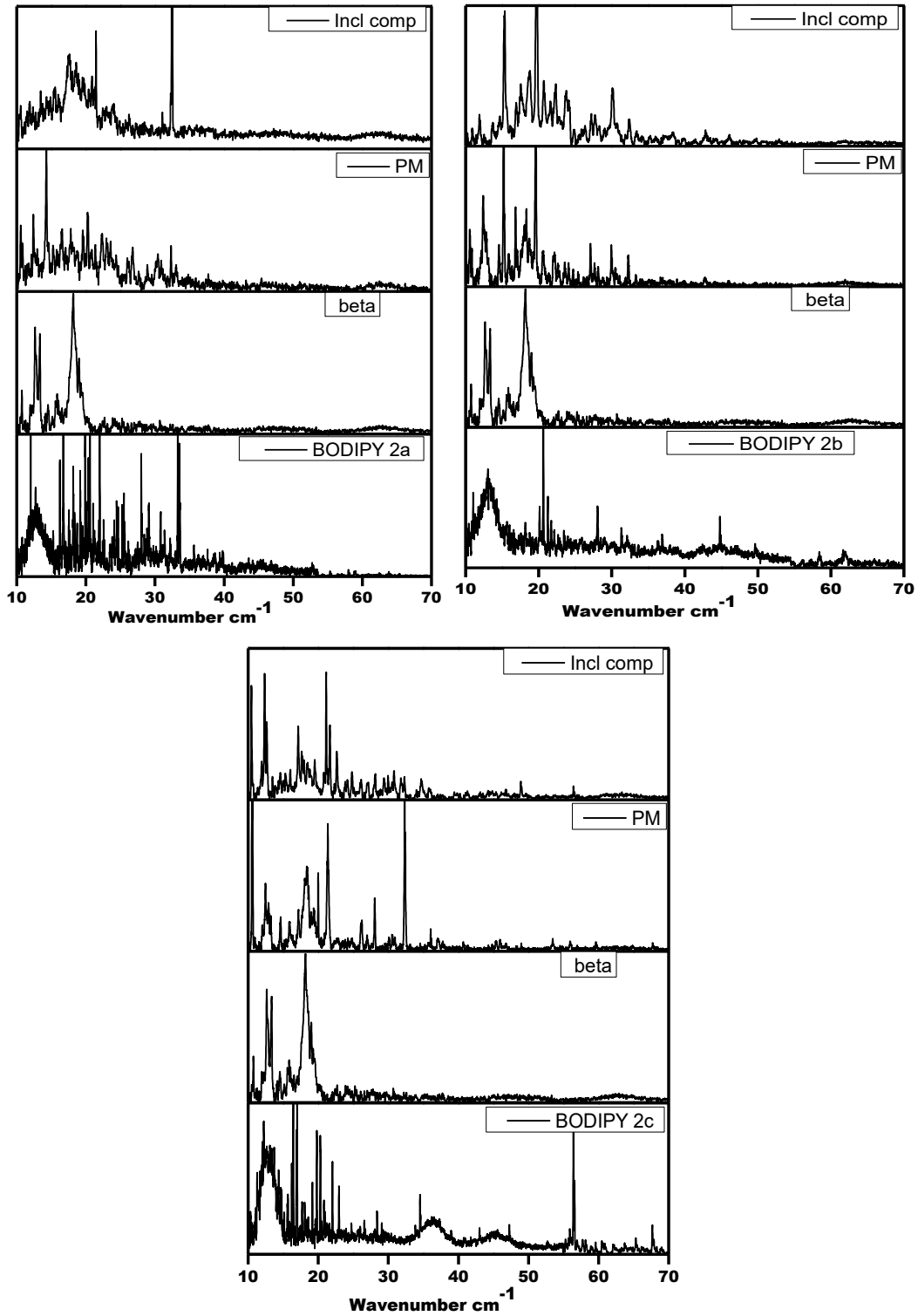

Figure 68. X-ray diffraction patterns of BODIPY **2a**, BODIPY **2b** and BODIPY **2c** with β-cyclodextrin.

In the β-cyclodextrin studies, the physical mixtures obtained were also a superimposition of the diffraction patterns of the respective BODIPY dye and β-cyclodextrin, with no parent pattern being more prominent for the BODIPY **2a**- and **2b**-(β-cyclodextrin) physical mixtures while the BODIPY diffraction pattern is more prominent for **2c**. When included in β-cyclodextrin, new patterns of a mixed amorphous and crystalline nature are observed and these are different from those of the BODIPY alone, cyclodextrin alone and the physical mixtures except for the **2b**-(β-cyclodextrin) complex which exhibits some similarities to the BODIPY diffraction pattern.

5.2.5. Circular dichroism

In essence, circular dichroism spectroscopy is used to identify both chromophore orientation and the direction of the electric dipole transition moment. The sign of the induced CD (ICD) spectrum shows the type of inclusion which has occurred, and this is based on the electronic transitions taking place.[45,87,190–192] A positive ICD signal shows that the electronic transitions occur parallel to the molecular axis of the cyclodextrin (axial inclusion) while a negative one shows that the electronic transitions occur parallel to the molecular axis of the cyclodextrin (equatorial inclusion). When the ICD signals of the short and long axis polarised transitions are both negative in sign, a third type of inclusion, the lid-type has occurred.[45,87,190–192] Attempts were made to obtain the CD spectra in deionised water but for all the complexes studied here, the CD spectra did not give satisfactory results as there was no clearly detectable induced signal. This was most probably due to the BODIPY and cyclodextrin forming the inclusion complexes not possessing strong enough interactions to generate ICD and/or the relatively large energy separation between the main BODIPY

spectral band in the 520–540 nm region and those of the cyclodextrin that lie below 300 nm.

5.2.6. Fluorescence spectroscopy

Another spectroscopic technique that is typically used in the assessment of guest inclusion into the cyclodextrin cavity is fluorescence spectroscopy, wherein a fluorescent guest is studied both before and after inclusion. In this instance, the BODIPY dyes used are not soluble in water hence it was not possible to assess their fluorescence in water prior to inclusion; instead the fluorescence properties of the dyes were studied in organic media before inclusion and in water subsequent to inclusion into cyclodextrins. Representative emission spectra are shown (**Figure 69**) and these belong to BODIPY **2b** in ethanol and the BODIPY **2b**-(α-cyclodextrin) inclusion complex in water.

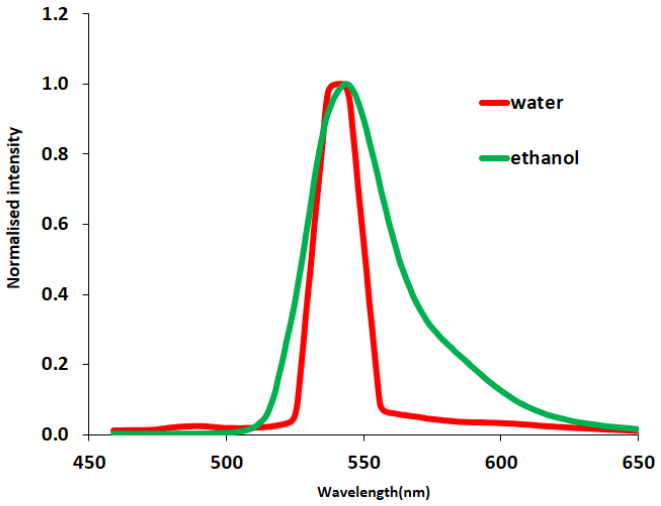

Figure 69. Emission spectra of BODIPY **2b** in ethanol (green) and the BODIPY **2b**-(α-cyclodextrin) inclusion complex in water (red).

From the spectrum, it is evident that the dye possesses the typical BODIPY emission spectrum as shown by the sharp emission maximum; but this is not the case for the inclusion complex in water as can be seen from the significantly broadened and flat

emission spectrum. This broadening is thought to be due to both aggregation in the water solution and the quenching effects of water. For all the other inclusion complexes in both α- and β-cyclodextrin, the observations were generally similar.

Concluding remarks and future outlook

A short series of BODIPY-cyclodextrin inclusion complexes have been successfully formed and characterised in solution using UV-visible absorption, fluorescence and circular dichroism spectroscopies and in the solid state using FT-IR, XRD and SEM; challenges were encountered in solution, however. Attempts to quantify the singlet oxygen generation of the inclusion complexes in water using both an Ekspla NT342B-20-AW laser and a Thorlabs mounted M530L3 LED as light sources. It was expected that the singlet oxygen generated from the brominated BODIPY dyes within the complexes should breakdown ADMA. However, no decrease in the concentration of the ADMA solution was observed and this implies either one of the following: that the BODIPY dyes included in the cyclodextrins were either unable to generate singlet oxygen; or that the molecular oxygen in the solution was not close enough to the BODIPY dyes to allow energy transfer to take place; or that the experimental setups used were not suitable in some regard.

Having successfully included heavy atom containing BODIPY dyes into α- and β-cyclodextrins and achieved water solubility, the next step to carry forward this research is to optimise the necessary conditions and experimental setup to be able to quantify any singlet oxygen that is generated under aqueous conditions. Additionally, assessing the toxicity of the inclusion complexes to bacterial cultures and in biological media would be another possible avenue of research if further progress is made.

Chapter 6:

Spectroscopic assessment of pH-sensitivity of a distyryl BODIPY in organic media

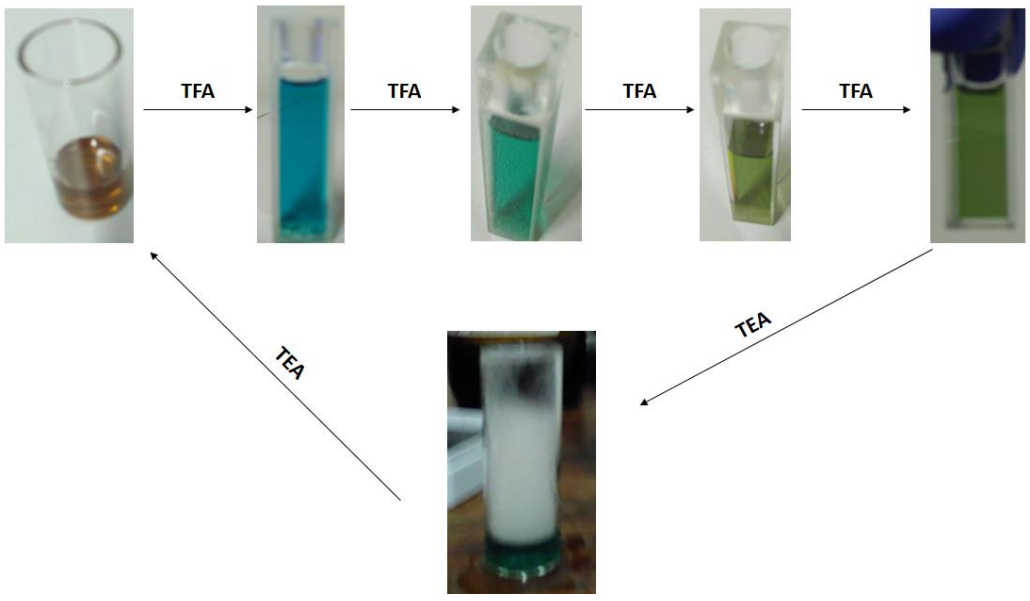

As described in Chapter 1, BODIPY dyes have been extensively studied for their potential in sensing cations and anions, metal ions, enzymes and reactive oxygen species.[114,131,133,135] Additionally, pH-sensitive fluorescent probes are also worth researching since pH is an indicator in many cellular events e.g. abnormal cell growth, inflammation and cancer are all characterised by pH values lower than those of normal cells.[136]

The focus of this chapter is an analysis of the suitability of BODIPY **8** in sensing pH changes (in organic media for the purposes of this study). The mechanism of interest here is ICT using a BODIPY dye, the design of which will allow turn-on fluorescence in the presence of an acid (**Figure 70**). During the ICT process, electronic interactions between electron donating and electron accepting groups occur. For the purposes of this study, the ($N(CH_3)_2$) group acts as an electron donor. The addition of an acid is expected to eliminate this ICT process, thereby enhancing the fluorescence intensity of the dye and also result in spectral changes. The BODIPY dye of interest contains two dimethyl-aminophenyl groups ($N(CH_3)_2$) at the 3,5-positions and these act as a receptors; ($N(CH_3)_2$) containing BODIPY dyes have their fluorescence quenched in polar solvents but upon protonation the fluorescence process is activated due to the inhibition of charge transfer processes.[112,132,133,135,137]

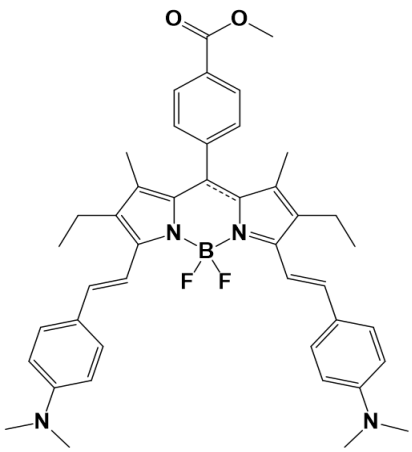

Figure 70. Structure of BODIPY **8**, the dye that was used for pH sensing.

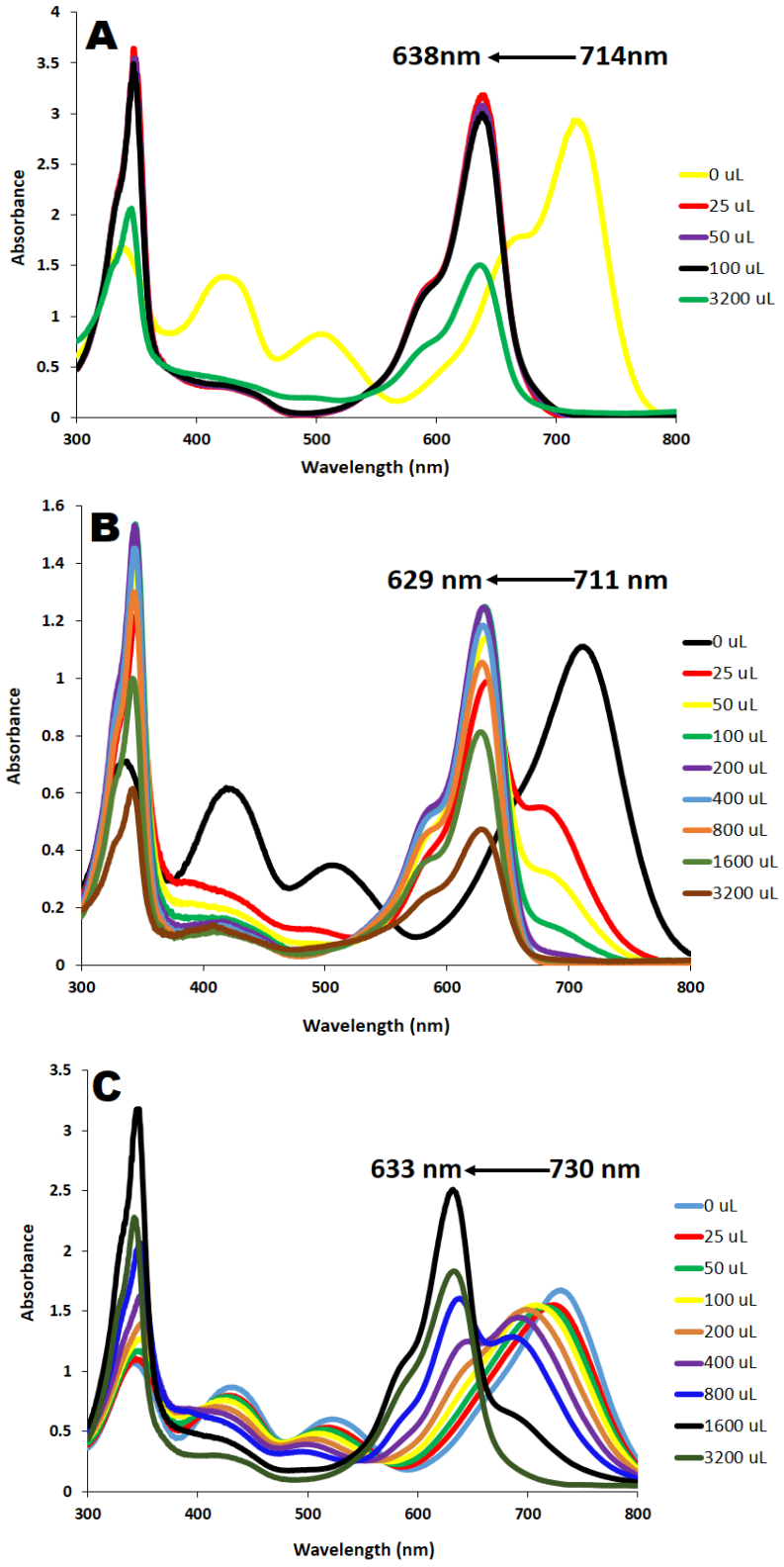

Figure 71. Absorption spectra of BODIPY **8** in the presence of increasing amounts of TFA. A: Benzene, B: acetonitrile and C: DMSO.

During this study, three different solvents with increasing polarities were used, and absorption spectra (**Figure 71A**–**Figure 71C**) were measured in the presence of increasing amounts of TFA. The solvents are benzene (polarity index 2.7), acetonitrile (polarity index 5.8) and DMSO (polarity index 7.2). Absorption spectra were measured from initial concentrations of 2.8×10^{-5} M for benzene and acetonitrile and at a concentration of 1.4×10^{-4} M for DMSO because 2.8×10^{-5} M for DMSO gave a significantly lower absorbance reading.

In benzene, the absorption spectrum is significantly red-shifted in the absence of an acid and possesses more pronounced charge transfer (CT) bands between 400 and 550 nm. Upon addition of minimal TFA (25 µL), the main absorption band blue-shifts and the CT bands disappear; this is an indication that charge transfer has been eliminated (**Figure 71A**). Upon increasing the polarity of the solvent, more acid was required to eliminate ICT. This is evident in the spectra recorded in acetonitrile and DMSO, wherein the dye does not instantaneously change from the unprotonated to the protonated form. Instead, as the amount of TFA increases the absorption maximum (associated with the main transition) for the unprotonated dye gradually decreases while the absorption maximum for the protonated form of the dye appears immediately. In addition, as the intensity of the absorption band associated with the unprotonated dye gradually decreases, the wavelength decreases to an intermediate value between that of the protonated and unprotonated form; this may signal the existence of a mixture of unprotonated, mono-protonated and di-protonated species. According to the absorption spectra, in acetonitrile, the di-protonated or fully protonated dye is completely formed after the addition of 200 µL of TFA whereas in DMSO it is observed after addition of 3200 µL (**Figure 71B** and **Figure 71C**). A final point

worth noting in relation to solvent polarity is that the absorption maximum seems to be highly dependent on solvent polarity because there is significant red-shifting in the most polar solvent, as can be seen from the absorption maxima at 714 nm for benzene and 730 nm for DMSO when unprotonated (**Figure 71A** and **Figure 71C**).

In each of the solvents, the fluorescence spectra (**Figure 72**–**Figure74**), quantum yields and lifetimes were obtained (**Table 35**). In benzene, in the absence of an acid, there are two emission maxima at 680 and 754 nm while the maxima are not significantly different in the more polar acetonitrile and DMSO in the presence of 25 and 100 µL TFA, occurring at 657 and 658 nm, respectively. The emission intensity drops by 12% on increasing the amount of TFA from 25 to 100 µL in benzene.

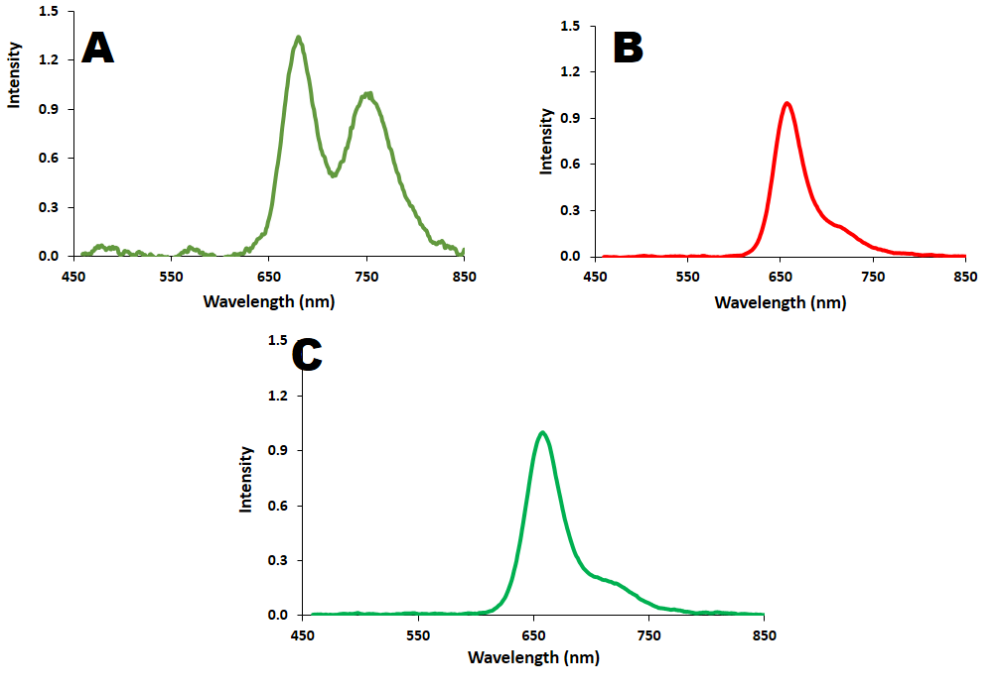

Figure 72. Emission spectra of BODIPY **8** in benzene, in the presence of increasing amounts of TFA. A: no acid, B: 25 µL TFA present and C: 100 µL TFA present.

The starting amounts of TFA for acetonitrile and DMSO are much higher, but, as can be observed in **Figure 73** and **Figure 74**, the emission spectra are weak despite the higher amounts of TFA added to eliminate ICT; this is has been previously observed to be the case for more polar solvents.[132,137]

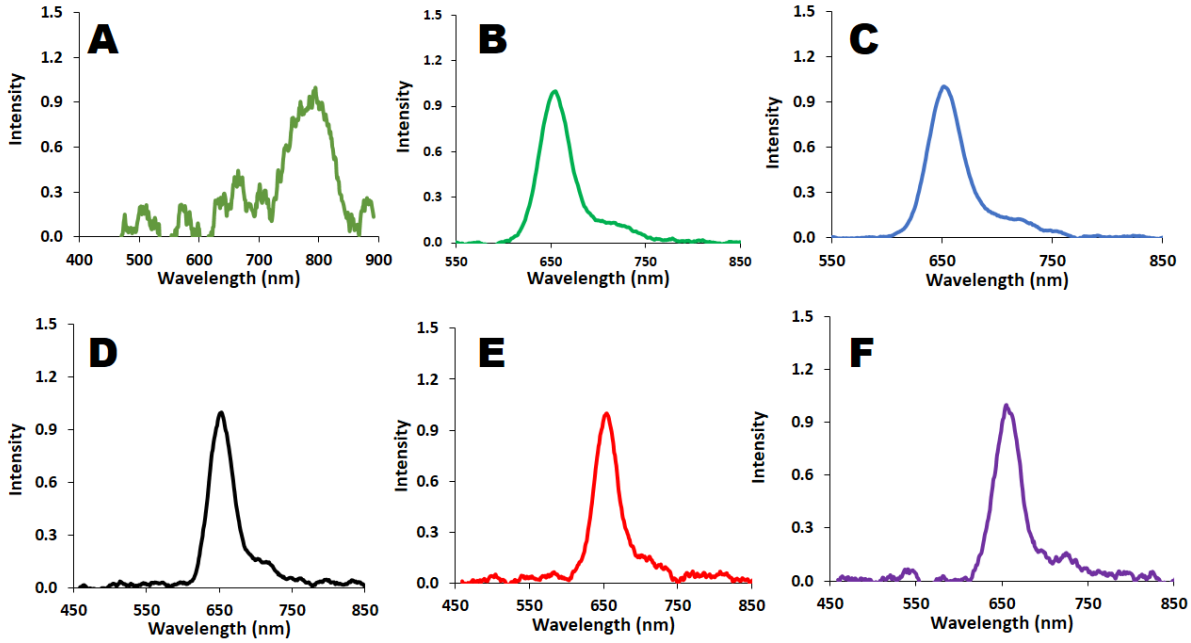

Figure 73. Emission spectra of BODIPY **8** in acetonitrile, in the presence of increasing amounts of TFA. A: no acid, B: 100 µL TFA present, C: 200 µL TFA present, D: 800 µL TFA present, E: 1600 µL TFA present and F: 3200 µL TFA present.

In acetonitrile, the emission intensity decreases gradually as the amount of acid is increased and finally drops by 65% on increasing the amount of TFA from 100 to 3200 µL; this huge decrease can be attributed to a dilution effect of the acid on the BODIPY-containing organic solution as large amounts of acid were used in the last three samples, as is evident from their weak emission spectra relative to the first three (**Figure 73**).

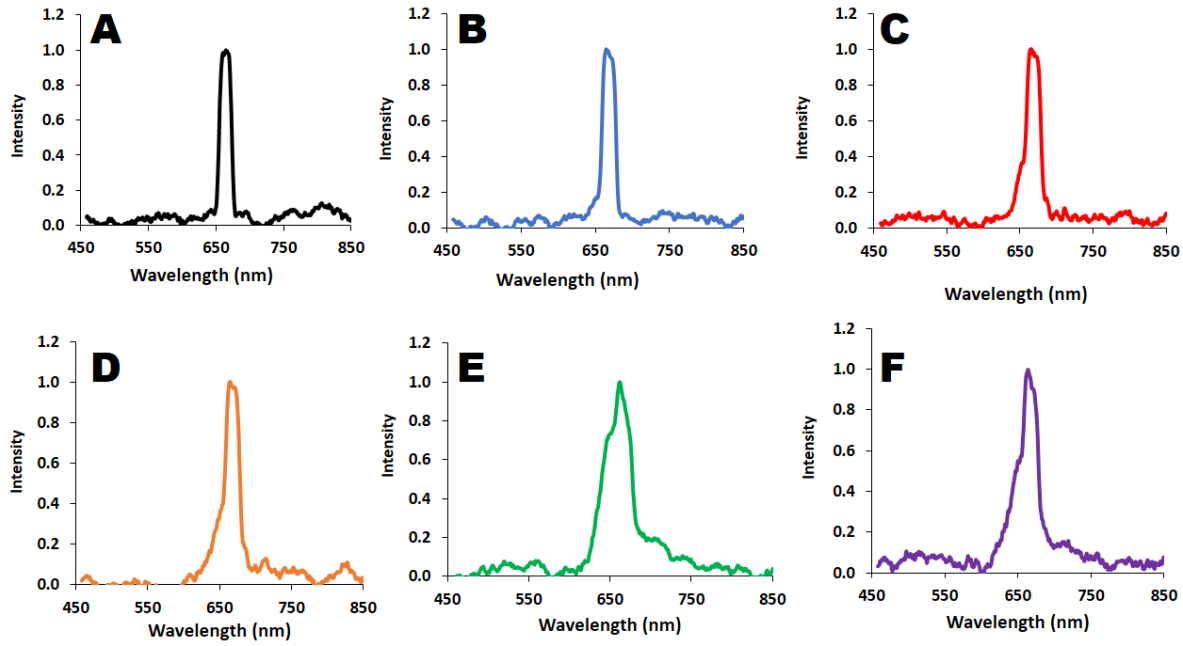

Figure 74. Emission spectra of BODIPY **8** in DMSO, in the presence of increasing amounts of TFA. A: no acid, B: 200 µL TFA present, C: 800 µL TFA present, D: 1600 µL TFA present, E: 3200 µL TFA present and F: 6400 µL TFA present.

In DMSO, there is no distinct fluorescence as the emission spectra are not similar to the typical BODIPY spectrum for all samples except the ones containing 3200 µL TFA and 6400 µL TFA. On increasing the amount of TFA from 100 µL to 3200 µL, the intensity increases and reaches a maximum at 3200 µL before dropping by 31% on increasing TFA volume to 6400 µL, further showing the dilution effects of the large amount of acid used (**Figure 74**).

Table 36. Photophysical data for BODIPY **8** in different organic solvents in the presence and absence of increasing volumes of TFA.

Solvent	λ_{Abs} (nm)	λ_{Exc} (nm)*	λ_{Em} (nm)*	Stokes shift (nm)	Φ_F	τ_F (ns)*
Benzene	714	660	680; 754	40	0.09	2.63
Benzene + 25 µL TFA	638	640	657	19	0.31	NS
Benzene + 100 µL TFA	638	639	658	20	0.27	4.60
Acetonitrile	711	717	794	83	0.02	NS
Acetonitrile + 100 µL TFA	632	632	654	22	0.08	NS
Acetonitrile + 3200 µL TFA	622	633	655	33	0.02	NS
DMSO	730	n.d	n.d	-	0.02	0.75 (97%) 3.301 (3%)
DMSO + 100 µL TFA	708	n.d	n.d	-	0.02	

DMSO + 3200 µL TFA	633	633	662	29	0.03	0.26 (73%) 1.99 (27%)

*fluorescence lifetimes were only determined in the absence of TFA and in the presence of excess TFA

*NS = not studied; *n.d = not detected

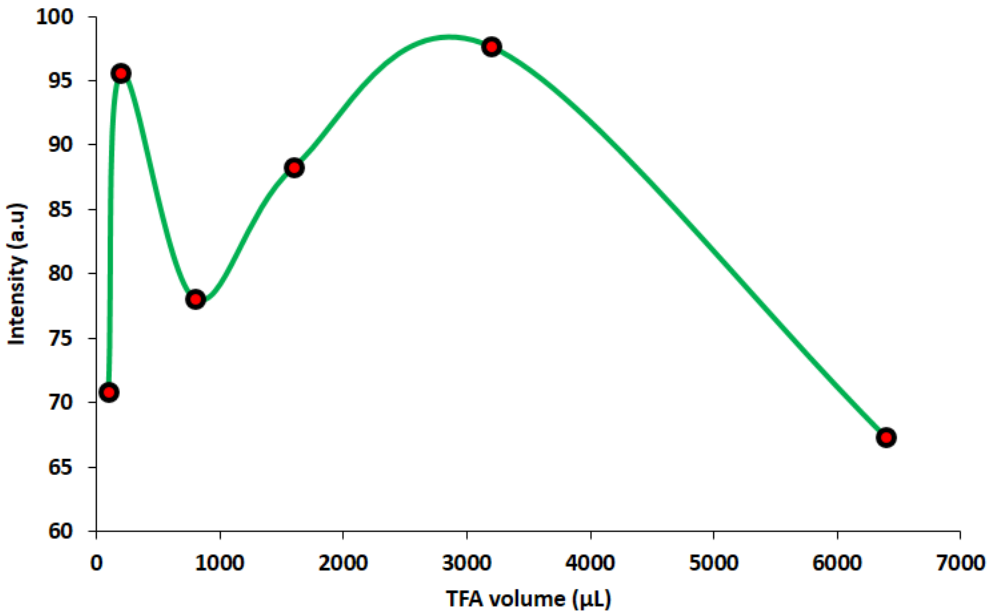

Figure 75. Changes in fluorescence emission intensity in DMSO, in the presence of increasing amounts of TFA.

As expected, the amount of acid required to eliminate ICT in the less polar benzene is not as large as in more polar solvents, and the fluorescence intensity significantly decreases in the more polar acetonitrile and DMSO relative to the measurements in benzene.[132,137] This is evident in the fluorescence lifetimes and quantum yields which are very low for acetonitrile and DMSO relative to benzene (**Table 35**).

To assess the reversibility of protonation of the dimethylamino moieties of the dye, TEA was added in aliquots to a solution of BODIPY **8** in DMSO, at a concentration of 1.4×10^{-4} M in

the presence of 3200 µL TFA and the absorption spectra recorded (**Figure 76**). From the recorded spectra, it is evident that the protonation process is easily reversible. Furthermore, when small amounts of TFA were added, there was no shift in the wavelength of the maximum absorption band; a shift was only visible when 3200 µL of TEA was added, shifting the absorption band from 633 nm to 725 nm. The spectrum observed displayed a weak signal as can be seen but this changed when the amount of TEA was gradually increased, wherein the wavelength continued shifting so that the band maximum lies at 768 nm in the presence of 8000 µL TEA, which represents a red shift of ca. 38 nm relative to the spectrum in DMSO with no acid or base added. The reversibility of the spectral changes further demonstrates the potential utility of BODIPY **8** as an "off-on" fluorescence switch.

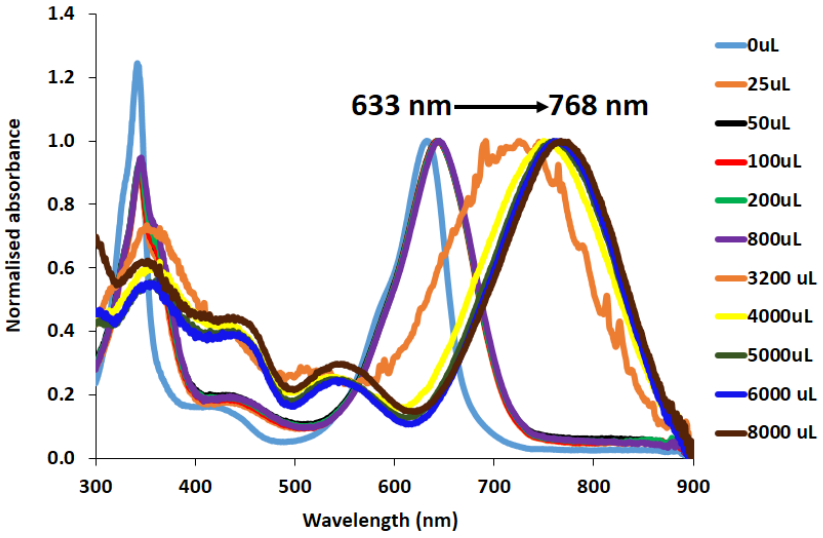

Figure 76. Normalised absorption spectra of BODIPY **8** in the presence of increasing amounts of TEA. Spectra measured in DMSO.

The reversibility which is observed spectroscopically (**Figure 76**) is also visible to the naked eye. The colour of the solution gradually changes from brown to green as TFA is added to a

solution of BODIPY **8**, following the red-shift occurring in the absorption spectrum. When TEA is added in excess to reverse the process, the original brown colour returns (**Figure 77**).

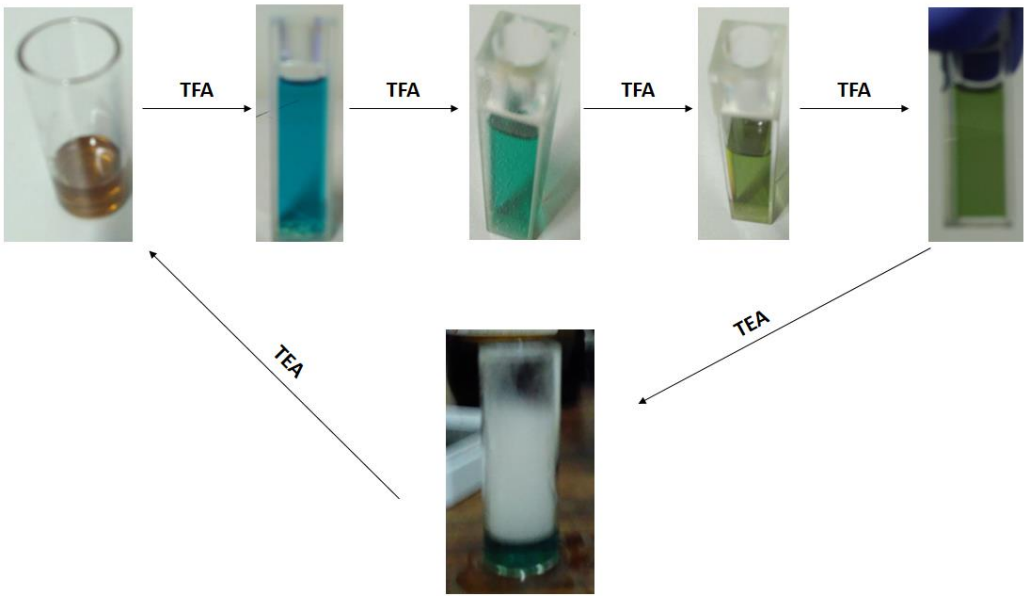

Figure 77. Colourimetric changes visualised upon addition of increasing amounts of TFA and TEA to a solution of BODIPY **8** in DMSO.

Concluding remarks

It has been successfully demonstrated using BODIPY **8** can be used as pH-sensitive fluorescent probe in three different solvents of differing polarity. The sensor process involves BODIPY dyes which have their fluorescence quenched in polar solvents due to ICT but upon protonation, the fluorescence process is activated due to its inhibition.[112,132,133,135,137] This is what was observed in this study, wherein the amount of acid required to eliminate ICT was higher in the most polar solvent. The elimination of ICT and the "turn on" effect on the fluorescence properties was reversible through the addition of a base, further demonstrating that BODIPY **8** is able to behave as an "off-on" fluorescence switch in the presence and absence of species which can interact with the styryl

dimethylamino moieties. The most interesting aspect of this study is the potential suitability of BODIPY **8** as a sensor for pH in biological studies, since pH is a useful indicator of many cellular events. Abnormal cell growth, inflammation and cancer are all characterised by pH values lower than those of normal cells.[136] More research still needs to be carried out in this regard, however, since non-toxicity and water solubility or the ability to include the molecule in a water-soluble carrier which can be easily excreted of metabolised if and when in a biological system, are key requirements for the biological application of any molecular dye. The main limitation in this regard is that the study was carried out in organic media.

Chapter 7:

Molecular modelling

7.1. Geometry Optimisation and TD-DFT calculations

Molecular modelling calculations have been used to elucidate trends in the predicted spectra and the electronic structures of a set of synthesised compounds, BODIPYs **1e**, **2e**, **5** and **6**. To perform the calculations, density functional theory (DFT) was used to carry out geometry optimisations using the Beck, three-Parameter, Lee-Yang-Parr (B3LYP) functional with 6-31G(d) basis sets using the Gaussian09 software package.[139] Because the B3LYP functional typically underestimates long-range charge transfer excitation, which is frequently found in BODIPY dyes, the Coulomb-attenuated B3LYP (CAM-B3LYP) functional was used to perform TD-DFT calculations so as to predict the electronic absorption properties.[193,194] This is particularly important because the CAM-B3LYP functional, unlike B3LYP combines elements of the hybrid B3LYP functional with increasing fractions of Hartree-Fock (HF) exchange parameters, resulting in a functional with improved long-range capabilities.[194]

7.2. Molecular modelling for BODIPYs 1e, 2e, 5 and 6

According to the TD-DFT calculations, the lowest lying $S_0 \rightarrow S_1$ transition is almost entirely associated with the HOMO → LUMO one-electron transition (**Table 36**). The C_{2V} symmetry adopted by BODIPY dyes upon complexation with a boron difluoride ligand makes the HOMO and LUMO energetically well-separated from other MOs (**Figure 78**) and this is significant because when the effect of structural changes on the optical properties are considered, it is primarily the HOMO and LUMO which should be considered, i.e. the other MOs are largely uninvolved in the observed changes. Hence, a red-shift of the BODIPY main

spectral band is observed because of structural changes which affect the energies of the HOMO and LUMO, resulting in a narrowing of the HOMO–LUMO band gap.

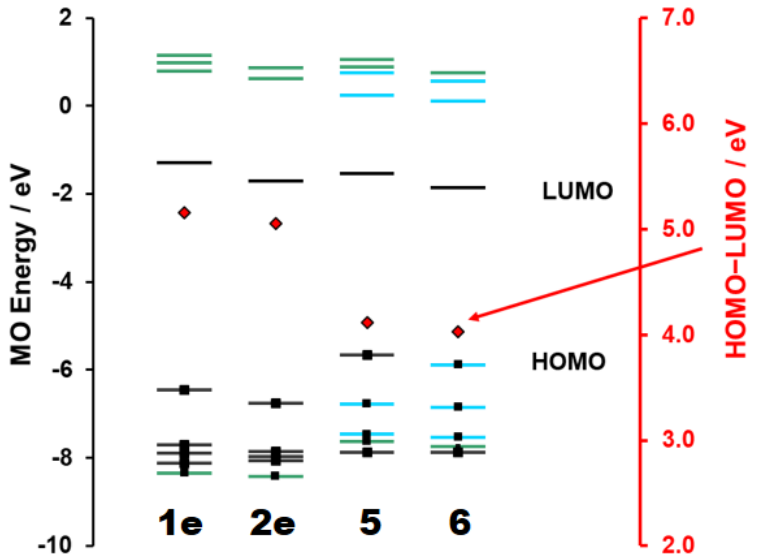

Figure 78. MO energies of BODIPYs **1e**, **2e**, **5** and **6** at the CAM-B3LYP/6-31 G(d) level of theory. Blue and green lines are used to denote the primary localisation of MOs on the styryl and phenyl moieties, respectively. The HOMO and LUMO gaps are plotted against a secondary axis and are denoted by large red diamonds. The occupied MOs are highlighted with small black squares.

Upon the addition of bromine atoms on going from BODIPY **1e** to BODIPY **2e** there is a destabilisation of both the HOMO and LUMO (**Figure 78**) but because the HOMO has significant MO coefficients at the 2,6-positions, while the LUMO only possesses small MO coefficients (**Figure 79**), the net effect of the addition of these bromine atoms is the destabilisation of the HOMO relative to the LUMO thereby narrowing the HOMO–LUMO gap and this results in the ca. 18 nm red-shift that is observed in the calculated TD-DFT spectrum

for BODIPY **2e** (**Figure 80**). This is usually observed for other 2,6-dibrominated dyes, hence this is expected to be the case with the other BODIPY dyes synthesised in this work.

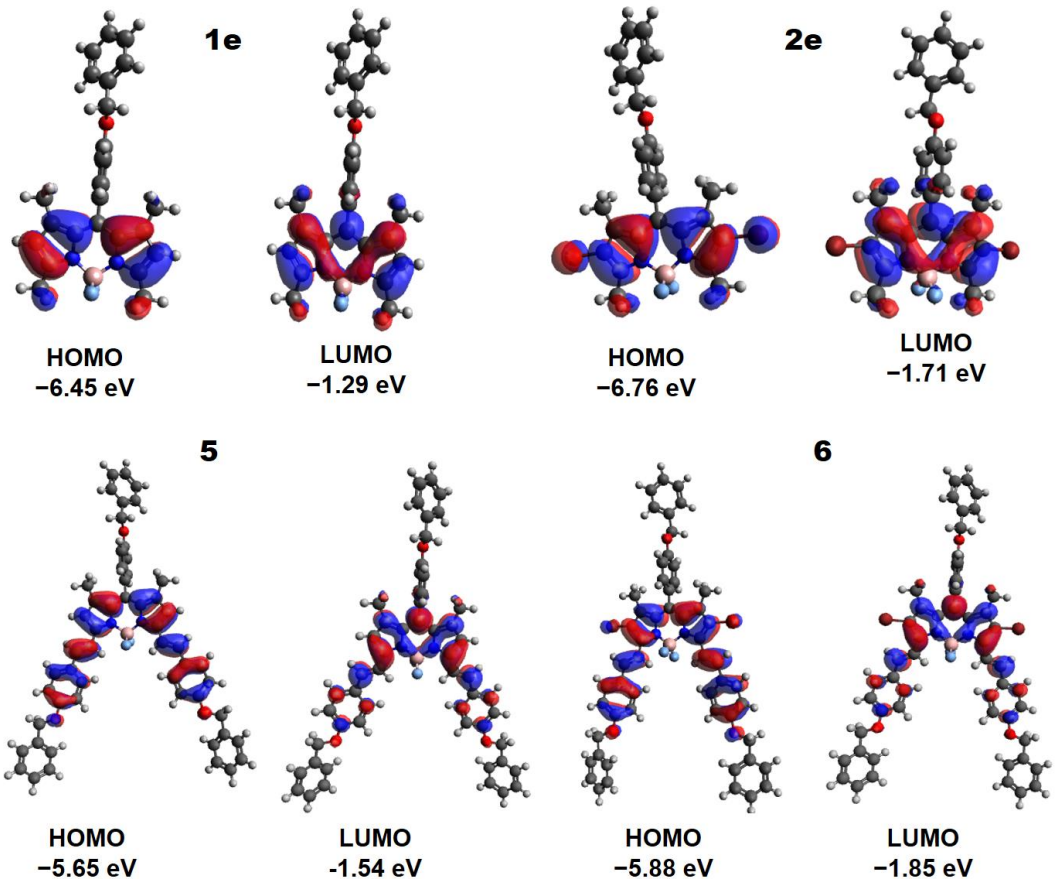

Figure 79. Angular nodal patterns and MO energies of BODIPYs **1e**, **2e**, **5** and **6** for the HOMO and LUMO (at an isosurface value of 0.02 a.u).

The MO coefficients at the 3,5-positions are unevenly distributed on the HOMO and LUMO of BODIPY **2e** as is evident from the larger MO coefficient that is observed in the HOMO (**Figure 79**) and as such any structural modifications at these positions are expected to result in a change in the size of the HOM–LUMO band gap because the HOMO is more significantly affected. As can be seen, the introduction of the styryl groups at the 3,5-positions results in a further red-shift of ca. 110 nm for BODIPY **5** and ca. 127 nm for BODIPY **6** (**Figure 80** and **Table 36**). Although the main absorption band is still due to the HOMO-LUMO one-electron

transitions for both dyes, other transitions are predicted to result in intense bands in the visible region, since large oscillator strengths are predicted both for the main absorption band (**Table 36**) and the absorption bands observed in the 300–450 nm region (**Figure 80**). These observations are typical of those made with other distyryl dyes, hence this is expected to also be the case with the other BODIPY dyes synthesised in this work, notwithstanding the fact that the substituents present on the styryl groups will also have an effect on the extent of red-shift of the main spectral band, since differing electron withdrawing and donating effects will change the degree of destabilization of the HOMO relative to the LUMO.

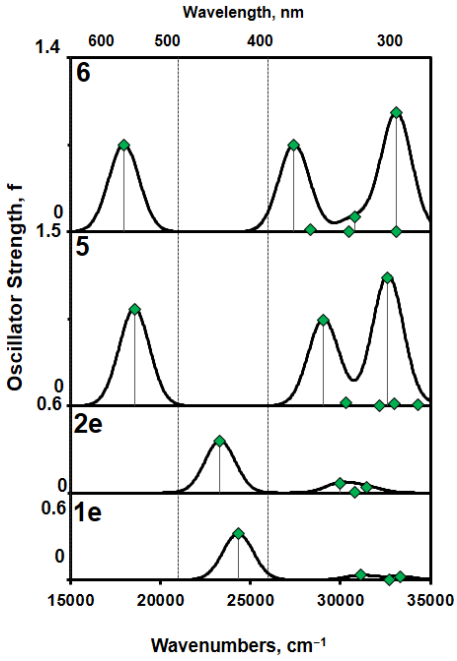

Figure 80. Calculated TD-DFT spectra of BODIPYs **1e**, **2e**, **5** and **6** at the CAM-B3LYP/6-31 G(d) level of theory. The main spectral bands associated with the HOMO → LUMO transition are found between 400 and 500 nm for BODIPYs **1e** and **2e**, and between 500 and 670 nm for BODIPYs **5** and **6**. Simulated spectra were calculated using the Chemcraft program[195] by using bandwidths of 30 nm.

Table 36. TD-DFT calculations at the CAM-B3LYP/6-31 G(d) level for B3LYP optimised BODIPY **1e**, **2e**, **5** and **6** structures

BODIPY	#[a]	E (eV)[b]	λ_{calc} (nm)[c]	f[d]	Wavefunction[e]
1e	1	3.01	411	0.53	97% (H → L); …
	2	3.86	321	0.05	96% (H-2 → L); …
	3	4.06	305	0.00	94% (H-1 → L); …
	4	4.13	300	0.04	99% (H-3 → L); …
2e	1	2.89	429	0.60	97% (H → L); …
	2	3.72	334	0.11	96% (H-2 → L); …
	3	3.82	324	0.00	94% (H-1 → L); …
	4	3.9	318	0.06	93% (H-3 → L); …
5	1	2.30	539	1.11	96% (H → L); …
	2	3.6	344	0.98	93% (H-1 → L); …
	3	3.76	330	0.04	89% (H-4 → L); 6% (H-2 → L); …
	4	3.99	311	0.00	92% (H-3 → L); 3% (H-3 → L+2); …
	5	4.05	306	1.48	89% (H → L+2); 5% (H-1 → L+2); 3% (H-6 → L); …
	6	4.09	303	0.03	77% (H-6 → L); 15% (H-5 → L); 4% (H → L+1); …
6	1	2.23	556	1.00	96% (H → L); …
	2	3.40	365	0.99	93% (H-1 → L); …
	3	3.51	353	0.02	58% (H-4 → L); 38% (H-2 → L); …
	4	3.78	328	0.00	93% (H-3 → L); 2% (H-3 → L+2); …
	5	3.82	325	0.17	93% (H-5 → L); …
	7	4.11	302	1.36	91% (H → L+1); 6% (H-1 → L+2); …

a- Excited state number assigned in increasing energy in the TD-DFT calculations. b- Calculated band energies in eV. c- Calculated wavelengths in nm. d- Calculated oscillator strengths. e- Wavefunctions of MOs involved in the transition, and their respective contributions, based on eigenvectors predicted by TD-DFT. H and L refer to the HOMO and LUMO, respectively.

Concluding remarks

The TD-DFT calculations performed have proven to be a useful tool for establishing trends in the energy of BODIPY molecular orbitals, which when studied they provide insight into the spectroscopic properties of BODIPY dyes in relation to structural modifications. This is useful in the design of specific BODIPY dyes for various applications such as optical limiting and fluorescence sensing, wherein the dyes must be significantly red-shifted and the intermolecular electron transfers taking place understood, respectively. The trends in the calculations match the experimental electronic absorption spectra, as observed not only in the series of BODIPY dyes modelled but also those of other dyes that have been synthesised, particularly the brominated BODIPYs **2a**, **2b**, **2c** and **2d** and the other distyryl dyes.

Chapter 8:

Conclusions, limitations and future prospects

8.1. Conclusions

The main aim of this work was to synthesise and study a series of structurally diverse BODIPY dyes that have properties that make them suitable for use as photosensitizers, in NLO and in fluorescence sensing. The applications envisaged included the use of BODIPY dye-cyclodextrin inclusion complexes in biomedical studies, optical limiting in the context of aviation and the development of a pH-sensitive colourimetric and fluorescence sensor suitable for use in the NIR region.

To understand the properties of these dyes, it was also necessary to assess their photophysical properties.The starting point in achieving the aims listed above was to synthesise five BODIPY dyes, **1a**–**1e** using the classic "one-pot three-step" acid-catalysed condensation reaction. These dyes have different functional groups at the *para* position of the *meso*-phenyl ring. BODIPYs **1a**–**d** have many favourable photophysical properties and they all have similar absorption properties, typical of BODIPY dyes derived from 2,4-dimethylpyrrole, since the *meso*-aryl ring lies orthogonal to the BODIPY core. The dyes did, however, exhibit significant differences when it comes to their fluorescence properties, with BODIPY **1a** only highly fluorescent in the presence of an acid to eliminate ICT between the dimethylamino moiety and the BODIPY core; BODIPY **1c** also possessed weak fluorescence due to the quenching effect of the nitro group which is known to strongly quench fluorescent dyes through what is suggested to be an electron-withdrawing effect.[161] BODIPYs **1b** and **1d** were significantly fluorescent and independent of solvent polarity. The absorption maxima were not significantly altered by changing the solvent.

To further red-shift the spectra and to make the dyes capable of generating singlet oxygen, BODIPYs **1a**–**1e** were brominated at the 2,6-positions (and BODIPY **1a** on the *meso*-phenyl ring), yielding BODIPYs **2a**–**2e** whose absorption spectra are red shifted by ca. 30 nm relative to their parent dyes. BODIPYs **2a**–**2d** possessed fair singlet oxygen quantum yields in the range of solvents studied. This creates an avenue for use in singlet oxygen applications, such as photodynamic antimicrobial chemotherapy,[195] which do not require a red-shifted photosensitizer and to couple this singlet oxygen generating ability with the typical requirement for water-soluble photosensitizers, a short series of BODIPY-cyclodextrin inclusion complexes was formed using BODIPYs **2a**–**2c** and α- and β- cyclodextrins. These complexes were characterised in solution and in the solid state, and the singlet oxygen generating ability assessed in water using ADMA as a singlet oxygen scavenger. There was no decrease in the concentration of the ADMA solution, however, and this may imply that the complexes were unable to generate singlet oxygen, due to rapid non-emissive deactivation of the S_1 state, or that the molecular oxygen in the solution was not close enough to the BODIPY dyes to allow energy transfer to take place; or that the light sources used were not suitable for this particular application. Further work is needed in this area.

BODIPY **2d** was used to synthesise BODIPY **3**, a new mono-styryl BODIPY dye whose structural characterisation was also successful. In addition, five novel di-styryl BODIPYs, BODIPYs **5**, **6**, **8**, **9** and **10** were synthesised from BODIPYs **1e** and **2e** for BODIPYs **5** and **6**, respectively and from 4,4'-difluoro-8-(4-carbomethoxyphenyl)-2,6-diethyl-1,3,5,7-tetramethyl-4-bora-3a,4a-diaza-*s*-indacene for BODIPYs **8**, **9** and **10**. These were synthesised using a modified version of the Knoevenagel condensation reaction.[1,3] Their main absorption band maxima are significantly red-shifted far above 532 nm, the second

harmonic of the Nd:YAG laser which is used to study the nonlinear optical limiting properties of these dyes. BODIPY **6** was red-shifted into the therapeutic window, with absorption maxima at 663 and 667 nm in DCM and DMSO, respectively; this red-shift coupled with the ability of the dye to generate singlet oxygen species with moderate quantum yield values makes **6** potentially suitable for use as a photosensitizer for singlet oxygen applications such as PDT. The nonlinear optical properties of BODIPYs **5**, **6**, **8**, **9** and **10** were investigated together with two other previously reported BODIPYs, **4** and **7**.[95,150,151] All of these BODIPY dyes showed very promising optical limiting responses on the nanosecond at 532 nm in solution, in the range of solvents used, and this provided further evidence that π-expanded BODIPY dyes have considerable potential in this context.

The potential application of BODIPY **8** as a pH-sensitive fluorescent probe was assessed in three different solvents of increasing polarity. It was successfully demonstrated that the addition of an acid to an organic solution of BODIPY **8** leads to the elimination of ICT, turning on the fluorescence of the dye. This was reversible upon the addition of a base, further demonstrating that BODIPY **8** is able to behave as an "off-on" fluorescence switch in the presence and absence of species which can interact with the dimethylamino moieties at the *para*-positions of the styryl groups.

8.2. Limitations and future prospects

- With respect to optical limiting, it will be essential to fabricate thin films to demonstrate the potential practical application of any molecules as optical limiters, for use in aviation safety or to protect sensitive optical equipment. This is one possible future avenue worth pursuing in relation to the structures studied here. In addition, the remarkable OL

response from BODIPY **4** with its unusually large permanent dipole moment provides the basis for the rational design of more novel BODIPY dyes with donor-π-acceptor type structures to be investigated for use as optical limiters on the nanosecond timescale, at 532 nm.

- On the BODIPY-cyclodextrin inclusion complexes, the next possible step to ensure successful singlet oxygen generation in aqueous media is to optimise both the experimental conditions and setup so that there is significant generation of singlet oxygen. Additionally, assessing the phototoxicity of the inclusion complexes to bacterial cultures and in biological media is another possible avenue of future research should progress be made in this regard.

- The ability of BODIPY **8** to act as a pH-sensitive fluorescent probe was assessed in organic media, but the limitation in this regard is that the biological application of any molecule typically requires non-toxicity and water solubility or the ability to include the molecule in a water-soluble carrier. This creates a possible future research avenue for the application of BODIPY dyes as pH indicators for cellular events and as fluorescence probes to detect abnormal cells, particularly when included in any suitable water-soluble carrier such as cyclodextrins or micelles.

References

(1) Atilgan, S.; Ekmekci, Z.; Dogan, A. L.; Guc, D.; Akkaya, E. U. Water Soluble Distyryl-Boradiazaindacenes as Efficient Photosensitizers for Photodynamic Therapy. *Chem. Commun.* **2006**, *43* (42), 4398–4400.

(2) Dost, Z.; Atilgan, S.; Akkaya, E. U. Distyryl-Boradiazaindacenes: Facile Synthesis of Novel near IR Emitting Fluorophores. *Tetrahedron* **2006**, *62* (36), 8484–8488.

(3) Lu, H.; Mack, J.; Yang, Y.; Shen, Z. Structural Modification Strategies for the Rational Design of red/NIR Region BODIPYs. *Chem. Soc. Rev.* **2014**, *43* (13), 4778–4823.

(4) Schmitt, A.; Hinkeldey, B.; Wild, M.; Jung, G. Synthesis of the Core Compound of the BODIPY Dye Class: 4,4'-difluoro-4-Bora-(3a,4a)-Diaza-*s*-Indacene. *J. Fluoresc.* **2009**, *19* (4), 755–758.

(5) Ulrich, G.; Ziessel, R.; Harriman, A. The Chemistry of Fluorescent BODIPY Dyes: Versatility Unsurpassed. *Angew. Chem Int. Ed.* **2008**, *47* (7), 1184–1201.

(6) Leen, V. Synthesis and Application of Reactive BODIPY Dyes, PhD thesis, Katholieke Universiteit Leuven, Leuven, Belgium, 2010.

(7) Treibs, A.; Kreuzer, F. Difluorboryl-Komplexe von Di und Tripyrrylmethenen. *Justus Liebigs Ann. Chem.* **1968**, *718*, 208–223.

(8) Deniz, E.; Isbasar, G. C.; Bozdemir, Ö. A.; Yildirim, L. T.; Siemiarczuk, A.; Akkaya, E. U. Bidirectional Switching of near IR Emitting Boradiazaindacene Fluorophores. *Org. Lett.* **2008**, *10* (16), 3401–3403.

(9) Loudet, A.; Burgess, K. BODIPY Dyes and Their Derivatives: Syntheses and

Spectroscopic Properties. *Chem. Rev.* **2007**, *107* (11), 4891–4932.

(10) Rohand, T.; Baruah, M.; Qin, W.; Boens, N.; Dehaen, W. Functionalisation of Fluorescent BODIPY Dyes by Nucleophilic Substitution. *Chem. Commun.* **2006**, *43* (3), 266–268.

(11) Saki, N.; Dinc, T.; Akkaya, E. U. Excimer Emission and Energy Transfer in Cofacial Boradiazaindacene (BODIPY) Dimers Built on a Xanthene Scaffold. *Tetrahedron* **2006**, *62* (11), 2721–2725.

(12) Chen, J.; Burghart, A.; Derecskei-Kovacs, A.; Burgess, K. 4,4-Difluoro-4-Bora-3a,4a-Diaza-*s*-Indacene (BODIPY) Dyes Modified for Extended Conjugation and Restricted Bond Rotations. *J. Org. Chem.* **2000**, *65* (10), 2900–2906.

(13) Rohand, T.; Qin, W.; Boens, N.; Dehaen, W. Palladium-Catalyzed Coupling Reactions for the Functionalization of BODIPY Dyes with Fluorescence Spanning the Visible Spectrum. *Eur. J. Org. Chem.* **2006**, *2006* (20), 4658–4663.

(14) Ulrich, G.; Goze, C.; Guardigli, M.; Roda, A.; Ziessel, R. Pyrromethene Dialkynyl Borane Complexes for “cascatelle” Energy Transfer and Protein Labeling. *Angew. Chem Int. Ed.* **2005**, *44* (24), 3694–3698.

(15) OpenStax, https://archive.cnx.org/contents/df95ff5a-7f2f-43b4-b54c-c35fe9150b25@1/fluorescence-characterization-and-its-application-in-dna-detection, Houston, United States (accessed Dec 12, 2017).

(16) Kasha, M. Characterization of Electronic Transitions in Complex Molecules. *Discuss. Faraday Soc.* **1950**, *9*, 14–19.

(17) López Arbeloa, F.; Bañuelos, J.; Martínez, V.; Arbeloa, T.; López Arbeloa, I. Structural, Photophysical and Lasing Properties of Pyrromethene Dyes. *Int. Rev. Phys. Chem.* **2005**, *24* (2), 339–374.

(18) Awuah, S. G.; Polreis, J.; Biradar, V.; You, Y. Singlet Oxygen Generation by Novel NIR BODIPY Dyes. *Org. Lett.* **2011**, *13* (15), 3884–3887.

(19) Yang, Y.; Guo, Q.; Chen, H.; Zhou, Z.; Guo, Z.; Shen, Z. Thienopyrrole-Expanded BODIPY as a Potential NIR Photosensitizer for Photodynamic Therapy. *Chem. Commun.* **2013**, *49* (38), 3940.

(20) Yogo, T.; Urano, Y.; Ishitsuka, Y.; Maniwa, F.; Nagano, T. Highly Efficient and Photostable Photosensitizer Based on BODIPY Chromophore. *J. Am. Chem. Soc.* **2005**, *127* (35), 12162–12163.

(21) Wang, Y. W.; Descalzo, A. B.; Shen, Z.; You, X. Z.; Rurack, K. Dihydronaphthalene-Fused Boron-Dipyrromethene (BODIPY) Dyes: Insight into the Electronic and Conformational Tuning Modes of BODIPY Fluorophores. *Chem. Eur. J.* **2010**, *16* (9), 2887–2903.

(22) Monsma, F. J.; Barton, C.; Kang, H. C.; Brassard, D. L.; Haugland, R. P.; Sibley, D. R. Characterization of Novel Fluorescent Ligands with High Affinity for D1 and D2 Dopaminergic Receptors. *J. Neurochem.* **1989**, *52*, 1641–1644.

(23) Coskun, A; Akkaya, E. Ion Sensing Coupled to Resonance Energy Transfer: A Highly Selective and Sensitive Ratiometric Fluorescent Chemosensor for Ag (I) by a Modular Approach. *J. Am. Chem. Soc.* **2005**, *127*, 10464–10465.

(24) Li, F.; Yang, S. I.; Ciringh, Y.; Seth, J.; Martin, C. H.; Singh, D. L.; Kim, D.; Birge, R. R.; Bocian, D. F.; Holten, D.; Lindsey, J. S. Design, Synthesis, and Photodynamics of Light-Harvesting Arrays Comprised of a Porphyrin and One, Two, or Eight Boron-Dipyrrin Accessory Pigments. *J. Am. Chem. Soc.* **1998**, *120* (39), 10001–10017.

(25) Yee, M. C.; Fas, S. C.; Stohlmeyer, M. M.; Wandless, T. J.; Cimprich, K. A. A Cell-Permeable, Activity-Based Probe for Protein and Lipid Kinases. *J. Biol. Chem.* **2005**, *280* (32), 29053–29059.

(26) Bañuelos, J.; Martín, V.; Gómez-Durán, C. F. A.; Córdoba, I. J. A.; Peña-Cabrera, E.; García-Moreno, I.; Costela, Á.; Pérez-Ojeda, M. E.; Arbeloa, T.; Arbeloa, Í. L. New 8-Amino-BODIPY Derivatives: Surpassing Laser Dyes at Blue-Edge Wavelengths. *Chem. Eur. J.* **2011**, *17* (26), 7261–7270.

(27) Niu, S. L.; Massif, C.; Ulrich, G.; Renard, P. Y.; Romieu, A.; Ziessel, R. Water-Soluble Red-Emitting Distyryl-Borondipyrromethene (BODIPY) Dyes for Biolabeling. *Chem. Eur. J.* **2012**, *18* (23), 7229–7242.

(28) He, H.; Lo, P.-C.; Yeung, S.-L.; Fong, W.-P.; Ng, D. K. P. Preparation of Unsymmetrical Distyryl BODIPY Derivatives and Effects of the Styryl Substituents on Their in Vitro Photodynamic Properties. *Chem. Commun.* **2011**, *47* (16), 4748–4750.

(29) Huang, X.; El-Sayed, M. A. Plasmonic Photo-Thermal Therapy (PPTT). *Alexandria J. Med.* **2011**, *47* (1), 1–9.

(30) Dickerson, E. B.; Dreaden, E. C.; Huang, X.; El-Sayed, I. H.; Chu, H.; Pushpanketh, S.; McDonald, J. F.; El-Sayed, M. A. Gold Nanorod Assisted near-Infrared Plasmonic

Photothermal Therapy (PPTT) of Squamous Cell Carcinoma in Mice. *Cancer Lett.* **2008**, *269* (1), 57–66.

(31) Meirow, D.; Nugent, D. The Effects of Radiotherapy and Chemotherapy on Female Reproduction. *Hum. Reprod. Update* **2001**, *7* (6), 535–543.

(32) Awuah, S. G.; You, Y. Boron Dipyrromethene (BODIPY)-Based Photosensitizers for Photodynamic Therapy. *RSC Adv.* **2012**, *2* (30), 11169–11183.

(33) Agostinis, P.; Berg, K.; Cengel, K. A.; Foster, T. H.; Girotti, A. W.; Gollnick, S. O.; Hahn, S. M.; Hamblin, M. R.; Juzeniene, A.; Kessel, D.; Korbelik, D.; Moan, J.; Mroz, P.; Nowis, D.; Piette, J.; Wilson, B. C.; Golab, J. Photodynamic Therapy of Cancer : An Update. *Am. Cancer Soc.* **2011**, *61*, 250–281.

(34) Paszko, E.; Ehrhardt, C.; Senge, M. O.; Kelleher, D. P.; Reynolds, J. V. Nanodrug Applications in Photodynamic Therapy. *Photodiagnosis Photodyn. Ther.* **2011**, *8* (1), 14–29.

(35) Wainwright, M.; Byrne, M. N.; Gattrell, M. A. Phenothiazinium-Based Photobactericidal Materials. *J. Photochem. Photobiol. B* **2006**, *84* (3), 227–230.

(36) Dai, T.; Fuchs, B. B.; Coleman, J. J.; Prates, R. A.; Astrakas, C.; St. Denis, T. G.; Ribeiro, M. S.; Mylonakis, E.; Hamblin, M. R.; Tegos, G. P. Concepts and Principles of Photodynamic Therapy as an Alternative Antifungal Discovery Platform. *Front. Microbiol.* **2012**, *3*, 1–16.

(37) Sakamoto, K.; Ohno-Okumura, E. Syntheses and Functional Properties of Phthalocyanines. *Materials* **2009**, *2* (3), 1127–1179.

(38) Durmus, M.; Nyokong, T. Synthesis, Photophysical and Photochemical Properties of Tetra- and Octa-Substituted Gallium and Indium Phthalocyanines. *Polyhedron* **2007**, *26* (13), 3323–3335.

(39) Eastburn, S. D.; Tao, B. Y. Applications of Modified Cyclodextrins. *Biotechnol. Adv.* **1994**, *12* (2), 325–339.

(40) Del Valle, E. M. M. Cyclodextrins and Their Uses: A Review. *Process Biochem.* **2004**, *39* (9), 1033–1046.

(41) Das, S. K.; Rajabalaya, R.; David, S.; Gani, N.; Khanam, J.; Nanda, A. Cyclodextrins-the Molecular Container. *Res. J. Pharm. Biol. Chem. Sci.* **2013**, *4* (2), 1694–1720.

(42) Brewster, M. E.; Loftsson, T. Cyclodextrins as Pharmaceutical Solubilizers. *Adv. Drug Deliv. Rev.* **2007**, *59* (7), 645–666.

(43) Larsen, K. L. Large Cyclodextrins. *J. Incl. Phenom.* **2002**, *43* (1–2), 1–13.

(44) Loftsson, T.; Brewster, M. E. Pharmaceutical Applications of Cyclodextrins: Drug Solubilisation and Stabilization. *J. Pharm. Sci.* **1996**, *85* (11), 1017–1025.

(45) Marconi, G.; Mayer, B. Conformational and Circular Dichroism Studies on Cyclodextrin Inclusion Complexes. *Pure Appl. Chem.* **1997**, *69* (4), 779–783.

(46) Loftsson, T.; Duchêne, D. Cyclodextrins and Their Pharmaceutical Applications. *Int. J. Pharm.* **2007**, *329* (1–2), 1–11.

(47) Del Valle, E. M. M. Cyclodextrins and Their Uses: A Review. *Process Biochem.* **2004**, *39* (9), 1033–1046.

(48) Szejtli, J. Introduction and General Overview of Cyclodextrin Chemistry. *Chem. Rev.* **1998**, *98* (5), 1743–1754.

(49) Freudenberg, K.; Jacobi, R. Über Schardingers Dextrine aus Stärke. *Justus Liebigs Ann. Chem.* **1935**, *518*, 102–108.

(50) Baudin, C.; Pean, C.; Perly, B.; Gosselin, P. Inclusion of Organic Pollutants in Cyclodextrins and Derivatives. *Int. J. Environ. Anal. Chem.* **2000**, *77* (3), 233–242.

(51) Desseaux, V.; Koukiekolo, R.; Moreau, Y.; Santimone, M.; Marchis-Mouren, G. Mechanism of Porcine Pancreatic α-Amylase (PPA). Inhibition of Amylose and Maltopentaose Hydrolysis by α- , β- and ϒ-Cyclodextrins. *Eur. J. Biochem.* **2002**, *11*, 163–170.

(52) Hedges, A. R. Industrial Applications of Cyclodextrins. *Chem. Rev.* **1998**, *98* (5), 2035–2044.

(53) Kumar, R.; Dahiya, J. S.; Singh, D.; Nigam, P. Biotransformation of Cholesterol Using *Lactobacillus Bulgaricus* in a Glucose-Controlled Bioreactor. *Bioresour. Technol.* **2001**, *78* (2), 209–211.

(54) Stella, V. J.; Rao, V. M.; Zannou, E. A.; Zia, V. Mechanisms of Drug Release from Cyclodextrin Complexes. *Adv. Drug Deliv. Rev.* **1999**, *36* (1), 3–16.

(55) Uekama, K.; Hirayama, F.; Irie, T. Cyclodextrin Drug Carrier Systems. *Chem. Rev.* **1998**, *98* (81), 2045–2076.

(56) Szejtli, J. The Cyclodextrins and Their Applications in Biotechnology. *Carbohydr. Polym.* **1990**, *12* (4), 375–392.

(57) Brunet, C.; Lamare, S.; Legoy, M. D. Studies of Specific Cyclodextrin Production Starting from Pure Maltooligosaccharides Using *Thermoanaerobacter* Sp. Cyclodextrin GlycosylTransferase. *Biocatal. Biotransformation* **1998**, *16* (4), 317–327.

(58) Tonkova, A. Bacterial Cyclodextrin Glucanotransferase. *Enzyme Microb. Technol.* **1998**, *22* (8), 678–686.

(59) Bhardwaj, R.; Dorr, R. T.; Blanchard, J. Approaches to Reducing Toxicity of Parenteral Anticancer Drug Formulations Using Cyclodextrins. *PDA J. Pharm. Sci. Technol.* **2000**, *54* (3), 233–239.

(60) Dufossé, L.; Souchon, I.; Feron, G.; Latrasse, A.; Spinnler, H. E. In Situ Detoxification of the Fermentation Medium during γ-Decalactone Production with the Yeast Sporidiobolus Salmonicolor. *Biotechnol. Prog.* **1999**, *15* (1), 135–139.

(61) Lezcano, M.; Al-Soufi, W.; Novo, M.; Rodríguez-Núñez, E.; Vázquez Tato, J. Complexation of Several Benzimidazole-Type Fungicides with α- and β-Cyclodextrins. *J. Agric. Food Chem.* **2002**, *50* (1), 108–112.

(62) Schollmeyer, E.; Buschmann, H. Applications of Cyclodextrins in Cosmetic Products: A Review. *J. Cosmet. Sci.* **2002**, *53*, 185–191.

(63) Szejtli, J. Downstream Processing Using Cyclodextrins. *Trends Biotechnol.* **1989**, *7* (7), 170–174.

(64) Winkler RG, Fioravanti S, Ciccotti G, Margheritis C, V. M. Hydration of Beta-Cyclodextrin: A Molecular Dynamics Simulation Study. *J. Comput. Aided Mol. Des.* **2000**, *14*, 659–667.

(65) Bone, S. Dielectric Studies of Water Clusters in Cyclodextrins: Relevance to the Transition between Slow and Fast Forms of Thrombin. *J. Phys. Chem. B* **2006**, *110* (41), 20609–20614.

(66) Hakkarainen, B.; Fujita, K.; Immel, S.; Kenne, L.; Sandström, C. ^{1}H NMR Studies on the Hydrogen-Bonding Network in Mono-Altro-β-Cyclodextrin and Its Complex with Adamantane-1-Carboxylic Acid. *Carbohydr. Res.* **2005**, *340* (8), 1539–1545.

(67) Lichtenthaler, F. W.; Immel, S. On the Hydrophobic Characteristics of Cyclodextrins: Computer-Aided Visualization of Molecular Lipophilicity Patterns. *Liebigs Ann.* **1996**, 27–37.

(68) Schneiderman, E.; Stalcup, A. M. Cyclodextrins: A Versatile Tool in Separation Science. *J. Chromatogr. B* **2000**, *745* (1), 83–102.

(69) Szente, L.; Szejtli, J. Highly Soluble Cyclodextrin Derivatives: Chemistry, Properties, and Trends in Development. *Adv. Drug Deliv. Rev.* **1999**, *36*, 17–28.

(70) Matsuda, H.; Arima, H. Cyclodextrins in Transdermal and Rectal Delivery. *Adv. Drug Deliv. Rev.* **1999**, *36* (1), 81–99.

(71) Uekama, K.; Hirayama, F.; Arima, H. Recent Aspect of Cyclodextrin-Based Drug Delivery System. *J. Incl. Phenom. Macrocycl. Chem.* **2006**, *56* (1–2), 3–8.

(72) Strickley, R. G. Solubilizing Excipients in Oral and Injectable Formulations. *Pharm. Res.* **2004**, *21* (2), 201–230.

(73) Loftsson, T.; Brewster, M. E.; Masson, M. Role of Cyclodextrins in Improving Oral Drug Delivery. *Am. J. Drug Deliv.* **2004**, *2* (4), 261–275.

(74) Davis, M. E.; Brewster, M. E. Cyclodextrin-Based Pharmaceutics: Past, Present and Future. *Nat. Rev. Drug Discov.* **2004**, *3* (12), 1023–1035.

(75) Avdeef, A.; Bendels, S.; Tsinman, O.; Tsinman, K.; Kansy, M. Solubility-Excipient Classification Gradient Maps. *Pharm. Res.* **2007**, *24* (3), 530–545.

(76) Hirayama, F.; Uekama, K. Cyclodextrin-Based Controlled Drug Release System. *Adv. Drug Deliv. Rev.* **1999**, *36* (1), 125–141.

(77) Szejtli, J.; Szente, L. Elimination of Bitter, Disgusting Tastes of Drugs and Foods by Cyclodextrins. *Eur. J. Pharm. Biopharm.* **2005**, *61* (3), 115–125.

(78) Lantz, A. W.; Rodriguez, M. A.; Wetterer, S. M.; Armstrong, D. W. Estimation of Association Constants between Oral Malodor Components and Various Native and Derivatized Cyclodextrins. *Anal. Chim. Acta* **2006**, *557* (1–2), 184–190.

(79) Irie T., U. K. Pharmaceutical Applications of Cyclodextrins. III. Toxicological Issues and Safety Evaluation. *J. Pharm. Sci.* **1997**, *86* (2), 147–162.

(80) Lina, B. A. R.; Bär, A. Subchronic Oral Toxicity Studies with α-Cyclodextrin in Rats. *Regul. Toxicol. Pharmacol.* **2004**, *39*, S14–S26.

(81) Bellringer, M. E.; Smith, T. G.; Read, R.; Gopinath, C.; Oliver, P. β- Cyclodextrin: 52-Week Toxicity Studies in the Rat and Dog. *Food Chem. Toxicol.* **1995**, *33* (5), 367–376.

(82) Szente, L.; Szejtli, J.; Kis, G. L. Spontaneous Opalescence of Aqueous Gamma-Cyclodextrin Solutions: Complex Formation or Self-Aggregation? *J. Pharm. Sci.* **1998**, *87* (6), 778–781.

(83) Munro, I. C.; Newberne, P. M.; Young, V. R.; Bär, A. Safety Assessment of γ-

Cyclodextrin. *Regul. Toxicol. Pharmacol.* **2004**, *39*, S3–S13.

(84) Koutsou, G. A.; Storey, D. M.; Bär, A. Gastrointestinal Tolerance of γ-Cyclodextrin in Humans. *Food Addit. Contam.* **1999**, *16* (7), 313–317.

(85) Hedges, A. R. Industrial Applications of Cyclodextrins. *Chem. Rev.* **1998**, *98* (5), 2035–2044.

(86) Loftsson, T.; Olafsdottir, B. J.; Frioriksdottir, H.; Jonsdottir, S. Cyclodextrin Complexation of Nsaids - Physicochemical Characteristics. *Eur. J. Pharm. Sci.* **1993**, *1*, 95–101.

(87) Hamai, S.; Koshiyama, T. Electronic Absorption, Fluorescence, and Circular Dichroism Spectroscopic Studies on the Inclusion Complexes of tetrakis(4-Sulfonatophenyl)porphyrin with Cyclodextrins in Basic Aqueous Solutions. *J. Photochem. Photobiol. A* **1999**, *127* (1–3), 135–141.

(88) Manka, J. S.; Lawrence, D. S. Self-Assembly of a Hydrophobic Groove. *Tetrahedron Lett.* **1989**, *30* (52), 7341–7344.

(89) Mosseri, S.; Mialocq, J. C.; Perly, B.; Hambright, P. Porphyrins-Cyclodextrin .1. Photooxidation of Zinc Tetrakis(4-Sulfonatophenyl)Porphyrin in Cyclodextrin Cavities - the Characterization of ZnTSPP Dication - Photolysis, Radiolysis, and NMR Studies. *J. Phys. Chem.* **1991**, *95* (6), 2196–2203.

(90) Mosseri, S.; Mialocq, J. C.; Perly, B.; Hambright, P. Porphyrins-Cyclodextrin .2. Dissociation, Reduction, and Proton Relaxivity of an Iron(iii) Porphyrin μ-Oxo Dimer in Cyclodextrin Solutions. *J. Phys. Chem.* **1991**, *95* (12), 4659–4663.

(91) Zhou, G.; Wang, X.; Wang, D.; Wang, C.; Shao, Z.; Fang, Q.; Jiang, M. Two-Photon Absorption and Nonlinear Optical Properties of a New Organic Dye PSPI. *Opt. Commun.* **2001**, *190* (1–6), 345–349.

(92) Barkana, Y.; Belkin, M. Laser Eye Injuries. *Surv. Ophthalmol.* **2000**, *44* (6), 459–478.

(93) Chen, Y.; Hanack, M.; Araki, Y.; Ito, O. Axially Modified Gallium Phthalocyanines and Naphthalocyanines for Optical Limiting. *Chem. Soc. Rev.* **2005**, *34* (6), 517–529.

(94) Dini, D.; Barthel, M.; Hanack, M. Phthalocyanines as Active Materials for Optical Limiting. *Eur. J. Org. Chem.* **2001**, *2001* (20), 3759–3769.

(95) Harris, J.; Gai, L.; Kubheka, G.; Mack, J.; Nyokong, T.; Shen, Z. Optical Limiting Properties of 3,5-Dithienylenevinylene BODIPY Dyes at 532 nm. *Chem. Eur. J.* **2017**, 1–9.

(96) Kubheka, G.; Achadu, O.; Mack, J.; Nyokong, T. Optical Limiting Properties of 3,5-Diphenyldibenzo-azaBODIPY at 532 nm. *New J. Chem.* **2017**, *41* (20), 12319–12325.

(97) de laTorre, G.; Vazquez, P.; Agullo-Lopez, F.; Torres, T. Role of Structural Factors in the Nonlinear Optical Properties of Phthalocyanines and Related Compounds. *Chem. Rev.* **2004**, *104* (9), 3723–3750.

(98) de la Torre, G.; Vazquez, P.; Agullo-Lopez, F.; Torres, T. Phthalocyanines and Related Compounds: Organic Targets for Nonlinear Optical Applications. *J. Mater. Chem.* **1998**, *8* (8), 1671–1683.

(99) Kandasamy, K.; Shetty, S. J.; Puntambekar, P. N.; Srivastava, T. S.; Kundu, T.; Singh, B. P. Non-Resonant Third-Order Optical Non-Linearity of Porphyrin Derivatives. *Chem.*

Commun. **1997**, *33* (13), 1159–1160.

(100) Ogawa, K.; Zhang, T.; Yoshihara, K.; Kobuke, Y. Large Third-Order Optical Nonlinearity of Self-Assembled Porphyrin Oligomers. *J. Am. Chem. Soc.* **2002**, *124* (1), 22–23.

(101) Sheik-bahae, M.; Said, A. A.; Van Stryland, E. W. High-Sensitivity, Single-Beam n_2 Measurements. *Opt. Lett.* **1989**, *14* (17), 955–957.

(102) Zhu, M.; Jiang, L.; Yuan, M.; Liu, X.; Ouyang, C.; Zheng, H.; Yin, X.; Zuo, Z.; Liu, H.; Li, Y. Efficient Tuning Nonlinear Optical Properties: Synthesis and Characterization of a Series of Novel Poly(aryleneethynylene)s Co-Containing BODIPY. *J. Polym. Sci. A Polym. Chem.* **2008**, *46* , 7401–7410.

(103) Sheik-Bahae, M.; Said, A. A.; Wei, T.-H.; Hagan, D. J.; Van Stryland, E. W. Sensitive Measurement of Optical Nonlinearities Using a Single Beam. *Quantum Electron. IEEE J.* **1990**, *26* (4), 760–769.

(104) Sutherland, R. L.; Mclean, D. G.; Kirkpatrick, S. *Handbook of Nonlinear Optics*, 2nd ed.; New York, 2003.

(105) Matthes, R. Commission on non-ionizing radiation protection. Revision of Guidelines on Limits of Exposure to Laser Radiation of Wavelengths between 400 nm and 1.4 µm. *Health Phys.* **2000**, *79* (4), 431–440.

(106) Hollins, R. C. Materials for Optical Limiters. *Curr. Opin. Solid State Mater. Sci.* **1999**, *4* (2), 189–196.

(107) Bankole, O. M.; Nyokong, T. Mercaptopyridine-substituted Indium, Zinc, and Metal-Free Phthalocyanines: Nonlinear Optical Studies in Solution and on Polymer Matrices.

J. Coord. Chem. **2015**, *68* (20), 3727–3740.

(108) Piechocki, C.; Simon, J.; André, J. J.; Guillon, D.; Petit, P.; Skoulios, A.; Weber, P. Synthesis and Physico-Chemical Studies of Neutral and Chemically Oxidized Forms of Bis(octaalkyloxyphthalocyaninato) Lutetium. *Chem. Phys. Lett.* **1985**, *122* (1–2), 124–128.

(109) Sanusi, K.; Antunes, E.; Nyokong, T. Optical Nonlinearities in Non-Peripherally Substituted Pyridyloxy Phthalocyanines: A Combined Effect of Symmetry, Ring-Strain and Demetallation. *Dalton. Trans.* **2014**, *43* (3), 999–1010.

(110) Misra, R.; Kumar, R.; PrabhuRaja, V.; Chandrashekar, T. K. Modified Push-Pull Expanded Corroles: Syntheses, Structure and Nonlinear Optical Properties. *J. Photochem. Photobiol. A* **2005**, *175* (2–3), 108–117.

(111) Marder, S. R.; Perry, J. W. Molecular Materials for Second-Order Nonlinear Optical Applications. *Adv. Mater.* **1993**, *5* (11), 804–815.

(112) Wong, J.; Todd, M.; Rutledge, P. Recent Advances in Macrocyclic Fluorescent Probes for Ion Sensing. *Molecules* **2017**, *22* (2), 200–200.

(113) Hulanicki, A.; Stanislaw, G.; FolKe, I. Chemical Sensors: Definitions and Classification. *Pure Appl. Chem.* **1991**, *63* (9), 1247–1250.

(114) Ni, Y.; Wu, J. Far-Red and near Infrared BODIPY Dyes: Synthesis and Applications for Fluorescent pH Probes and Bio-Imaging. *Org. Biomol. Chem.* **2014**, *12* (23), 3774–3791.

(115) Basabe-Desmonts, L.; Reinhoudt, D. N.; Crego-Calama, M. Design of Fluorescent

Materials for Chemical Sensing. *Chem. Soc. Rev.* **2007**, *36* (6), 993–1017.

(116) Ng, S. M.; Koneswaran, M.; Narayanaswamy, R. A Review on Fluorescent Inorganic Nanoparticles for Optical Sensing Applications. *RSC Adv.* **2016**, *6* (26), 21624–21661.

(117) New, E. J. Harnessing the Potential of Small Molecule Intracellular Fluorescent Sensors. *ACS Sensors* **2016**, *1*, 328–333.

(118) Li, C.; Shi, G. Carbon Nanotube-Based Fluorescence Sensors. *J. Photochem. Photobiol. C* **2014**, *19* (1), 20–34.

(119) Fabbrizzi, L.; Licchelli, M.; Mancin, F.; Pizzeghello, M.; Rabaioli, G.; Taglietti, A.; Tecilla, P.; Tonellato, U. Fluorescence Sensing of Ionic Analytes in Water: From Transition Metal Ions to Vitamin B13. *Chem. Eur. J.* **2002**, *8* (1), 94–101.

(120) Montes, S.; Rivera-mancia, S.; Diaz-ruiz, A.; Tristan-lopez, L.; Rios, C. Copper and Copper Proteins in Parkinson's Disease. *Oxid. Med. Cell. Longev.* **2014**, 2014, 147251.

(121) Jomova, K.; Vondrakova, D.; Lawson, M.; Valko, M. Metals, Oxidative Stress and Neurodegenerative Disorders. *Mol. Cell. Biochem.* **2010**, *345* (1–2), 91–104.

(122) Zhao, Y.; Zhang, X.-B.; Han, Z.-X.; Qiao, L.; Li, C.-Y.; Jian, L.-X.; Shen, G.-L.; Yu, R.-Q. Highly Sensitive and Selective Colorimetric and Off−On Fluorescent Chemosensor for Cu^{2+} in Aqueous Solution and Living Cells. *Anal. Chem.* **2009**, *81* (16), 7022–7030.

(123) Shen, C.; Kolanowski, J. L.; M-N Tran, C.; Kaur, A.; Akerfeldt, M. C.; Rahme, M. S.; Hambley, T. W.; New, E. J. A Ratiometric Fluorescent Sensor for the Mitochondrial Copper Pool. *Metallomics* **2016**, *8* (8), 915–919.

(124) Meaney, M. S.; McGuffin, V. L. Luminescence-Based Methods for Sensing and

Detection of Explosives. *Anal. Bioanal. Chem.* **2008**, *391* (7), 2557–2576.

(125) Sun, X.; Wang, Y.; Lei, Y. Fluorescence Based Explosive Detection: From Mechanisms to Sensory Materials. *Chem. Soc. Rev.* **2015**, *44* (22), 8019–8061.

(126) Chang, C. J.; Gunnlaugsson, T.; James, T. D. Sensor Targets. *Chem. Soc. Rev.* **2015**, *4176* (44), 4176–4178.

(127) Hayes, J. S. Synthesis, Characterization, and Evaluation of Novel BODIPY Dyes With Theranostic Applications, PhD thesis, Louisiana State University, Baton Rouge, United States, 2014.

(128) Yuan, L.; Lin, W.; Cao, Z.; Long, L.; Song, J. Photocontrollable Analyte-Responsive Fluorescent Probes: A Photocaged Copper-Responsive Fluorescence Turn-on Probe. *Chem. Eur. J.* **2011**, *17* (2), 689–696.

(129) Yin, S.; Leen, V.; Snick, S. Van; Boens, N.; Dehaen, W. A Highly Sensitive, Selective, Colorimetric and near-Infrared Fluorescent Turn-on Chemosensor for Cu^{2+} Based on BODIPY. *Chem. Commun.* **2010**, *46* (34), 6329–6331.

(130) Hudnall, T. W.; Gabbai, F. P. A BODIPY Boronium Cation for the Sensing of Fluoride Ions. *Chem. Commun.* **2008**, *45* (38), 4596–4597.

(131) Boens, N.; Leen, V.; Dehaen, W. Fluorescent Indicators Based on BODIPY. *Chem. Soc. Rev.* **2012**, *41* (3), 1130–1172.

(132) Huang, L.; Zhao, J. Switching of the Triplet Excited State of the C_{60}-Dimethylaminostyryl BODIPY Dyads/triads. *J. Mater. Chem. C* **2015**, *3* (3), 538–550.

(133) Li, L.; Han, J.; Nguyen, B.; Burgess, K. Syntheses and Spectral Properties of

Functionalized, Water-Soluble BODIPY Derivatives. *J. Org. Chem.* **2008**, *73* (5), 1963–1970.

(134) Kálai, T.; Hideg, K. Synthesis of New, BODIPY-Based Sensors and Labels. *Tetrahedron* **2006**, *62* (44), 10352–10360.

(135) Kang, H.; Si, Y.; Liu, J.; Chen, L.; Li, Y.; Chen, H.; Groeper, J.; Yang, B. An Experimental and Theoretical Study of Dimethylaminostyryl BODIPY-Perylenetetracarboxylic Derivative Dyads: Synthesis, Properties and DFT Calculation. *RSC Adv.* **2016**, *6* (28), 23094–23101.

(136) Han, J.; Burgess, K. Fluorescent Indicators for Intracellular pH. *Chem. Rev.* **2009**, *110* (5), 2709–2728.

(137) Rurack, K.; Kollmannsberger, M.; Daub, J. A Highly Efficient Sensor Molecule Emitting in the near Infrared (NIR): 3,5-Distyryl-8-(*p*-Dimethylaminophenyl)difluoroboradiaza-*s*-Indacene. *New J. Chem.* **2001**, *25* (2), 289–292.

(138) Bruker Corporation, https://www.bruker.com/products/x-ray-diffraction-and-elemental-analysis/x-ray-diffraction/xrd-software/eva/overview.html, Billerica, United States (accessed Jan 5, 2018).

(139) Frisch, M. J.; Trucks, G. W.; Schlegel, H. B.; Scuseria, G. E.; Robb, M. A.; Cheeseman, J. R.; Scalmani, G.; Barone, V.; Petersson, G. A.; Nakatsuji, H.; Li, X.; Caricato, M.; Marenich, M.; Bloino, J.; Janesko, B. G.; Gomperts, R.; Mennuci, B.; Hratachian, H. P.; Oritiz, J. V.; Izmoylov, A. F.; Sonnenberg, J. L.; Williams-Young. D.; Ding, F.; Lipparini, F.; Egidi, F.; Goings, J.; Peng, B.; Petrone, A.; Henderson, T.; Ranasinghe, D.;

Zakrzewski, V. G.; Gao, J.; Rega, N.; Zheng, G.; Liang, W.; Hada, M.; Ehara, M.; Toyota, K.; Fukuda, R.; Hasegawa, J.; Ishida, M.; Nakajima, T.; Honda, Y.; Kitao, O.; Nakai, H.; Vreven, T.; Throssell, K.; Montgomery, J. A.; Peralta, J. E.; Ogliaro, F.; Bearpark, M.; Heyd, J. J.; Brothers, E.; Kudin, K. N.; Staroverov, V. N.; Keith, T.; Kobayashi, R.; Normand, J.; Raghavachari, K.; Rendell, A.; Burant, J. C.; Iyengar, S. S.; Tomasi, J.; Cossi, M.; Millam, J. M.; Klene, M.; Adamo, C.; Cammi, R.; Ochterski, J. W.; Martin, R. L.; Morokuma, K.; Farkas, O.; Foresman, J. B.; Fox, D. J. Gaussian 09, Revision D.01. Gaussian, Inc.: Wallingford CT 2016.

(140) Hanwell, M. D.; Curtis, D. E.; Lonie, D. C.; Vandermeersch, T.; Zurek, E.; Hutchison, G. R. Avogadro: An Advanced Semantic Chemical Editor, Visualization, and Analysis Platform. *J. Cheminform.* **2012**, *4* (8), 1–17.

(141) López Arbeloa, F.; López Arbeloa, T.; López Arbeloa, I.; García-Moreno, I.; Costela, A.; Sastre, R.; Amat-Guerri, F. Photophysical and Lasing Properties of Pyrromethene 567 Dye in Liquid Solution. Environment Effects. *Chem. Phys.* **1998**, *236* (1–3), 331–341.

(142) Fery-Forgues, S.; Lavabre, D. Are Fluorescence Quantum Yields So Tricky to Measure? A Demonstration Using Familiar Stationery Products. *J. Chem. Educ.* **1999**, *76* (9), 1260-1264.

(143) Fletcher, A. .; Kubin, R. F. Fluorescence Quantum Yields of Some Rhodamine Dyes. *J. Lumin*. **1982**, *27*, 455–462.

(144) Ogunsipe, A.; Chen, J.; Nyokong, T. Photophysical and Photochemical Studies of Zinc(II) phthalocyanine derivatives-effects of substituents and solvents. *New J. Chem.* **2004**, *28*, 822–827.

(145) Wu, W.; Guo, H.; Wu, W.; Ji, S.; Zhao, J. Organic Triplet Sensitizer Library Derived from a Single Chromophore (BODIPY) with Long-Lived Triplet Excited State for Triplet-Triplet Annihilation Based Upconversion. *J. Org. Chem.* **2011**, *76* (17), 7056–7064.

(146) Luo, G.-G.; Lu, H.; Zhang, X.-L.; Dai, J.-C.; Wu, J.-H.; Wu, J.-J. The Relationship between the Boron Dipyrromethene (BODIPY) Structure and the Effectiveness of Homogeneous and Heterogeneous Solar Hydrogen-Generating Systems as well as DSSCs. *Phys. Chem. Chem. Phys.* **2015**, *17* (15), 9716–9729.

(147) Seotsanyana-Mokhosi, I.; Nyokong, T. Synthesis and Photochemical Studies of Substituted Adjacent Binaphthalophthalocyanines. *J. Porphyrins Phthalocyanines.* **2004**, *8* (10), 1214–1221.

(148) Ogunsipe, A.; Nyokong, T. Effects of Central Metal on the Photophysical and Photochemical Properties of Non-Transition Metal Sulfophthalo- Cyanine. *J. Porphyrins Phthalocyanines.* **2005**, *9 (2)*, 121–129.

(149) Redmond, R. W.; Gamlin, J. N. A Compilation of Singlet Oxygen Yields from Biologically Relevant Molecules. *Photochem. Photobiol.* **1999**, *70* (4), 391–475.

(150) Stone, J. Synthesis and Photophysical Studies of Crown Ether-Bodipy Dyes and the Fabrication of Bodipy Embedded Fluorescent Nanofibers, MSc thesis, Rhodes University, Grahamstown, South Africa, 2016.

(151) Harris, J. BODIPY Dyes for Singlet Oxygen and Optical Limiting Applications, MSc thesis, Rhodes University, Grahamstown, South Africa, 2018.

(152) Quan, L.; Lin, W.; Sun, T.; Xie, Z.; Huang, Y.; Jing, X. Green Photocatalysis with Oxygen

Sensitive BODIPYs under Visible Light. *Catal. Lett.* **2014**, *144* (2), 308–313.

(153) Hoogendoorn, S.; Blom, A. E. M.; Willems, L. I.; Van Der Marel, G. A.; Overkleeft, H. S. Synthesis of pH-Activatable Red Fluorescent BODIPY Dyes with Distinct Functionalities. *Org. Lett.* **2011**, *13* (20), 5656–5659.

(154) Qin, W.; Baruah, M.; Stefan, A.; Van Der Auweraer, M.; Boens, N. Photophysical Properties of BODIPY-Derived Hydroxyaryl Fluorescent pH Probes in Solution. *ChemPhysChem* **2005**, *6* (11), 2343–2351.

(155) Huh, J. O.; Do, Y.; Lee, M. H. A BODIPY-Borane Dyad for the Selective Complexation of Cyanide Ion. *Organometallics* **2008**, *27* (6), 1022–1025.

(156) Xiaolin, Z.; Yi, X.; Xuhong, Q. Highly Efficient Energy Transfer in the Light Harvesting System Composed of Three Kinds of Boron-Dipyrromethene Derivatives. *Org. Lett.* **2008**, *10* (1), 29–32.

(157) Lv, Y.; Xu, J.; Guo, Y.; Shao, S. A Sandwich Anion Receptor by a BODIPY Dye Bearing Two calix[4]pyrrole Units. *Chem. Pap.* **2011**, *65* (4), 553–558.

(158) Wu, W.; Sun, J.; Cui, X.; Zhao, J. Observation of the Room Temperature Phosphorescence of BODIPY in Visible Light-Harvesting Ru(ll) Polyimine Complexes and Application as Triplet Photosensitizers for Triplet–Triplet-Annihilation Upconversion and Photocatalytic Oxidation. *J. Mater. Chem. C* **2013**, *1* (30), 4577–4589.

(159) Sun, J.; Zhong, F.; Yi, X.; Zhao, J. Efficient Enhancement of the Visible-Light Absorption of Cyclometalated Ir(III) Complexes Triplet Photosensitizers with BODIPY and

Applications in Photooxidation and Triplet-Triplet Annihilation Upconversion. *Inorg. Chem.* **2013**, *52* (11), 6299–6310.

(160) Algi, M. P.; Tirkes, S.; Ertan, S.; Ergun, E. G. C.; Cihaner, A.; Algi, F. Design and Synthesis of New 4,4′-Difluoro-4-Bora-3a,4a-Diaza-*S*-Indacene Based Electrochromic Polymers. *Electrochim. Acta.* **2013**, *109*, 766–774.

(161) Ueno, T.; Urano, Y.; Kojima, H.; Nagano, T. Mechanism-Based Molecular Design of Highly Selective Fluorescence Probes for Nitrative Stress. *J. Am. Chem. Soc.* **2006**, *128* (33), 10640–10641.

(162) Qin, W.; Baruah, M.; De Borggraeve, W. M.; Boens, N. Photophysical Properties of an On/off Fluorescent pH Indicator Excitable with Visible Light Based on a Borondipyrromethene-Linked Phenol. *J. Photochem. Photobiol. A* **2006**, *183* (1–2), 190–197.

(163) Inoue, N.; Suzuki, Y.; Yokoyama, K.; Karube, I. Novel Fluorescent Probe for Analysis of Hydroperoxides Based on Boron Dipyrromethane Fluorophore. *Biosci. Biotechnol. Biochem.* **2009**, *73* (5), 1215–1217.

(164) Frenette, M.; Hatamimoslehabadi, M.; Bellinger-Buckley, S.; Laoui, S.; Bag, S.; Dantiste, O.; Rochford, J.; Yelleswarapu, C. Nonlinear Optical Properties of Multipyrrole Dyes. *Chem. Phys. Lett.* **2014**, *608*, 303–307.

(165) Zhou, Z.; Yang, W. Syntheses of 2-Aryl Benzothiazoles via Photocatalyzed Oxidative Condensation of Amines with 2-Aminothiophenol in the Presence of BODIPY Derivatives. *Synth. Commun.* **2014**, *44* (21), 3189–3198.

(166) Saleh, B. E. A.; Teich, M. C. *Fundamentals of Photonics*; Wiley: New York, 1991.

(167) Kumar, R. S. S.; Rao, S. V.; Giribabu, L.; Rao, D. N. Femtosecond and Nanosecond Nonlinear Optical Properties of Alkyl Phthalocyanines Studied Using Z-Scan Technique. *Chem. Phys. Lett.* **2007**, *447* (4–6), 274–278.

(168) Mkhize, C.; Britton, J.; Nyokong, T. Enhanced Nonlinear Optical Properties of Octa-Substituted Lead and Cadmium Phthalocyanines When Embedded in Poly(bisphenol A Carbonate) as Thin Films. *Polyhedron* **2014**, *81*, 607–613.

(169) Sekhosana, K. E.; Amuhaya, E.; Nyokong, T. Nanosecond Nonlinear Optical Limiting Properties of New Trinuclear Lanthanide Phthalocyanines in Solution and as Thin Films. *Polyhedron* **2015**, *85*, 347–354.

(170) Frenette, M.; Hatamimoslehabadi, M.; Bellinger-Buckley, S.; Laoui, S.; La, J.; Bag, S.; Mallidi, S.; Hasan, T.; Bouma, B.; Yelleswarapu, C.; Rochford, J. Shining Light on the Dark Side of Imaging: Excited State Absorption Enhancement of a Bis-Styryl BODIPY Photoacoustic Contrast Agent. *J. Am. Chem. Soc.* **2014**, *136* (45), 15853–15856.

(171) Kubheka, G.; Sanusi, K.; Mack, J.; Nyokong, T. Optical Limiting Properties of 3,5-dipyrenylvinyleneBODIPY Dyes at 532 nm. *Spectrochim. Acta A* **2018**, *191*, 357–364.

(172) Jiao, L.; Pang, W.; Zhou, J.; Wei, Y.; Mu, X.; Bai, G.; Hao, E. Regioselective Stepwise Bromination of Boron Dipyrromethene (BODIPY) Dyes. *J. Org. Chem.* **2011**, *76* (24), 9988–9996.

(173) Kamkaew, A.; Lim, S. H.; Lee, H. B.; Kiew, L. V.; Chung, L. Y.; Burgess, K. BODIPY Dyes in Photodynamic Therapy. *Chem. Soc. Rev.* **2013**, *42* (1), 77–88.

(174) May, A. K.; Stone, J.; Ngoy, B. P.; Mack, J.; Nyokong, T.; Kimura, M.; Kobayashi, N., accepted for publication in the *Journal of Porphyrins and Phthalocyanines* in **2018**. [doi: 10.1142/S1088424617500869]

(175) Astray, G.; Gonzalez-Barreiro, C.; Mejuto, J. C.; Rial-Otero, R.; Simal-Gándara, J. A Review on the Use of Cyclodextrins in Foods. *Food Hydrocoll.* **2009**, *23* (7), 1631–1640.

(176) Schmid, G. Cyclodextrin Glycosyltransferase Production: Yield Enhancement by Overexpression of Cloned Genes. *Trends Biotechnol.* **1989**, *7* (9), 244–248.

(177) Sapkal, N. P.; Kilor, V. A.; Bhursari, K. P.; Daud, A. S. Evaluation of Some Methods for Preparing Gliclazide-β-Cyclodextrin Inclusion Complexes. *Trop. J. Pharm. Res.* **2007**, *6* (4), 833–840.

(178) Osadebe, P. O.; Onugwu, L. E.; Attama, A. A. Energetics of the Interaction between Piroxicam and Beta-Cyclodextrin (β-CD) in Inclusion Complexes. *Sci. Res. Essays* **2008**, *3* (3), 86–93.

(179) Miller, L. A.; Carrier, R. L.; Ahmed, I. Practical Considerations in Development of Solid Dosage Forms That Contain Cyclodextrin. *J. Pharm. Sci.* **2007**, *96* (7), 1691–1707.

(180) Challa, R.; Ahuja, A.; Ali, J.; Khar, R. K. Cyclodextrins in Drug Delivery: An Updated Review. *AAPS PharmSciTech.* **2005**, *6* (2), E329–E357.

(181) Waleczek, K. J.; Cabral-Marques, H. M.; Hempel, B.; Schmidt, P. C. Phase Solubility Studies of Pure (−)-α-Bisabolol and Camomile Essencial Oil with β-Cyclodextrin. *Eur. J. Pharm. Biopharm.* **2003**, *55* (2), 247–251.

(182) Moraes, C. M.; Abrami, P.; De Araujo, D. R.; Braga, A. F. A.; Issa, M. G.; Ferraz, H. G.; De Paula, E.; Fraceto, L. F. Characterization of Lidocaine:hydroxypropyl-β-Cyclodextrin Inclusion Complex. *J. Incl. Phenom. Macrocycl. Chem.* **2007**, *57* (1–4), 313–316.

(183) Bratu, I.; Hernanz, A.; Gavira, J. M.; Bora, G. H. FT-IR Spectroscopy of Inclusion Complexes of β-Cyclodextrin with Fenbufen and Ibuprofen. *Romanian J. Phys.* **2005**, *50* (9–10), 1063–1069.

(184) Kim, H.; Yiluo, H.; Park, S.; Lee, J. Y.; Cho, E.; Jung, S. Characterization and Enhanced Antioxidant Activity of the Cysteinyl β-Cyclodextrin-Baicalein Inclusion Complex. *Molecules* **2016**, 21 (6), 703–703.

(185) Periasamy, R.; Kothainayaki, S.; Rajamohan, R.; Sivakumar, K. Spectral Investigation and Characterization of Host-Guest Inclusion Complex of 4,4'-Methylene-bis(2-Chloroaniline) with β-Cyclodextrin. *Carbohydr. Polym.* **2014**, *114*, 558–566.

(186) Srinivasan, K.; Sivakumar, K.; Stalin, T. 2,6-Dinitroaniline and β-Cyclodextrin Inclusion Complex Properties Studied by Different Analytical Methods. *Carbohydr. Polym.* **2014**, *113*, 577–587.

(187) Job, P. Formation and Stability of Inorganic Complexes in Solution. *Ann. Chim.* **1928**, *9*, 113–203.

(188) Dotsikas, Y.; Kontopanou, E.; Allagiannis, C.; Loukas, Y. L. Interaction of 6-*P*-Toluidinylnaphthalene-2-sulphonate with β-Cyclodextrin. *J. Pharm. Biomed. Anal.* **2000**, *23*, 997–1003.

(189) Loukas, Y. L. Multiple Complex Formation of Fluorescent Compounds with

Cyclodextrins: Efficient Determination and Evaluation of the Binding Constant With Improved Fluorometric Studies. *J. Phys. Chem. B* **1997**, *101*, 4863–4866.

(190) Kobayashi, N. Lid-Type Inclusion. *Chem. Commun.* **1988**, 24 (14), 918–919.

(191) Harata, K.; Uedaira, H. The Circular Dichroism Spectra of the β-Cyclodextrin Complex with Naphthalene Derivatives. *Bull. Chem. Soc. Jpn* **1975**, *48* (2), 375–378.

(192) Kobayashi, N.; Fukuda, T. Phthalocyanine, Porphyrin, Cyclodextrin, and Polymer Systems Suitable for Studying by Circular Dichroism, Magnetic Circular Dichroism, and/or Electrochemistry. *Bull. Chem. Soc. Jpn* **2009**, *82* (6), 631–663.

(193) Komatsu, T.; Urano, Y.; Fujikawa, Y.; Kobayashi, T.; Kojima, H.; Terai, T.; Hanaoka, K.; Nagano, T. Development of 2,6-Carboxy-Substituted Boron Dipyrromethene (BODIPY) as a Novel Scaffold of Ratiometric Fluorescent Probes for Live Cell Imaging. *Chem. Commun.* **2009**, *46* (45), 7015–7017.

(194) Yanai, T.; Tew, D. P.; Handy, N. C. A New Hybrid Exchange-Correlation Functional Using the Coulomb-Attenuating Method (CAM-B3LYP). *Chem. Phys. Lett.* **2004**, *393* (1–3), 51–57.

(195) Chemcraft version 1.8, Andrienko GA. http://www.chemcraftprog.com (accessed Jan 18, 2018).

(196) Kubheka, G.; Uddin, I.; Amuhaya, E.; Mack, J.; Nyokong, T. Synthesis and Photophysicochemical Properties of BODIPY Dye Functionalized Gold Nanorods for Use in Antimicrobial Photodynamic Therapy. *J. Porphyrins Phthalocyanines* **2016**, 20 (08n11), 1016–1024.